MACHINABILITY CHARACTERISTICS IN DRILLING OF GLASS MICROBALLOON/EPOXY SYNTACTIC FOAM

Thesis

Submitted in partial fulfillment of the requirements for the degree of

DOCTOR OF PHILOSOPHY

by

ASHRITH H. S.

DEPARTMENT OF MECHANICAL ENGINEERING

NATIONAL INSTITUTE OF TECHNOLOGY KARNATAKA,

SURATHKAL, MANGALORE -575025

MAY, 2019

D E C L A R A T I O N

I hereby *declare* that the Research Thesis entitled **"MACHINABILITY CHARACTERISTICS IN DRILLING OF GLASS MICROBALLOON/EPOXY SYNTACTIC FOAM"** which is being submitted to the **National Institute of Technology Karnataka, Surathkal** in partial fulfillment of the requirements for the award of the Degree of **Doctor of Philosophy** in **Department of Mechanical Engineering** is a *bonafide report of the research work carried out by me*. The material contained in this Research Thesis has not been submitted to any University or Institution for the award of any degree.

Register Number : **155067ME15F01**

Name of the Research Scholar : **ASHRITH H. S.**

Signature of the Research Scholar :

Department of Mechanical Engineering

Place **: NITK, Surathkal**

Date **:**

CERTIFICATE

This is to *certify* that the Research Thesis entitled **"MACHINABILITY CHARACTERISTICS IN DRILLING OF GLASS MICROBALLOON/EPOXY SYNTACTIC FOAM"** submitted by **Mr. ASHRITH H. S.** (**Register Number: 155067ME15F01**) as the record of the research work carried out by him, is *accepted as the Research Thesis submission* in partial fulfillment of the requirements for the award of degree of **Doctor of Philosophy.**

Research Guide

Dr. Mrityunjay Doddamani
Assistant Professor
Department of Mechanical Engineering
NITK, Surathkal

Chairman–DRPC

Date:

ACKNOWLEDGEMENT

I would like to extend my gratitude to Dr. Mrityunjay Doddamani, Assistant Professor, Mechanical Engineering, National Institute of Technology Karnataka (NITK), Surathkal for the invaluable constructive guidance and encouragement extended throughout my study. Sincere gratitude is expressed to Prof. Nikhil Gupta of New York University, USA and Prof. Vinayak Gaitonde of B V B College of Engineering and Technology, India for the encouragement and the help provided.

I would like to thank my Research Progress Assessment Committee members Dr. Ramesh M. R. and Dr. Raviraj H. M. for their valuable inputs.

I would like to thank former Head of Department Prof. Narendranath S., and Prof. Shrikantha S Rao, Head of Mechanical Engineering Department and all the faculty members at Mechanical Engineering Department for their support throughout this research work.

Constant encouragement of my family to pursue higher studies has made it possible for me to reach at this stage. I wish to thank all my family members for love, help and encouragement provided. I express my sincere thanks to our research team for their help and kind cooperation extended throughout this research work. Special note of thanks to all my friends and well-wishers for their constant help, encouragement and understanding.

ABSTRACT

Polymer composites are steadily substituting the conventional materials in aerospace, marine, automobile and many other engineering applications owing to their unique properties such as lightweight feature combined with high specific strength and superior corrosion resistance. Weight reduction of composite materials is of great interest in aerospace, marine and automobile applications to meet the stringent guidelines of fuel consumption and emissions in the coming years. Structural weight reduction without compromising the desired properties can be achieved by using a unique class of composite called syntactic foams, wherein the matrix is filled with hollow particles called microballoons. Even though the composites are produced to near-net shape, drilling is unavoidable during final stage of production process for the assembly of various structural components using fasteners. Many problems arise during drilling of composites due to non-homogeneous and anisotropic nature of the material. Nearly 60% of the composite parts are rejected during aircraft assembly due to drilling induced damages. The focus of the present study is to achive good quality holes in drilling of glass microballoon/epoxy syntactic foams by selecting appropriate process parameters.

In the present investigation, epoxy resin (LAPOX L-12) is used as the matrix resin and borosilicate glass microballoon (GMB) is used as hollow filler without any surface treatment. Syntactic foams are fabricated by dispersing 20, 40 and 60 vol.% GMBs in epoxy matrix using manual stirring method. Nine different types of syntactic foams specimens with 20, 40 and 60 vol.% of GMBs are fabricated using three different densities (varying wall thickness) of GMBs (SID-200Z: 200 kg/m^3, SID-270Z: 270 kg/m^3 and SID-350Z: 350 kg/m^3). All the prepared samples are coded as per EYYY-*R* convention. Epoxy resin is denoted by ‘E’ and ‘YYY’ represents density of GMBs. Neat epoxy specimens are also fabricated under similar processing conditions for comparison. Extensive micrography of fabricated foams confirms the uniform distribution of GMBs in the epoxy matrix without forming the clusters. Experimental density of all the fabricated syntactic foams is lower than neat epoxy resin. Density of foams decreases with decreasing GMB wall thickness and increasing volume fraction of GMBs. Density reduction in the range of 18-53% is noted as compared to neat epoxy indicating significant weight saving potential of the proposed syntactic foams.

Experiments are conducted using vertical computer numerical control machine and TiAlN coated tungsten carbide twist drills of varying diameter based on full factorial design (FFD). Cutting speed (*v*), feed (*f*), GMB content (*R*), GMB wall thickness (*w*) and drill diameter (*D*) are taken as input parameters, while thrust force, surface roughness, specific cutting coefficient, cylindricity, exit side circularity error and exit side damage factor are considered as responses for evaluating the quality of drilled hole. Three levels for each input process parameters (*v*: 25, 75 and 125 m/min; *f*: 0.04, 0.08 and 0.12 mm/rev; *R*: 20, 40 and 60 vol.%; *w*: 0.716, 0.925 and 1.080 µm; *D*: 8, 12 and 16 mm) are selected to consider the nonlinear effects among the parameters. Experiments are repeated for three times and the average values are used for analysis. Mathematical models based on response surface methodology (RSM) are developed using Minitab 14 software for analyzing the influence of the input parameters on the measured responses. Adequacy of the developed mathematical models is confirmed using analysis of variance. Higher R-squared values indicate that the developed mathematical models can be effectively used as a tool in industrial practices to predict the machinability characteristics of GMB reinforced epoxy foams during drilling.

Individual and interaction effect of process parameters on the responses are analyzed using RSM based mathematical models. Individual effects are studied by varying one parameter at a time in the mathematical models while keeping all the remaining process parameters at the intermediate levels. Two parameters are varied at the same time while keeping the other parameters at the intermediate level in the mathematical models to study the interaction effect of process parameters on the chosen responses. Thrust force is found to be increasing with increasing feed and drill diameter, while it decreases with increasing GMB content. Thrust force of all the foams is found to be lower as compared to neat epoxy resin. Thrust force is observed to be decreased by 40-55% as compared to neat epoxy due to the incorporation of GMBs. Drill diameter, feed and GMB content have a significant effect on the thrust force while the effect of cutting speed is found to be insignificant. $v_{125}f_{0.04}R_{60}D_8$ is the optimum condition for minimizing thrust force of E200 and E270 foams while performing machining at $v_{25}f_{0.04}R_{60}D_8$ minimizes the thrust force of E350 syntactic foam. Extensive microscopy is conducted on the drilled specimens to understand crack initiation and propagation mechanisms. Surface roughness of the drilled hole is measured using Mitutoyo surftest with a cut-off length of 0.8 mm. As compared to neat epoxy, the surface roughness of syntactic foams increases by 14-20 times. However, surface roughness in foams decreases with increasing GMB volume fraction. Surface roughness is strongly governed by drill diameter and cutting speed. Minimum surface roughness for E200 and E270 foams is obtained at $v_{25}f_{0.12}R_{60}D_{16}$, while $v_{25}f_{0.12}R_{60}D_{12}$ is found to be optimum for E350 foam.

Specific cutting coefficient increases with increasing drill diameter and decreasing feed. Increasing GMB content significantly decreases specific cutting coefficient by 40-55% as compared to neat epoxy specimens. $v_{25}f_{0.12}R_{60}D_8$ is the optimum condition for E350 foam, while machining at $v_{125}f_{0.12}R_{60}D_8$ is found to be beneficial for E200 and E270 foams for minimizing specific cutting coefficient. Coordinate measuring machine is used to measure the cylindricity, exit side circularity and maximum diameter of drilled hole for damage estimations. Cylindricity of the foams increases with increasing the cutting speed, feed and drill diameter. Increasing GMB content decreases the cylindricity by 46-69% as compared to neat epoxy. Drill diameter, feed and GMB content have a significant effect on cylindricity of drilled holes. $v_{25}f_{0.04}R_{60}D_8$ is noted to be the optimum conditions for E200 and E270 foams while $v_{75}f_{0.04}R_{60}D_8$ parametric setting is most suitable for thick-walled (E350) foams to minimize cylindricity.

Circularity error increases with increasing cutting speed and drill diameter, while it decreases with increasing feed and GMB content. Increasing the microballoon volume fraction decreases the circularity error of foams by 18-67% as compared to neat epoxy. Circularity error of the holes is highly influenced by drill diameter followed by GMB volume fraction and wall thickness. $v_{25}f_{0.12}R_{60}D_8$ is the optimum condition for minimizing the circularity error of all the type of foams. The damage factor is dependent on the thrust force developed during drilling process. Drill diameter, feed and GMB content have a significant effect on damage factor of the drilled holes. Optimum conditions for minimizing damage factor is observed to same as that of thrust force. A reduction in the damage factor by 26-42% is noted in foams with increasing GMB content as compared to neat epoxy. Optimum conditions based on response surface

methodology for minimizing all the responses are not same and the trade-off among various process parameters necessitates multi-response optimization. In the present work, grey relation analysis (GRA) is used for finding a specific combination of process parameters for minimizing all the response at the same time to obtain a good quality hole in drilling GMB/Epoxy syntactic foams. According to GRA, $v_{125}f_{0.08}R_{60}D_{8}$ is the optimal condition for producing a quality hole in E200 foams, whereas $v_{25}f_{0.12}R_{60}D_{8}$ is found to be optimal for E270 and E350 syntactic foams. Higher GMB content is preferred in the foams from drilling operations perspective, which is also beneficial for weight sensitive applications.

Influence of GMB wall thickness on the responses is studied by keeping the GMB content at 60 vol.%, as higher filler content significantly improves the hole quality. Response surface plots for varying wall thickness of GMBs are plotted using the developed mathematical models to study the interaction effects among input process parameters. Increasing microballoon wall thickness from $w_{0.716}$ to $w_{1.080}$ increases thrust force, specific cutting coefficient and damage factor by 40%. Surface roughness, cylindricity and circularity error of drilled holes are significantly affected by GMB wall thickness and is found to be decreased by 30, 41 and 56% respectively. Combination of higher particle wall thickness and feed with lower cutting speed and drill diameter ($v_{25}f_{0.12}w_{1.080}D_{8}$) is the optimum condition for producing a sound hole quality as observed from GRA. Hole quality is highly influenced by drill diameter followed by the interaction between cutting speed and GMB wall thickness. Finally, microscopy is conducted to analyze the shape and size of chips produced during drilling. Cutting tools are inspected using a confocal microscope post drilling operation and micrographs show negligible tool wear due to the superior wear resistance of TiAlN coating. Observations and parameters settings explored in this work offers guidelines for the industrial practitioners to produce quality holes in drilling of GMB reinforced epoxy composites.

Keywords: *Syntactic foam; Glass microballoon; Epoxy; Drilling; Design of experiments; Response surface methodology; Analysis of variance; Machinability; Grey relation analysis; Multi-response optimization.*

CONTENTS

LIST OF FIGURES

LIST OF TABLES

ABBREVIATIONS

ABS	: Acrylonitrile Butadiene Styrene
AJM	: Abrasive Jet Machining
AlTiN	: Aluminium Titanium Nitride
ANN	: Artificial Neural Network
ANOVA	: Analysis of Variance
ASTM	: American Society for Testing and Materials
AWJM	: Abrasive Water Jet Machining
CCF	: Central Composite Face Centred Design
CFRP	: Carbon Fiber Reinforced Polymer
CMC	: Ceramic Matrix Composite
CNC	: Computer Numerical Control
CNF	: Carbon Nanofiber
Co	: Cobalt
CTE	: Coefficient of Thermal Expansion
DoE	: Design of Experiments
EBM	: Electron Beam Machining
FFD	: Full Factorial Design
GA	: Genetic Algorithm
GFRP	: Glass Fiber Reinforced Polymer
GMB	: Glass Microballoon
GRA	: Grey Relational Analysis
HSS	: High Speed Steel
LBM	: Laser Beam Machining
MMC	: Metal Matrix Composite
PMC	: Polymer Matrix Composite
PP	: Polypropylene
PVC	: Polyvinyl Chloride
RSM	: Response Surface Methodology
SF	: Syntactic Foam

TiAlN	: Titanium Aluminium Nitride
USM	: Ultrasonic Machining
WC	: Tungsten Carbide
WJM	: Water Jet Machining

NOMENCLATURE

v	Cutting speed	m/min
CYL	Cylindricity	mm
ρ	Density	kg/m^3
ρ_g	Density of glass	kg/m^3
ρ_{MB}	Density of GMB	kg/m^3
ρ_m	Density of matrix	kg/m^3
Δ_{oi}	Deviation sequence	-----
D	Drill diameter	mm
C_{e-Exit}	Exit side circularity error	mm
F_{d-Exit}	Exit side damage factor	-----
ρ_e	Experimental density	kg/m^3
ρ_{e-E}	Experimental density of neat epoxy	kg/m^3
ρ_{e-SF}	Experimental density of syntactic foam	kg/m^3
f	Feed	mm/rev
Φ_w	Filler content	weight %
R	Filler content	volume %
$\Phi_{\mu P}$	GMB porosity	volume %
$\xi_i(k)$	Grey relation coefficient	-----
γ_i	Grey relation grade	-----
ζ	Identification coefficient	-----
r_i	Inner radius of GMB	µm
V_m	Matrix content	volume %
Φ_v	Matrix porosity	volume %
$D_{\max}$	Maximum diameter of damage zone	mm
$X_i^{o}(k)$	Original data sequence	-----
r_o	Outer radius of GMB	µm
$d_{\mu m}$	Particle diameter	µm
$X_i^{*}(k)$	Pre-processed data sequence	-----
η	Radius ratio	-----

$X_o^*(k)$	Reference sequence	-----
K_f	Specific cutting coefficient	MPa
R_a	Surface roughness	µm
ρ_t	Theoretical density	kg/m^3
F_t	Thrust force	N
m	Total number of experiments	-----
n	Total number of parameters	-----
Φ_t	Total porosity	volume %
w	Wall thickness of GMB	µm

1 INTRODUCTION

1.1 Composite material

Conventional materials cannot always meet the ever increasing demands of technological advances. Performance requirements of advanced technologies necessitate materials to have diverse properties like high specific strength, high stiffness, high toughness, etc. and this leads to the development of composite materials. Composite material is defined as a structural material that consists of two or more constituents that are combined at a macroscopic level and are not soluble in each other (Kaw 2005). In other words, composite materials are defined as multiphase materials obtained by artificially combining different materials to achieve properties that the individual components by themselves cannot accomplish (Chung 2010). Composite material consists of a reinforcing phase in the form of fiber or particle which is surrounded by a continuous phase called matrix. Composite material exhibits various advantages over conventional material such as high strength to weight ratio, high stiffness to weight ratio, superior mechanical properties, improved impact resistance, excellent corrosion resistance and better design flexibility (Singh et al. 2013).

Composites are broadly classified based on the matrix and reinforcement. Based on the matrix material composites are classified as polymer matrix composites (PMCs), carbon matrix composites (or carbon-carbon composites), metal matrix composites (MMCs) and ceramic matrix composites (CMCs). Based on the reinforcement form, composites are classified as particulate reinforced, whisker reinforced and fiber reinforced composites. PMCs are most commonly used composites than metal-matrix, carbon-matrix, and ceramic-matrix composites because of the relatively low processing temperatures required for fabrication (Chung 2010). PMCs find applications in lightweight structures (aircraft, sporting goods, wheelchairs, etc.), vibration dampers, electronic enclosures, etc.

Based on the type of matrix used PMCs are classified as thermoset and thermoplastic composites. Thermoset is defined as a polymeric material which can be formed by the application of heat and pressure, as a result of a chemical reaction, permanently cross-links and cannot be reformed upon further application of heat and pressure (Dodiuk and

Goodman 2014). Thermosets, especially epoxy resins are currently used more than other matrices in structural applications because of their resistance towards moisture and other environmental influences. For many applications, thermoset polymers offer an invincible combination of handling characteristics, processing flexibility, lower cure shrinkage and better mechanical properties at acceptable cost. Epoxy matrix structural components are extensively used in U.S. Air Force and Navy since 1972, and in-service performance of these components has been very satisfactory (Donaldson and Miracle 2001).

Particulate composites are the class of particle reinforced composite where large amounts of particles (usually less than 1000 μm) are dispersed in the matrix resin. Particulate composites are usually synthesized by dispersing particles in a liquid resin to form a slurry and then poured into the molds to form a composite. In these composites, particles are incorporated to obtain an unusual combination of properties like reduced density, enhanced mechanical properties and to reduce the cost of the composite. Increasing demands for lightweight structures in automobiles, marine and aerospace application has led to the development of a new class of structural composites called syntactic foams. Syntactic foams are fabricated by dispersing hollow microballoons in the matrix material. These closed cell foams help to save fuel, increase payload capacity and reduce environmental pollution (Gupta et al. 2013). Properties of syntactic foams can be tailored according to requirements by varying microballoon volume fraction or wall thickness. Varying microballoon properties allows the development of multifunctional syntactic foams for a wide range of applications (Pinisetty et al. 2015).

1.2 Syntactic foam composites

Lightweight multifunctional materials are in high demand in all the modes of transportation because the structural weight reduction results in better fuel economy and associated environmental benefits. Syntactic foams (SFs) are the particulate composite materials synthesized by dispersing hollow particles called microspheres (microballoons) in a matrix medium. Unlike open-cell foams, the porosity in SFs is enclosed inside the shell of microspheres forming closed-cell structure (Gupta and

Woldesenbet 2004). Even though the SFs are developed in the 1960s, most of the effort has been made by many researchers in the last 15 years to investigate the behavior of these materials. Earlier applications of SFs are limited to marine structures where buoyancy of the materials is an important consideration along with low moisture absorption and high hydrostatic compression. Effort has been made in the recent years to tailor the various properties of SFs such as mechanical, thermal and electrical properties resulting in the increased application of syntactic foams (Gupta et al. 2014). Syntactic foams exhibit high damage tolerance and energy absorption under various loading conditions. Sandwich composites use SFs as core materials for structural applications (Porfiri and Gupta 2009). Other than structural applications, SFs are also used in electronic packing, sports equipments, furnitures, thermal insulation, acoustic transducers, etc.

Generally, SFs are two-phase structures, consisting of hollow microballoons and the matrix resin. Figure 1.1 shows the schematic representation of syntactic foam microstructure. Syntactic foams are closed cell foams because the porosity is enclosed within the stiff shell of hollow microballoons (Figure 1.1). Microballoon porosity in foams is desired and can be controlled by varying microballoon volume fraction and wall thickness. Entrapment of air in the matrix resin during syntactic foams fabrication results in formation of voids called matrix porosity. Presence of matrix porosity makes syntactic foams a three-phase structures which should be kept as low as 10 vol.% (Gupta et al. 2013).

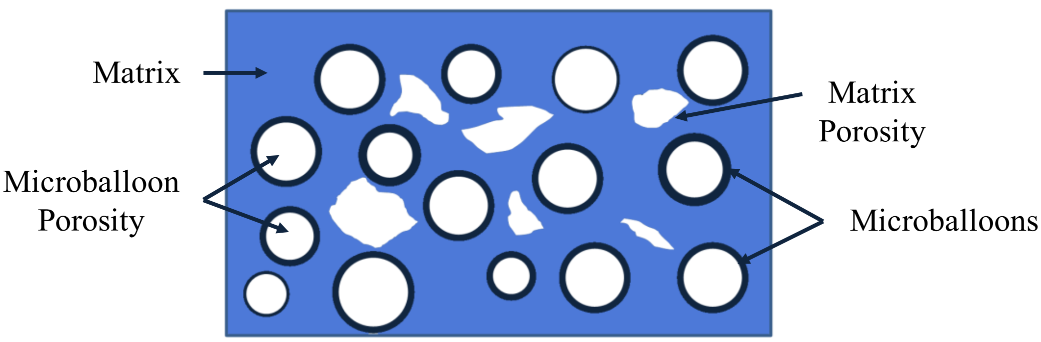

Figure 1.1 Schematic representation of syntactic foam microstructure.

Properties of syntactic foams can be enhanced by incorporating micro and nanoscale reinforcements making syntactic foam a multi-phase structure. Addition of reinforcements to syntactic foams enhances its modulus, strength, energy absorption, and thermal properties. Glass, carbon and aramid fibers, nanoclay, carbon nanotubes, and rubber particles are generally used as reinforcements in syntactic foam fabrication (Gupta et al. 2013). High dimensional and thermal stability of syntactic foams makes them suitable candidates for automotive, aerospace, marine and civil structural applications (Pinisetty et al. 2015).

1.2.1 Fillers

Syntactic foams density can be controlled by varying the hollow particles density (wall thickness) and volume fraction. Variety of particles can be used as fillers in SFs fabrication. Incorporation of hollow particles reduces the density of composite material and replaces the expensive matrix resin. Hollow particles also enhance the mechanical properties, tribological characteristics, thermal and dimensional stability of SFs. Hollow particles of glass, carbon, phenolic, ceramics and fly ash particles have been used as fillers (Cochran 1998, Jayavardhan et al. 2017, Shahapurkar et al. 2018, Yi-Jen et al. 2010). Various shapes of engineered hollow particles like spherical, cuboidal or cylindrical are available these days. Among them, spherical hollow particles of diameter and density in the range of 10-250 μm and 150-500 kg/m^3 respectively are most commonly used for SFs fabrication (Gupta et al. 2013). Cenospheres, an industrial waste is also used as fillers to develop inexpensive SFs. However, the defects present on the surface and within the cenosphere walls leads to inferior mechanical properties as compared to the foams reinforced with engineered hollow glass particles (Koopman et al. 2004).

Glass microballoons (GMBs) are the most commonly used fillers for syntactic foam fabrication. GMBs are finely dispersed, free-flowing powders containing spherical glass particles of diameter and wall thickness in the range of 10-200 µm and 0.5-2.0 µm respectively. Most commonly used method for fabrication of GMBs involves passing glass powders through the flame of a gas-air burner at a temperature of 1100-1500°C so that the solid particles of glass are converted into hollow microballoons

(Budov 1994). American Standard Oil Co. used GMBs for the first time as a protective layer to prevent evaporation of highly volatile products. These hollow particles exhibit a unique combination of properties such as low density, relatively high strength, good thermal insulation and dielectric properties. This makes them important technogenic fillers for polymeric materials. GMBs not only used to modify the properties significantly but also used to improve the technological conditions of polymer processing like decreasing the shrinkage and viscosity of filled polymeric composites, ensure stable dimensions of molded articles, and decrease wear of molding equipment (Budov 1994, Shutov 1986).

1.2.2 Matrix

Polymers are the newest and at the same time oldest basic materials known to humans. Polymers are made by chemical processing, i.e., by joining many small molecules called monomers together to form very large molecules called macromolecules that possess a chain-like structure. Polymer is derived from Greek word *poly* means many and *meros* means parts. Atoms in the molecules are held together by the strong covalent bond. Polymers are considered as organic chemical because most of them are carbon-based. Polymers are broadly classified into thermoplastics and thermosets. In thermosets strong covalent bonds leads to cross-linking of molecules in addition to Van der Waals forces. Thermosets cannot be subjected to repeated heating and cooling cycles as they have a tendency to degrade. Thermoplastics are usually solid at room temperature and cross-linking between molecules takes place as a result of Van der Waals forces. Thermoplastics can be reheated and reshaped repeatedly during processing without degradation. Thermoplastics nearly constitute 70% of the world's synthetic plastic consumption (Groover 2007).

Thermoplastics are generally used in packing materials, paints, varnishes, to make thin films, fibers and sheets. Commonly used thermoplastics are acetals, acrylics, acrylonitrile-butadiene-styrene (ABS), polyamides, polyethylene, polypropylene (PP), polystyrene, polyvinylchloride (PVC), etc. Thermosets are generally more rigid, brittle, less soluble in common solvents and capable of higher service temperatures. Thermosets finds applications in adhesives, surface coatings, flooring, glass fiber-reinforced composites, brake linings, abrasive wheels, printed circuit boards, paints, varnishes, medical tubing, protective clothing fibers, etc. Examples of commercially available thermosets include amino resins, epoxies, phenolics, polyesters, polyimides, polyurethanes and silicones (Groover 2007).

Epoxy resins are first produced in the early 1940s in Europe and United States simultaneously. Earlier application of epoxy resins is limited to casting compounds and coatings. Epoxies belong to the class of thermoset plastics and extensively used for fabrication of structural composites because of a unique combination of properties such as high strength, low cost, high dimensional stability, good wettability, high electrical insulation, chemical resistance and low toxicity. Epoxy resins are available in wide varieties starting form low-viscosity liquid to high-melting solids. Epoxy resins are combined with fibers and filler to fabricate complex composite structures in military aerospace applications that include wings, fuselage, ventilation ducts, flooring panels, etc. Epoxies are also used in bicycle frames, musical instruments, race cars, golf clubs and snowboards. Epoxies are readily compatible with substrates making them well suited for composites applications (Donaldson and Miracle 2001).

1.2.3 Processing of syntactic foams

Manufacturing is the process of transforming raw materials into products of greater value using physical and chemical processes (Groover 2007). A suitable manufacturing method must be chosen to transform the material into its final form. Syntactic foams can be processed by free pouring, molding, casting, or extrusion, depending on the matrix and filler concentration. The matrix used for syntactic foam fabrication should have low viscosity, low shrinkage, good wettability and must be compatible with fillers (Shutov 1986). Dispersion of hollow particle in matrix resins is a challenging task. Processing route for syntactic foam fabrication must be carefully designed so that uniform distribution of fillers in matrix resins without filler breakage and formation of clusters is obtained (Gupta et al. 2013).

Figure 1.2 shows the fabrication method commonly used for the preparation of GMBs reinforced epoxy syntactic foam. Two-step mixing process is adopted in this method.

In the first step, GMBs of required quantity is mixed with epoxy resin and stirred slowly until the homogeneous slurry is formed and care should be taken to avoid the breakage of GMBs. In the second step, hardener is added and stirred slowly to initiate the polymerization process. Finally, the mixture is poured into the molds of required dimension and then cured as per the requirements of the resin.

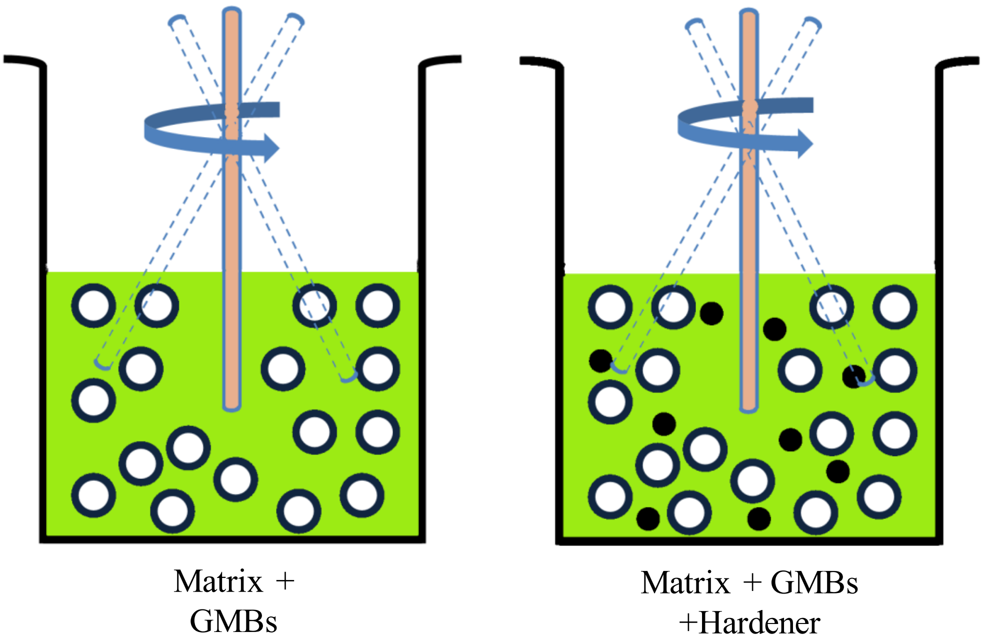

Figure 1.2 Illustration of syntactic foam fabrication method (Pinisetty et al. 2015).

Volume fraction of GMBs that can be incorporated in matrix material is the limitation of stirring methods. Since the density of GMBs is less than half the density of epoxy resins, mixing below 20 vol.% of particles is not recommended as GMBs tends to float to the top of the foam during curing. Mixing over 60 vol.% of GMBs is difficult because the GMBs tend to break and agglomeration becomes an issue during processing. High volume fraction of GMBs reinforced syntactic foams can be fabricated by reducing the viscosity of the matrix resin. Viscosity can be reduced by heating the matrix resin to a higher temperature. Another method used for reducing the matrix viscosity is by adding the diluents which should be chosen carefully to avoid the adverse effect on mechanical properties of syntactic foams (Gupta et al. 2013, Pinisetty et al. 2015).

1.3 Drilling of polymer composites

Composites are slowly replacing the conventional materials like metals in military, aerospace and civilian applications because of its unique properties. Composites can be produced to near net shape; however machining of composites are unavoidable for assembly purpose and to meet the needs of end user. Machinability refers to the ease or difficulty with which the materials can be machined. Machinability is the process of the evaluating material's response to different cutting conditions (Sheikh-Ahmad 2009). Machining of composite material is a difficult task due to anisotropic and heterogeneous nature of the material and also due to the presence of highly abrasive reinforcements. Properties and volume fraction of the constituents significantly influence the machining of composite material. In composite material, brittle fracture contributes to material removal rather than plastic deformation (Teti 2002). Composites can be machined using both conventional and non-conventional machining process. Figure 1.3 shows the different process that can be used for machining of polymer matrix composites. However, conventional processes are preferred over non-conventional machining processes because of simple operation and low operating cost (Pihtili and Canpolat 2009).

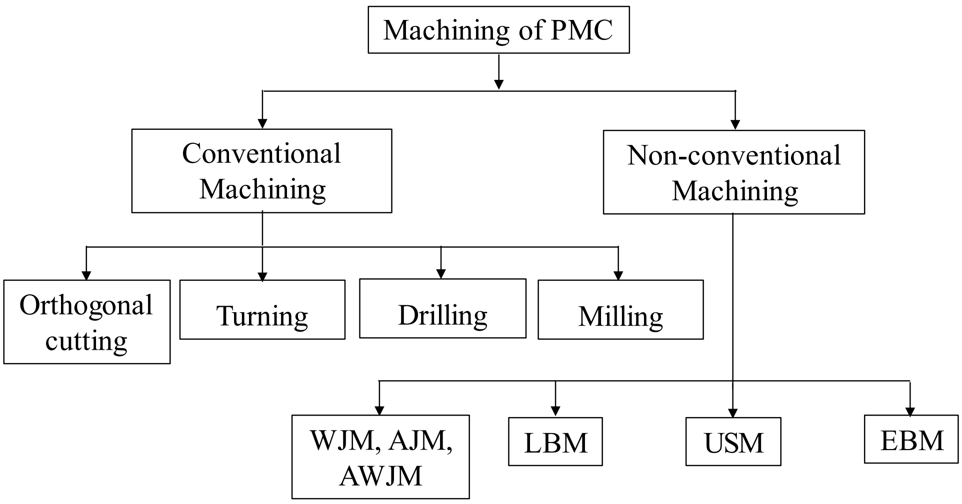

Figure 1.3 Different processes used for the machining of PMC.

Drilling is the most commonly used machining process to make holes for joining and assembly of automobiles and aircrafts complex structures. For example, a single wing in Airbus A380 requires drilling of 750,000 holes. But drilling of composite material is different than drilling of conventional metals because the drill has to move alternatively through the constituents of the material having different properties. Since the matrix and reinforcement have different physical and chemical properties, mechanism of material removal is quite complex. Drills with different geometries like twist drill, saw drill, candlestick drill, core drill, and step drill can be used to perform drilling operation (Hocheng and Tsao 2006). Damages are induced around the hole in drilling of composite material. Process parameters and their levels significantly affect the quality of the drilled hole. Nearly 60% of the composite parts are rejected due to poor hole quality which results in significant increase in the production cost (Singh et al. 2013). The different elements which significantly influence the drilling of polymer composites are shown in Figure 1.4. Defect-free drilling can be achieved by selecting optimum process parameters. Performing drilling operation with backup plate support also helps to achieve damage free holes (Singh et al. 2012).

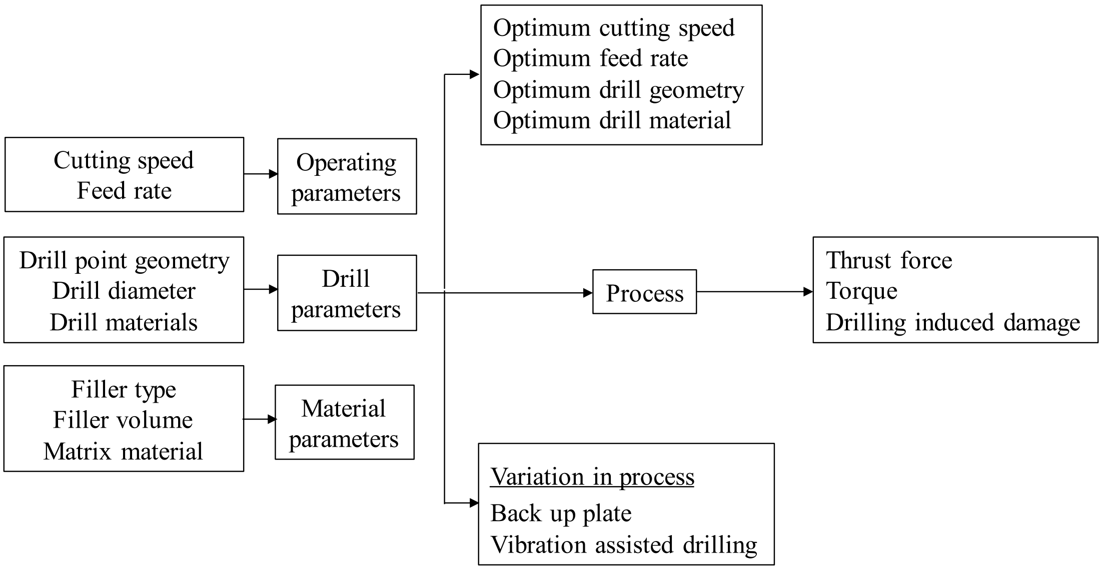

Figure 1.4 Elements of PMC drilling (Singh et al. 2012).

1.4 Response surface methodology (RSM)

Response surface methodology is a collection of mathematical and statistical techniques primarily developed for establishing the relationship between the various process parameters and the responses (Manakari et al. 2015). Since RSM models can be developed with minimum knowledge of the process, it is the most widely used tool for the approximation of responses in industries. RSM was initially used to model the experimental responses and later it is applied for modeling numerical experiments (Box and Draper 1987). Simple quadratic polynomials are generally used to construct response surface models for approximating the responses. The accuracy response surface models are limited to small design space. Non-linearities present in a large design space cannot be modeled effectively using polynomials of a lower order. RSM involves carefully designing a set of experiments with the objective to optimize a response which is influenced by several input parameters. Various machining processes such as turning, drilling and milling are successfully analyzed by adopting RSM mathematical models. Using RSM approach the interaction effects among various process parameters can be easily analyzed. The independent process parameters are represented in a quantitative form and response can be expressed as (Montgomery 2017),

$$Y = \varphi(x_1, x_2, x_3, ...x_k) \tag{1.1}$$

where, Y is the response, $x_1, x_2, x_3, ...x_k$ are the quantitative factors and φ is the response function. Better correlation between the response and process parameters can be obtained by employing polynomial equations of higher order which results in the increased experimentation costs (Basavarajappa et al. 2011).

1.4.1 Design of experiments (DoE)

Experiment is referred to a series of tests, called runs, where input variables are changed to identify the response. Experiments must be planned carefully for developing a response surface methodology based mathematical model (Basavarajappa et al. 2011). The conventional method involves the variation of one parameter at a time keeping other parameters at fixed levels. Moreover, the conventional method not only requires a large number of experiments to be performed but also does not include the interaction effects among the process parameters (Gaitonde et al. 2011). The experimental planning based on the design of experiments requires minimum number of experiments than the conventional method and hence reduces the time and cost of experimentation. Many types of experimental designs can be used for this purpose, but the most common ones are full factorial design, fractional factorial design and central composite design (Montgomery 2017).

A factorial experiment is one in which input parameters are varied simultaneously, instead of varying one at a time like in conventional methods. The experimental design systematically defines the efficient set of experimental sampling points at which the responses must be computed or observed. Number of experiments grows exponentially in a factorial design and hence it is suited for modeling the problems with five or fewer input parameters. A three-level design is usually written as 3^k factorial design, where k refers to the numbers of factors considered at three levels. Three levels are usually referred as low (0), intermediate (1) and high levels (2). Possible curvature in response function can be modeled using 3^k factorial design. Second order mathematical models are generally fitted using full factorial design of experiments. A general second-order model is given by (Montgomery 2017),

$$Y = \begin{pmatrix} b_0 + b_1 \times v + b_2 \times f + b_3 \times D + b_4 \times R + b_{11} \times v^2 + b_{22} \times f^2 + b_{33} \times D^2 + b_{44} \times R^2 + b_{12} \times v \times f \\ + b_{13} \times v \times D + b_{14} \times v \times R + b_{23} \times f \times D + b_{24} \times f \times R + b_{34} \times D \times R \end{pmatrix} \tag{1.2}$$

where, $b_0, b_1, b_2, ...b_{34}$ are the regression coefficients to be determined. The regression coefficients of the quadratic model are determined by,

$$B = (X^T X)^{-1} X^T Y \tag{1.3}$$

where, B is a matrix of parameter estimates, X is calculation matrix which includes linear, quadratic and interaction terms, X^T is the transpose of X and Y is a matrix of response.

1.5 Grey relational analysis (GRA)

Response surface methodology with single response optimization is widely used in drilling studies. A single set of process parameters may be optimal for single quality characteristic, but the same settings may yield detrimental results for other quality features (Kumar and Singh 2014). Therefore, multi-objective optimization is the solution to optimize multiple responses simultaneously like in GRA. GRA has successfully been implemented in the past for process parameter optimization in the drilling process (Palanikumar 2011, Palanikumar et al. 2012, Sheth and George 2016). Grey relation analysis is relatively a new analysis method founded by Chinese Professor Julong Deng from Huazhong University of Science and Technology for providing an efficient solution to uncertainty, multi-input, and discrete data problems. It involves the measurement of absolute values of data differences between the sequences (Nagpal et al. 2014). GRA is widely used multi-response optimization technique because of its comparative simplicity. GRA is used to quantify the influence of various input parameters on the output parameters known as responses by computing the grey relational grades. The overall evaluation of experimental data for the multi-response process can be obtained using grey relational grade. Larger grey relation grade indicates the combination of optimal parameters which significantly influencing the response (Sreenivasulu and Rao 2012). GRA is considered more advantageous than the statistical regression analysis (Palanikumar et al. 2012).

1.6 Literature survey

Composites are continuously replacing the conventional materials in various engineering applications due to their exceptionally good mechanical properties. Polymer composites especially fiber reinforced composites are widely used in the structural application of aerospace industry. Syntactic foams are lightweight composites used prominently in weight saving applications. Glass microballoon reinforced syntactic foams possess attractive mechanical, thermal, electrical properties, better dimensional stability and are cost effective. In the recent past, many researchers have put their efforts for evaluating the various properties of glass microballoon reinforced syntactic foams and are presented in Table 1.1.

Even though composites are produced to near net shapes, machining of lightweight composites are unavoidable for joining and assembly purpose. Drilling is the most commonly used machining process for making holes in the composites. It is necessary to understand the behavior of the material to produce good quality holes economically. Life of the structural joint is significantly affected by the quality of the drilled hole, which in turn depends on the selection of appropriate process parameters. Machining performance can be significantly improved by proper selection of drill and process parameters. A number of research publications on drilling of polymer matrix composite have been published in the recent year are presented in Table 1.2 to identify the significant process parameters and their effects on quality of drilled hole. Notations used to represent the summary of literature are as follows:

ρ	Density	kg/m^3
Φ_w	Filler content	weight %
R	Filler content	volume %
$d_{\mu m}$	Particle diameter	μm

Table 1.1 Literature review on glass microballoon reinforced syntactic foam.

Author	Matrix and Filler	Properties Investigated	Remarks
Gupta et al. (1999)	Epoxy resin Araldite LY5052 ρ : 1150 GMBs Φ_w : 1.52 and 1.84 $d_{\mu m}$: 10-100 ρ : 250	Physical and mechanical properties	• A novel approach is developed for fabrication of SF to reduce the void content. • Rigorous stirring increases void content of the SF due to the entrapment of air. • Strength of SF increases with decreasing void content.
Kim and Khamis (2001)	Epoxy resin Bisphenol A and F ρ : 1108 GMBs $d_{\mu m}$: 10-100 ρ : 125 R: 0, 15, 31, 45, 51, 65	Fracture toughness, flexural properties and impact performance	• GMBs are not having any significant effect on specific fracture toughness of SF. • Increasing GMBs content decreases the specific flexural strength and marginally increases the specific flexural modulus of SF. • Impact performance of SF can be enhanced by increasing the GMBs content.
Kim and Plubrai (2004)	Epoxy resin Bisphenol A and F ρ : 1073 GMBs ρ : 125	Compression properties	• Increasing matrix volume percentage increases the compressive strength and modulus of foams. • SFs with lowest density fails due to longitudinal splitting. • Layered crushing is the reason for the failure of high density SF.
Park et al. (2005)	Epoxy resin Bisphenol A ρ : 1160 GMBs	Fracture behavior, thermal and electrical properties	• SFs exhibit lower coefficient of thermal expansion as compared to neat epoxy. • Increasing GMBs content decreases the dielectric constant and

Author	Matrix and Filler	Properties Investigated	Remarks
	Φ_w : 0-2 $d_{\mu m}$: 10-150		increases the fracture toughness of foams. • SFs exhibit higher glass transition temperature and mechanical properties than neat epoxy.
Kishore et al. (2005)	Epoxy resin ρ : 1180 GMBs R : 25.9, 34.9, 39.8 and 43.9	Tensile strength and modulus	• Tensile strength of foams increases from 23.8 to 41.9 MPa with the decreasing GMBs content. • Decreasing GMB content increases the tensile modulus of syntactic foam 2 to 2.47 GPa.
Wouterson et al. (2005)	Epoxy resin Epicote 1006 GMBs ρ : 150 and 460 $d_{\mu m}$: 70 and 43.6 R : 10, 20, 30, 40 and 50	Specific strength, specific modulus and fracture toughness	• SFs reinforced with high density microspheres exhibit superior compressive properties. • Types and volume fractions of microspheres significantly influence the specific properties of syntactic foam. • Increase in microsphere density and thickness-to-radius ratio led to an increase in specific tensile stiffness.
Nikhil and Ruslan (2006)	Epoxy resin DER 332 ρ : 1160 GMBs R : 30, 40, 50 and 60 ρ : 220, 320, 380 and 460	Tensile properties	• Increasing the density of GMBs increases the tensile modulus and tensile strength of the SFs. • Increasing GMB content decreases the tensile strength of SFs. • The effect of volume fraction is found to be insignificant on tensile modulus of SFs with higher density GMBs.

Author	Matrix and Filler	Properties Investigated	Remarks
Gupta and Ricci (2006)	Epoxy resin DER 332 GMBs R : 30, 40,50,60 and 65 $d_{\mu m}$: 35-40 ρ : 220, 320, 380, and 460	Compression properties	• A novel approach is proposed for fabricating functionally graded syntactic foams (FGSFs) by varying the wall thickness of GMBs. • Increasing density of FGSFs leads to the increased compressive strength and modulus. • Wall thickness gradient SFs shows 3-5 times higher total energy absorption compared to neat and volume fraction gradient SFs.
Gupta et al. (2006)	Epoxy resin DER 332 GMBs R : 30, 40,50,60 and 65 $d_{\mu m}$: 35-40 ρ : 220, 320, 380, 460	Compression and electric properties	• Compressive strength and modulus increase with increasing GMB wall thickness and decreasing volume fraction of GMB. • Increasing density of SFs linearly increases the compressive strength and modulus. • Dielectric constant and dielectric loss of SFs increases with increasing GMB wall thickness and decreasing volume fraction.
Yung et al. (2009)	Epoxy resin Epon 8008 and Epon 1031 GMBs R : 0-51.3 ρ : 600	Thermal mechanical analysis, thermal conductivity and dielectric properties	• Increasing GMB content simultaneously decreases dielectric constant and dielectric loss of the composites. • Coefficient of thermal expansion and the glass transition temperature of SFs enhances with increasing GMB content. • The thermal conductivity of the SFs is found to be decreased with increasing GMB content.

Author	Matrix and Filler	Properties Investigated	Remarks
Hu and Yu (2011)	Epoxy resin E-44 ρ : 1148 GMBs	Tensile, thermal and dynamic mechanical properties	• Thermogravimetric analysis and dynamic mechanical analysis results show the existence of stronger interfacial bonding between matrix and GMBs and high loss factor. • Increasing GMBs content decreases the tensile strength and specific properties of all types of SFs.
Swetha and Kumar (2011)	Epoxy resin Araldite GY257 ρ : 1150 GMBs $d_{\mu m}$: 60, 35 and 40 ρ : 150, 220, 460	Compression properties	• Results show that the strength of SFs decreases linearly with increasing GMB content. • Using higher density GMBs increases strength of the SFs. • Energy absorption capacity of syntactic foams is found to be increasing till 40 vol.% GMBs and later found to be decreased.
Zhu et al. (2012)	Epoxy resin Epon 8008 and Epon 1031 GMBs $d_{\mu m}$: 32.5, 32.5, 20 and 15 ρ : 125, 200, 380 and 600	Thermal, dielectric and compressive properties	• Results show that increasing GMB content decreases thermal conductivity, dielectric constant and dielectric loss of SFs. • Increasing GMB content to 60 vol.% decreases thermal conductivity, dielectric constant and dielectric loss of SFs by 56, 51 and 54% respectively as compared to neat epoxy. • Thermal, dielectric and compressive properties of SFs can be tailored according to the requirements by varying GMB content and density.

Author	Matrix and Filler	Properties Investigated	Remarks
Colloca et al. (2013)	Epoxy resin DER 332 GMBs $d_{\mu m}$: 35 and 40 ρ : 220 and 460 R : 30 and 50 CNFs ρ :1950	Tensile properties	• Increasing density of GMB leads to the increased modulus and strength of the SFs. • A higher value of tensile strength is observed in CNF reinforced SFs compared to unreinforced SFs. • Specific tensile modulus of all CNF reinforced SFs is found to be higher than that of the CNF reinforced epoxy resin.
Wang et al. (2014)	Epoxy resin Bisphenol-A GMBs $d_{\mu m}$: 55 ρ : 250 Φ_w : 15 Glass fiber Φ_w : 0, 0.5 and 1.5	Flexural properties	• Higher values of flexural strength and modulus is noted for glass fiber reinforced SFs compared to plain SFs. • Reinforcing SFs with two layers of fiberglass mesh increases the flexural strength and modulus by 2.5 and 2 times. • The flexural properties of SFs are highly influenced by the position and layers of fiberglass mesh.
Zhang et al. (2016)	Epoxy resin Epolam 5015 ρ : 1100 GMBs $d_{\mu m}$: 65 ρ : 125 R : 0, 5, 10, 15, 20	Mechanical properties	• Tensile strength is influenced by strain rate and an increase in strain rate increases the tensile strength of foams. • Increasing filler content decreases tensile strength at constant strain rate. • Increasing filler content decreases compressive strength, while the compressive modulus increases with increasing strain rate.

Table 1.2 Literature review on drilling of polymer matrix composite materials.

Author	Material & tool	Drilling parameters	Investigation	Remarks
Lin and Chen (1996)	CFRP composite Carbide drills	Cutting speed, feed rate and drilled length Multifacet and twist drill	Thrust force, torque, tool wear and hole quality FFD	• Increasing cutting speed accelerates tool wear which in turn increases the thrust force. • Effect of cutting speed on tool wear is significant than the effect of drilled length. • Torque slightly increases with increasing cutting speed. • Twist drill exhibits superior performance compared to multifacet drill.
El-Sonbaty et al. (2004)	GFRP composite HSS twist drills	Cutting speed, feed, drill diameter and fiber volume fraction	Thrust force, torque and surface roughness	• Cutting speed has insignificant effect on the thrust force and surface roughness of neat epoxy. • Thrust force and torque increases with increasing feed, drill size, fiber volume fraction and decreasing cutting speed. • Drill diameter combined with feed has a significant effect on surface roughness.
Khashaba (2004)	GFRP composite HSS drills	Cutting speed, feed, matrix type, filler and fiber shape	Thrust force, torque, delamination	• Cutting forces and delamination increases with increasing cutting speed for sand filler reinforced continuous-winding composite.

Author	Material & tool	Drilling parameters	Investigation	Remarks
				• Cutting forces and delamination decreases with increasing cutting speed in cross-winding, woven and chopped fiber composites. • Thrust force is three times higher in drilling of continuous-winding than cross-winding.
Tsao and Hocheng (2004)	CFRP composite HSS drills	Feed rate, spindle speed, drill diameter and type of drill	Delamination Taguchi's method, ANOVA	• Feed rate and drill diameter are significant process parameters on delamination. • Candlestick drill and saw drill exhibits superior performance than a twist drill.
Mohan et al. (2005)	GFRP composite Coated carbide drills	Speed, feed rate, drill size and specimen thickness	Thrust and torque Taguchi's method, ANOVA	• Speed and drill size are the most significant parameters influencing thrust force. • Torque is highly influenced by specimen thickness and drill size.
Mohan et al. (2007)	GFRP composite Coated carbide twist drills	Speed, feed rate, drill size and specimen thickness.	Delamination Taguchi's method, RSM	• Delamination is highly influenced by specimen thickness, feed rate and cutting speed. • Minimum delamination, better surface finish and tool life is achieved by employing high cutting speed and low feed.

Author	Material & tool	Drilling parameters	Investigation	Remarks
Velayudham and Krishnamurthy (2007)	GFRP composite Cemented carbide drills	Cutting speed, feed rate and drill geometry	Thrust, torque and delamination	• Thrust and delamination are significantly influenced by drill point angle. • Minimum delamination is achieved by using tripod geometry solid carbide drill.
Campos Rubio et al. (2008)	GFRP composite Cemented carbide drills	Spindle speed, feed and type of drill	Delamination factor	• Delamination factor increases with increasing feed and decreasing spindle speed. • At higher spindle speed delamination is less sensitive to the variation of feed. • Twist drill with 85° point angle provides lower delamination factor as compared to 115° point angle at low and intermediate spindle speeds. • Brad and Spur drill produces lesser delamination compared to twist drills at high spindle speed.
Campos Rubio et al. (2008)	CFRP composite Cemented carbide drills	Spindle speed, feed speed and type of drill	Delamination factor	• Drill with 85° point angle produces lower delamination values. • Brad and Spur drill produces lesser delamination with increased material removal rate. • Larger material removal rates with minimum

Author	Material & tool	Drilling parameters	Investigation	Remarks
				delamination can be achieved by employing high spindle speeds.
Faria et al. (2008)	GFRP composite Twist drills	Cutting speed, feed rate and type of drill	Thrust force and tool wear	• Cemented carbide drill presented superior wear resistance compared to HSS drill. • Titanium nitride coating on carbide drill doesn't have any significant effect on tool wear and thrust force. • Thrust force increases with increasing feed rate due to the increase in the shear area. • Cutting speed has insignificant effect on thrust force generated during drilling using a cemented carbide drill.
Gaitonde et al. (2008)	CFRP composite Cemented carbide twist drills	Cutting speed, feed rate and point angle	Delamination FFD, RSM, ANOVA	• Delamination decrease with an increase in cutting speed. • Delamination can be minimized by using lower values of feed rate and point angle.
Karnik et al. (2008)	CFRP composite Cemented	Spindle speed, feed rate and point angle	Delamination FFD, ANN	• Delamination factor reduces with increased spindle speed.

Author	Material & tool	Drilling parameters	Investigation	Remarks
	carbide twist drills			• Delamination can be reduced by employing a low point angle and feed rates. • ANN model developed shows a good correlation for both the training and testing data sets, thus validating the model.
Palanikumar et al. (2008)	GFRP composite Cemented carbide twist drills	Spindle speed, feed rate and point angle	Delamination factor RSM, ANOVA	• Delamination decreases with the increase in the spindle speed. • At low spindle speed delamination increases with increasing feed rate. • Combination of higher speed, low feed, and point angle is necessary to minimize the delamination factor.
Tsao and Hocheng (2008)	CFRP composite Candlestick drill	Feed rate, spindle speed and drill diameter	Thrust force and surface roughness Taguchi method and ANN	• Thrust force is significantly affected by feed rate and drill diameter. Surface roughness is highly influenced by feed rate and spindle speed. • ANN analysis is found be more effective than multi-variable regression analysis in investigating the delamination of drilled hole.

Author	Material & tool	Drilling parameters	Investigation	Remarks
Khashaba et al. (2010)	GFRP composite Cemented carbide twist drills	Cutting speed, feed and drill diameter	Thrust force, delamination, surface roughness and bearing strength.	• Load carrying capacity of composite structure improves with the decreasing thrust force. • Delamination increases with increasing feed and drill diameter due to the increased thrust force. • Surface roughness increases with increasing the cutting feed, while no clear effect of the cutting speed is observed.
Kilickap (2010)	GFRP composite HSS twist drill	Cutting speed, feed rate and point angle	Entry and exit delamination Taguchi method and ANOVA	• Feed rate is the most influential factor on the delamination followed by cutting speed. • Minimum delamination is obtained at lower cutting speed and feed rate. • Increasing the point angle (118-135°) increases the delamination.
Basavarajappa et al. (2011)	GFRP composite reinforced with silicon carbide Solid carbide drill	Spindle speed and feed	Thrust force, surface roughness and specific cutting coefficient FFD, RSM, ANOVA	• Thrust force increases with increasing feed, while it is found to be less sensitive to increasing spindle speed. • Surface roughness decreases with the increasing speed and decreasing feed.

Author	Material & tool	Drilling parameters	Investigation	Remarks
				• Specific cutting coefficient is minimal at a combination of low speed and medium feed. • Composites reinforced with silicon carbide provide better machinability.
Gaitonde et al. (2011)	CFRP composite Cemented carbide twist drills	Cutting speed, feed rate and point angle	Delamination Taguchi's method and ANOVA	• Optimization results indicate that point angle is the most significant factor on delamination followed by feed and spindle speed. • Delamination can be minimized by using higher cutting speeds.
Palanikumar (2011)	GFRP composite Brad and Spur drill	Spindle speed and feed rate	Thrust force, surface roughness and delamination factor Taguchi method and GRA	• Increasing spindle speed up to certain value decreases thrust force with further increase in the spindle speed slightly increases thrust force. • Increasing feed rates leads to increased thrust force. • Surface roughness decreases with increasing speed and decreasing feed. • Grey relational analysis indicates that feed rate is the most influential parameter than spindle speed.

Author	Material & tool	Drilling parameters	Investigation	Remarks
				• According to GRA machining at high spindle speed and lower feed rate provides a good quality hole.
Khashaba et al. (2012)	GFRP composite Cemented carbide twist drills	Feed, speed and drill pre-wear	Thrust force, torque, delamination, surface roughness, and bearing strength. RSM, ANN	• Increasing speed and feed increases thrust force which in turn increases the delamination of the drilled hole. • At high feeds, irrespective of thrust force constant push-out delamination is observed in drilling of GFRP composites. • ANN models are found to be more significant than the regression model in prediction. • Ultimate bearing strength of composite reduces when drilling at high feeds due to a reduction in the stiffness of the material.
Krishnaraj et al. (2012)	CFRP composite Carbide twist drills	Spindle speed and feed rate	Hole diameter, circularity and delamination ANOVA, GA	• Feed rate has a significant influence on thrust force, push-out delamination and diameter of the hole. Thrust force and push-out delamination can be minimized by using lower values of feed rates.

Author	Material & tool	Drilling parameters	Investigation	Remarks
				• Circularity of the drilled hole largely depends on the spindle speed. • According to GA the optimized spindle speed and feed rate for drilling CFRP laminates were found to be 12,000 rpm and 0.137 mm/rev respectively.
Palanikumar et al. (2012)	GFRP composite Brad and Spur drills	Spindle speed, feed rate and drill diameter	Thrust force and surface roughness Taguchi's method, GRA	• Thrust force and surface roughness are significantly affected by feed rate followed by drill diameter. • Spindle speed is not having any significant effect on the thrust force and surface roughness in drilling of GFRP composites.
Rajamurugan et al. (2013)	GFRP composite Brad and Spur cemented carbide drills	Fiber orientation angle, feed rate, speed and tool diameter	Delamination RSM, ANOVA	• Increase in feed rate and drill diameter increases the delamination, whereas fiber orientation angle is not having any significant effect. • The spindle speed shows only little effect on delamination in drilling of GFRP composites. • Feed rate and drill diameter are the most significant parameter influencing delamination.

Author	Material & tool	Drilling parameters	Investigation	Remarks
Raju et al. (2013)	GFRP composite reinforced with silica and alumina	Cutting speed feed, HSS and cemented carbide	Thrust force and torque	• Increasing feed and cutting speed increases the thrust force and torque. • Carbide drill performs better than HSS drill during drilling of reinforced composites. • Better machinability is achieved in alumina reinforced composite compared to unfilled and silica reinforced composites using carbide drills.
Reddy et al. (2013)	GFRP composite	Point angle, drill diameter, material thickness, feed rate, and speed	Thrust force and delamination FFD	• Carbide drill exhibits better performance as under all drilling conditions. • Thrust force is highly influenced by work material thickness
Wang et al. (2013)	CFRP composite Twist drills	Uncoated, diamond coated and coated carbide drills	Tool wear	• Cutting edge rounding wear is significantly reduced in diamond-coated tools. • No significant correlation is found between the abrasive wear resistance of the coatings and the drilling experiment wear measurements.
Eneyew and Ramulu (2014)	CFRP composite Polycrystalline	Cutting speed and feed	Thrust force, surface roughness and	• Feed significantly affects the thrust force than the cutting speed.

Author	Material & tool	Drilling parameters	Investigation	Remarks
	diamond tipped eight facet drill		damage	• Better quality holes are obtained at a combination of higher cutting speed and lower feed rate.
Vankanti and Ganta (2014)	GFRP composite	Cutting speed, feed, point angle and chisel edge width	Thrust force, torque, surface roughness and circularity. Taguchi's method, ANOVA	• Thrust force is significantly affected by feed rate followed by cutting speed, chisel edge width and point angle. • Torque is highly influenced by cutting speed, whereas circularity of the drilled hole is significantly affected by feed followed by chisel edge width and point angle.
Merino-Perez et al. (2016)	CFRP composite Uncoated WC-Co drill	Cutting speed and workpiece constituents	Thrust force and torque	• Type of matrix showed significant impact on thrust force and torque. • The type of carbon fiber fabric and cutting speed showed negligible effects on the thrust force. • All the factors considered showed a significant impact on the maximum torque developed.
Ramesh et al. (2016)	GFRP composite Cemented carbide twist	Spindle speed, feed and coolant pressure	Drill flank temperature and damage factor	• Drill temperature increases with increasing spindle speed and feed. • Damage factor increases with increasing feed, but

Author	Material & tool	Drilling parameters	Investigation	Remarks
	drills		CCF, RSM, ANOVA	it remains constant with increasing spindle speed. • Damage factor is highly influenced by feed. • Optimum conditions are found to be different for different cooling methods.
Ravichandran et al. (2016)	GFRP composite reinforced with aluminium oxide and graphite HSS and carbide drills	Cutting speed and feed rate	Thrust, torque, delamination, specific cutting pressure and surface roughness.	• HSS drills produced better quality holes in neat composites, whereas carbide drills produce better quality holes in particulate filled composites. • Variation of thrust force with increasing speed using carbide drill is found to be very small and neglected due to the superior wear resistance of carbide drills. • Surface roughness of drilled holes increases with increasing speed, feed and addition of reinforcements.
Gaugel et al. (2016)	CFRP composite carbide	Uncoated and diamond-coated tungsten carbide drills	Tool wear and delamination	• Uncoated tools exhibit abrasion wear during CFRP drilling leading to progressive rounding, whereas a diamond-coated tool shows negligible tool wear.

Author	Material & tool	Drilling parameters	Investigation	Remarks
				• Cutting edge rounding measurement is found to be an effective method to characterize the tool wear of uncoated tool. • The porosity of the workpiece is not having any effect on the tool wear in CFRP drilling. • Tool life of diamond coated dills is found to be eight times more than the uncoated drills.
Akhil et al. (2017)	GFRP composite HSS	Cutting speed, feed rate and drill diameter	Delamination and surface roughness. Taguchi's method, ANOVA, GRA	• Delamination and surface roughness is highly influenced by the cutting speed. • Machining at higher cutting speed and lower feed rate with smaller drill diameter produce a good quality hole.
Ameur et al. (2017)	CFRP composite	Spindle speeds, feed rate and tool material	Thrust force, torque, exit delamination and cylindricity FFD, RSM, ANOVA	• Thrust force and delamination factor is highly influenced by the tool materials and feed rate. • Cylindricity of drilled holes is highly influenced by spindle speed and can be minimized using lower spindle speed and higher feed rate. • Combination of high spindle speed and low feed

Author	Material & tool	Drilling parameters	Investigation	Remarks
				rate leads to lower torque values. • Coated carbide drills present superior performance compared to HSS drill.
Feito et al. (2018)	CFRP composite Coated tungsten carbide drills	Cutting speed feed rate and drill geometry	Thrust force, torque and delamination	• Using step drill reduces the thrust force and torque, but delamination is found to be reduced only at low feed rates. • It is found that increasing cutting speed and feed rate increases thrust force and damage factor. It is also found that providing backplate reduces damage on the drilled hole.

From the preceding literature survey, it is very much clear that the research reports on drilling of lightweight materials as potential structural members having superior machinability characteristics are not available. Further, the relationship among the influencing parameters and their effects on machinability are unknown during the drilling process of syntactic foams. Hence, the present work deals with the machinability characteristics in drilling of GMB/Epoxy syntactic foam composites.

1.7 Motivation of work

Syntactic foams are used in wide variety of weight sensitive applications, primarily in marine and aerospace sectors. The complex assembly of structural parts is carried out using fasteners and riveted bolts, which requires a large number of holes to be drilled. The drilling action results in damage of the composite material around the hole, which reduces part quality and does not facilitate easy assembly of structural components. Poor hole quality leads to the formation of cracks in the structural component, which can reduce their service life and add extra costs for maintenance. Drilling damages can be minimized by optimizing the operating, drill and work material parameters.

Many researchers have put their efforts into evaluating the effect of process parameters on the machinability of polymer matrix composites, but no systematic study has been reported on the drilling of GMB/Epoxy syntactic foam. The present study attempts to fill the gap by reporting the experimental investigations in drilling of GMB/Epoxy syntactic foam composites using coated tungsten carbide twist drill to evaluate machinability characteristics.

1.8 Objectives and scope of the work

From the preceding literature survey, it is clear that hollow glass microballoons are found to be the promising entrant for developing lightweight composite material, and no study has been reported on the drilling of GMB/Epoxy syntactic foams. Hence, the present study deals with the experimental investigations in drilling of glass microballoon reinforced epoxy composites using coated tungsten carbide twist drills. The influence of operating (cutting speed and feed), drill (drill diameter) and work material parameters (filler wall thickness and volume fraction) on various machinability characteristics like thrust force, specific cutting coefficient, surface roughness, circularity error, cylindricity and damage factor are studied in drilling of GMB/Epoxy syntactic foam.

The work undertaken pursues the following objectives:

1 Preparing the hollow glass microballoons reinforced epoxy composites by varying volume fraction and wall thickness of fillers.
2 Identifying the important process parameters and their levels which significantly influence the machinability characteristics of the developed composites.
3 Performing the drilling experiments as per the selected design of experiments (DoE) and development of response surface methodology (RSM) based mathematical models for evaluating machinability characteristics.
4 Analyze the interaction effects of process parameters using the developed mathematical models and optimization of the drilling process parameters to achieve sound quality hole.

Scope of the present work includes synthesizing epoxy syntactic foam composites by varying GMB content by 20, 40 and 60 vol.% using three different types of GMB. SFs are fabricated by conventional casting method, i.e., by mechanically mixing the GMBs in epoxy resin. Scanning electron microscopy is conducted on as cast samples to confirm the uniform dispersion of GMBs in epoxy resin. Densities of all the syntactic foams are reported based on ASTM C271-16 standard. Cast samples are drilled using computer numerical control vertical machining center to investigate the influences of process parameters on machinability characteristics. Response surface methodology based mathematical models are developed to analyze the interaction effect of process parameter. Analysis of variance is performed to identify the percentage contribution of process parameters followed by grey relation analysis for optimizing the process parameters.

1.9 Outline of the thesis

The systematic study conducted with respect to above objectives is presented in the thesis. A brief skeletal structure of the thesis is detailed as below.

- Chapter 1 provides an introduction to composite materials, drilling process, modeling and multi-objective optimization technique. This chapter also presents the exhaustive literature survey on drilling of polymer composites followed by the research objectives.

- Chapter 2 focuses on the constituents used for the development of thermoset syntactic foam composites; processing route adopted and testing methodology.
- Chapter 3 illustrates the effect of various process parameters on machinability characteristics in drilling of GMB/Epoxy syntactic foams. Statistical analysis is performed based on response surface methodology and analysis of variance. Further grey relation analysis is performed for identifying optimum cutting conditions.
- Chapter 4 illustrates the significant conclusions drawn from the results of drilling GMB/Epoxy syntactic foam composites.

2 MATERIALS AND METHODS

2.1 Constituents

In the present work, lightweight thermoset syntactic foams are fabricated by dispersing borosilicate hollow glass microballoons in Lapox L-12 epoxy resin. Particulars about these constituents are explained in the following sections.

2.1.1 Glass microballoon

Three different types (SID-200Z, SID-270Z and SID-350Z) of hollow borosilicate glass microballoons (GMBs) procured from Trelleborg Offshore, USA are used as fillers (Figure 2.1a) for syntactic foam fabrication. GMBs are used in as received conditions without any surface treatment. The average particle size of GMBs is noted to be 53, 50 and 45 μm respectively for SID-200Z, SID-270Z and SID-350Z. Even though the average particle size of all the GMBs is almost same, the difference in density is due to variation in their wall thickness. Compared to particle size, the wall thickness of GMBs are relatively thin. Table 2.1 presents the basic properties of three different types of GMBs used in the present work. Wall thickness of the GMBs is related to the radius ratio (η) which is defined as the ratio of inner radius (r_i) to the outer radius (r_o) of hollow particle and is given by (Pinisetty et al. 2015),

$$\eta = \frac{r_i}{r_o} \tag{2.1}$$

Radius ratio of GMBs can also be estimated by knowing the true particle density of GMBs (ρ_{MB}) and density of glass (ρ_g) using (Pinisetty et al. 2015),

$$\eta = \left(1 - \frac{\rho_{MB}}{\rho_g}\right)^{1/3} \tag{2.2}$$

The pycnometer is used to experimentally measure the densities of GMBs and glass (2540 kg/m^3).

Wall thickness of the hollow particle is computed using (Pinisetty et al. 2015),

$$w = r_o(1-\eta) \tag{2.3}$$

Table 2.1 Properties of hollow glass microballoons.

Type	Average particle size* (μm)	True particle density* (kg/m^3)	Radius ratio#	Wall thickness# (μm)
SID-200Z	53	200	0.973	0.716
SID-270Z	50	270	0.973	0.925
SID-350Z	45	350	0.952	1.080

*As specified by the supplier
#Computed value

2.1.2 Matrix

Epoxy resin (Lapox L-12) with polyamine hardener (K-6) procured from Atul Ltd., Valsad, Gujarat, India, is the matrix system used for syntactic foam fabrication (Figure 2.1b).

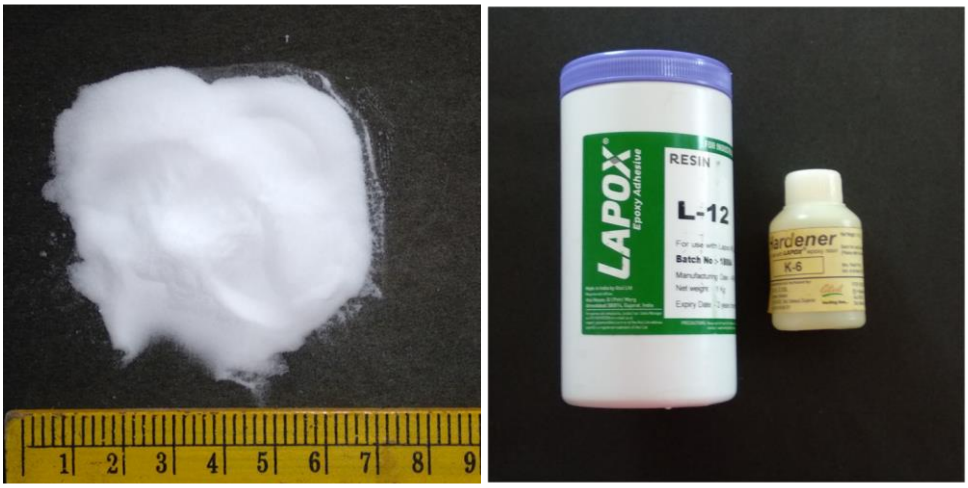

(a) (b)

Figure 2.1 (a) GMBs and (b) Matrix system used for syntactic foam fabrication.

Lapox L-12 is a medium viscosity unmodified epoxy resin compatible with most of the hardeners. Lapox L-12 exhibits a shell-life of two years if stored properly away from excessive heat and humid environment. K-6 is a low viscosity light yellow colored polyamine hardener widely used to cure epoxy resin at room temperature. Polyamine hardener provides shorter pot life and rapid curing when used along with epoxy resins. It should be stored in a cool and dry place using a sealed container and should not be exposed to direct sunlight. If stored in a sealed container (18-25°C) away from excessive heat and humid environment, K-6 hardener exhibits a shell-life of one year. Table 2.2 presents the properties of epoxy resin and hardener.

Table 2.2 Properties of LAPOX L-12[#] and K-6[#].

Properties	Test method	Values	
		LAPOX L-12	K-6
Appearance	Visual	Clear, viscous liquid	Clear liquid
Color (GS)	ASTM D1544	Max 1	Max 1
Viscosity @ 25°C (m Pas)	ASTM D2196	9,000-12,000	-----
Epoxy content (Eq/kg)	ASTM D1652	5.26-5.55	-----
Specific gravity @ 25°C	ASTM D792	1.1-1.2	-----
Refractive index	-----	-----	1.494-1.50
Pot life @ 25°C (min)	ASTM D2471	-----	30-40
Recommended ratio (w/w)	-----	-----	10

[#]As specified by the manufacturer

2.2 Sample preparation

Syntactic foams are fabricated by dispersing 20, 40 and 60 vol.% of GMBs in Lapox L-12 resin to cover a wide range of material compositions. GMBs of desired volume fraction are added into the epoxy matrix at room temperature and stirred slowly for 15 minutes until a homogeneous slurry is formed. Hardener by 10 wt.% is added to the slurry and stirred for additional 5 min and degassed for 10 min prior pouring into the molds of dimensions 35 mm diameter and 16 mm height coated with silicone releasing agent (Figure 2.2a). The specimens are cured at room temperature for 24 h and then post-cured for 2 h at 90°C. Finally cast specimens are trimmed using disc polishing machine to the required dimensions (Figure 2.2b).

Nine different types of syntactic foams specimens with 20, 40 and 60 vol.% of GMBs are fabricated using three different density grades of GMBs. Neat epoxy specimens are also fabricated under similar processing conditions for comparison. Specimen coding begins with “E” to indicate epoxy resin and is followed by YYY-*R*, which signifies the true particle density and volume fraction of GMBs. For example, “E350-60” syntactic foam indicates 350 kg/m^3 density 60 vol.% GMBs are dispersed in epoxy resin.

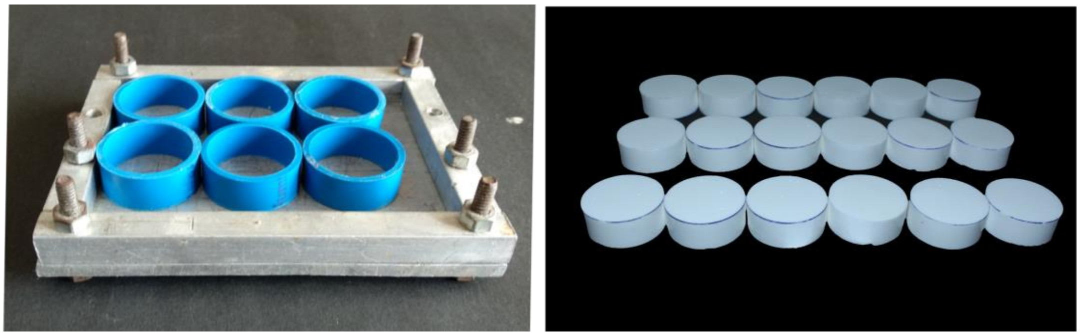

(a) (b)

Figure 2.2 (a) Molds used for sample preparation and (b) Syntactic foam specimens.

2.3 Density measurement

Densities of all the specimens are measured according to ASTM C271-16 . The density of neat epoxy is measured to be 1192 kg/m^3, which is used in the rule of mixtures to estimate theoretical density (ρ_t) of syntactic foams (Nikhil and Ruslan 2006). Theoretical density of syntactic foams is estimated using (Manakari et al. 2015, Pinisetty et al. 2015),

$$\rho_t = \rho_m V_m + \rho_{MB} R \tag{2.4}$$

Ignoring the fraction of crushed GMBs during syntactic foam synthesis, the entrapped matrix porosity (Φ_v) is estimated by (Nikhil and Ruslan 2006),

$$\Phi_v = \frac{\rho_t - \rho_e}{\rho_t} \times 100 \tag{2.5}$$

The volume fraction of GMB porosity in syntactic foams is calculated by,

$$\Phi_{\mu P} = R \times \eta^3 \tag{2.6}$$

The total porosity of syntactic foams (Φ_t) is a summation of matrix and GMB porosities and is given by,

$$\Phi_t = \Phi_v + \Phi_{\mu P} \tag{2.7}$$

Weight saving potential of the developed syntactic foams as compared to neat epoxy is computed using (Shahapurkar et al. 2018),

$$Weight\ saving\ potential = \frac{\rho_{e-E} - \rho_{e-SF}}{\rho_{e-E}} \times 100 \tag{2.8}$$

2.4 Drilling experiments

2.4.1 Cutting tools

Coated solid tungsten carbide twist drills are the most commonly and widely used tools for producing cylindrical holes. From the literature it is found that coating on the drill bit significantly improves tool life. Hence in the present work, experiments are conducted using coated solid tungsten carbide twist drills procured from Sri Vinayaka Cutting Tools, Bengaluru, Karnataka (Figure 2.3). Table 2.3 presents the specification of the cutting tools used in the present study.

8 mm 12 mm 16 mm

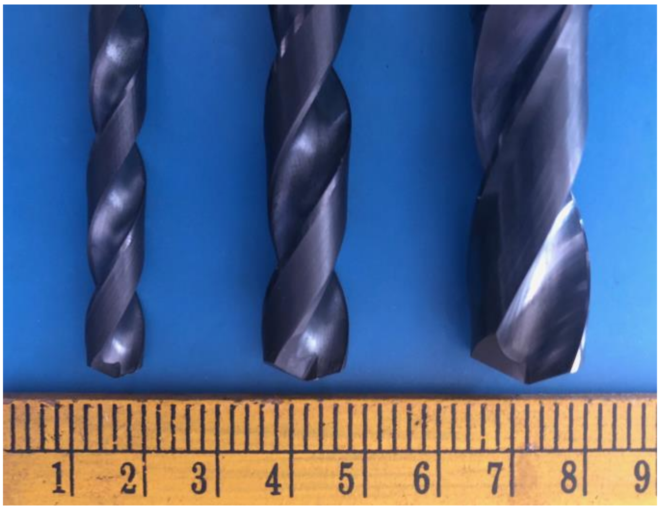

Figure 2.3 Twist drills used in the present work.

Table 2.3 Drill bit specifications.

Specification	Tool geometry
Number of flutes	2
Flute length	50 mm
Overall length	100 mm
Helix angle	30°
Point angle	135°
Diameter	8, 12 and 16 mm
Tool material	Tungsten carbide
Coating	TiAlN

2.4.2 Process parameters

Exhaustive literature survey is conducted to identify the process parameters and their levels which significantly affect the quality of the drilled hole. From the literature it is found that cutting speed (v), feed (f) and drill diameter (D) are the significant process parameters that influence the quality of the hole in drilling polymer composites (Palanikumar 2011) and hence considered in the present work along with filler content (R) for initial investigation. Levels of the chosen input parameters are selected based on earlier studies (El-Sonbaty et al. 2004, Gaitonde et al. 2008, Gupta et al. 2013, Palanikumar 2011). From the literature survey, it is observed that the cutting speed in the range of 20-200 m/min and feed in the range of 0.03-0.5 mm/rev is typically employed in drilling of polymer composites (Abrao et al. 2007, Gaitonde et al. 2009). Also, using high cutting speed results in high cutting temperature which may reduce the life of the drill. GMB content (20-60 vol.%) is chosen to cover a wide range of material compositions. Drill diameters are selected to suit the application requirements of syntactic foams. Based on this criterion, the process parameters and their levels presented in Table 2.4 are considered for conducting the drilling experiments.

Table 2.4 Process parameter and their levels for neat epoxy[#] and syntactic foams[#,*].

Parameters	Level		
	1	2	3
[#]v	25	75	125
[#]f	0.04	0.08	0.12
[#]D	8	12	16
[*]R	20	40	60

2.4.3 Design of experiments

Development of mathematical models based on RSM necessitates careful planning of experiments. Hence, in the present investigation experiments are planned based on full factorial design to analyze the effect of input parameters on the responses. Table 2.5 presents the layout plan for experimentation based on full factorial design.

Table 2.5 Experimental layout plan.

Exp. No.	Cutting conditions R_{20}			Exp. No.	Cutting conditions R_{40}			Exp. No.	Cutting conditions R_{60}		
1			D_8	28			D_8	55			D_8
2		$f_{0.04}$	D_{12}	29		$f_{0.04}$	D_{12}	56		$f_{0.04}$	D_{12}
3			D_{16}	30			D_{16}	57			D_{16}
4			D_8	31			D_8	58			D_8
5	v_{25}	$f_{0.08}$	D_{12}	32	v_{25}	$f_{0.08}$	D_{12}	59	v_{25}	$f_{0.08}$	D_{12}
6			D_{16}	33			D_{16}	60			D_{16}
7			D_8	34			D_8	61			D_8
8		$f_{0.12}$	D_{12}	35		$f_{0.12}$	D_{12}	62		$f_{0.12}$	D_{12}
9			D_{16}	36			D_{16}	63			D_{16}
10			D_8	37			D_8	64			D_8
11		$f_{0.04}$	D_{12}	38		$f_{0.04}$	D_{12}	65		$f_{0.04}$	D_{12}
12			D_{16}	39			D_{16}	66			D_{16}
13			D_8	40			D_8	67			D_8
14	v_{75}	$f_{0.08}$	D_{12}	41	v_{75}	$f_{0.08}$	D_{12}	68	v_{75}	$f_{0.08}$	D_{12}
15			D_{16}	42			D_{16}	69			D_{16}
16			D_8	43			D_8	70			D_8
17		$f_{0.12}$	D_{12}	44		$f_{0.12}$	D_{12}	71		$f_{0.12}$	D_{12}
18			D_{16}	45			D_{16}	72			D_{16}
19			D_8	46			D_8	73			D_8
20		$f_{0.04}$	D_{12}	47		$f_{0.04}$	D_{12}	74		$f_{0.04}$	D_{12}
21			D_{16}	48			D_{16}	75			D_{16}
22			D_8	49			D_8	76			D_8
23	v_{125}	$f_{0.08}$	D_{12}	50	v_{125}	$f_{0.08}$	D_{12}	77	v_{125}	$f_{0.08}$	D_{12}
24			D_{16}	51			D_{16}	78			D_{16}
25			D_8	52			D_8	79			D_8
26		$f_{0.12}$	D_{12}	53		$f_{0.12}$	D_{12}	80		$f_{0.12}$	D_{12}
27			D_{16}	54			D_{16}	81			D_{16}

Cutting speed, feed, drill diameter and filler content are taken as input parameters, while thrust force (F_t), surface roughness (R_a), specific cutting coefficient (K_f), cylindricity (CYL), exit side circularity error ($C_{e\text{-}Exit}$) and exit side damage factor ($F_{d\text{-}Exit}$) are taken as the responses. The parameters and their levels are selected based on the earlier investigations. Three levels are selected for each of the process parameters to consider the non-linearity. A total of 81 experiments are planned based on a full factorial design with three replicates for each test condition (Table 2.5).

The experimental values obtained are used for proposing regression model based on RSM, which has been effectively used previously in the modeling of drilling behavior (Basavarajappa et al. 2011, Gaitonde et al. 2008, Rajamurugan et al. 2013). Individual effect plots are plotted by varying one parameter at a time within the chosen range, keeping the other parameters at intermediate level in the developed mathematical models to predict the general trends and significant parameter. Interaction effects among the input process parameters are studied by varying two parameters at a same time in the developed mathematical models while keeping the other two parameters at their intermediate levels as per the scheme presented in Table 2.6.

Table 2.6 Two-way interaction parameters used in the study for syntactic foams.

Interaction		Response
Parameter 1	Parameter 2	
v	D, f and R	F_t, R_a, K_f, CYL, $C_{e\text{-}Exit}$ and $F_{d\text{-}Exit}$
f	D and R	
R	D	

2.4.4 Experimental setup

Drilling experiments are conducted as per full factorial design with coated solid tungsten carbide twist drills fitted on a vertical CNC machine (Figure 2.4) with specifications listed in Table 2.7, along with the specifications of dynamometer used to measure the thrust force. Surface roughness of the drilled hole is measured using Mitutoyo surftest (SJ 301, Japan) as shown in Figure 2.5. Specific cutting coefficient (K_f) is defined as the ratio of total energy input rate to material removal rate and is seen as an important material characteristic. It gives a good indication of the machining effort and is given by (Basavarajappa et al. 2011),

$$K_f = \frac{2 \times F_t}{f \times D} \tag{2.9}$$

Table 2.7 Machine tool specification used in drilling study.

Machining center		Drilling tool dynamometer	
Make	MTAB Engineers Pvt. Ltd., India	Make	Syscon Instruments Pvt. Ltd., India
Model	MAX MILL PLUS+	Product	Drill Tool Sensors
Voltage	415 V ± 2%, 3 Phase	Type	Strain gauge
Axis Travel (X×Y × Z)	480×360×500 mm	Voltage	230 V AC, 50 Hz, 1 Phase
Table Size (L×W)	600×350 mm	Maximum thrust	500 kg
Max. Table Load	250 kg	Maximum torque	10 kg-m
Control system	Fanuc Oi Mate MD	Safe overload	125% of rated capacity
Max. spindle speed	9000 rpm	Maximum overload	150% of rated capacity
Spindle motor power	7.5 kW	Fatigue rating	10 E6 full cycles
Axis accuracy	0.01 mm	Excitation maximum	10 VDC
Axis repeatability	± 0.005 mm	Sensitivity	1 mV/V (Nominal)
Rapid feed	30 m/min	Temperature range	10 to 50 °C
Programmable feed rate	0 - 6000 mm/min		

Coordinate measuring machine (Evolution 20.12.10, METRIS, UK) as shown in Figure 2.6 is used to measure the cylindricity, circularity error and maximum diameter of the damaged zone ($D_{\max}$) of drilled holes. Since syntactic foam is a particulate composite (non-laminate) damage factor is considered instead of delamination factor (Ramesh et al. 2016). Drilling-induced damage on the exit side is more severe than on the entry side (Xu et al. 2013). Also, the damage observed on the entry side in the present work is found to be very small compared to damage on the exit side, and hence it is not considered during the investigation. Damage factor at the hole exit is estimated using most commonly used approach and is given by (Ramesh et al. 2016)

$$F_d = \frac{D_{\max}}{D} \tag{2.10}$$

Input parameters (I) and their levels (L) are coded together as I_L. For example, D_{12} represents 12 mm drill diameter.

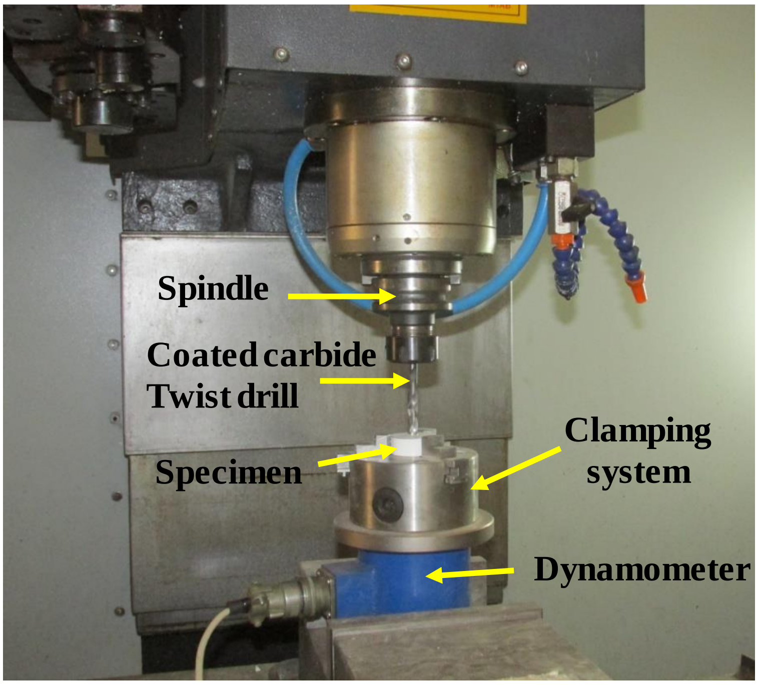

Figure 2.4 Experimental setup.

Figure 2.5 Surface roughness tester (Surftest SJ-301).

Figure 2.6 Coordinate measuring machine (CMM).

2.4.5 Imaging

Microstructural examinations are carried out using a scanning electron microscope (JSM 6380LA, JEOL, Japan). JFC-1600 auto fine coater (JEOL, Japan) is used to sputter coat the samples with gold. Confocal microscope (LEXT, OLS4000, OLYMPUS, Japan) is used for inspecting the drilling tool.

2.4.6 Grey relation analysis

GRA provides an efficient solution to uncertainty, multi-input and discrete data problems. It involves the measurement of absolute value of data differences between the sequences. Steps involved in optimizing the process parameters are as follows:

Step 1: Data normalization/pre-processing

The experimental data of the responses to be used in GRA must be pre-processed to be in the range of 0 to 1 for comparison. Smaller-the-better characteristic of grey relation is used for data normalization since the objective is to minimize the responses. The equation used to normalize the data is given by (Sheth and George 2016)

$$X_i^*(k) = \frac{\max X_i^o(k) - X_i^o(k)}{\max X_i^o(k) - \min X_i^o(k)} \tag{2.11}$$

here $i = 1 \ldots m$; $k = 1 \ldots n$.

Step 2: Grey relation co-efficient and grades

Grey relation coefficient is calculated using (Sheth and George 2016),

$$\xi_i(k) = \frac{\Delta_{\min} + \zeta\Delta_{\max}}{\Delta_{oi}(k) + \zeta\Delta_{\max}} \tag{2.12}$$

$$\Delta_{oi}(k) = \left\| X_o^*(k) - X_i^*(k) \right\| \tag{2.13}$$

$$\Delta_{\max}(k) = \max\max \left\| X_o^*(k) - X_i^*(k) \right\| \tag{2.14}$$

$$\Delta_{\min}(k) = \min\min \left\| X_o^*(k) - X_i^*(k) \right\| \tag{2.15}$$

ζ is the identification coefficient and ζ = 0.5 is generally used for analysis (Palanikumar 2011). Finally, grey relation grade is calculated by taking the averages of the grey relation coefficient. The grey relation grade is calculated using

$$\gamma_i = \frac{1}{n}\sum_{k=1}^{n} \xi_i(k) \tag{2.16}$$

According to grey relational analysis, highest grey relational grade value corresponds to better machining performance. Therefore, the optimized condition is obtained at a specific combination of process parameters with the highest grey relational grade value. By performing machining at the optimized condition, responses can be effectively minimized to achieve sound hole quality.

3 RESULT AND DISCUSSION

3.1 Syntactic foam microstructure and density

Uniform dispersion of hollow glass microballoons in the epoxy matrix with minimum particle failure and cluster formation is quite challenging. In the present work GMB/Epoxy syntactic foams are fabricated using mechanical mixing method (Figure 1.2). Extensive micrography is conducted on the as-cast syntactic foam specimens and representative micrographs having the lowest and highest density are presented in Figure 3.1. Microballoons are found to be uniformly distributed throughout the epoxy matrix without forming the clusters. Shear forces induced during mechanical mixing effectively breaks the clusters of particles resulting in proper wetting and uniform distribution. No particle debris embedded in the epoxy resin is observed, affirming the fact that the damage and fracture of GMBs during processing was not significant.

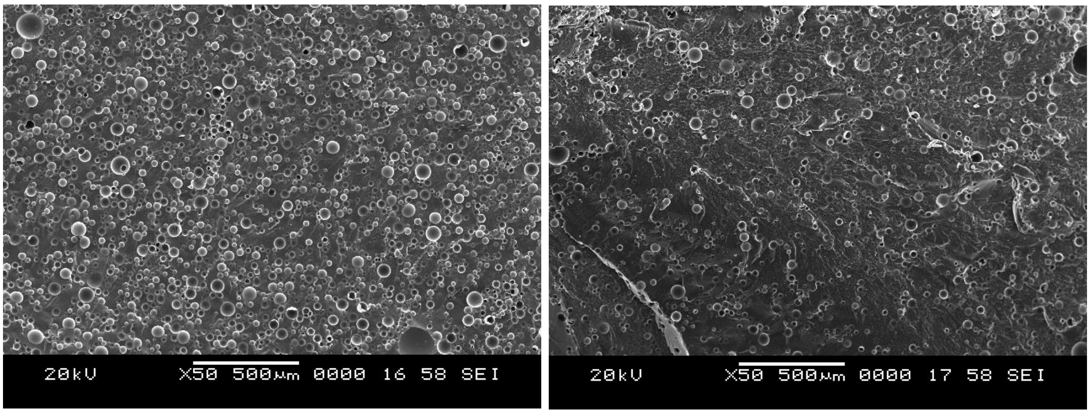

(a) (b)

Figure 3.1 Scanning electron micrographs of (a) E200-60 and (b) E350-20 syntactic foams showing the uniform dispersion of GMBs in the epoxy matrix.

Densities of syntactic foams along with matrix porosity are presented in Table 3.1. During syntactic foam fabrication air is entrapped in the matrix resin leading to matrix porosity. Matrix porosity is calculated using Equation 2.5. Experimental density is found to be lesser than the theoretical density of syntactic foams indicating the presence of hollow microballoons and air entrapment in the matrix resin. Calculations show the matrix porosity to be less than 9 vol.% and is found to be increasing with increasing GMB content and wall thickness (Table 3.1). Increasing GMB content increases the stirring time required for uniform dispersion of particles leading to the increased air entrapment. Also, thick-walled GMBs being stiffer requires more force to disperse them in the matrix leading to increased air entrapment, which subsequently increases matrix porosity. Weight saving potential of the fabricated syntactic foams is calculated using Equation 2.8. Density reduction in the range of 18-53% is noted for the fabricated syntactic foams with respect to neat resin density indicating significant weight saving potential.

Table 3.1 Density and porosity estimations of neat epoxy and their syntactic foams.

Sample type	ρ_t	ρ_e	Φ_v	$\Phi_{\mu P}$	Φ_t	Weight saving potential (%) compared to 'E'
E	1192	1192	0.0	0.0	0.0	-----
E200-20	993.60	971.01±3.65	2.27	18.42	20.70	18.54
E200-40	795.20	768.37±9.68	3.37	36.85	40.22	35.54
E200-60	596.80	566.3±13.12	5.11	55.27	60.38	52.49
E270-20	1007.60	974.32±3.02	3.30	17.86	21.16	18.26
E270-40	823.20	790.2±8.97	4.01	35.72	39.73	33.71
E270-60	638.80	586.22±10.14	8.23	53.58	61.81	50.82
E350-20	1023.60	977.33±2.56	4.52	17.26	21.78	18.01
E350-40	855.20	798.07±8.65	6.68	34.51	41.19	33.05
E350-60	686.80	625.26±12.45	8.96	51.77	60.73	47.55

3.2 Investigation on drilling characteristics of syntactic foams

Cutting speed, feed and drill diameter are significant process parameters that influence quality of the drilled hole and hence are considered in the present work along with filler content. A total of 81 experiments with three replicates for each condition are conducted to evaluate the drilling characteristics of syntactic foams reinforced with three different grades of GMBs using the experimental layout plan presented in Table 2.5. The experimental results are used to develop the mathematical models based on RSM to evaluate the individual and interaction effect of process parameters on the considered responses.

3.2.1 Thrust force

Thrust force is defined as the reaction force against the advancement of tool into the workpiece material (Basavarajappa et al. 2011). Figure 3.2a and Figure 3.2b shows the schematic representation of drilling mechanism in syntactic foams. As drill bit advances, GMBs present next to lip get debonded or sheared resulting in crack and debris formation. These cracks in the brittle matrix lead to lower thrust force (Basavarajappa et al. 2011), and such effect enhances with increasing filler content (Figure 3.2b). The micrograph in Figure 3.2c shows the virgin and drilled hole surface of a representative E350-20 at an intermediate drilling step to check the crack initiation. Crack is visible in the matrix at the GMB/Epoxy interface as shown in Figure 3.2d. Experimentally measured values of thrust force for neat epoxy and their syntactic foams are presented in Table 3.2.

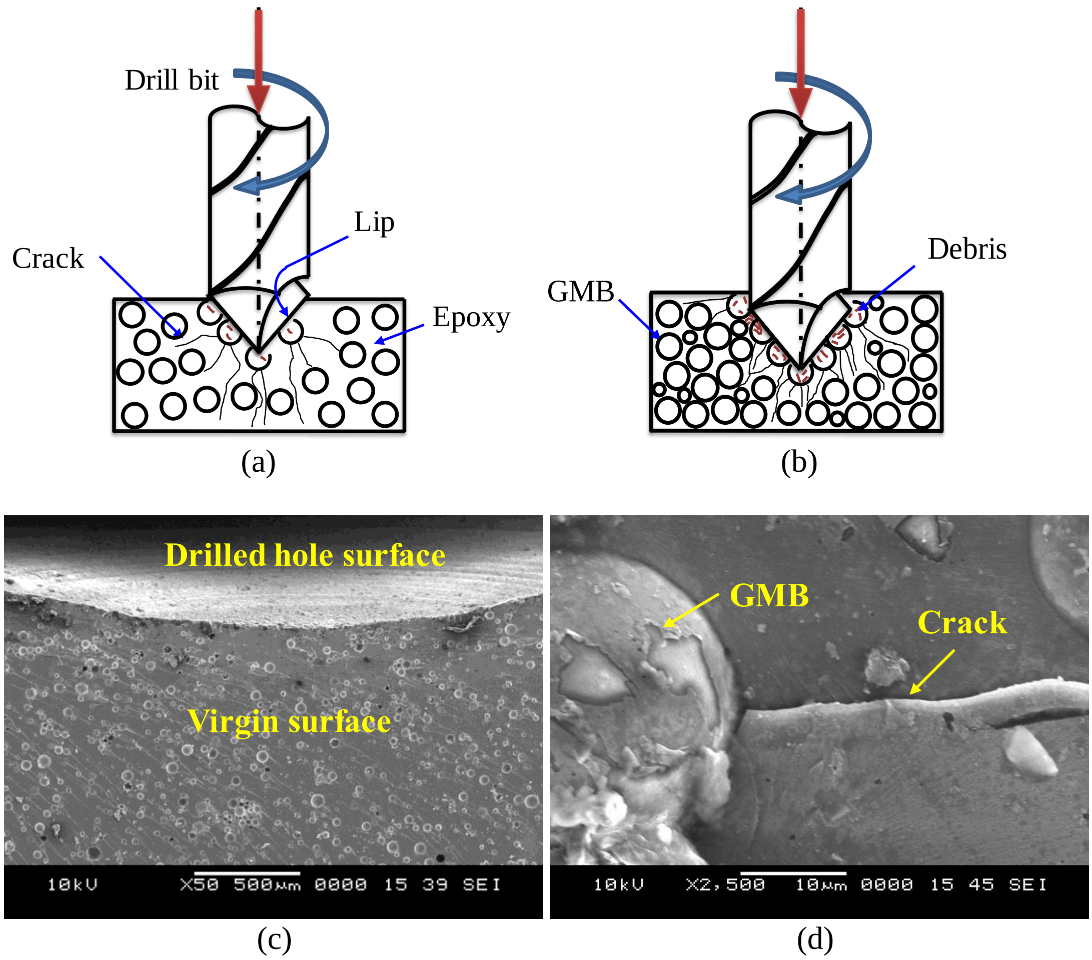

Figure 3.2 Schematic representation of drilling in (a) 20 and (b) 60 vol.% GMBs reinforced samples. (c-d) Scanning electron micrographs showing crack formation at the intermittent drilled surface of E350-20 sample at different magnification.

Table 3.2 Experimentally measured values of thrust force for neat epoxy and their syntactic foams.

v	f	D	E0	E200			E270			E350		
				R_{20}	R_{40}	R_{60}	R_{20}	R_{40}	R_{60}	R_{20}	R_{40}	R_{60}
25	0.04	8	68.67	39.24	29.43	19.62	39.24	39.24	29.43	39.24	39.24	29.43
		12	107.91	58.86	49.05	39.24	68.67	58.86	49.05	68.67	68.67	49.05
		16	156.96	88.29	78.48	58.86	98.10	78.48	58.86	127.53	88.29	78.48
	0.08	8	98.10	49.05	49.05	29.43	58.86	49.05	39.24	58.86	49.05	39.24
		12	156.96	88.29	78.48	49.05	88.29	78.48	68.67	88.29	68.67	58.86
		16	215.82	117.72	107.91	78.48	147.15	117.72	88.29	156.96	117.72	98.10
	0.12	8	107.91	58.86	58.86	39.24	58.86	58.86	39.24	68.67	58.86	39.24
		12	176.58	98.10	88.29	68.67	98.10	88.29	68.67	107.91	88.29	68.67
		16	245.25	137.34	127.53	98.10	166.77	137.34	107.91	166.77	127.53	98.10
75	0.04	8	58.86	29.43	29.43	19.62	39.24	39.24	29.43	39.24	39.24	29.43
		12	98.10	49.05	49.05	29.43	58.86	58.86	39.24	78.48	58.86	39.24
		16	147.15	78.48	68.67	49.05	98.10	78.48	58.86	117.72	78.48	68.67
	0.08	8	88.29	49.05	39.24	29.43	49.05	49.05	39.24	58.86	49.05	39.24
		12	137.34	78.48	68.67	49.05	88.29	78.48	58.86	107.91	78.48	68.67
		16	186.39	107.91	98.10	68.67	137.34	117.72	78.48	147.15	117.72	107.91
	0.12	8	107.91	49.05	49.05	29.43	58.86	58.86	39.24	68.67	58.86	49.05
		12	166.77	88.29	78.48	58.86	98.10	88.29	58.86	107.91	88.29	68.67
		16	225.63	117.72	107.91	88.29	147.15	127.53	98.10	176.58	137.34	117.72
125	0.04	8	49.05	29.43	29.43	19.62	39.24	29.43	19.62	49.05	29.43	19.62
		12	98.10	49.05	49.05	29.43	58.86	58.86	39.24	88.29	58.86	49.05
		16	137.34	68.67	68.67	39.24	88.29	78.48	58.86	117.72	88.29	78.48
	0.08	8	88.29	39.24	39.24	19.62	49.05	49.05	29.43	68.67	49.05	39.24
		12	127.53	68.67	58.86	39.24	88.29	68.67	58.86	88.29	78.48	68.67
		16	176.58	98.10	88.29	58.86	127.53	107.91	78.48	176.58	127.53	107.91

v	*f*	*D*	E0	E200			E270			E350		
				R_{20}	R_{40}	R_{60}	R_{20}	R_{40}	R_{60}	R_{20}	R_{40}	R_{60}
		8	98.10	49.05	39.24	29.43	58.86	58.86	39.24	98.10	58.86	49.05
	0.12	12	156.96	78.48	68.67	49.05	107.91	78.48	58.86	107.91	98.10	78.48
		16	215.82	117.72	107.91	68.67	147.15	127.53	98.10	186.39	156.96	117.72

Table 3.3 Summary of ANOVA results for the developed mathematical models of thrust force.

Responses	Sum of squares		Degrees of freedom		Mean square		F-ratio	P-Value	CoD
	Regression	Residual	Regression	Residual	Regression	Residual			
$F_{t(E200)}$	$6.48×10^4$	$6.98×10^2$			$4.63×10^3$	10.57	437.66[a]	<0.001	0.9893
$F_{t(E270)}$	$8.58×10^4$	$1.43×10^3$	14	66	$6.13×10^3$	21.60	283.67[a]	<0.001	0.9837
$F_{t(E350)}$	$1.14×10^5$	$3.29×10^3$			$8.15×10^3$	49.78	163.69[a]	<0.001	0.9720

[a]F-table = 2.36. Significance at 99 % confidence interval.

3.2.1.1 Development of mathematical models based on experimental data

Mathematical models for thrust force are developed based on experimental results (Table 3.2) using commercially available Minitab 14 software. Regression equations for predicting the thrust force of different syntactic foams are given as,

$$F_{t(E200)} = \begin{pmatrix} -49.82 + 0.03 \times v + 487.09 \times f + 1.60 \times R + 4.93 \times D + 0.001 \times v^2 - 2270.83 \times \\ f^2 - 0.02 \times R^2 + 0.08 \times D^2 - 1.23 \times v \times f + 0.0003 \times v \times R - 0.01 \times v \times D - 2.73 \\ \times f \times R + 37.47 \times f \times D - 0.06 \times R \times D \end{pmatrix} \tag{3.1}$$

$$F_{t(E270)} = \begin{pmatrix} -34.38 - 0.02 \times v + 554.08 \times f + 1.62 \times R + 2.10 \times D + 0.0003 \times v^2 - 3633.33 \times \\ f^2 - 0.01 \times R^2 + 0.25 \times D^2 - 5.25 \times 10^{-15} \times v \times f - 0.0003 \times v \times R - 0.01 \times v \times D \\ -4.43 \times f \times R + 51.09 \times f \times D - 0.10 \times R \times D \end{pmatrix} \tag{3.2}$$

$$F_{t(E350)} = \begin{pmatrix} 26.30 - 0.23 \times v + 513.21 \times f - 0.08 \times R - 2.66 \times D + 0.001 \times v^2 - 3065.63 \times f^2 \\ +0.01 \times R^2 + 0.51 \times D^2 + 1.91 \times v \times f - 0.001 \times v \times R + 0.01 \times v \times D - 4.09 \times f \times \\ R + 35.77 \times f \times D - 0.10 \times R \times D \end{pmatrix} \tag{3.3}$$

Equation 3.1-Equation 3.3 are used to predict the thrust force within the chosen range of input process parameters. Adequacy of the developed mathematical models are confirmed using ANOVA and are presented in Table 3.3. According to ANOVA, the computed F-ratio should be more than the F-table for the models to be adequate. Higher CoD values of the developed mathematical models of thrust force for E200 (0.98), E270 (0.98) and E350 (0.97) syntactic foams indicate a good correlation is existing between the experimental and predicted values. The average errors between the experimental and predicted values are found to be 0.20, 0.45 and 0.70% for thrust force of E200, E270 and E350 syntactic foams respectively as shown in Figure 3.3. Hence, the developed mathematical models can be effectively used as a tool in industrial practices to predict the thrust force of GMB reinforced epoxy foams during drilling.

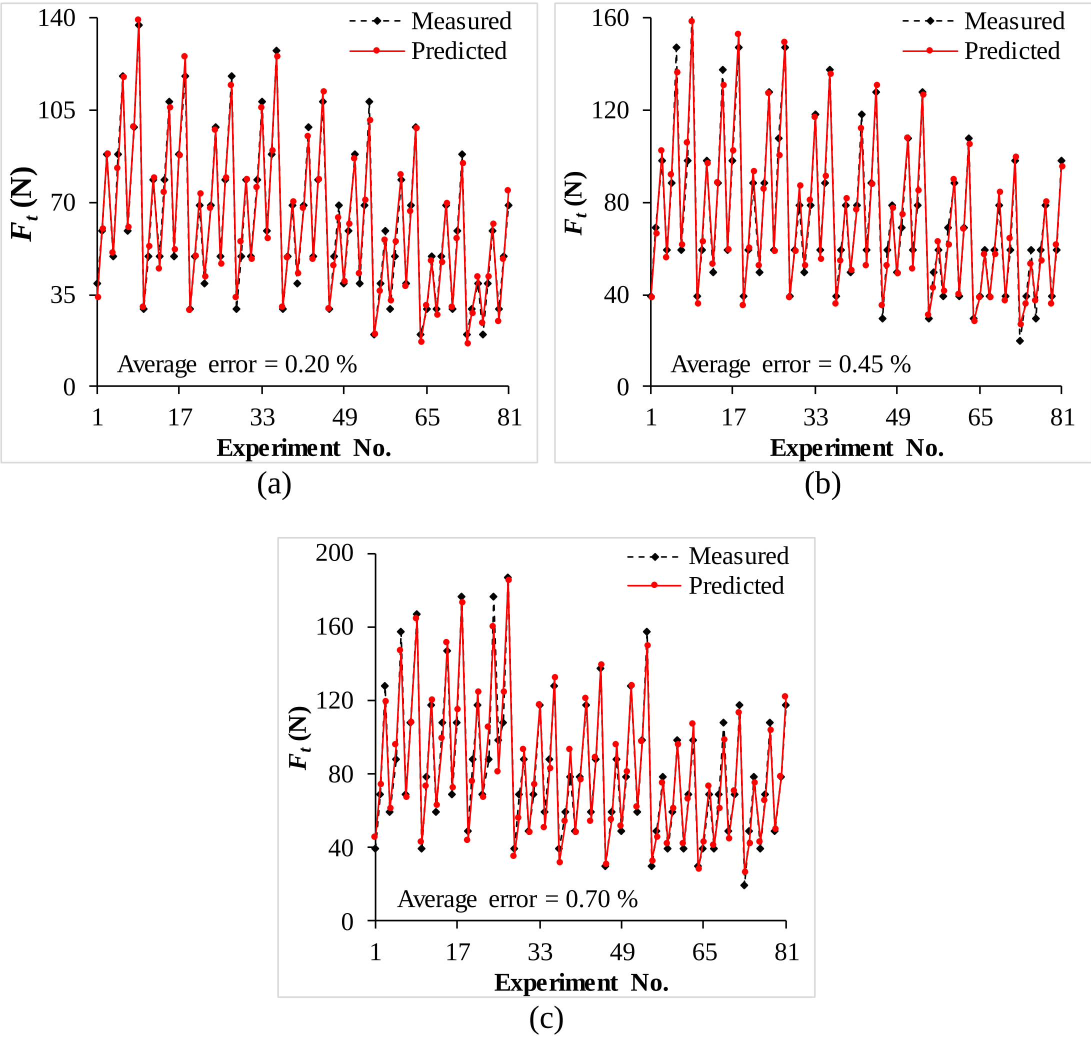

Figure 3.3 Comparison between measured and predicted values of F_t for (a) E200, (b) E270 and (c) E350 syntactic foams.

3.2.1.2 Effects of individual parameters

Cutting speed, feed, drill diameter and filler content are varied one at a time within the chosen range, keeping the other parameters at intermediate level in Equation 3.1-Equation 3.3 to predict the general trend of F_t as presented in Figure 3.4. F_t of all the syntactic foams increases with increasing f (Figure 3.4a, Figure 3.4c and Figure 3.4e) but decreases with increasing R and decreasing D (Figure 3.4b, Figure 3.4d and Figure 3.4f). With increasing v the F_t is found to be decreasing for E200 and E270 syntactic foams as shown in Figure 3.4a and Figure 3.4c respectively while it marginally increases for E350 syntactic foam (Figure 3.4e). These plots can serve as a reference to understand the general relationships among various parameters.

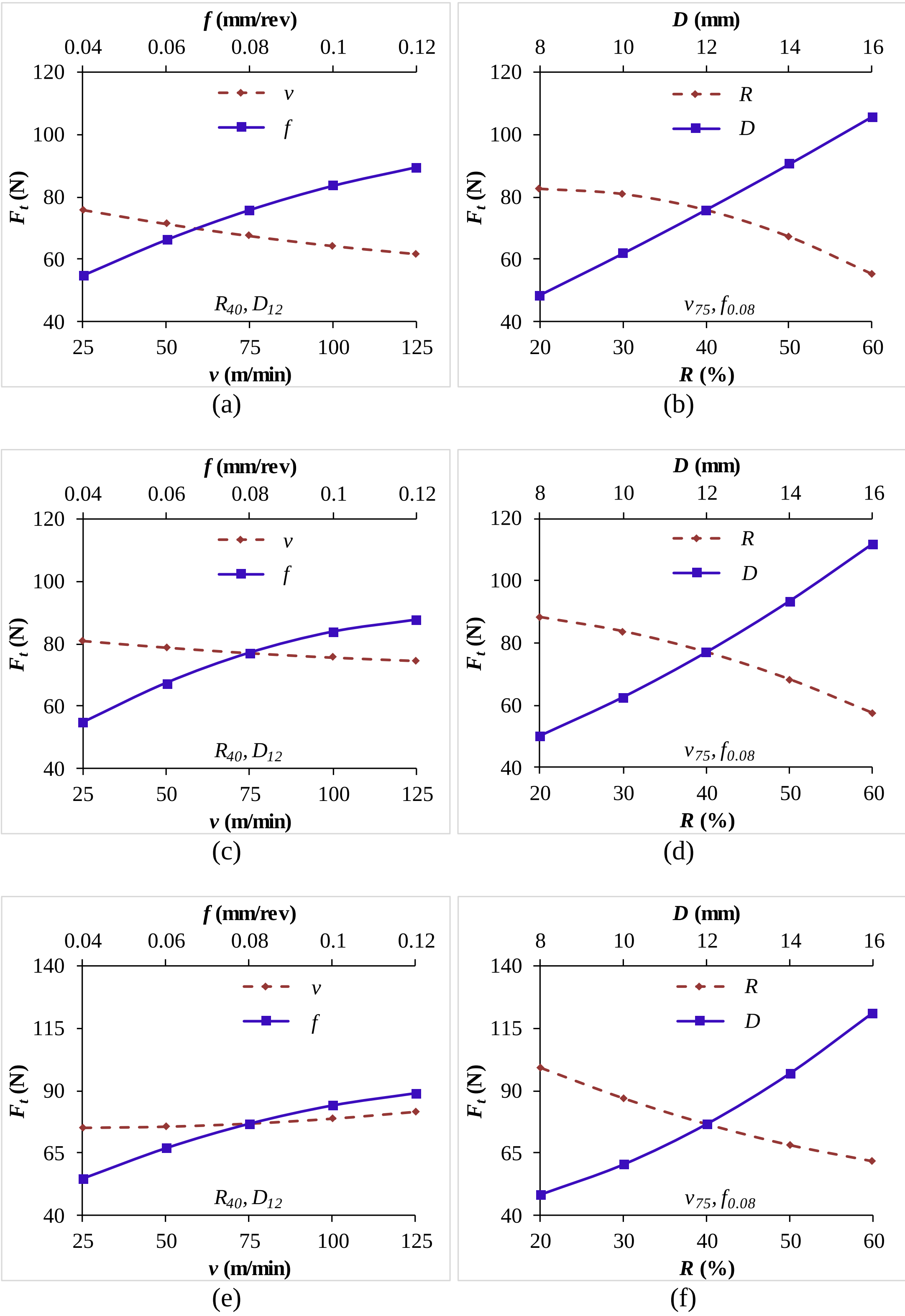

Figure 3.4 Individual effect plots of F_t for (a-b) E200, (c-d) E270 and (e-f) E350 syntactic foams.

3.2.1.3 Effects of two-parameter interactions

Interaction effects among the input process parameters on the thrust force in drilling of syntactic foams are studied by varying two parameters at the same time in Equation 3.1-Equation 3.3, keeping the other two at their intermediate levels as per the scheme presented in Table 2.6.

Figure 3.5a show that the thrust force decreases with increasing cutting speed and decreasing drill diameter for E200 syntactic foam. A similar effect of v on F_t is observed for E270 syntactic foam as shown in Figure 3.6a, while F_t marginally increases with increasing v for E350 syntactic foam (Figure 3.7a). With the increasing cutting speed from v_{25} - v_{125}, at higher drill diameter F_t decreases by 19 and 8% for E200 and E270 syntactic foams respectively, whereas it increases by 9% for E350 syntactic foam. Increasing v raises the tool and work material interface temperature, resulting in the softening of syntactic foam leading to decreased thrust force (Ameur et al. 2017) in E200 and E270 syntactic foams. Increasing F_t with increasing cutting speed for E350 syntactic foam is attributed to the increased compressive strength and thermal stability of the foam compared to E200 and E270 syntactic foams (Zeltmann et al. 2017). Thrust force as a function of cutting speed and feed is presented in Figure 3.5b, Figure 3.6b and Figure 3.7b for E200, E270 and E350 syntactic foams respectively. At higher feeds F_t decreases by 21 and 7% for E200 and E270 syntactic foams respectively, while it increases by 17% for E350 syntactic foam, with the increasing cutting speed. Thrust force decreases with increasing GMB content for all the syntactic foams (Figure 3.5c, Figure 3.6c and Figure 3.7c). F_t decreases by 67, 57 and 52% as compared to neat epoxy for E200, E270 and E350 syntactic foams respectively. As the drill advances into the syntactic foam specimen, axial and tangential forces exerted by the tool promote debonding between GMB and epoxy matrix, leading to the reduced uncut material. GMBs being relatively brittle than the matrix, a large number of particles shear at higher filler loadings resulting in declining trend of F_t. The presence of porosity inside GMBs leads to lower thrust forces because fracture of particle exposes the void for the drill to advance without any resistance (Basavarajappa et al. 2011, Gaitonde et al. 2011).

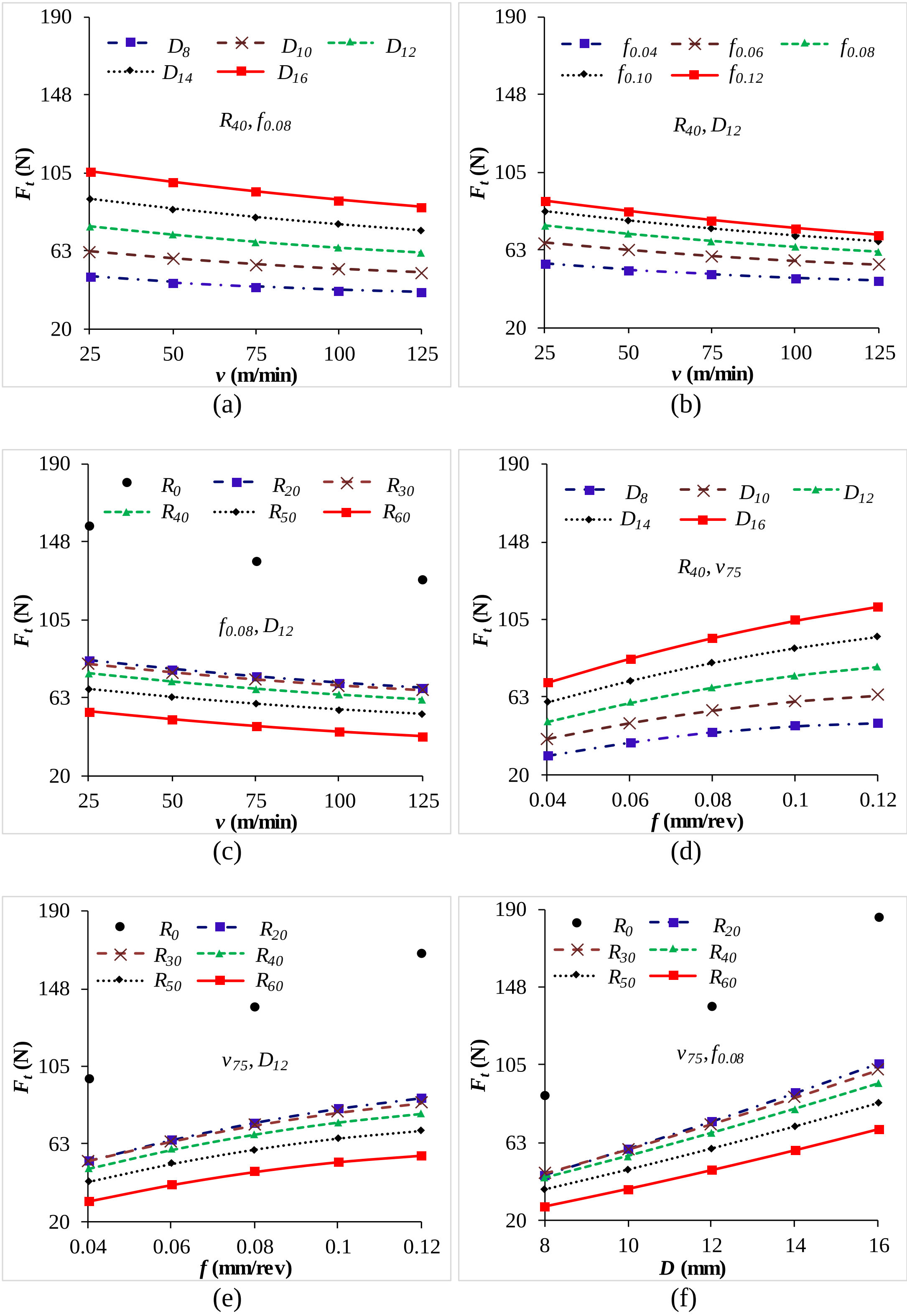

Figure 3.5 Variation of F_t with respect to v at different (a) D, (b) f and (c) R. F_t with respect to f at different (d) D and (e) R. (f) F_t with respect to D at different R for E200 syntactic foam.

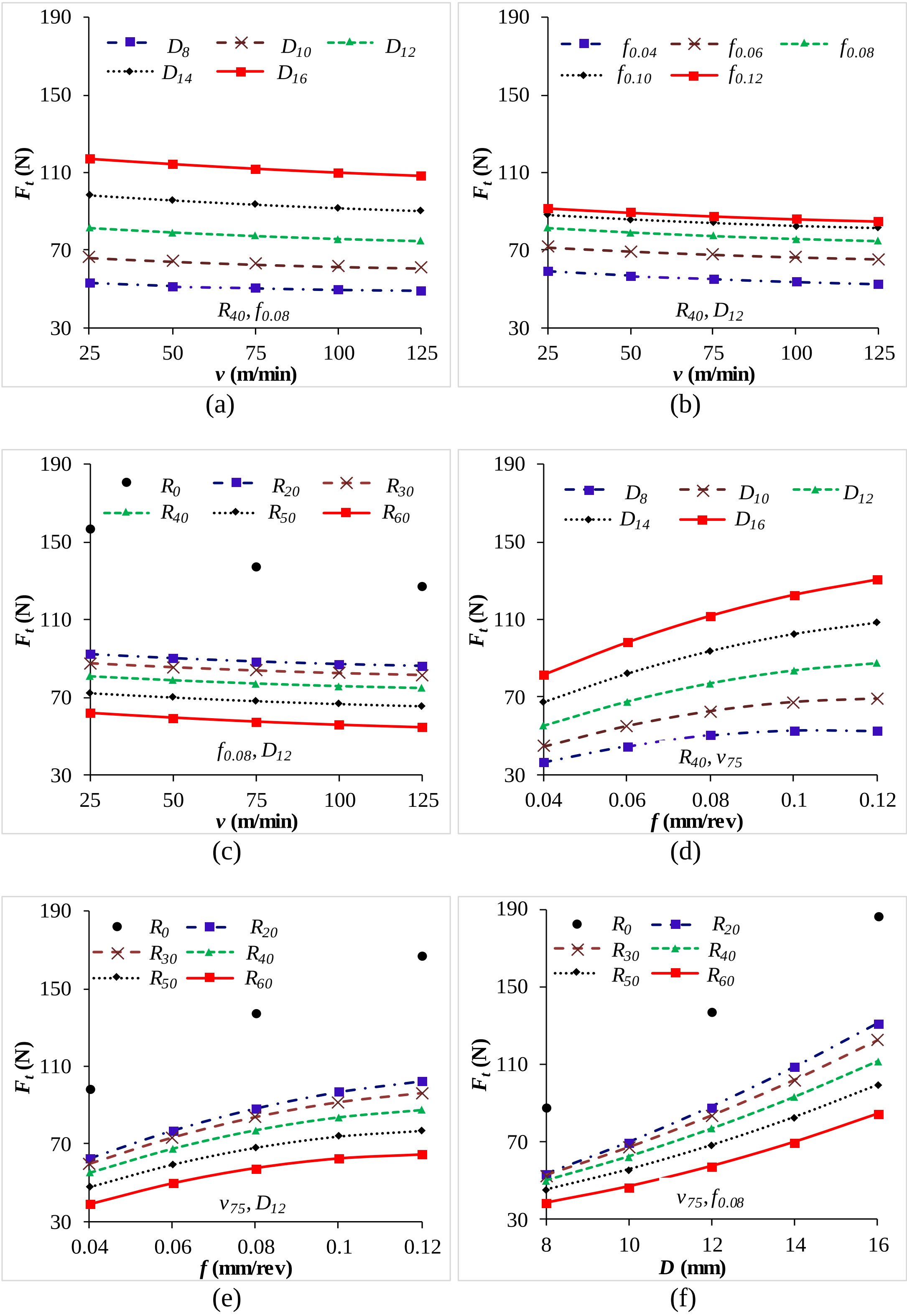

Figure 3.6 Variation of F_t with respect to v at different (a) D, (b) f and (c) R. F_t with respect to f at different (d) D and (e) R. (f) F_t with respect to D at different R for E270 syntactic foam.

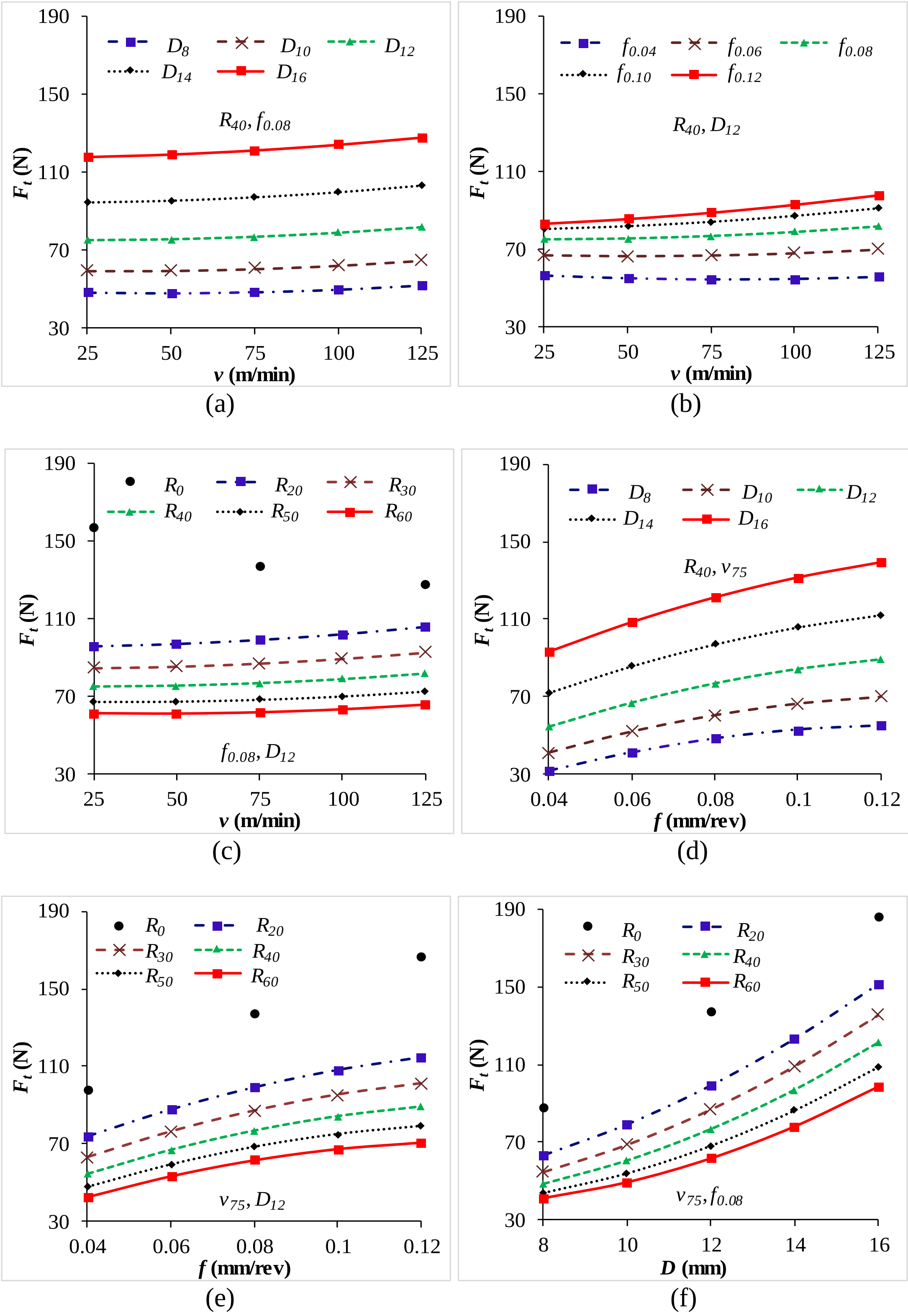

Figure 3.7 Variation of F_t with respect to v at different (a) D, (b) f and (c) R. F_t with respect to f at different (d) D and (e) R. (f) F_t with respect to D at different R for E350 syntactic foam.

Thrust force is found to increase with increasing feed and drill diameter as shown in Figure 3.5d, Figure 3.6d and Figure 3.7d for all type of SFs. F_t increases in the range of 58-59, 45-60 and 49-72% for E200, E270 and E350 SFs respectively with increasing feed from $f_{0.04}$ - $f_{0.12}$. At higher feeds, the resistance offered by substrate raises in the direction of cutting, resulting in increased friction between tool and substrate leading to higher thrust forces. Material removal rate also increases due to the increased contact area leading to higher values of F_t (Basavarajappa et al. 2011, Gaitonde et al. 2009).

Figure 3.5e, Figure 3.6e and Figure 3.7e show the variation of feed and filler content as a function of thrust force for E200, E270 and E350 SFs respectively. The thrust force increases with increasing feed and decreasing filler content. The thrust force reduces by 65-68, 58-61 and 56-58% as compared to that of neat epoxy for E200, E270 and E350 SFs respectively with increasing feed from $f_{0.04}$ - $f_{0.12}$.

The variation of F_t with drill diameter and filler content is presented in Figure 3.5f, Figure 3.6f and Figure 3.7f for all the syntactic foams. With increasing drill diameter from D_8 - D_{16}, F_t increases in the range of 121-157, 120-145 and 139-141% for E200, E270 and E350 SFs respectively. As drill diameter increases, the contact area of the drilled hole increases leading to higher thrust forces (El-Sonbaty et al. 2004, Rajamurugan et al. 2013).

3.2.2 Surface roughness

Experimentally measured values of surface roughness for neat epoxy and their syntactic foams are presented in Table 3.4. Results analysis, discussions and interpretations are presented herewith.

Table 3.4 Experimentally measured values of surface roughness for neat epoxy and their syntactic foams.

v	*f*	*D*	E0	E200			E270			E350		
				R_{20}	R_{40}	R_{60}	R_{20}	R_{40}	R_{60}	R_{20}	R_{40}	R_{60}
25	0.04	8	0.16	4.28	4.19	4.12	3.60	3.44	3.03	2.06	2.94	2.78
		12	0.14	3.20	2.98	2.81	2.34	2.47	2.54	1.44	1.13	0.87
		16	0.12	2.85	2.35	2.11	1.63	1.61	1.08	1.55	2.23	2.10
	0.08	8	0.15	4.19	3.22	3.20	3.44	3.02	2.94	2.30	2.34	2.22
		12	0.13	2.89	2.89	2.20	2.27	2.31	1.26	1.26	1.21	0.79
		16	0.12	2.20	1.99	1.97	1.38	1.34	1.08	1.70	2.64	1.15
	0.12	8	0.13	3.69	3.12	3.12	3.00	2.55	2.06	3.32	2.38	1.92
		12	0.12	2.58	2.56	2.19	1.82	1.82	1.14	1.30	1.08	1.00
		16	0.12	1.56	1.54	1.29	1.31	1.15	1.07	1.32	1.56	1.11
75	0.04	8	0.22	4.28	4.24	4.12	4.23	3.86	3.26	2.86	2.56	2.96
		12	0.15	3.90	3.28	3.11	3.33	3.08	2.75	1.50	1.66	1.78
		16	0.13	2.88	2.88	2.16	2.85	2.05	2.03	2.89	2.23	2.65
	0.08	8	0.17	4.23	3.61	3.39	4.23	3.49	3.09	3.24	2.10	3.00
		12	0.15	3.12	2.98	2.88	3.02	2.81	2.43	1.66	1.26	1.55
		16	0.12	2.62	2.32	2.32	2.53	1.74	1.95	2.21	2.38	1.72
	0.12	8	0.17	3.75	3.39	3.15	3.54	3.30	2.54	3.42	3.30	2.39
		12	0.14	2.88	2.92	2.77	2.86	2.68	2.20	1.09	1.45	1.44
		16	0.12	1.98	1.64	1.63	1.89	1.60	1.52	2.41	2.42	2.56
125	0.04	8	0.22	4.83	4.39	4.25	4.42	4.28	4.76	3.03	3.46	3.58
		12	0.16	4.24	3.97	3.32	3.96	3.60	3.00	1.22	2.01	1.33
		16	0.16	3.29	3.08	2.99	3.20	2.98	2.64	3.87	3.52	1.90
	0.08	8	0.20	4.38	3.99	3.99	4.26	3.71	3.84	3.34	3.62	4.75
		12	0.15	4.18	3.77	3.19	3.40	3.53	2.68	1.29	1.32	1.66
		16	0.14	3.10	2.85	2.56	2.58	2.56	2.15	1.90	3.44	1.42

v	f	D	E0	E200			E270			E350		
				R_{20}	R_{40}	R_{60}	R_{20}	R_{40}	R_{60}	R_{20}	R_{40}	R_{60}
		8	0.18	4.30	3.73	3.73	3.54	3.52	3.79	3.51	3.47	3.68
	0.12	12	0.15	3.55	3.00	2.66	3.20	2.89	2.68	1.47	1.21	1.00
		16	0.12	2.29	2.31	2.20	2.13	2.23	1.55	3.22	2.80	1.26

Table 3.5 Summary of ANOVA results for the developed mathematical models of surface roughness.

Responses	Sum of squares		Degrees of freedom		Mean square		F-ratio	P-Value	CoD
	Regression	Residual	Regression	Residual	Regression	Residual			
$R_{a(E200)}$	50.99	2.43			3.64	0.037	98.78[a]	<0.001	0.9544
$R_{a(E270)}$	62.12	3.76	14	66	4.44	0.057	77.95[a]	<0.001	0.9430
$R_{a(E350)}$	48.83	15.65			3.49	0.240	14.71[a]	<0.001	0.7574

[a]F-table = 2.36. Significance at 99 % confidence interval.

3.2.2.1 Development of mathematical models based on experimental data

Mathematical models for analysing surface roughness of different syntactic foams are developed based on experimental results (Table 3.4) using Minitab 14 software. Regression equations for predicting the surface roughness of different syntactic foams are given as,

$$R_{a(E200)} = \begin{pmatrix} 6.73 - 0.002 \times v - 6.90 \times f - 0.03 \times R - 0.21 \times D + 3.38 \times 10^{-5} \times v^2 - 9.72 \times f^2 \\ + 0.0001 \times R^2 - 0.0002 \times D^2 + 0.01 \times v \times f - 2.36 \times 10^{-5} \times v \times R + 0.0003 \times v \times \\ D + 0.03 \times f \times R - 0.25 \times f \times D + 0.0005 \times R \times D \end{pmatrix} \tag{3.4}$$

$$R_{a(E270)} = \begin{pmatrix} 5.92 + 0.02 \times v - 8.62 \times f - 0.01 \times R - 0.31 \times D - 4.4 \times 10^{-5} \times v^2 - 5.80 \times f^2 - \\ 0.0001 \times R^2 + 0.003 \times D^2 - 0.02 \times v \times f + 2.73 \times 10^{-5} \times v \times R + 0.0002 \times v \times D - \\ 0.01 \times f \times R + 0.25 \times f \times D + 0.0002 \times R \times D \end{pmatrix} \tag{3.5}$$

$$R_{a(E350)} = \begin{pmatrix} 10.77 + 0.02 \times v + 7.15 \times f + 0.06 \times R - 1.83 \times D - 4.00 \times 10^{-5} \times v^2 + 49.56 \times f^2 \\ -0.0004 \times R^2 + 0.08 \times D^2 - 0.003 \times v \times f + 1.53 \times 10^{-6} \times v \times R - 0.0003 \times v \times D \\ -0.15 \times f \times R - 0.95 \times f \times D - 0.002 \times R \times D \end{pmatrix} \tag{3.6}$$

Equation 3.4-Equation 3.6 are used to predict the surface roughness of the drilled hole within the chosen range of input process parameters. ANOVA is used to check the adequacy of the developed mathematical models and the results are presented in Table 3.5. Higher CoD (R-squared) values of the developed mathematical models (Equation 3.4-Equation 3.6) of surface roughness for E200 (0.95), E270 (0.94) and E350 (0.76) syntactic foams indicate a good correlation is existing between the experimental and predicted values. The average errors between the experimental and predicted values are found to be 0.36, 0.77 and 3.55% for surface roughness of E200, E270 and E350 syntactic foams respectively as shown in Figure 3.8. Hence, the developed mathematical models can be effectively used as a tool in industrial practices to predict the surface roughness of GMB reinforced epoxy foams during drilling.

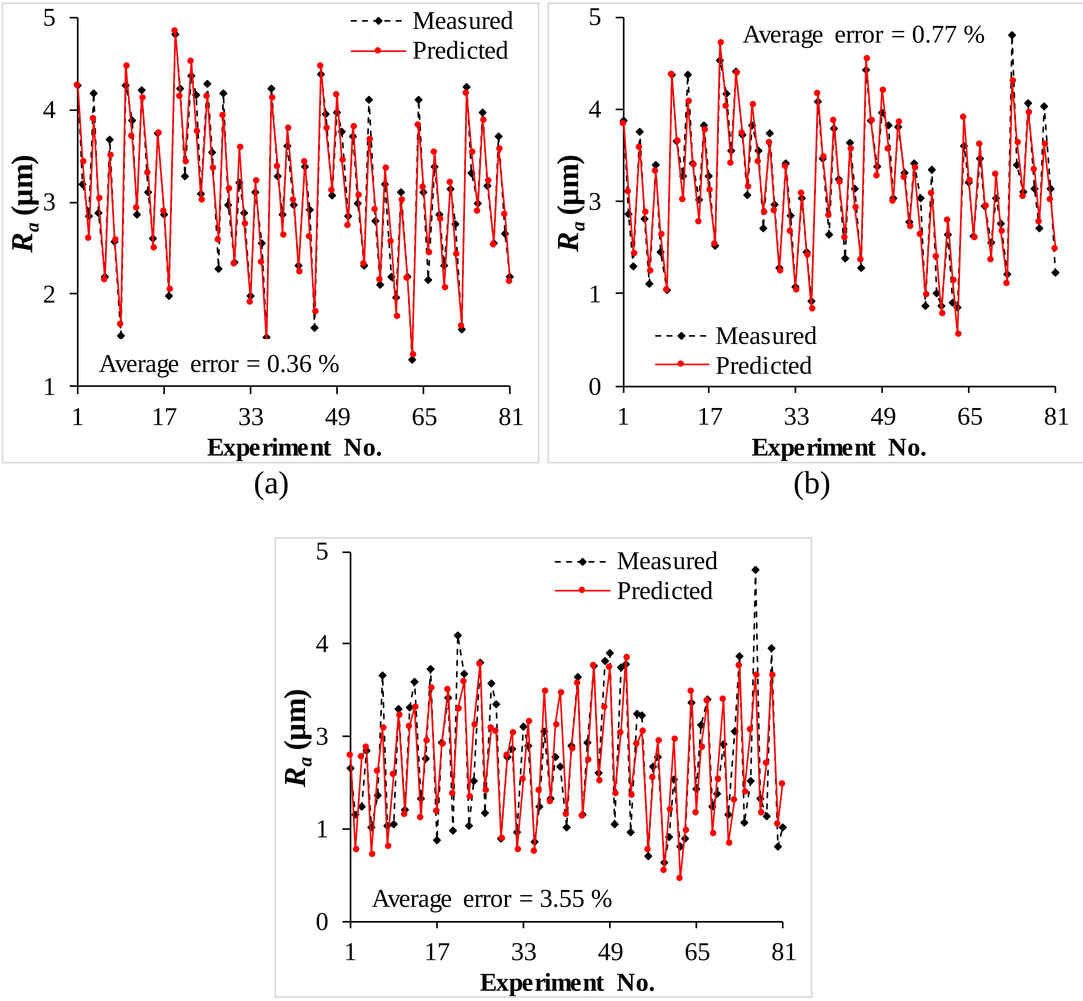

(a) (b)
(c)

Figure 3.8 Comparison between measured and predicted values of R_a for (a) E200, (b) E270 and (c) E350 syntactic foams.

3.2.2.2 Effects of individual parameters

Only one parameter is varied at a time in Equation 3.4-Equation 3.6 within the chosen range, while other parameters are kept constant at the intermediate level for predicting the general trend of surface roughness (Figure 3.9). Surface roughness increases with increasing cutting speed while decreases with increasing feed (Figure 3.9a, Figure 3.9c and Figure 3.9e) and filler content (Figure 3.9b, Figure 3.9d and Figure 3.9f) for all the syntactic foams. R_a is found to be decreasing for E200 (Figure 3.9b) and E270 (Figure 3.9d) syntactic foams with increasing drill diameter, whereas it decreases with increasing drill diameter up to D_{12} and later shows increasing trend beyond for E350 syntactic foam as seen from Figure 3.9f. These plots serve as a reference to understand the general relationships among various parameters.

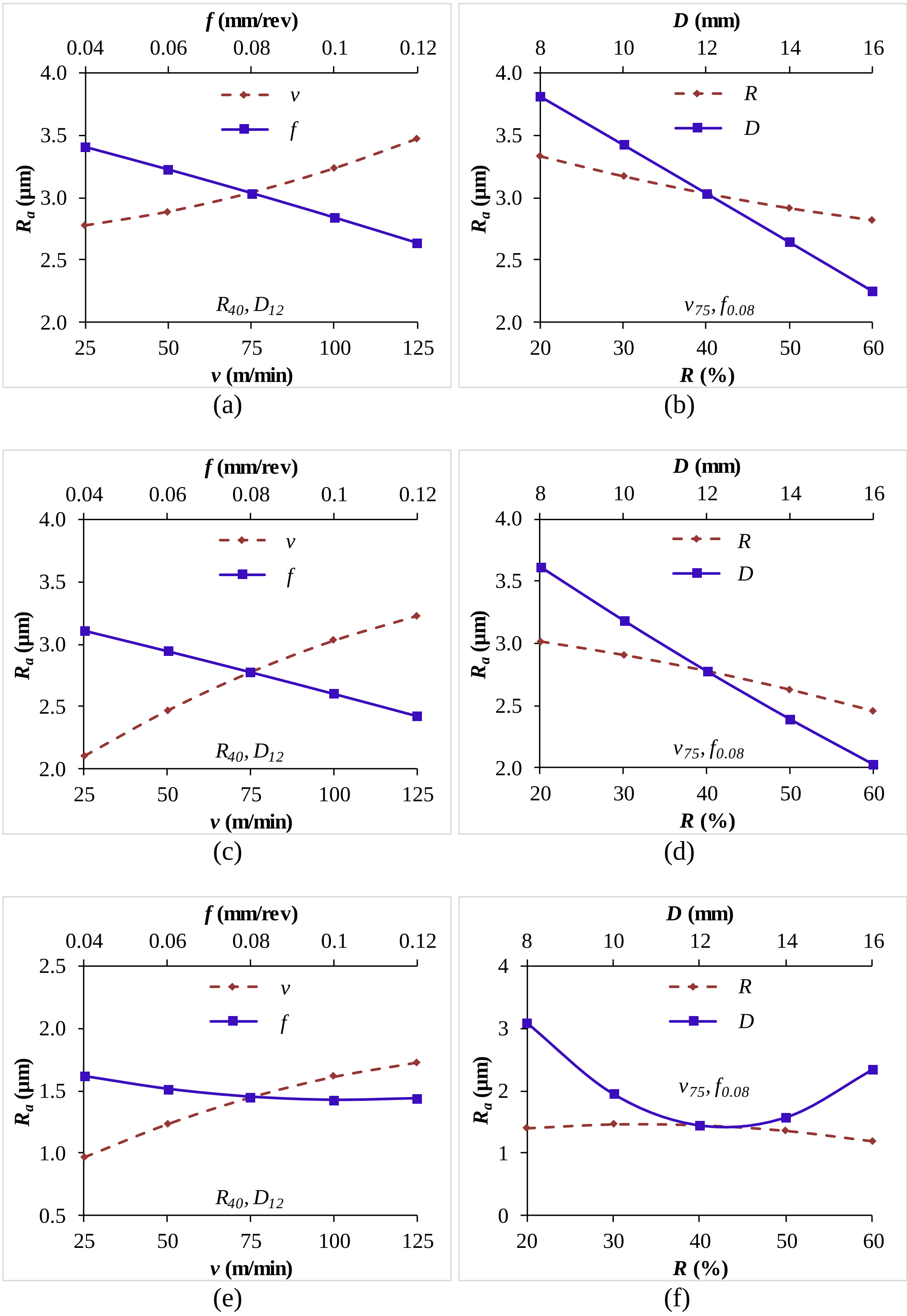

Figure 3.9 Individual effect plots of R_a for (a-b) E200, (c-d) E270 and (e-f) E350 syntactic foams.

3.2.2.3 Effects of two-parameter interactions

Equation 3.4-Equation 3.6 are used to analyze the interaction effects among the input process parameters on the surface roughness of drilled hole by varying two parameters at the same time and keeping the other two at their intermediate levels as per the scheme presented in Table 2.6. Surface roughness increases with the increasing cutting speed at all levels of drill diameter for all the syntactic foams (Figure 3.10a, Figure 3.11a and Figure 3.12a). It increases in the range of 16-43, 35-91 and 33-79% with increasing cutting speed from v_{25}-v_{125} for E200, E270 and E350 syntactic foams respectively at different levels of drill diameter. Increasing cutting speed raises the temperature at the tool-workpiece interface leading to rough surfaces (Campos Rubio et al. 2008, Gaitonde et al. 2011, Giasin et al. 2015). Surface roughness increases with cutting speed while it decreases with increasing feed for all the foams as shown in Figure 3.10b, Figure 3.11b and Figure 3.12b. R_a increases in the range of 21-31, 51-59 and 68-80% for E200, E270 and E350 foams respectively with increasing cutting speed at different levels of feeds.

Effect of filler (GMB) content on surface roughness of the drilled hole is shown in Figure 3.10c, Figure 3.11c and Figure 3.12c for E200, E270 and E350 foams respectively. In comparison to R_a of neat epoxy, surface roughness in foams is observed to be increased in the range of 19-21, 13-19 and 5-10 times for E200, E270 and E350 foams respectively with increasing cutting speed. Nevertheless, in foams surface roughness decreases with increasing filler content owing to the burnishing and honing effect produced by abrasive fillers (Basavarajappa et al. 2011). Additionally, lower F_t with increased R results in reduced surface roughness (Gaitonde et al. 2011, Palanikumar 2011, Palanikumar et al. 2006). Surface roughness decreases with increasing feed at all the levels of drill diameter as shown in Figure 3.10d, Figure 3.11d and Figure 3.12d for all the syntactic foams. R_a decreases in the range of 17-32, 19-26 and 2-19% for E200, E270 and E350 SFs respectively with increasing feed from $f_{0.04}$-$f_{0.12}$. At higher feed, the temperature at tool-workpiece interface decreases due to reduced contact time between tool and samples leading to lower surface roughness values (Campos Rubio et al. 2008).

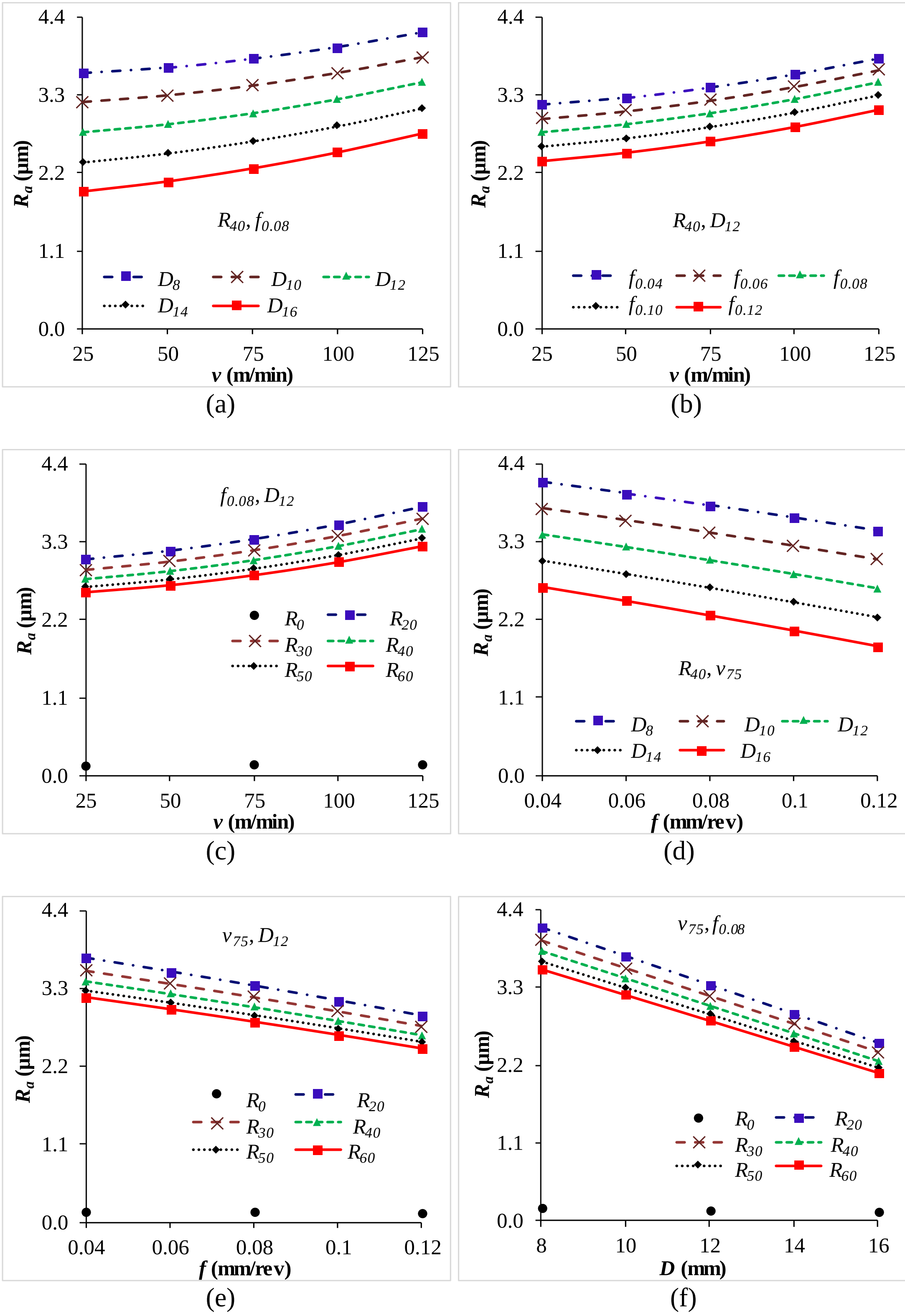

Figure 3.10 Variation of R_a with respect to v at different (a) D, (b) f and (c) R. R_a with respect to f at different (d) D and (e) R. (f) R_a with respect to D at different R for E200 syntactic foam.

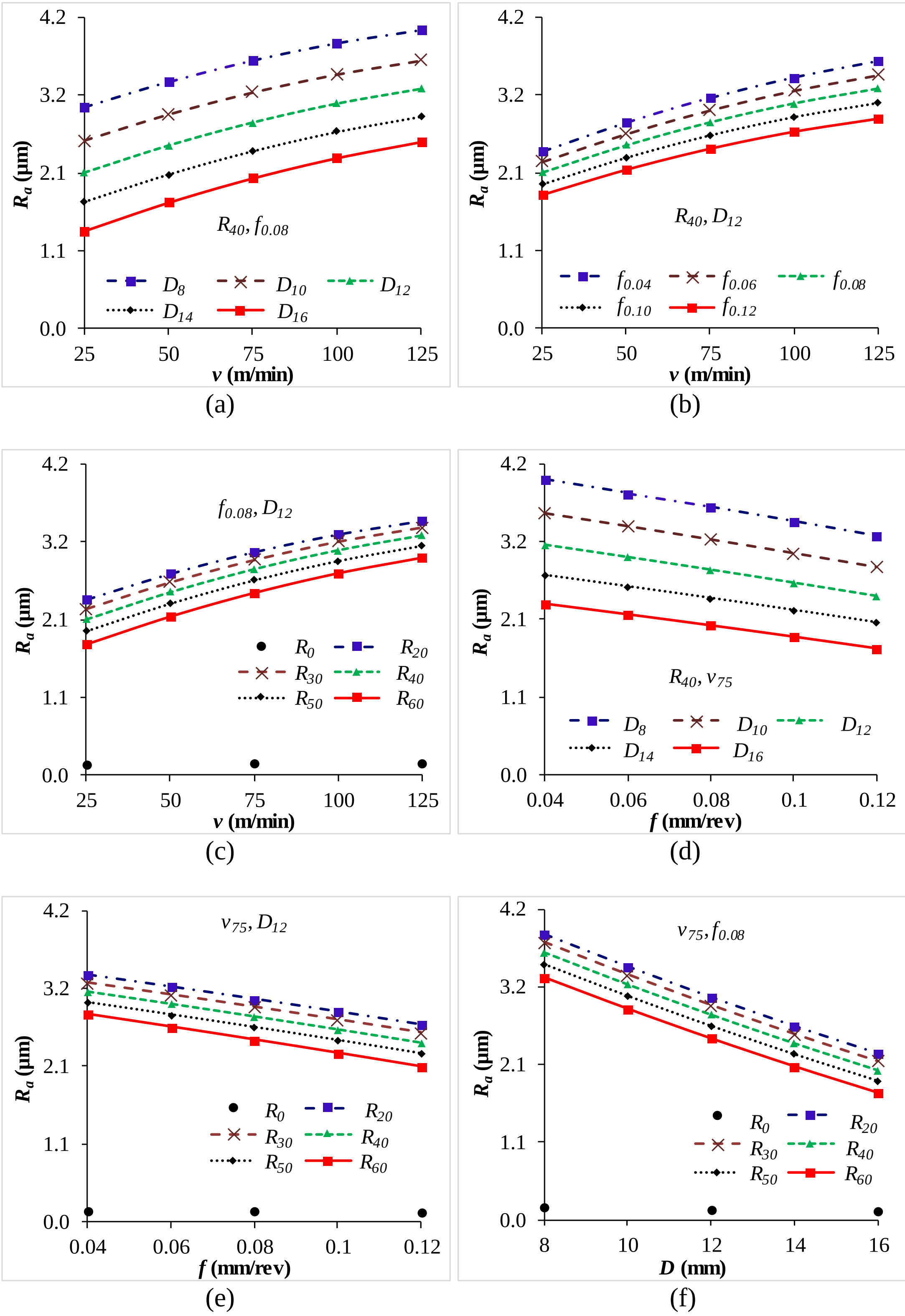

Figure 3.11 Variation of R_a with respect to v at different (a) D, (b) f and (c) R. R_a with respect to f at different (d) D and (e) R. (f) R_a with respect to D at different R for E270 syntactic foam.

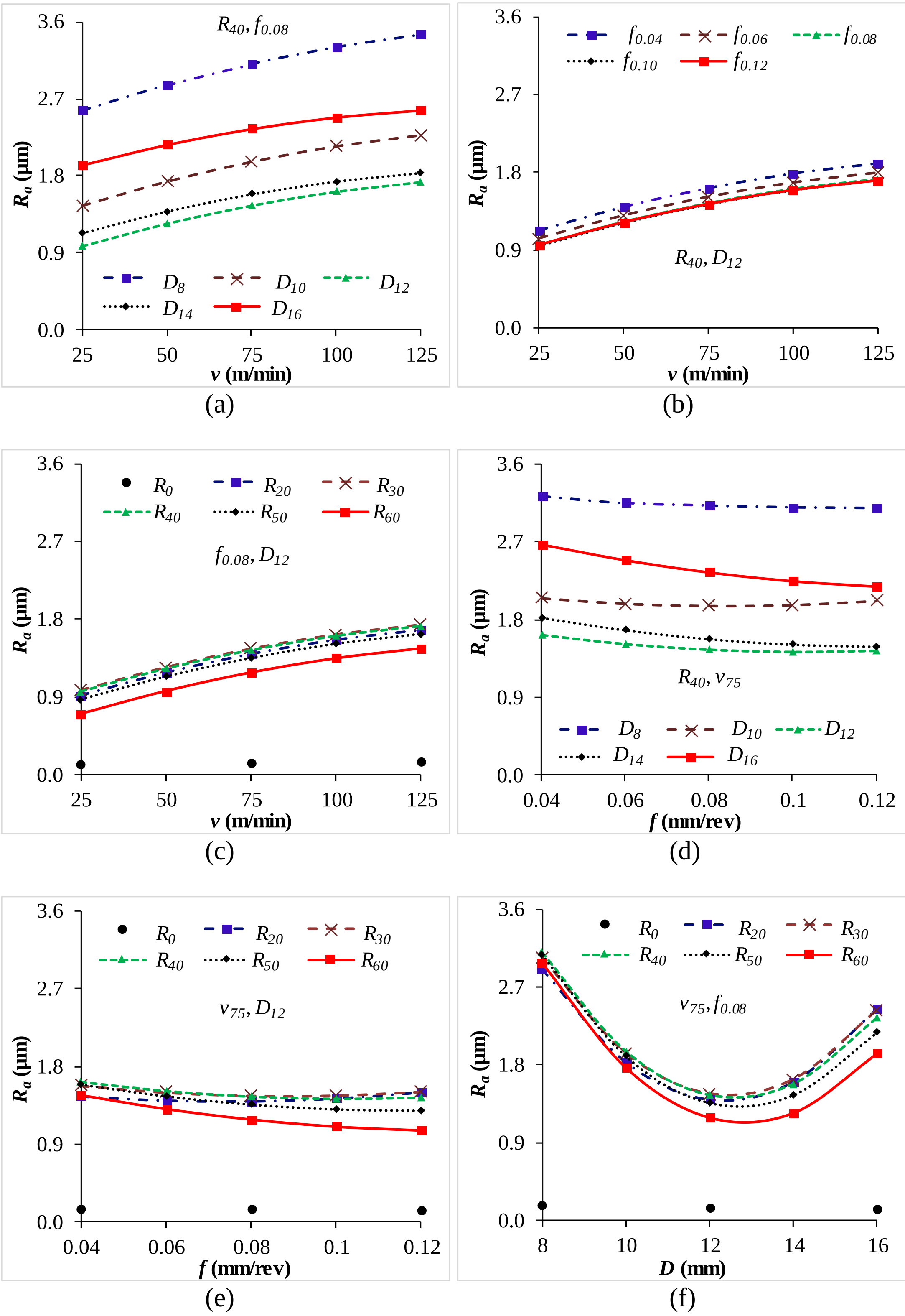

Figure 3.12 Variation of R_a with respect to v at different (a) D, (b) f and (c) R. R_a with respect to f at different (d) D and (e) R. (f) R_a with respect to D at different R for E350 syntactic foam.

Surface roughness decreases with increasing feed and filler content as observed from Figure 3.10e, Figure 3.11e and Figure 3.12e for E200, E270 and E350 SFs respectively. Surface roughness of SFs increases by 8-21 times as compared to neat epoxy with increasing feed from $f_{0.04}$ - $f_{0.12}$. Surface roughness decreases with increasing the drill diameter for E200 (Figure 3.10f) and E270 (Figure 3.11f) SFs, while it decreases up to D_{12} for E350 SF and later found to be increasing (Figure 3.12f). R_a decreases by 39-42, 42-48 and 16-35% with increasing drill diameter for E200, E270 and E350 SFs respectively. At any given cutting speed, D_{16} has a lower spindle speed than D_8 ($N = 1000 \times v / \pi \times D$) which results in lower surface roughness values (Gaitonde et al. 2011, Khashaba et al. 2010). Increasing surface roughness beyond D_{12} in E350 syntactic foam is attributed to the higher thrust force generated with larger diameter drills (El-Sonbaty et al. 2004, Rajamurugan et al. 2013). Figure 3.13 presents the surface texture of the drilled hole wall. Foams exhibit higher surface roughness as compared to neat epoxy samples due to the presence of broken GMBs as seen in Figure 3.13b. GMB debris and the exposed matrix voids result in higher surface roughness values of SFs as compared to neat resin surface (Figure 3.13a).

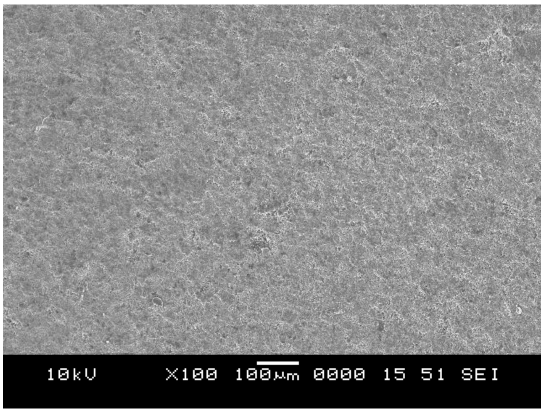

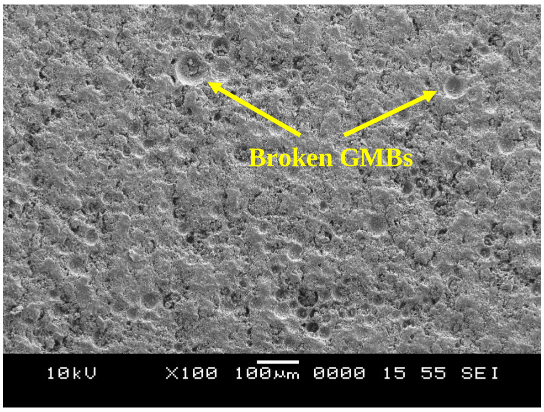

(a) (b)

Figure 3.13 Micrography of hole wall surface of (a) neat epoxy and (b) E200-60 specimens post drilling.

3.2.3 Specific cutting coefficient

Table 3.6 presents the experimentally measured values of specific cutting coefficient for neat epoxy and their syntactic foams.

Table 3.6 Experimentally measured values of specific cutting coefficient for neat epoxy and their syntactic foams.

v	*f*	*D*	E0	E200			E270			E350		
				R_{20}	R_{40}	R_{60}	R_{20}	R_{40}	R_{60}	R_{20}	R_{40}	R_{60}
25	0.04	8	429.19	245.25	183.94	122.63	245.25	245.25	183.94	245.25	245.25	183.94
		12	449.63	245.25	204.38	163.50	286.13	245.25	204.38	286.13	286.13	204.38
		16	490.50	275.91	245.25	183.94	306.56	245.25	183.94	398.53	275.91	245.25
	0.08	8	306.56	153.28	153.28	91.97	183.94	153.28	122.63	183.94	153.28	122.63
		12	327.00	183.94	163.50	102.19	183.94	163.50	143.06	183.94	143.06	122.63
		16	337.22	183.94	168.61	122.63	229.92	183.94	137.95	245.25	183.94	153.28
	0.12	8	224.81	122.63	122.63	81.75	122.63	122.63	81.75	143.06	122.63	81.75
		12	245.25	136.25	122.63	95.38	136.25	122.63	95.38	149.88	122.63	95.38
		16	255.47	143.06	132.84	102.19	173.72	143.06	112.41	173.72	132.84	102.19
75	0.04	8	367.88	183.94	183.94	122.63	245.25	245.25	183.94	245.25	245.25	183.94
		12	408.75	204.38	204.38	122.63	245.25	245.25	163.50	327.00	245.25	163.50
		16	459.84	245.25	214.59	153.28	306.56	245.25	183.94	367.88	245.25	214.59
	0.08	8	275.91	153.28	122.63	91.97	153.28	153.28	122.63	183.94	153.28	122.63
		12	286.13	163.50	143.06	102.19	183.94	163.50	122.63	224.81	163.50	143.06
		16	291.23	168.61	153.28	107.30	214.59	183.94	122.63	229.92	183.94	168.61
	0.12	8	224.81	102.19	102.19	61.31	122.63	122.63	81.75	143.06	122.63	102.19
		12	231.63	122.63	109.00	81.75	136.25	122.63	81.75	149.88	122.63	95.38
		16	235.03	122.63	112.41	91.97	153.28	132.84	102.19	183.94	143.06	122.63
125	0.04	8	306.56	183.94	183.94	122.63	245.25	183.94	122.63	306.56	183.94	122.63
		12	408.75	204.38	204.38	122.63	245.25	245.25	163.50	367.88	245.25	204.38
		16	429.19	214.59	214.59	122.63	275.91	245.25	183.94	367.88	275.91	245.25
	0.08	8	275.91	122.63	122.63	61.31	153.28	153.28	91.97	214.59	153.28	122.63
		12	265.69	143.06	122.63	81.75	183.94	143.06	122.63	183.94	163.50	143.06
		16	275.91	153.28	137.95	91.97	199.27	168.61	122.63	275.91	199.27	168.61

v	f	D	E0	E200			E270			E350		
				R_{20}	R_{40}	R_{60}	R_{20}	R_{40}	R_{60}	R_{20}	R_{40}	R_{60}
		8	204.38	102.19	81.75	61.31	122.63	122.63	81.75	204.38	122.63	102.19
	0.12	12	218.00	109.00	95.38	68.13	149.88	109.00	81.75	149.88	136.25	109.00
		16	224.81	122.63	112.41	71.53	153.28	132.84	102.19	194.16	163.50	122.63

Table 3.7 Summary of ANOVA results for the developed mathematical models of specific cutting coefficient.

Responses	Sum of squares		Degrees of freedom		Mean square		F-ratio	P-Value	CoD
	Regression	Residual	Regression	Residual	Regression	Residual			
$K_{f(E200)}$	1.87×10^5	5.92×10^3			1.34×10^4	89.66	149.37[a]	<0.001	0.9694
$K_{f(E270)}$	2.48×10^5	8.85×10^3	14	66	1.77×10^4	134.07	131.95[a]	<0.001	0.9655
$K_{f(E350)}$	3.68×10^5	2.56×10^4			2.63×10^4	387.83	67.87[a]	<0.001	0.9350

[a]F-table = 2.36. Significance at 99 % confidence interval

3.2.3.1 Development of mathematical models based on experimental data

Minitab 14 software is used to develop the mathematical models for specific cutting coefficient of different syntactic foams based on the experimental results presented in Table 3.6. Regression equations for predicting the specific cutting coefficient of different syntactic foams are given as,

$$K_{f(E200)} = \begin{pmatrix} 273.94 - 0.53 \times v - 2698.98 \times f + 0.70 \times R + 7.76 \times D + 0.001 \times v^2 + 8515.65 \times \\ f^2 - 0.04 \times R^2 - 0.04 \times D^2 + 0.85 \times v \times f + 0.002 \times v \times R - 0.01 \times v \times D + 13.84 \\ \times f \times R - 28.39 \times f \times D - 0.01 \times R \times D \end{pmatrix} \tag{3.7}$$

$$K_{f(E270)} = \begin{pmatrix} 356.57 - 0.38 \times v - 3468.93 \times f + 0.66 \times R + 3.32 \times D - 0.0001 \times v^2 + 9501.22 \\ \times f^2 - 0.03 \times R^2 + 0.16 \times D^2 + 2.51 \times v \times f - 0.001 \times v \times R + 0.01 \times v \times D + 13.13 \\ \times f \times R - 8.87 \times f \times D - 0.08 \times R \times D \end{pmatrix} \tag{3.8}$$

$$K_{f(E350)} = \begin{pmatrix} 457.05 - 0.26 \times v - 3739.77 \times f - 4.24 \times R + 2.24 \times D + 0.002 \times v^2 + 13443.62 \\ \times f^2 + 0.02 \times R^2 + 0.50 \times D^2 + 3.22 \times v \times f - 0.01 \times v \times R + 0.01 \times v \times D + 20.34 \\ \times f \times R - 83.38 \times f \times D - 0.06 \times R \times D \end{pmatrix} \tag{3.9}$$

Equation 3.7-Equation 3.9 are used to predict the specific cutting coefficient of the drilled hole within the chosen range of input process parameters. ANOVA is used to check the adequacy of the developed mathematical models and the results are presented in Table 3.7. Higher CoD values of the developed mathematical models (Equation 3.7-Equation 3.9) of specific cutting coefficient for E200 (0.97), E270 (0.97) and E350 (0.94) syntactic foams indicate a good correlation is existing between the experimental and predicted values. The average errors between the experimental and predicted values are found to be 0.33, 0.39 and 0.73% for specific cutting coefficient of E200, E270 and E350 syntactic foams respectively as shown in Figure 3.14. Hence, the developed mathematical models can be effectively used as a tool in industrial practices to predict the specific cutting coefficient of GMB reinforced epoxy foams during drilling.

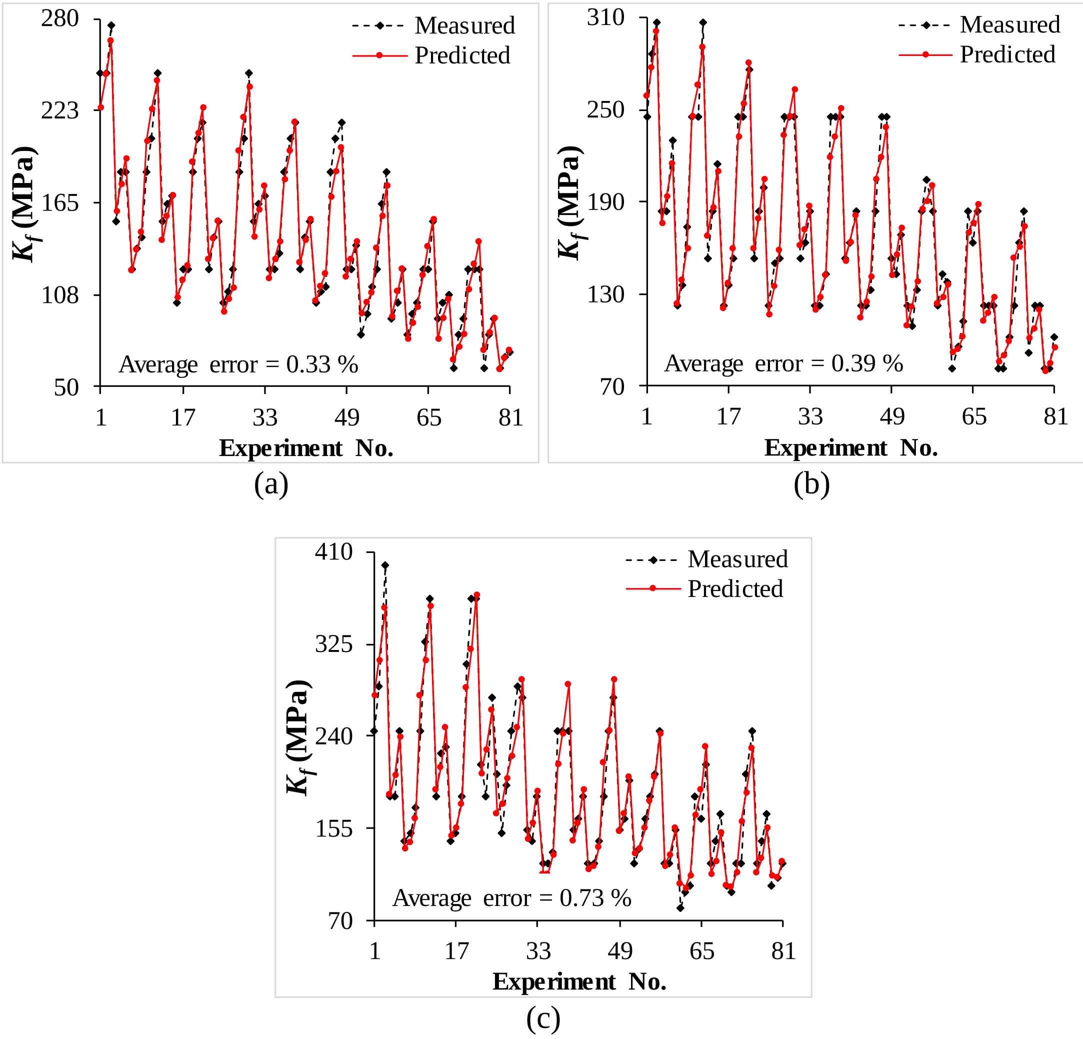

Figure 3.14 Comparison between measured and predicted values of K_f for (a) E200, (b) E270 and (c) E350 syntactic foams.

3.2.3.2 Effects of individual parameters

Input parameters (v, f, R and D) are varied one at a time within the chosen range, keeping the other parameters at intermediate level in Equation 3.7-Equation 3.9 to predict the trend of K_f as presented in Figure 3.15. K_f of all the syntactic foams decreases with increasing feed (Figure 3.15a, Figure 3.15c and Figure 3.15e), filler content and decreasing drill diameter (Figure 3.15b, Figure 3.15d and Figure 3.15f). With increasing v the K_f is found to be decreasing for E200 and E270 syntactic foam as shown in Figure 3.15a and Figure 3.15c while it marginally increases for E350 syntactic foam (Figure 3.15e). These plots can serve as a reference to understand the general relationships among various parameters.

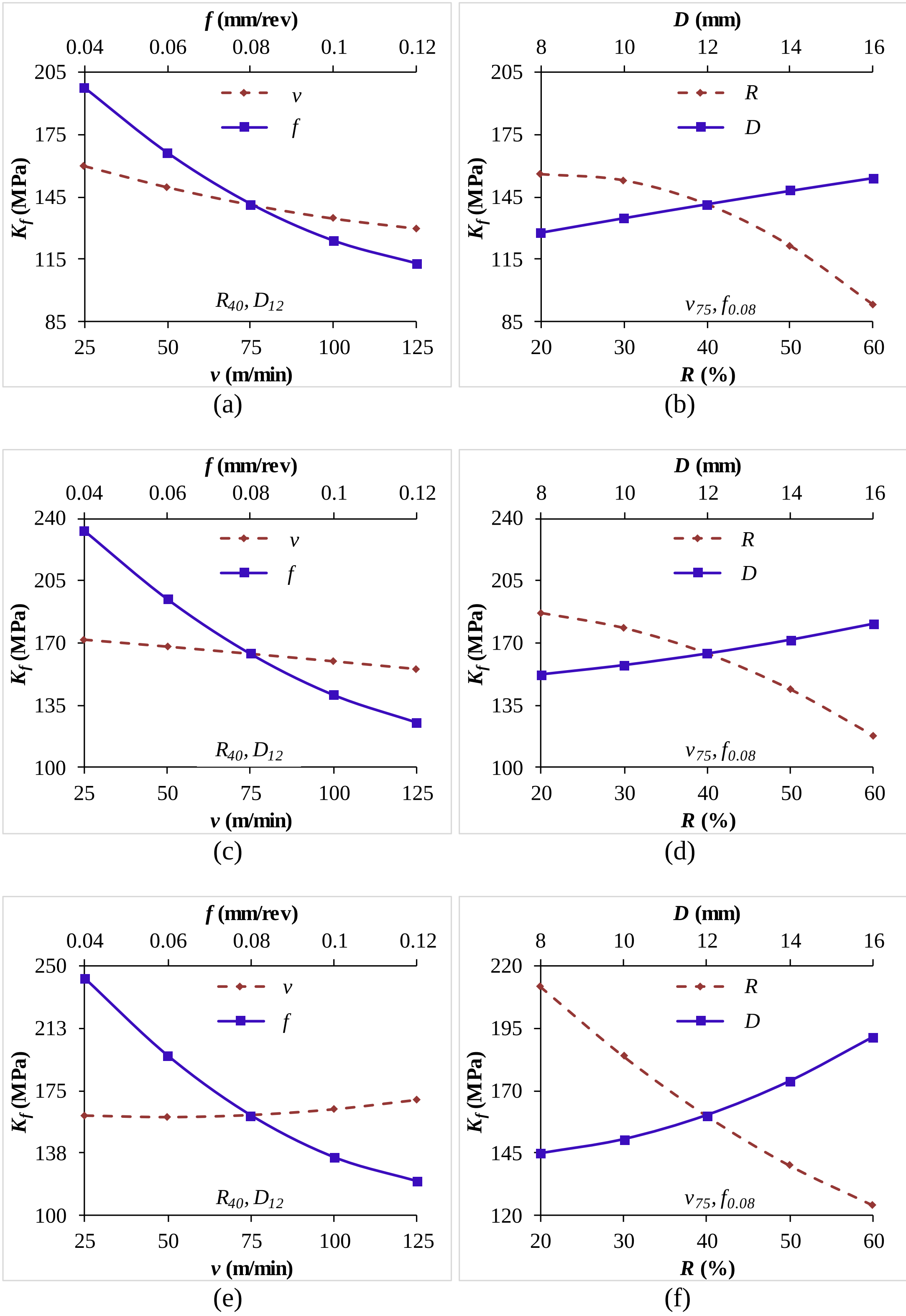

Figure 3.15 Individual effect plots of K_f for (a-b) E200, (c-d) E270 and (e-f) E350 syntactic foams.

3.2.3.3 Effects of two-parameter interactions

Two parameters are varied at the same time while keeping the other two parameters at their intermediate levels in Equation 3.7-Equation 3.9 to study the interaction effects among the input process parameters on the K_f.

Specific cutting coefficient is observed to be decreasing with increasing cutting speed for E200 (Figure 3.16a) and E270 (Figure 3.17a) SFs while it marginally increases for E350 SF (Figure 3.18a). With increasing the cutting speed from v_{25} - v_{125}, K_f decreases in the range of 18-20 and 7-12% for E200 and E270 SFs respectively. Decreased thrust force at higher cutting speed is the likely reason for decreased specific cutting coefficient. K_f is found to be increased in the range of 5-7% for E350 SF due to increased thrust forces at higher cutting speed (Davim et al. 2003). A similar effect of cutting speed on K_f is observed for all the syntactic foams at different levels of feed as shown in Figure 3.16b, Figure 3.17b and Figure 3.18b. K_f decreases in the range of 16-21 and 5-11% for E200 and E270 syntactic foams, while it increases in the range of 1-20% with increasing cutting speed for E350 syntactic foam.

Specific cutting coefficient is found to be decreasing with increasing GMB content as shown in Figure 3.16c, Figure 3.17c and Figure 3.18c for E200, E270 and E350 SFs respectively. K_f is observed to be decreased in the range of 67-69, 59-61 and 51-61% for E200, E270 and E350 SFs respectively as compared to neat epoxy with increasing speed. Lower K_f is attributed to the reduced thrust forces with increasing filler content (Basavarajappa et al. 2011, Davim et al. 2003). Figure 3.16d, Figure 3.17d and Figure 3.18d show the variation of K_f with feed and drill diameter for E200, E270 and E350 SFs respectively. Specific cutting coefficient decreases with increasing feed and decreasing drill diameter. K_f decreases in the range of 42-44, 44-48 and 45-52% with increasing feed from $f_{0.04}$ - $f_{0.12}$ for E200, E270 and E350 SFs respectively at different levels of drill diameter. At low feeds, the material is subjected to lower strain rates leading to increased specific cutting coefficient (Basavarajappa et al. 2011).

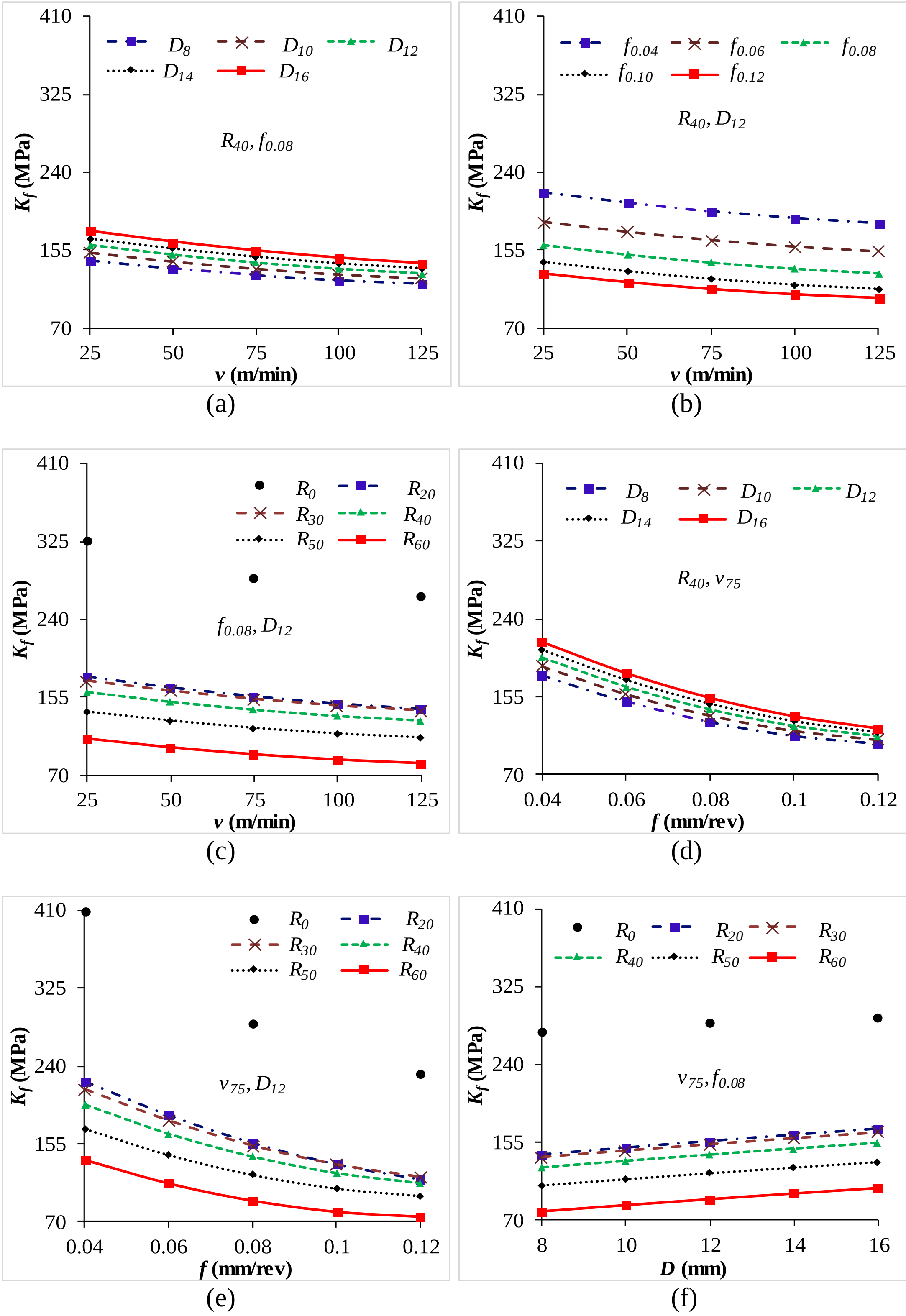

Figure 3.16 Variation of K_f with respect to v at different (a) D, (b) f and (c) R. K_f with respect to f at different (d) D and (e) R. (f) K_f with respect to D at different R for E200 syntactic foam.

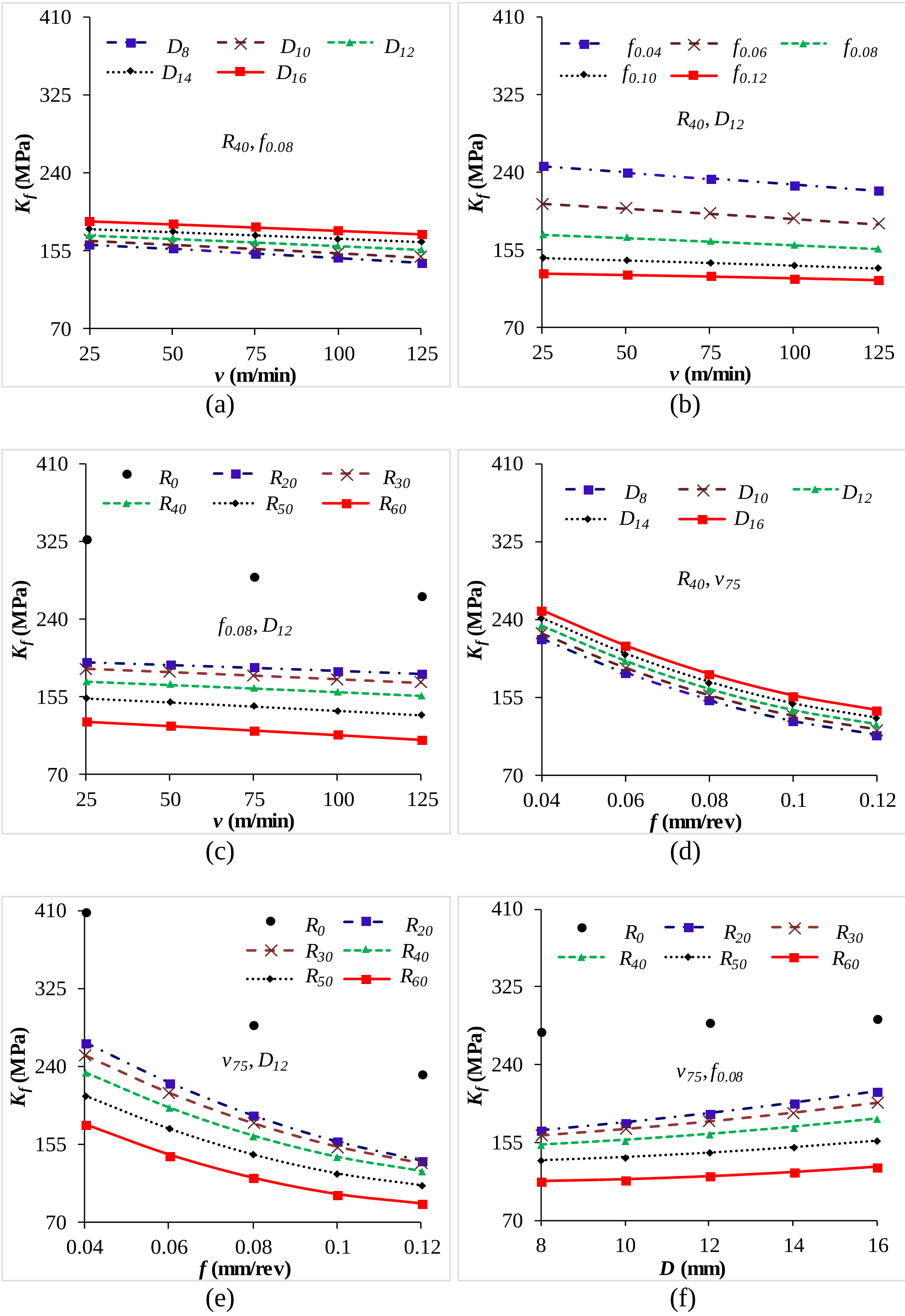

Figure 3.17 Variation of K_f with respect to v at different (a) D, (b) f and (c) R. K_f with respect to f at different (d) D and (e) R. (f) K_f with respect to D at different R for E270 syntactic foam.

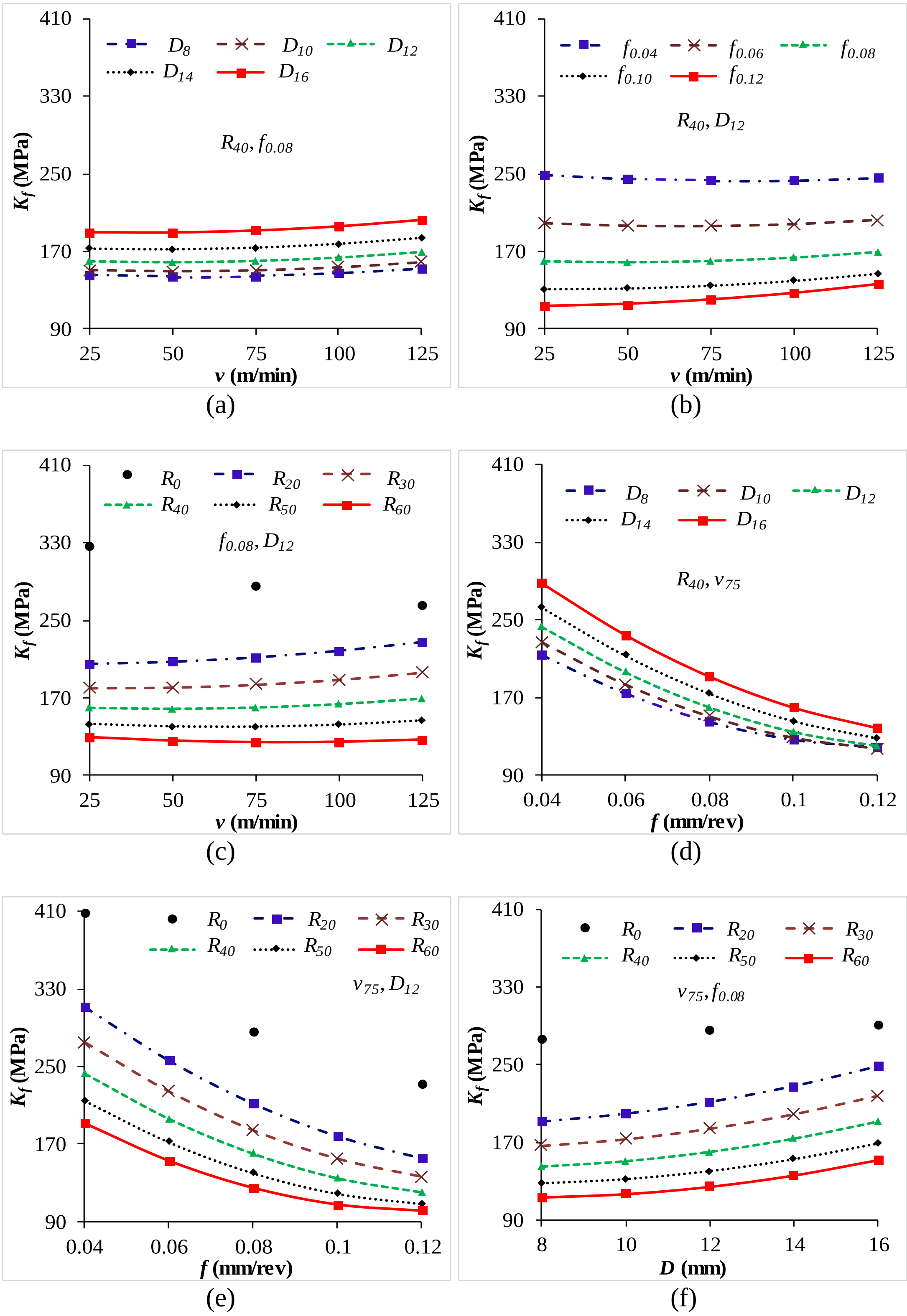

Figure 3.18 Variation of K_f with respect to v at different (a) D, (b) f and (c) R. K_f with respect to f at different (d) D and (e) R. (f) K_f with respect to D at different R for E350 syntactic foam.

The variation of specific cutting coefficient with filler content at various feeds are shown in Figure 3.16e, Figure 3.17e and Figure 3.18e for E200, E270 and E350 syntactic foams respectively. K_f decreases in the range of 66-68, 57-61 and 53-57% for E200, E270 and E350 syntactic foams respectively as compared to neat epoxy with increasing feed.

Specific cutting coefficient increases with increasing drill diameter and decreasing filler content for all the syntactic foams (Figure 3.16f, Figure 3.17f and Figure 3.18f). Increasing drill diameter increases K_f in the range of 20-32, 14-25 and 29-33% for E200, E270 and E350 syntactic foams respectively at different levels of filler content. Increasing thrust force with increasing drill diameter results in higher values of specific cutting coefficient (Davim et al. 2003, Gaitonde et al. 2010).

3.2.4 Cylindricity

Cylindricity is a 3D tolerance which refers to the degree by which the entire cylinder deviates or in other words it is a surface of revolution in which all the points of the surface are equidistant from a common axis (Kim and Ramulu 2004). Experimentally measured values of cylindricity for neat epoxy and their syntactic foams are presented in Table 3.8.

Table 3.8 Experimentally measured values of cylindricity for neat epoxy and their syntactic foams.

v	*f*	*D*	E0	E200			E270			E350		
				R_{20}	R_{40}	R_{60}	R_{20}	R_{40}	R_{60}	R_{20}	R_{40}	R_{60}
25	0.04	8	0.037	0.030	0.022	0.022	0.021	0.010	0.010	0.013	0.010	0.010
		12	0.061	0.030	0.029	0.024	0.023	0.019	0.014	0.018	0.018	0.012
		16	0.066	0.037	0.035	0.030	0.035	0.030	0.027	0.030	0.028	0.022
	0.08	8	0.040	0.030	0.030	0.024	0.023	0.014	0.014	0.016	0.014	0.014
		12	0.066	0.033	0.031	0.030	0.031	0.026	0.023	0.024	0.017	0.018
		16	0.081	0.044	0.038	0.035	0.041	0.034	0.030	0.039	0.033	0.028
	0.12	8	0.053	0.034	0.033	0.031	0.027	0.024	0.020	0.019	0.016	0.015
		12	0.072	0.038	0.035	0.032	0.031	0.028	0.026	0.019	0.023	0.023
		16	0.090	0.073	0.047	0.043	0.059	0.043	0.041	0.045	0.043	0.036
75	0.04	8	0.040	0.030	0.024	0.022	0.022	0.017	0.014	0.012	0.007	0.007
		12	0.065	0.033	0.031	0.027	0.024	0.024	0.019	0.015	0.012	0.012
		16	0.070	0.040	0.040	0.037	0.039	0.038	0.028	0.025	0.020	0.020
	0.08	8	0.046	0.031	0.030	0.025	0.024	0.024	0.016	0.016	0.016	0.010
		12	0.073	0.037	0.036	0.034	0.034	0.031	0.026	0.023	0.016	0.014
		16	0.089	0.052	0.043	0.040	0.048	0.041	0.037	0.028	0.028	0.027
	0.12	8	0.057	0.035	0.034	0.031	0.028	0.027	0.022	0.021	0.013	0.014
		12	0.080	0.040	0.039	0.035	0.040	0.035	0.033	0.021	0.021	0.015
		16	0.101	0.087	0.053	0.048	0.067	0.048	0.041	0.035	0.032	0.029
125	0.04	8	0.042	0.031	0.030	0.024	0.022	0.020	0.017	0.012	0.014	0.013
		12	0.083	0.035	0.033	0.031	0.028	0.026	0.025	0.019	0.022	0.018
		16	0.086	0.051	0.041	0.041	0.047	0.039	0.033	0.035	0.032	0.024
	0.08	8	0.048	0.033	0.031	0.025	0.028	0.026	0.018	0.023	0.016	0.016
		12	0.086	0.043	0.038	0.034	0.041	0.033	0.030	0.023	0.018	0.019
		16	0.093	0.092	0.058	0.042	0.054	0.044	0.041	0.048	0.042	0.031

v	f	D	E0	E200			E270			E350		
				R_{20}	R_{40}	R_{60}	R_{20}	R_{40}	R_{60}	R_{20}	R_{40}	R_{60}
		8	0.058	0.037	0.034	0.032	0.037	0.031	0.026	0.018	0.021	0.016
	0.12	12	0.101	0.087	0.043	0.040	0.043	0.040	0.033	0.027	0.024	0.024
		16	0.104	0.092	0.073	0.055	0.071	0.069	0.045	0.047	0.045	0.037

Table 3.9 Summary of ANOVA results for the developed mathematical models of cylindricity.

Responses	Sum of squares		Degrees of freedom		Mean square		F-ratio	P-Value	CoD
	Regression	Residual	Regression	Residual	Regression	Residual			
$CYL_{(E200)}$	1.57×10^{-2}	2.39×10^{-3}			1.12×10^{-3}	3.62×10^{-5}	30.93[a]	<0.001	0.8677
$CYL_{(E270)}$	1.20×10^{-2}	6.11×10^{-4}	14	66	8.58×10^{-4}	9.62×10^{-6}	92.65[a]	<0.001	0.9516
$CYL_{(E350)}$	6.99×10^{-3}	5.40×10^{-4}			5.00×10^{-4}	8.18×10^{-6}	61.08[a]	<0.001	0.9284

[a]F-table = 2.36. Significance at 99 % confidence interval

3.2.4.1 Development of mathematical models based on experimental data

Mathematical models for cylindricity are developed based on experimental results (Table 3.8) using Minitab 14 software. Regression equations for predicting the cylindricity of different syntactic foams are given as,

$$CYL_{(E200)} = \begin{pmatrix} 0.047 - 0.0002 \times v - 0.196 \times f + 0.0004 \times R - 0.005 \times D + 7.26 \times 10^{-7} \times v^2 + \\ 0.961 \times f^2 + 4.95 \times 10^{-6} \times R^2 + 0.0002 \times D^2 + 0.001 \times v \times f - 2.75 \times 10^{-6} \times v \times \\ R + 1.97 \times 10^{-5} \times v \times D - 0.004 \times f \times R + 0.027 \times f \times D - 4.93 \times 10^{-5} \times R \times D \end{pmatrix} \tag{3.10}$$

$$CYL_{(E270)} = \begin{pmatrix} 0.024 + 1.28 \times 10^{-5} \times v - 0.045 \times f + 0.0001 \times R - 0.003 \times D - 2.22 \times 10^{-8} \times v^2 \\ +0.486 \times f^2 + 6.94 \times 10^{-7} \times R^2 + 0.0002 \times D^2 + 0.0004 \times v \times f - 4.72 \times 10^{-7} \times \\ v \times R + 5.69 \times 10^{-6} \times v \times D - 0.001 \times f \times R + 0.014 \times f \times D - 2.19 \times 10^{-5} \times R \times D \end{pmatrix} \tag{3.11}$$

$$CYL_{(E350)} = \begin{pmatrix} 0.035 - 0.0003 \times v + 0.094 \times f + 0.0001 \times R - 0.005 \times D + 1.99 \times 10^{-6} \times v^2 - \\ 0.637 \times f^2 - 3.24 \times 10^{-7} \times R^2 + 0.0003 \times D^2 - 0.0001 \times v \times f - 2.50 \times 10^{-7} \times v \\ \times R + 2.08 \times 10^{-6} \times v \times D - 0.0001 \times f \times R + 0.010 \times f \times D - 1.49 \times 10^{-5} \times R \times D \end{pmatrix} \tag{3.12}$$

Equation 3.10-Equation 3.12 are used to predict the cylindricity within the chosen range of input process parameters. Adequacy of the developed mathematical models are confirmed using ANOVA and the results are presented in Table 3.9. According to ANOVA, the computed F-ratio should be more than the F-table for the models to be adequate. Higher CoD values of the developed mathematical models of cylindricity for E200 (0.87), E270 (0.95) and E350 (0.93) syntactic foams indicate a good correlation is existing between the experimental and predicted values. The average errors between the experimental and predicted values are found to be 0.96, 0.90 and 0.98% for cylindricity of E200, E270 and E350 syntactic foams respectively as shown in Figure 3.19. Hence, the developed mathematical models can be effectively used as a tool in industrial practices to predict the cylindricity of GMB reinforced epoxy foams during drilling.

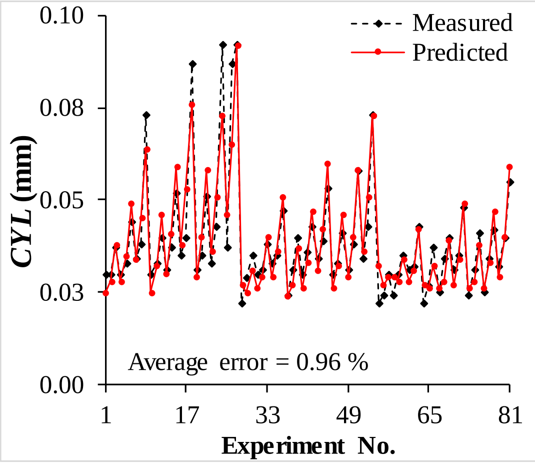

(a)

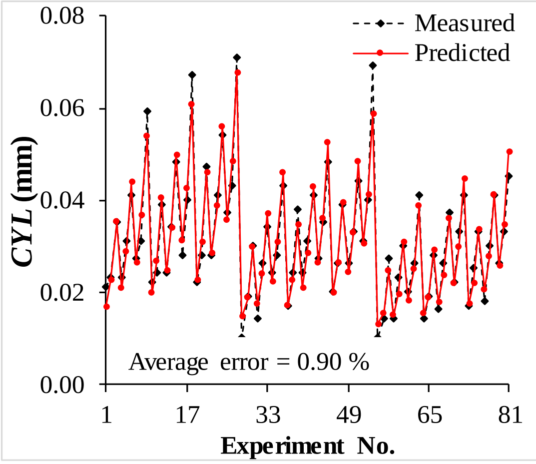

(b)

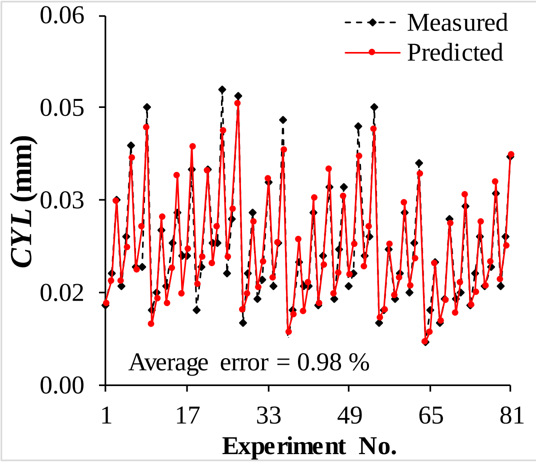

(c)

Figure 3.19 Comparison between measured and predicted values of *CYL* for (a) E200, (b) E270 and (c) E350 syntactic foams.

3.2.4.2 Effects of individual parameters

Cutting speed, feed, drill diameter and filler content are varied one at a time within the chosen range, keeping the other parameters at intermediate level in Equation 3.10-Equation 3.12 for predicting the trend of *CYL* and to identify significant process parameter (Figure 3.20). *CYL* of all the foams increases with increasing *f* (Figure 3.20a, Figure 3.20c and Figure 3.20e) but decreases with increasing *R* and decreasing *D* (Figure 3.20b, Figure 3.20d and Figure 3.20f). With increasing *v*, the *CYL* is found to be increasing for E200 and E270 foams as shown in Figure 3.20a and Figure 3.20c while it decreases up to v_{25} and later found to be increasing beyond for E350 foam (Figure 3.20e). These plots can serve as a reference to understand the general relationships among various parameters.

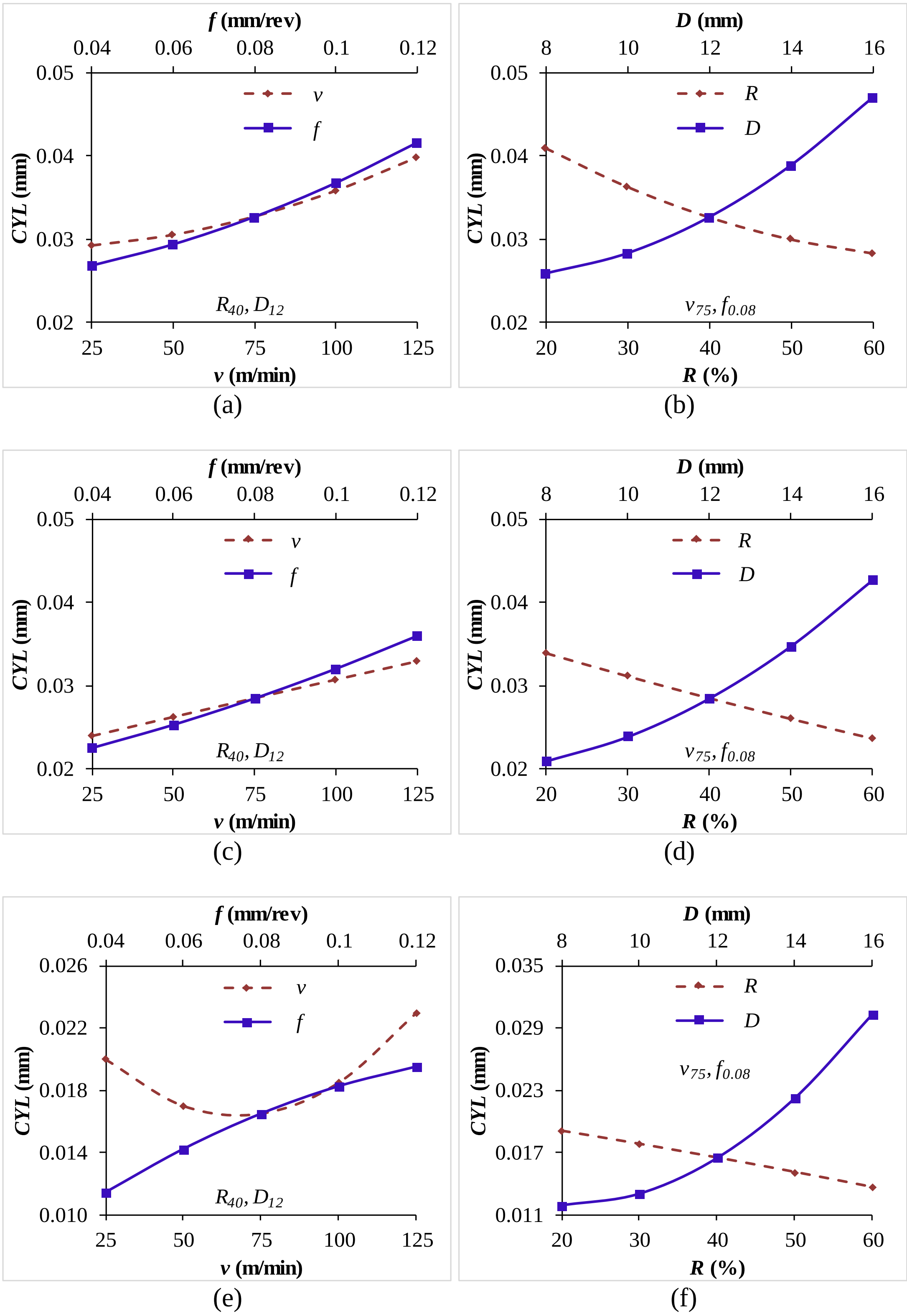

Figure 3.20 Individual effect plots of *CYL* for (a-b) E200, (c-d) E270 and (e-f) E350 syntactic foams.

3.2.4.3 Effects of two-parameter interactions

Interaction effects among the input process parameters on the cylindricity in drilling of syntactic foams are studied by varying two parameters at the same time in Equation 3.10-Equation 3.12 while keeping the other two parameters at their intermediate levels as per the scheme presented in Table 2.6.

Cylindricity is found to be increasing with increasing cutting speed for E200 (Figure 3.21a) and E270 (Figure 3.22a) SF, while it decreases up to v_{75} for E350 SF and later found to be increasing (Figure 3.23a). With the increasing v from v_{25} - v_{125}, CYL increases in the range of 7-45, 31-40 and 10-13% for E200, E270 and E350 SFs respectively. At higher cutting speeds the vibration of the cutting tool increases, which leads to the scatting of machine main shaft resulting higher CYL values (Kurt et al. 2008). Cylindricity as a function of cutting speed and feed is presented in Figure 3.21b, Figure 3.22b and Figure 3.23b for all the SFs. CYL is found to be increased in the range of 24-38, 35-40 and 9-20% for E200, E270 and E350 SFs respectively with increasing cutting speed at different levels of feed.

The variation of cylindricity with cutting speed at different filler content is shown in Figure 3.21c, Figure 3.22c and Figure 3.23c for E200, E270 and E350 SFs respectively. CYL decreases in the range of 58-63, 68-71 and 74-82% as compared to neat epoxy for E200, E270 and E350 SFs respectively. Increasing the GMB content decreases the thrust force generated during drilling leading to reduced cylindricity values (Basavarajappa et al. 2011, Gaitonde et al. 2011, Gowda et al. 2014). CYL is found to increase with increasing feed and drill diameter as shown in Figure 3.21d, Figure 3.22d and Figure 3.23d for all the SFs. CYL increases in the range of 27-64, 52-60 and 49-78% for E200, E270 and E350 SFs respectively with increasing feed from $f_{0.04}$ - $f_{0.12}$. At lower feeds, the tool moves slowly along the axis of the hole leading to lower CYL values or in other words better tool stability at lower feeds leads to reduced CYL values (Sultan et al. 2015). Also, at larger feeds thrust force increases due to the friction between tool and syntactic foams resulting higher CYL values (Basavarajappa et al. 2011, Gowda et al. 2014).

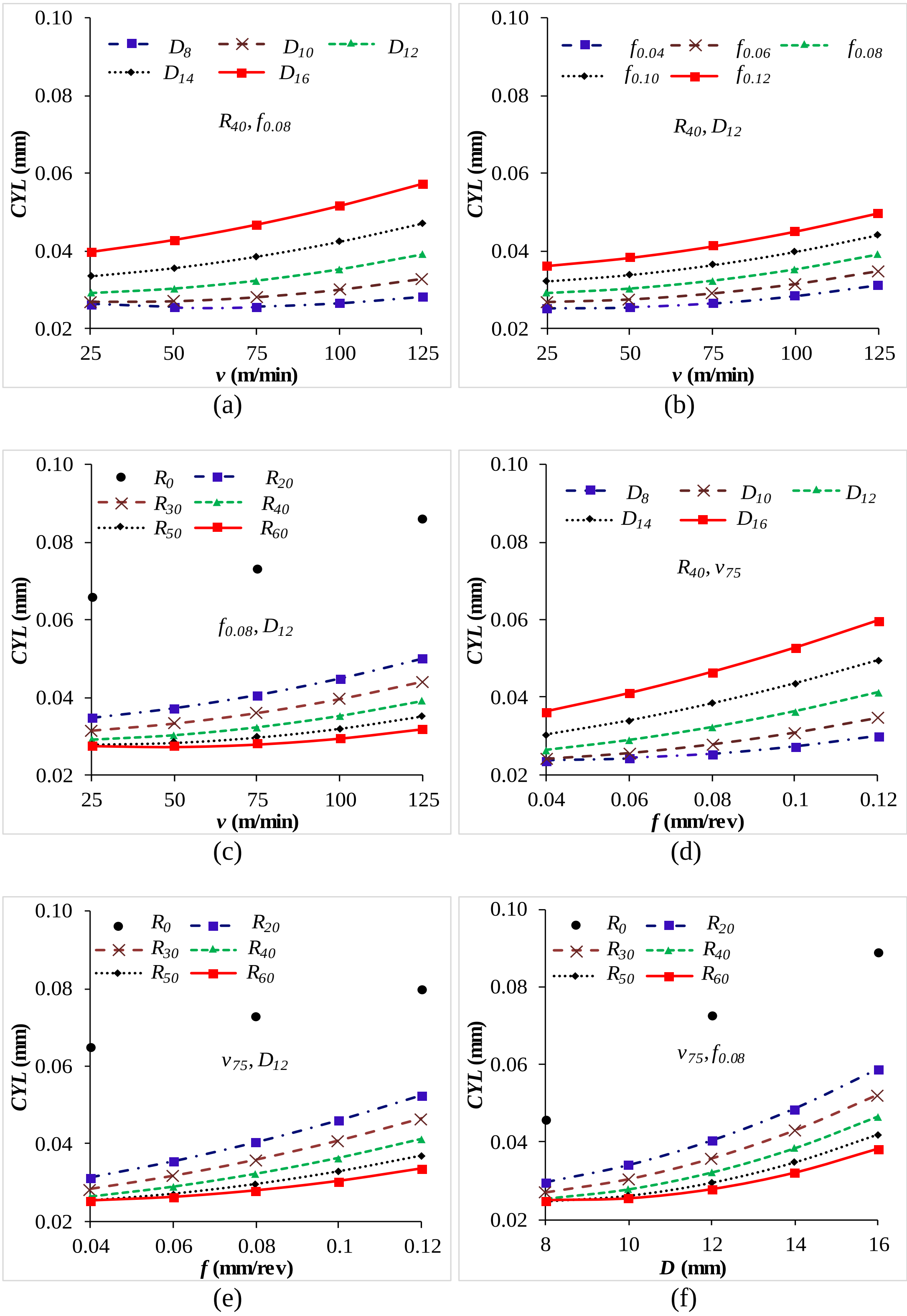

Figure 3.21 Variation of *CYL* with respect to *v* at different (a) *D*, (b) *f* and (c) *R*. *CYL* with respect to *f* at different (d) *D* and (e) *R*. (f) *CYL* with respect to *D* at different *R* for E200 syntactic foam.

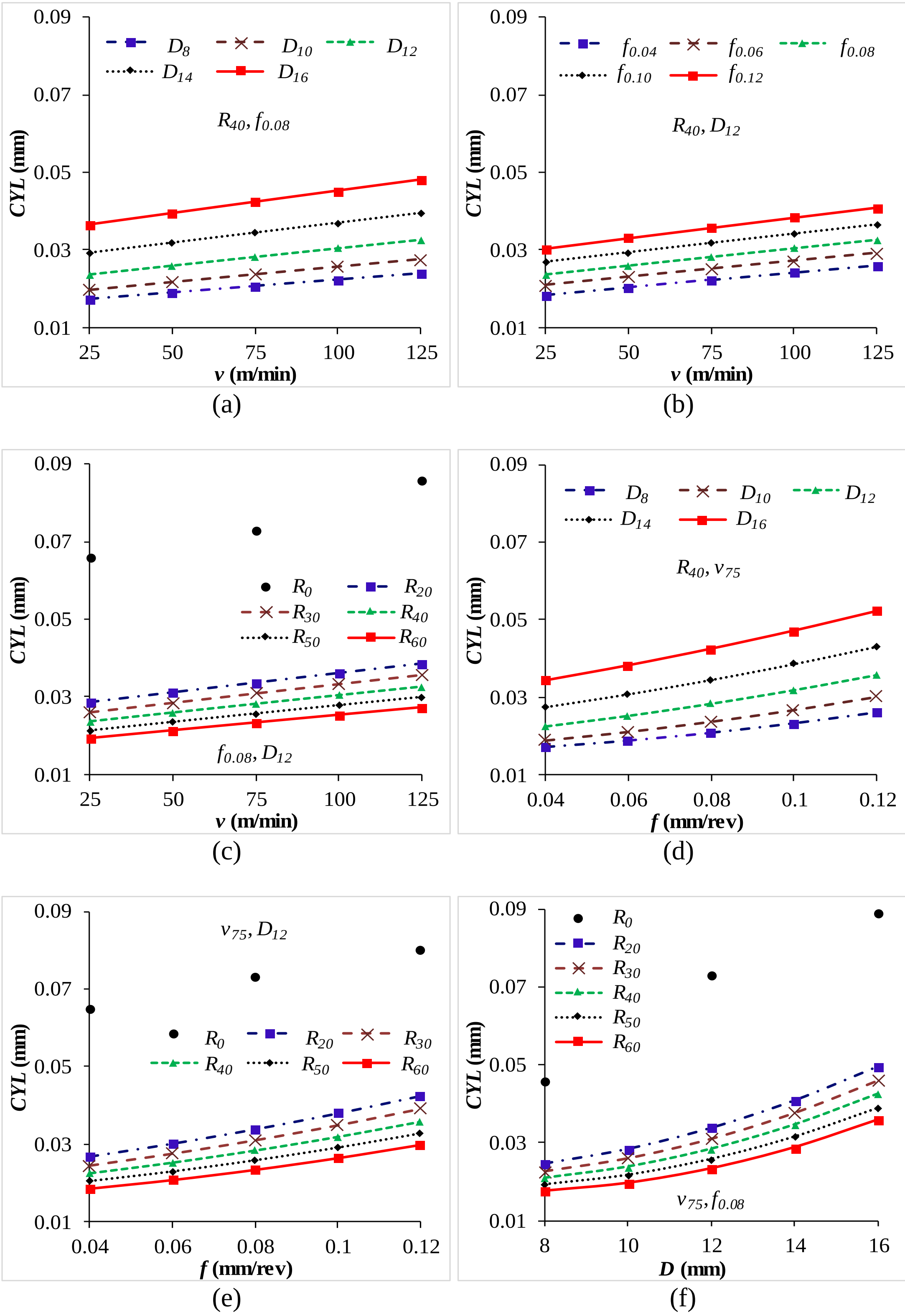

Figure 3.22 Variation of *CYL* with respect to *v* at different (a) *D*, (b) *f* and (c) *R*. *CYL* with respect to *f* at different (d) *D* and (e) *R*. (f) *CYL* with respect to *D* at different *R* for E270 syntactic foam.

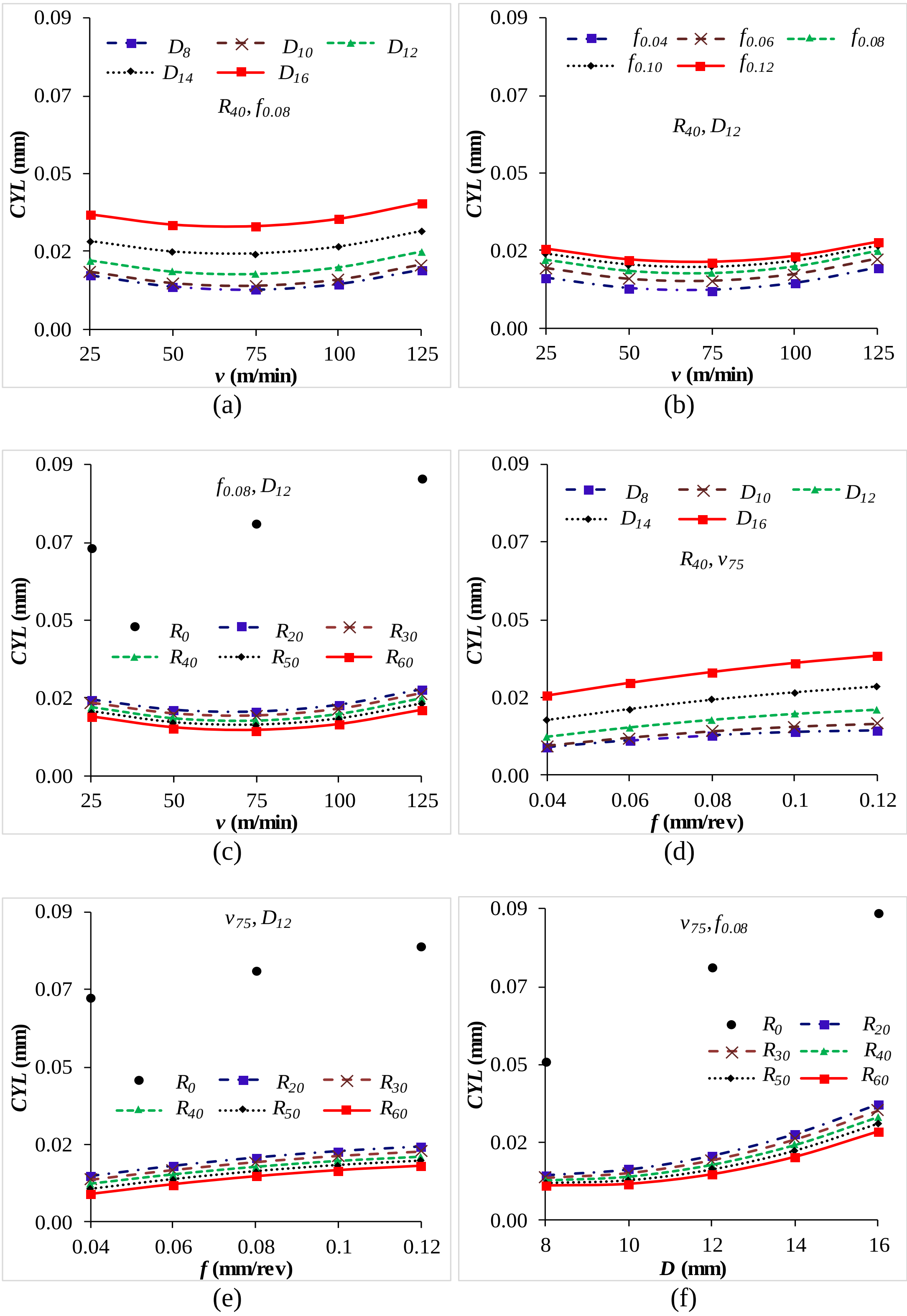

Figure 3.23 Variation of *CYL* with respect to *v* at different (a) *D*, (b) *f* and (c) *R*. *CYL* with respect to *f* at different (d) *D* and (e) *R*. (f) *CYL* with respect to *D* at different *R* for E350 syntactic foam.

Figure 3.21e, Figure 3.22e and Figure 3.23e show variation of cylindricity as a function of feed and filler content for E200, E270 and E350 SFs respectively. Cylindricity is found to be increasing with increasing feed and decreasing filler content. It reduces in the range of 58-62, 63-71 and 80-87% compared to that of neat epoxy for E200, E270 and E350 SFs respectively.

The variation of cylindricity with drill diameter at different levels of filler content is presented in Figure 3.21f, Figure 3.22f and Figure 3.23f for all the syntactic foams. With increasing drill diameter from D_8 - D_{16}, CYL increases in the range of 53-97, 103-104 and 159-162% for E200, E270 and E350 SFs respectively. As drill diameter increases, thrust force increases due to the increased contact area of the drilled hole leading to higher cylindricity values (El-Sonbaty et al. 2004, Gowda et al. 2014).

3.2.5 Exit side circularity error

Circularity error is a 2D radial tolerance that describes how close is a part with a diametrical cross-section to a true circle (Giasin and Ayvar-Soberanis 2017). Experimentally measured values of circularity error for neat epoxy and their syntactic foams are presented in Table 3.10.

Table 3.10 Experimentally measured values of exit side circularity error for neat epoxy and their syntactic foams.

v	f	D	E0	E200			E270			E350		
				R_{20}	R_{40}	R_{60}	R_{20}	R_{40}	R_{60}	R_{20}	R_{40}	R_{60}
25	0.04	8	0.034	0.030	0.027	0.024	0.017	0.018	0.013	0.007	0.007	0.006
		12	0.049	0.070	0.041	0.030	0.026	0.031	0.025	0.017	0.016	0.009
		16	0.069	0.096	0.049	0.044	0.045	0.038	0.026	0.027	0.024	0.023
	0.08	8	0.021	0.026	0.026	0.019	0.013	0.010	0.007	0.005	0.004	0.004
		12	0.043	0.036	0.031	0.030	0.026	0.021	0.010	0.013	0.008	0.007
		16	0.064	0.064	0.044	0.042	0.039	0.029	0.02	0.021	0.016	0.013
	0.12	8	0.018	0.024	0.019	0.016	0.007	0.006	0.004	0.005	0.003	0.003
		12	0.034	0.030	0.029	0.021	0.016	0.008	0.009	0.011	0.006	0.005
		16	0.055	0.060	0.036	0.031	0.02	0.027	0.015	0.018	0.013	0.011
75	0.04	8	0.050	0.038	0.033	0.028	0.022	0.018	0.017	0.012	0.011	0.010
		12	0.059	0.085	0.044	0.036	0.03	0.033	0.028	0.023	0.019	0.014
		16	0.080	0.115	0.057	0.056	0.051	0.048	0.036	0.039	0.032	0.026
	0.08	8	0.027	0.030	0.027	0.026	0.014	0.012	0.011	0.010	0.010	0.009
		12	0.050	0.046	0.039	0.034	0.029	0.026	0.016	0.019	0.014	0.011
		16	0.069	0.064	0.046	0.044	0.043	0.035	0.031	0.033	0.028	0.026
	0.12	8	0.019	0.025	0.023	0.018	0.010	0.008	0.009	0.007	0.007	0.007
		12	0.036	0.033	0.031	0.026	0.021	0.010	0.014	0.013	0.013	0.010
		16	0.063	0.064	0.041	0.040	0.039	0.033	0.019	0.027	0.025	0.017
125	0.04	8	0.050	0.043	0.040	0.030	0.031	0.028	0.021	0.016	0.015	0.014
		12	0.067	0.088	0.049	0.044	0.041	0.034	0.028	0.024	0.022	0.022
		16	0.089	0.150	0.068	0.060	0.056	0.061	0.055	0.045	0.040	0.037
	0.08	8	0.044	0.032	0.030	0.026	0.023	0.015	0.013	0.013	0.011	0.010
		12	0.056	0.049	0.043	0.040	0.028	0.031	0.023	0.023	0.020	0.017
		16	0.076	0.078	0.051	0.047	0.053	0.039	0.034	0.040	0.037	0.031

v	f	D	E0	E200			E270			E350		
				R_{20}	R_{40}	R_{60}	R_{20}	R_{40}	R_{60}	R_{20}	R_{40}	R_{60}
		8	0.024	0.030	0.025	0.019	0.023	0.013	0.011	0.018	0.010	0.010
	0.12	12	0.051	0.042	0.033	0.031	0.028	0.026	0.020	0.023	0.018	0.017
		16	0.073	0.067	0.043	0.042	0.043	0.039	0.030	0.042	0.039	0.029

Table 3.11 Summary of ANOVA results for the developed mathematical models of exit side circularity error.

Responses	Sum of squares		Degrees of freedom		Mean square		F-ratio	P-Value	CoD
	Regression	Residual	Regression	Residual	Regression	Residual			
$C_{e\text{-}Exit(E200)}$	3.49×10^{-2}	4.27×10^{-3}			2.50×10^{-3}	6.46×10^{-5}	38.62[a]	<0.001	0.8912
$C_{e\text{-}Exit(E270)}$	1.30×10^{-2}	7.88×10^{-4}	14	66	9.28×10^{-4}	1.19×10^{-5}	77.70[a]	<0.001	0.9428
$C_{e\text{-}Exit(E350)}$	8.59×10^{-3}	2.08×10^{-4}			6.14×10^{-4}	3.15×10^{-6}	195.20[a]	<0.001	0.9764

[a]F-table = 2.36. Significance at 99 % confidence interval.

3.2.5.1 Development of mathematical models based on experimental data

Minitab 14 software is used to develop the mathematical models for circularity error of syntactic foams based on the experimental results presented in Table 3.10. Regression equations for predicting the exit side circularity error of different syntactic foams are given as,

$$C_{e-Exit(E200)} = \begin{pmatrix} 0.0303+0.0002\times v-0.555\times f-0.001\times R+0.006\times D-2.2\times10^{-8}\times v^2+ \\ 2.708\times f^2+1.71\times10^{-5}\times R^2+0.0001\times D^2-0.001\times v\times f-1.69\times10^{-6}\times v \\ \times R+1.06\times10^{-5}\times v\times D+0.008\times f\times R-0.031\times f\times D-0.0001\times R\times D \end{pmatrix} \tag{3.13}$$

$$C_{e-Exit(E270)} = \begin{pmatrix} 0.013-4.00\times10^{-5}\times v-0.203\times f+0.0003\times R+0.0005\times D+3.48\times10^{-7}\times \\ v^2+0.961\times f^2-2.55\times10^{-6}\times R^2+0.0001\times D^2+0.0001\times v\times f-3.06\times10^{-7} \\ \times v\times R+9.44\times10^{-6}\times v\times D-0.0002\times f\times R-0.01\times f\times D-2.4\times10^{-5}\times R\times D \end{pmatrix} \tag{3.14}$$

$$C_{e-Exit(E350)} = \begin{pmatrix} 0.018-0.0001\times v-0.110\times f+0.0001\times R-0.002\times D+7.41\times10^{-9}\times v^2+ \\ 0.671\times f^2+6.02\times10^{-7}\times R^2+0.0002\times D^2+0.0004\times v\times f-3.89\times10^{-7}\times v \\ \times R+1.4\times10^{-5}\times v\times D-0.0002\times f\times R-0.008\times f\times D-2.05\times10^{-5}\times R\times D \end{pmatrix} \tag{3.15}$$

Equation 3.13-Equation 3.15 are used to predict the exit side circularity error of the drilled hole within the chosen range of input process parameters. ANOVA is used to check the adequacy of the developed mathematical models and the results are presented in Table 3.11. Higher CoD values of the developed mathematical models (Equation 3.13-3.15) of exit side circularity error for E200 (0.89), E270 (0.94) and E350 (0.98) syntactic foams indicates a good correlation is existing between the experimental and predicted values. The average errors between the experimental and predicted values are found to be 1.07, 1.91 and 0.80% for exit side circularity error of E200, E270 and E350 syntactic foams respectively as shown in Figure 3.24. Hence, the developed mathematical models can be effectively used as a tool in industrial practices to predict the exit side circularity error of GMB reinforced epoxy foams during drilling.

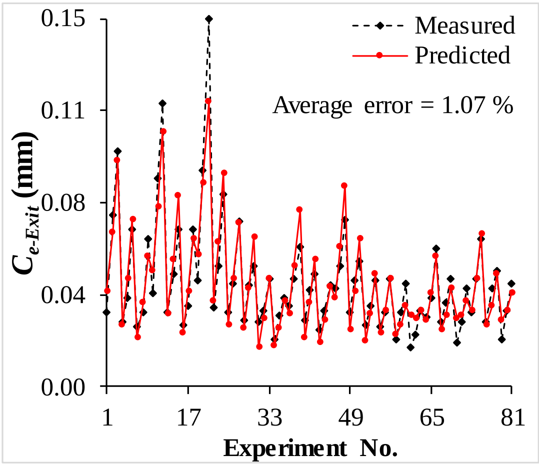

(a)

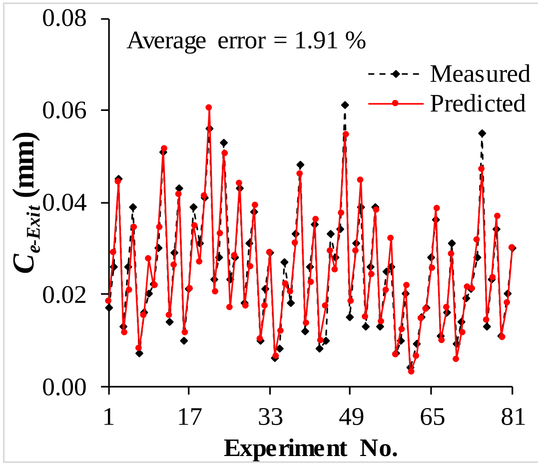

(b)

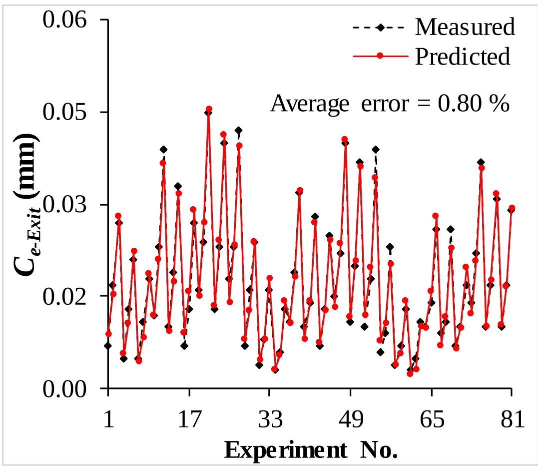

(c)

Figure 3.24 Comparison between measured and predicted values of $C_{e\text{-}Exit}$ for (a) E200, (b) E270 and (c) E350 syntactic foams.

3.2.5.2 Effects of individual parameters

Input parameters (v, f, R and D) are varied one at a time within the chosen range, keeping the other parameters at intermediate level in Equation 3.13-Equation 3.15 to predict the trend of C_{e-Exit} as presented in Figure 3.25. C_{e-Exit} of all the syntactic foams decreases with decreasing cutting speed and increasing feed (Figure 3.25a, Figure 3.25c and Figure 3.25e). Increasing GMB content decreases the C_{e-Exit}, while it is found to be increasing with increasing drill diameter (Figure 3.25b, Figure 3.25d and Figure 3.25f). These plots can serve as a reference to understand the general relationships among various parameters.

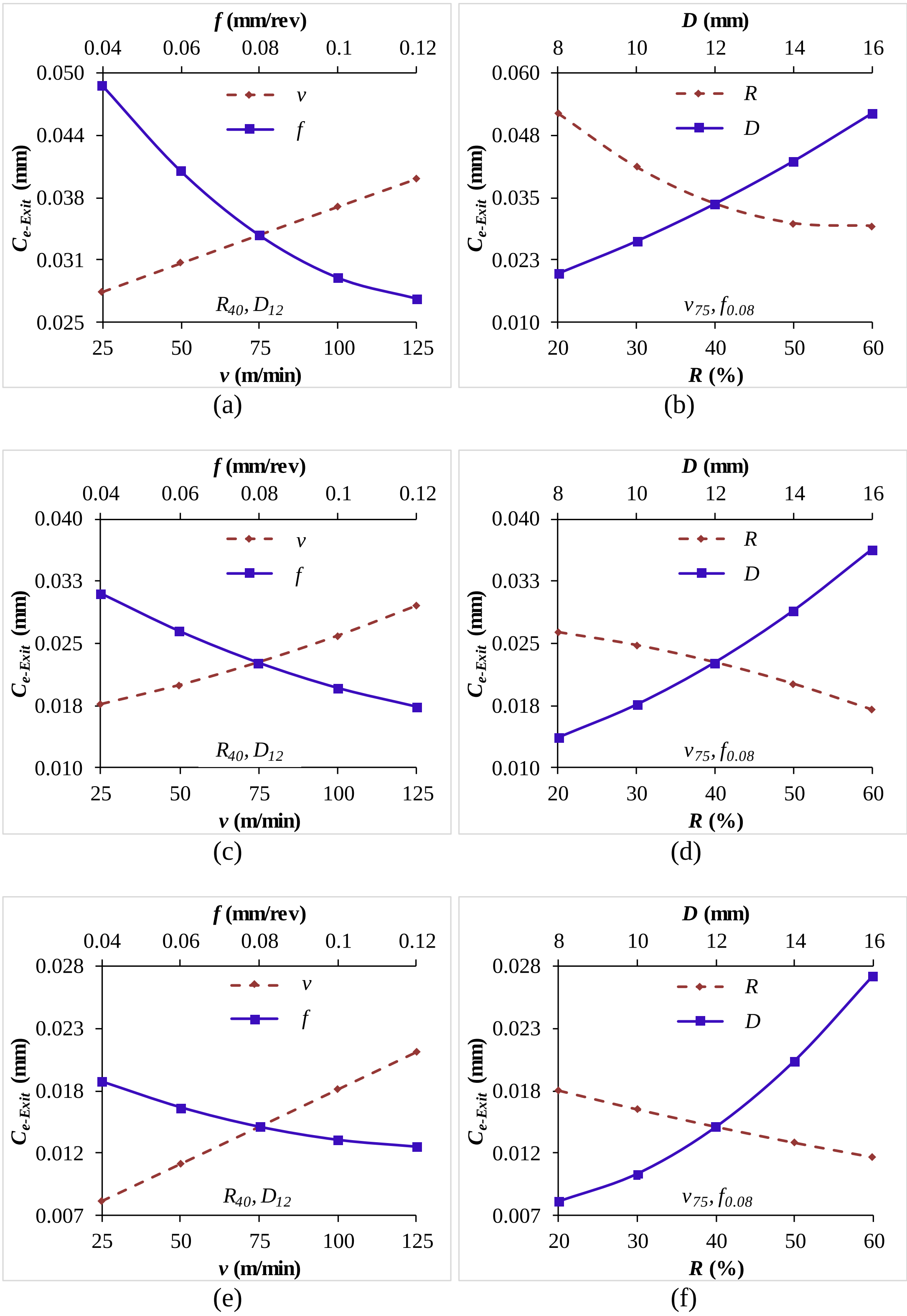

Figure 3.25 Individual effect plots of $C_{e\text{-}Exit}$ for (a-b) E200, (c-d) E270 and (e-f) E350 syntactic foams.

3.2.5.3 Effects of two-parameter interactions

Two parameters are varied at the same time while keeping the other two parameters at their intermediate levels in Equation 3.13-Equation 3.15 to study the interaction effects among the input process parameters on the C_{e-Exit} as per the scheme presented in Table 2.6.

Circularity error on the exit side of the hole is found to be increasing with increasing cutting speed for E200 (Figure 3.26a), E270 (Figure 3.27a) and E350 (Figure 3.28a) SFs. With the increasing v from v_{25} - v_{125}, C_{e-Exit} increases in the range of 34-40, 53-76 and 98-168% for E200, E270 and E350 SFs respectively. Stability of the cutting tool decreases with increasing cutting speed due to the increased chatter vibrations resulting in higher circularity errors. Also, at higher cutting speed frequency of the tool rubbing against the walls of hole increases causing high surface distortion leading to higher circularity errors (Giasin and Ayvar-Soberanis 2017). C_{e-Exit} as a function of cutting speed and feed is presented in Figure 3.26b, Figure 3.27b and Figure 3.28b for all the SFs. It is found to be increased by 40, 44 and 82% for E200, E270 and E350 SFs respectively with the increasing cutting speed.

The variation of circularity error with cutting speed at different filler content is shown in Figure 3.26c, Figure 3.27c and Figure 3.28c for E200, E270 and E350 syntactic foams respectively. C_{e-Exit} decreases in the range of 46-48, 61-74 and 70-87% as compared to neat epoxy for E200, E270 and E350 syntactic foams respectively. Increasing the GMB content increases the stiffness and thermal resistance of syntactic foams resulting in reduced circularity error values (Campos Rubio et al. 2013, Gaitonde et al. 2012). C_{e-Exit} is found to decreasing with increasing feed and decreasing drill diameter as shown in Figure 3.26d, Figure 3.27d and Figure 3.28d for all the syntactic foams. C_{e-Exit} decreases in the range of 39-44, 37-52 and 25-31% for E200, E270 and E350 syntactic foams respectively with increasing feed. Lower values of circularity error is observed at higher feeds due to the reduced tool-workpiece interface temperature (Campos Rubio et al. 2008).

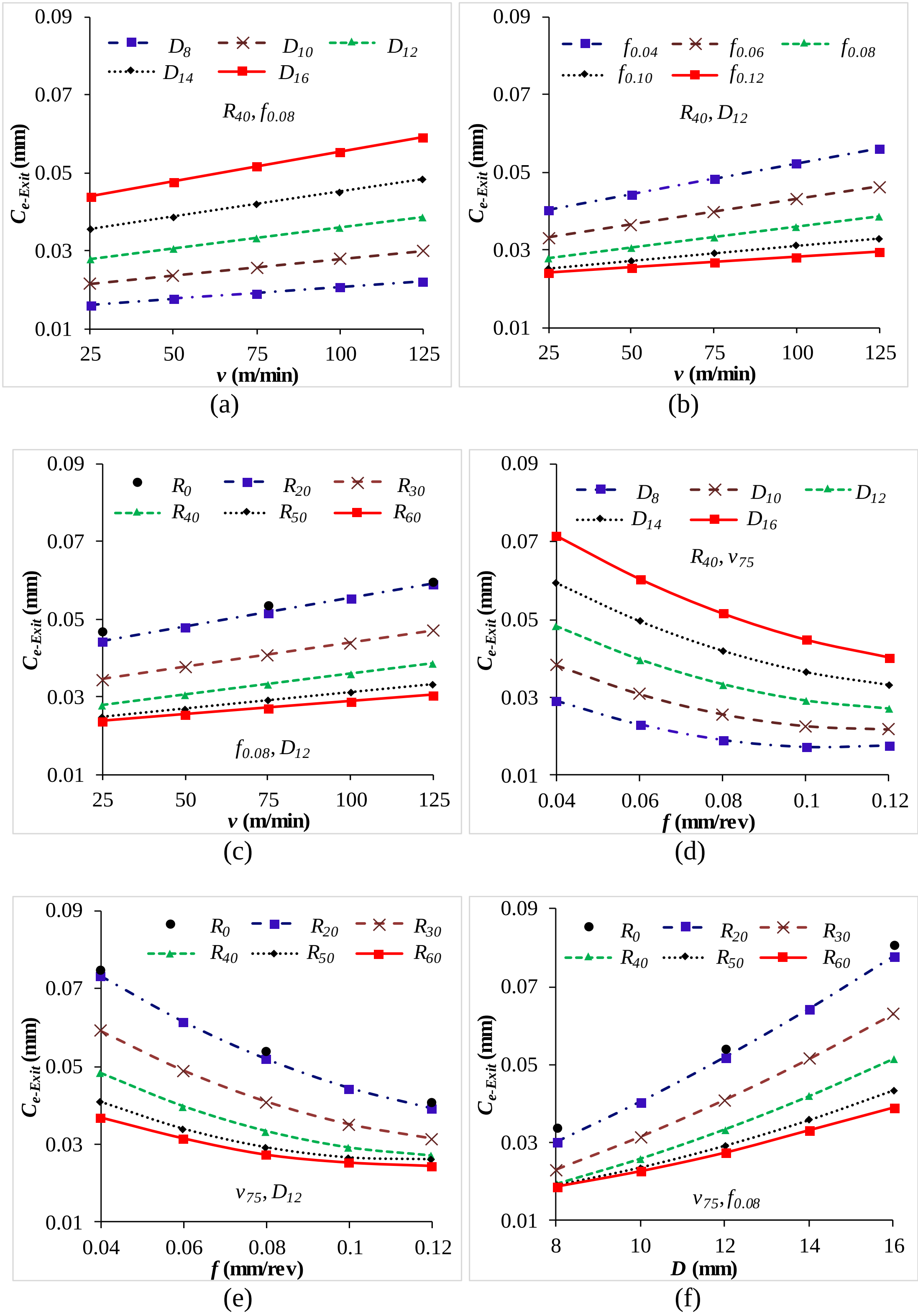

Figure 3.26 Variation of $C_{e\text{-}Exit}$ with respect to v at different (a) D, (b) f and (c) R. $C_{e\text{-}Exit}$ with respect to f at different (d) D and (e) R. (f) $C_{e\text{-}Exit}$ with respect to D at different R for E200 syntactic foam.

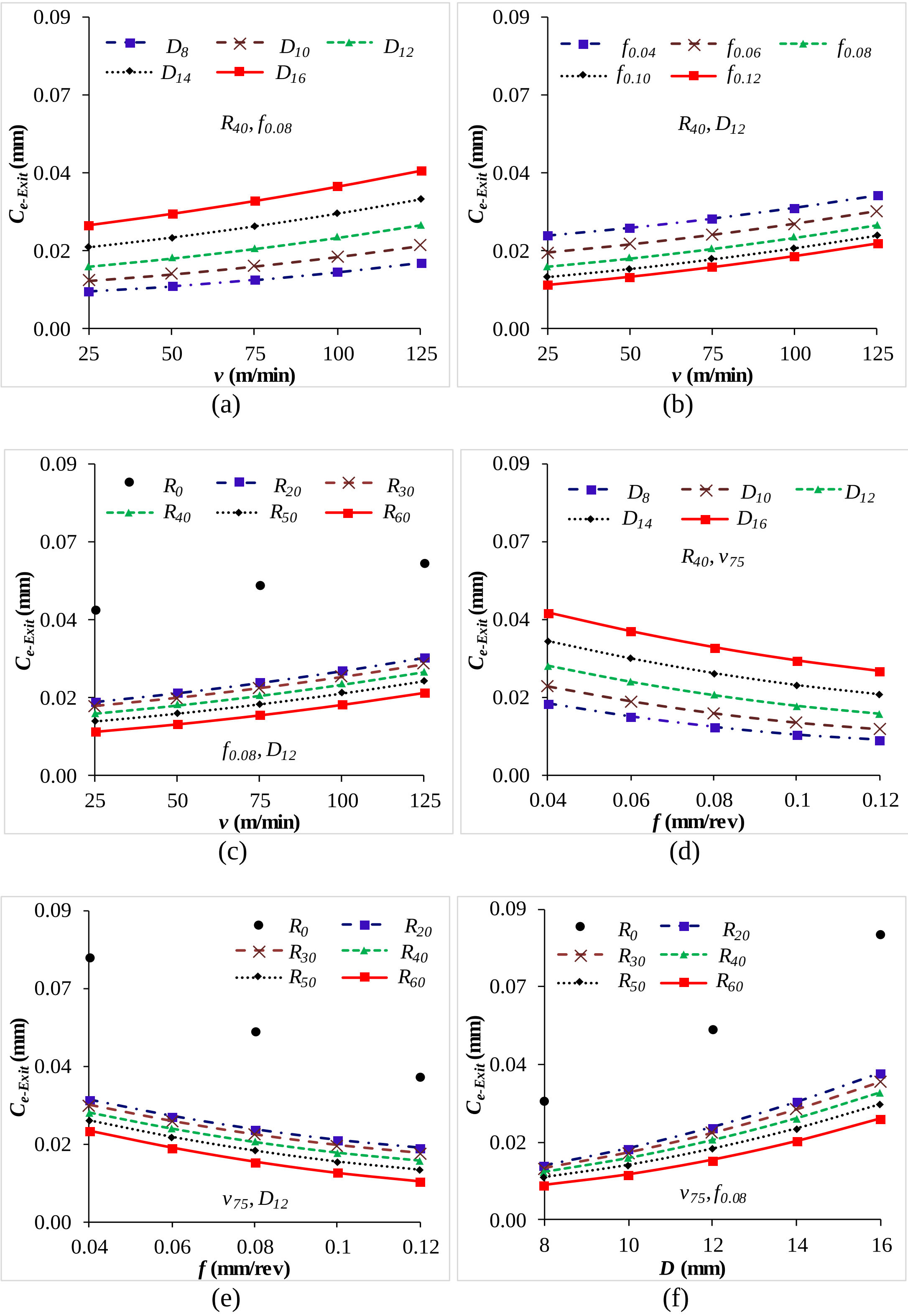

Figure 3.27 Variation of $C_{e\text{-}Exit}$ with respect to v at different (a) D, (b) f and (c) R. $C_{e\text{-}Exit}$ with respect to f at different (d) D and (e) R. (f) $C_{e\text{-}Exit}$ with respect to D at different R for E270 syntactic foam.

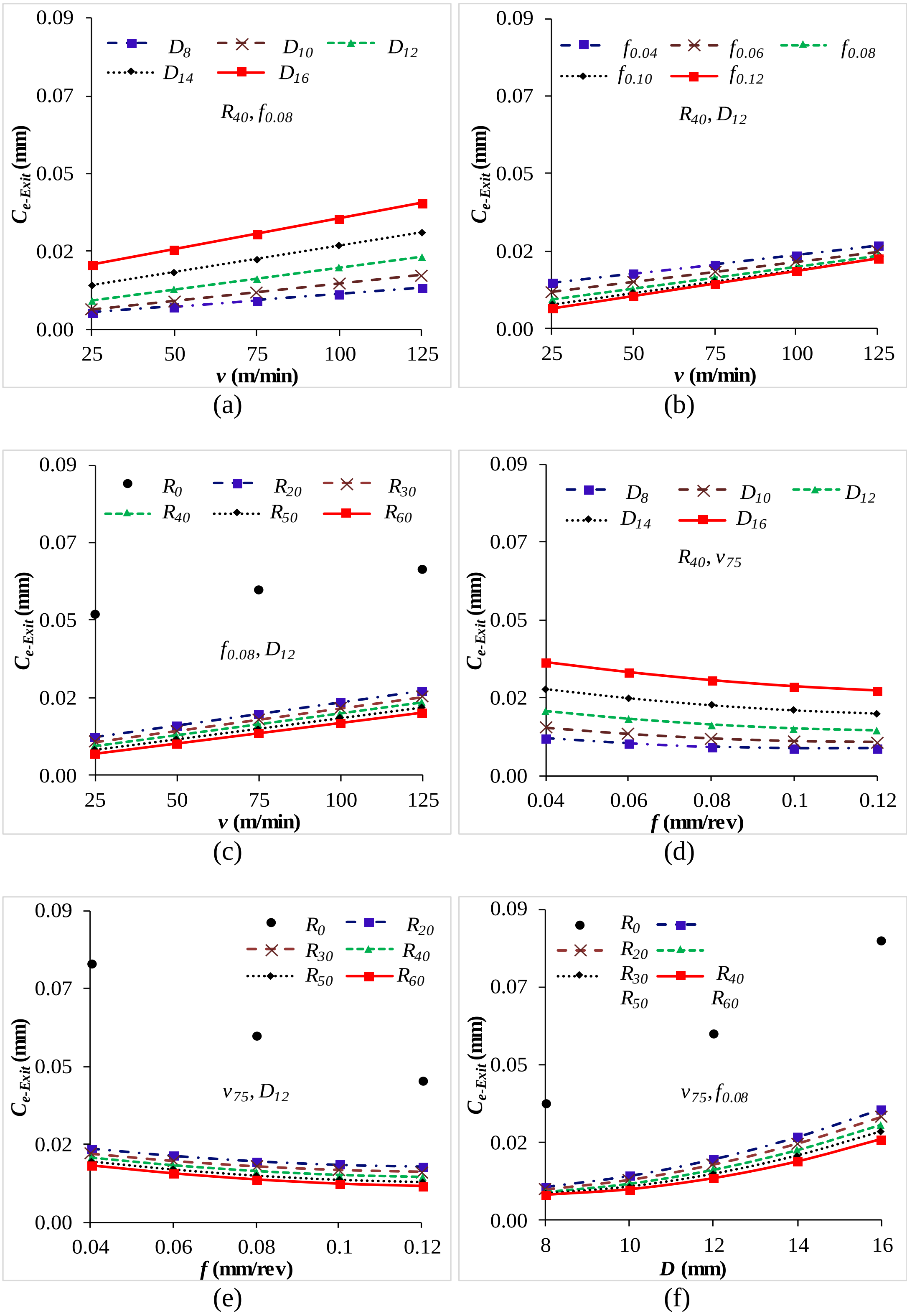

Figure 3.28 Variation of $C_{e\text{-}Exit}$ with respect to v at different (a) D, (b) f and (c) R. $C_{e\text{-}Exit}$ with respect to f at different (d) D and (e) R. (f) $C_{e\text{-}Exit}$ with respect to D at different R for E350 syntactic foam.

Figure 3.26e, Figure 3.27e and Figure 3.28e show variation of C_{e-Exit} as a function of feed and filler content for E200, E270 and E350 syntactic foams respectively. C_{e-Exit} is found to be decreasing with increasing feed and filler content. It reduces in the range of 40-51, 66-72 and 75-78% compared to that of neat epoxy for E200, E270 and E350 syntactic foams respectively with increasing feed from $f_{0.04}$ - $f_{0.12}$.

The variation of C_{e-Exit} with drill diameter at different levels of filler content is presented in Figure 3.26f, Figure 3.27f and Figure 3.28f for all the syntactic foams. With increasing drill diameter from D_8 - D_{12}, C_{e-Exit} increases in the range of 107-175, 165-187 and 216-234% for E200, E270 and E350 syntactic foams respectively. Increasing drill diameter increases the thrust force owing to the higher contact area of the drilled hole resulting higher values of circularity error (El-Sonbaty et al. 2004, Giasin and Ayvar-Soberanis 2017, Gowda et al. 2015).

3.2.6 Exit side damage factor

Experimentally measured values of exit side damage factor for neat epoxy and their syntactic foams are presented in Table 3.12.

Table 3.12 Experimentally measured values of exit side damage factor for neat epoxy and their syntactic foams.

v	*f*	*D*	E0	E200			E270			E350		
				R_{20}	R_{40}	R_{60}	R_{20}	R_{40}	R_{60}	R_{20}	R_{40}	R_{60}
25	0.04	8	1.0048	1.0034	1.0031	1.0028	1.0040	1.0033	1.0030	1.0030	1.0026	1.0032
		12	1.0082	1.0049	1.0048	1.0042	1.0071	1.0064	1.0046	1.0060	1.0050	1.0055
		16	1.0101	1.0080	1.0076	1.0065	1.0088	1.0078	1.0071	1.0081	1.0065	1.0071
	0.08	8	1.0053	1.0040	1.0033	1.0030	1.0040	1.0035	1.0037	1.0041	1.0036	1.0039
		12	1.0093	1.0054	1.0049	1.0048	1.0074	1.0068	1.0058	1.0068	1.0072	1.0059
		16	1.0140	1.0089	1.0083	1.0073	1.0092	1.0086	1.0076	1.0086	1.0079	1.0079
	0.12	8	1.0094	1.0040	1.0036	1.0043	1.0046	1.0042	1.0044	1.0041	1.0033	1.0045
		12	1.0119	1.0060	1.0057	1.0054	1.0079	1.0069	1.0062	1.0070	1.0070	1.0067
		16	1.0154	1.0090	1.0084	1.0081	1.0094	1.0090	1.0084	1.0093	1.0084	1.0086
75	0.04	8	1.0046	1.0033	1.0029	1.0014	1.0034	1.0030	1.0028	1.0038	1.0031	1.0030
		12	1.0078	1.0047	1.0046	1.0039	1.0058	1.0048	1.0043	1.0068	1.0068	1.0056
		16	1.0093	1.0075	1.0063	1.0060	1.0082	1.0069	1.0068	1.0084	1.0074	1.0073
	0.08	8	1.0048	1.0035	1.0030	1.0030	1.0038	1.0032	1.0032	1.0039	1.0041	1.0038
		12	1.0093	1.0049	1.0049	1.0048	1.0065	1.0058	1.0055	1.0073	1.0065	1.0069
		16	1.0115	1.0078	1.0081	1.0065	1.0084	1.0085	1.0072	1.0086	1.0090	1.0081
	0.12	8	1.0080	1.0038	1.0032	1.0032	1.0039	1.0035	1.0036	1.0042	1.0037	1.0044
		12	1.0099	1.0057	1.0054	1.0048	1.0078	1.0066	1.0055	1.0083	1.0078	1.0069
		16	1.0143	1.0085	1.0082	1.0078	1.0091	1.0085	1.0080	1.0093	1.0088	1.0085
125	0.04	8	1.0037	1.0024	1.0021	1.0007	1.0026	1.0024	1.0018	1.0044	1.0038	1.0038
		12	1.0059	1.0044	1.0033	1.0029	1.0047	1.0033	1.0043	1.0075	1.0065	1.0063
		16	1.0085	1.0063	1.0063	1.0047	1.0070	1.0065	1.0058	1.0090	1.0088	1.0079
	0.08	8	1.0042	1.0032	1.0029	1.0023	1.0033	1.0032	1.0029	1.0041	1.0035	1.0049
		12	1.0076	1.0049	1.0048	1.0038	1.0060	1.0054	1.0053	1.0083	1.0073	1.0073
		16	1.0094	1.0079	1.0074	1.0054	1.0080	1.0078	1.0066	1.0094	1.0095	1.0083

v	f	D	E0	E200			E270			E350		
				R_{20}	R_{40}	R_{60}	R_{20}	R_{40}	R_{60}	R_{20}	R_{40}	R_{60}
		8	1.0069	1.0036	1.0030	1.0030	1.0039	1.0030	1.0035	1.0056	1.0043	1.0056
	0.12	12	1.0088	1.0049	1.0049	1.0034	1.0065	1.0066	1.0054	1.0085	1.0078	1.0075
		16	1.0120	1.0083	1.0078	1.0072	1.0088	1.0082	1.0078	1.0096	1.0093	1.0093

Table 3.13 Summary of ANOVA results for the developed mathematical models of exit side damage factor.

Responses	Sum of squares		Degrees of freedom		Mean square		F-ratio	P-Value	CoD
	Regression	Residual	Regression	Residual	Regression	Residual			
$F_{d\text{-}Exit(E200)}$	3.20×10^{-4}	1.33×10^{-5}			2.29×10^{-5}	2.02×10^{-7}	113.39[a]	<0.001	0.9601
$F_{d\text{-}Exit(E270)}$	3.35×10^{-4}	7.49×10^{-6}	14	66	2.39×10^{-5}	1.14×10^{-7}	210.83[a]	<0.001	0.9781
$F_{d\text{-}Exit(E350)}$	3.27×10^{-4}	9.78×10^{-6}			2.33×10^{-5}	1.48×10^{-7}	157.45[a]	<0.001	0.9709

[a]F-table = 2.36. Significance at 99 % confidence interval.

3.2.6.1 Development of mathematical models based on experimental data

Mathematical models for F_{d-Exit} are developed based on experimental results (Table 3.12) using Minitab 14 software. Regression equations for predicting the damage factor of different syntactic foams are given as,

$$F_{d-Exit(E200)} = \begin{pmatrix} 1.001 + 7.04\times10^{-6}\times v + 0.018\times f + 2.01\times10^{-5}\times R - 0.0001\times D - 8.15\times10^{-8} \\ \times v^2 - 0.093\times f^2 - 2.31\times10^{-7}\times R^2 + 2.89\times10^{-5}\times D^2 + 0.0001\times v\times f - 1.39 \\ \times10^{-7}\times v\times R - 5.56\times10^{-7}\times v\times D + 3.47\times10^{-5}\times f\times R + 0.0003\times f\times D - 1.74 \\ \times10^{-6}\times R\times D \end{pmatrix} \tag{3.16}$$

$$F_{d-Exit(E270)} = \begin{pmatrix} 0.998 - 2.04\times10^{-5}\times v + 1.08\times10^{-2}\times f - 2.81\times10^{-5}\times R + 0.001\times D + 5.33 \\ \times10^{-9}\times v^2 - 0.076\times f^2 + 2.08\times10^{-7}\times R^2 - 1.49\times10^{-5}\times D^2 + 0.0001\times v\times f \\ +1.14\times10^{-7}\times v\times R - 2.11\times10^{-7}\times v\times D + 0.0001\times f\times R + 0.001\times f\times D - \\ 2.44\times10^{-6}\times R\times D \end{pmatrix} \tag{3.17}$$

$$F_{d-Exit(E350)} = \begin{pmatrix} 0.992 + 6.01\times10^{-6}\times v + 2.29\times10^{-2}\times f - 4.07\times10^{-5}\times R + 0.002\times D + 4.19 \\ \times10^{-8}\times v^2 - 0.089\times f^2 + 6.45\times10^{-7}\times R^2 - 4.48\times10^{-5}\times D^2 - 3.21\times10^{-5}\times v \\ \times f - 5.47\times10^{-8}\times v\times R + 1.78\times10^{-7}\times v\times D + 0.0001\times f\times R + 0.0003\times f\times \\ D - 2.53\times10^{-6}\times R\times D \end{pmatrix} \tag{3.18}$$

Equation 3.16-Equation 3.18 are used to predict the damage factor within the chosen range of input process parameters. Adequacy of the developed mathematical models are confirmed using ANOVA and are presented in Table 3.13. According to ANOVA, the computed F-ratio should be more than the F-table for the models to be adequate. Higher CoD values of the developed models of F_{d-Exit} for E200 (0.96), E270 (0.98) and E350 (0.97) SFs indicate a good correlation is existing between the experimental and predicted values. The average errors between the experimental and predicted values are found to be less than 0.001% for F_{d-Exit} of all the SFs as shown in Figure 3.29. Hence, the developed mathematical models can be effectively used as a tool in industrial practices to predict the F_{d-Exit} of GMB reinforced epoxy foams during drilling.

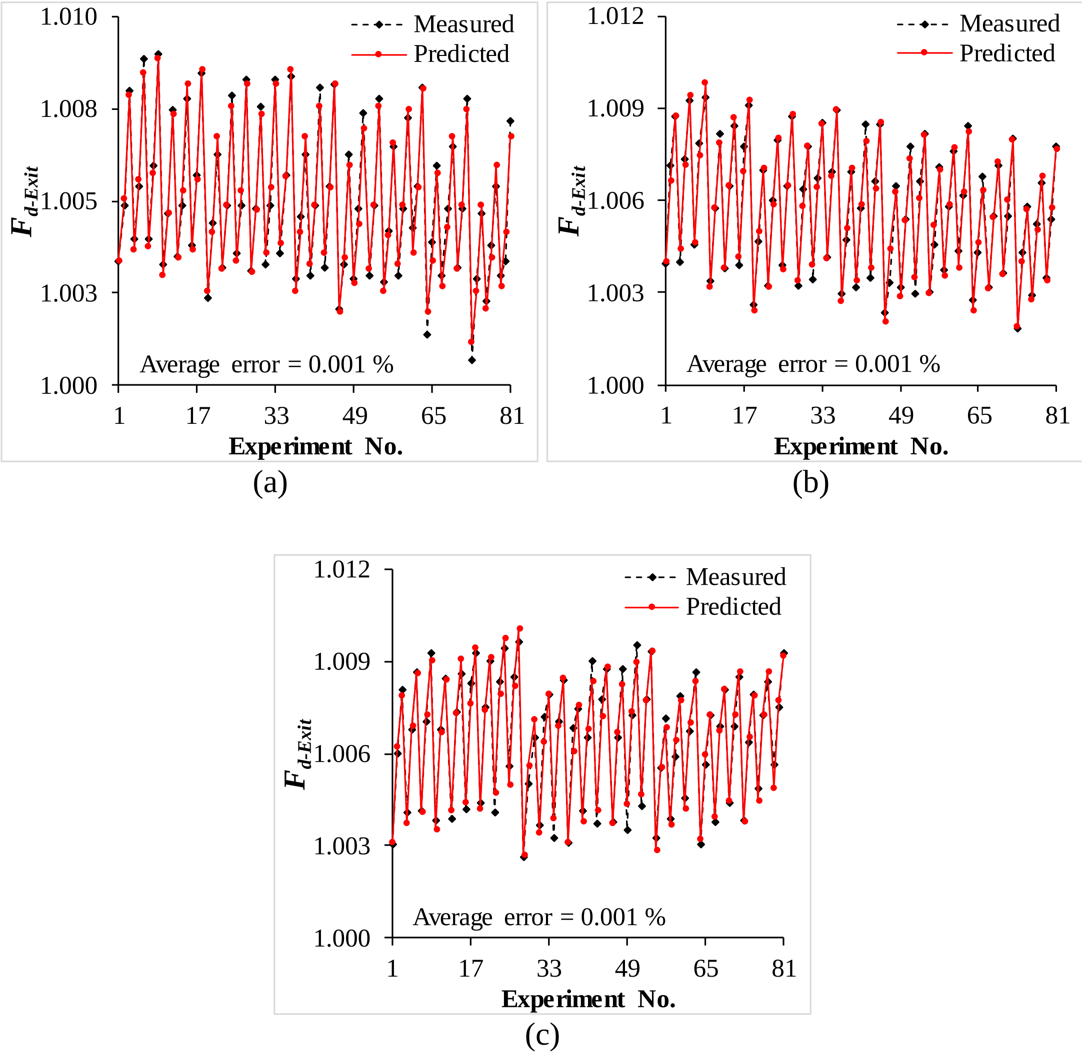

Figure 3.29 Comparison between measured and predicted values of $F_{d\text{-}Exit}$ for (a) E200, (b) E270 and (c) E350 syntactic foams.

3.2.6.2 Effects of individual parameters

Cutting speed, feed, filler content and drill diameter are varied one at a time within the chosen range, keeping the other parameters at intermediate level in Equation 3.16-Equation 3.18 to predict the trend of F_{d-Exit} as presented in Figure 3.30. F_{d-Exit} of all the syntactic foams increases with increasing f (Figure 3.30a, Figure 3.30c and Figure 3.30e) but decreases with increasing R and decreasing D (Figure 3.30b, Figure 3.30d and Figure 3.30f). With increasing v, the F_{d-Exit} is found to be decreasing for E200 and E270 syntactic foams as shown in Figure 3.30a and Figure 3.30c while it marginally increases for E350 syntactic foam (Figure 3.30e). These plots can serve as a reference to understand the general relationships among various parameters.

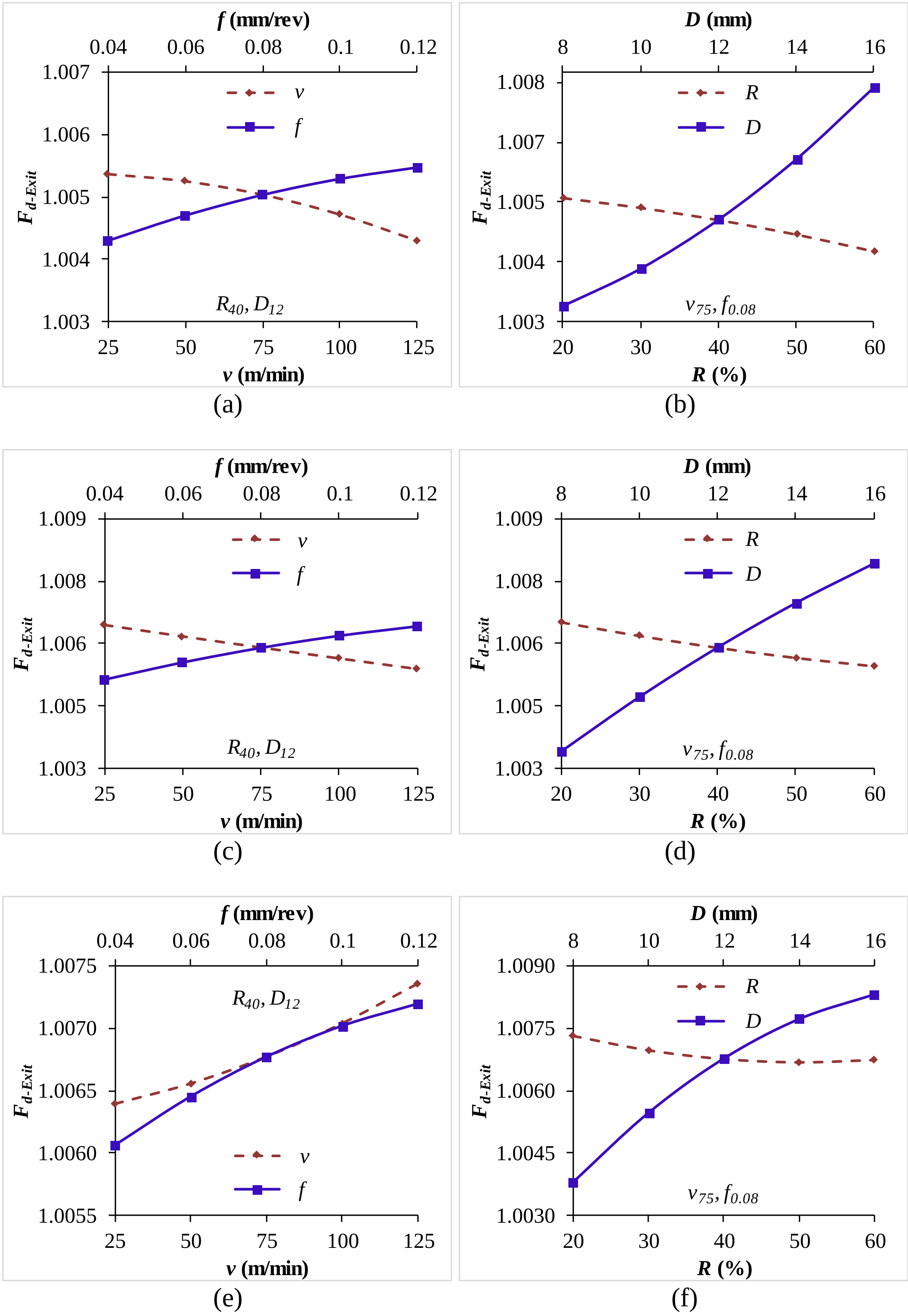

Figure 3.30 Individual effect plots of $F_{d\text{-}Exit}$ for (a-b) E200, (c-d) E270 and (e-f) E350 syntactic foams.

3.2.6.3 Effects of two-parameter interactions

Interaction effects among the input process parameters on the F_{d-Exit} in drilling of syntactic foams are studied by varying two parameters at the same time in Equation 3.16-Equation 3.18, keeping the other two at their intermediate levels as per the scheme presented in Table 2.6.

F_{d-Exit} is found to be decreased with increasing cutting speed for E200 and E270 SFs as shown in Figure 3.31a and Figure 3.32a, while it increases with increasing cutting speed for E350 SF (Figure 3.33a). With the increasing cutting speed from v_{25} - v_{125}, F_{d-Exit} decreases by 16-24 and 13-25% for E200 and E270 SFs respectively, whereas it increases by 13-26% for E350 SF at different levels of drill diameter. Damage factor solely dependents on the thrust force developed during drilling process (Palanikumar 2011). Increasing cutting speed decreases the thrust force due to the increased tool and work material interface temperature resulting in lower F_{d-Exit} values for E200 and E270 SFs. E350 SF being reinforced with high collapse strength (6500 psi) GMBs exhibits higher resistance for the advancement of tool into the work material leading to higher thrust forces which result in higher F_{d-Exit} values (El-Sonbaty et al. 2004, Palanikumar 2011). Variation of F_{d-Exit} as a function of cutting speed and feed is presented in Figure 3.31b, Figure 3.32b and Figure 3.33b for E200, E270 and E350 SFs respectively.

F_{d-Exit} decreases by 13-29 and 11-24% for E200 and E270 SFs respectively, while it increases by 12-20% for E350 SF with the increasing speed. F_{d-Exit} as a function of cutting speed and filler content is shown in Figure 3.31c, Figure 3.32c and Figure 3.33c for all the SFs. With increasing GMB content, F_{d-Exit} is found to be decreased in the range of 48-54, 33-41 and 5-31% as compared to neat epoxy for E200, E270 and E350 SFs respectively. Increasing GMB content decreases the thrust force due to increased brittle behavior of the foams resulting in reduced values of F_{d-Exit} (Gaitonde et al. 2011).

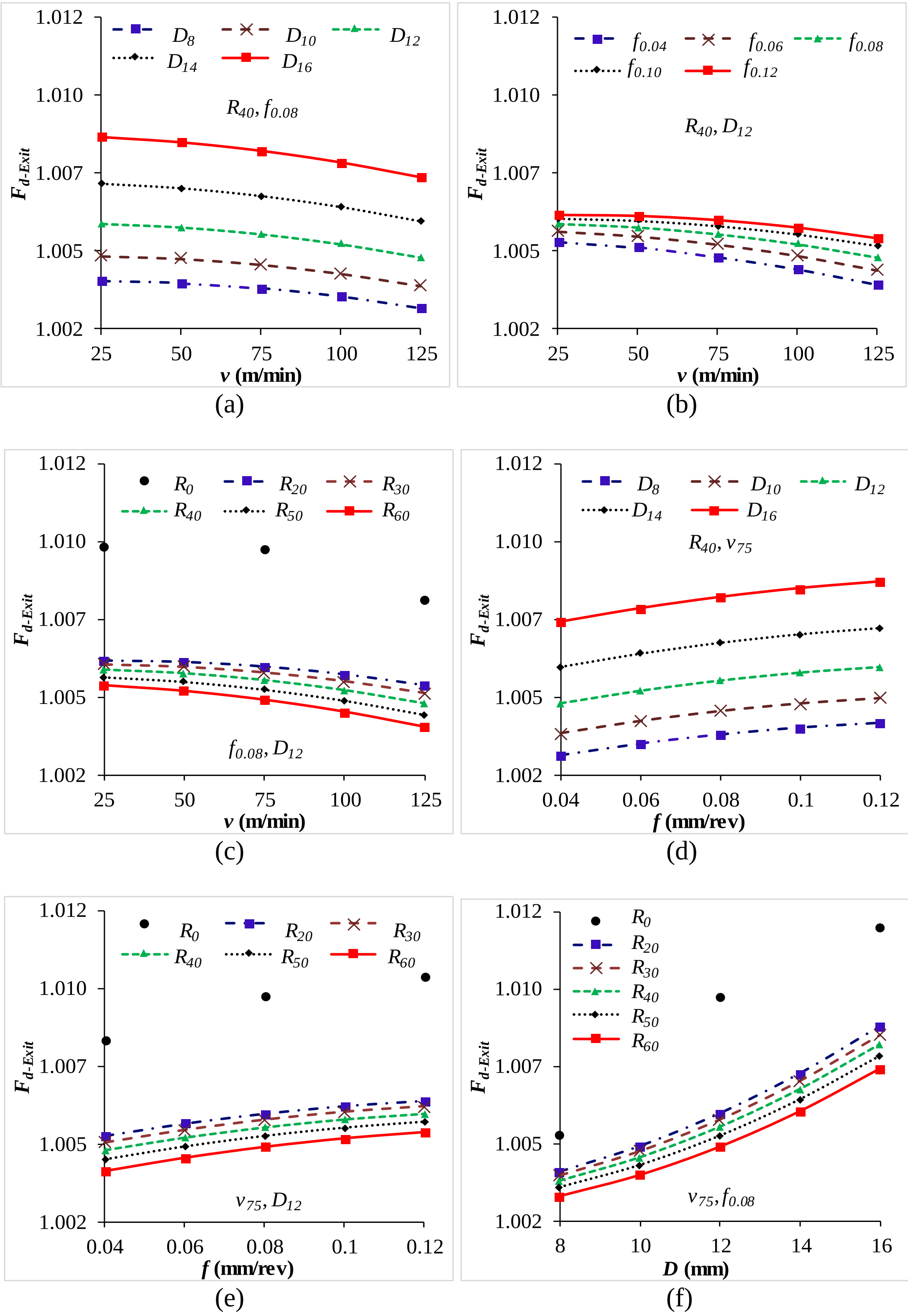

Figure 3.31 Variation of $F_{d\text{-}Exit}$ with respect to v at different (a) D, (b) f and (c) R. $F_{d\text{-}Exit}$ with respect to f at different (d) D and (e) R. (f) $F_{d\text{-}Exit}$ with respect to D at different R for E200 syntactic foam.

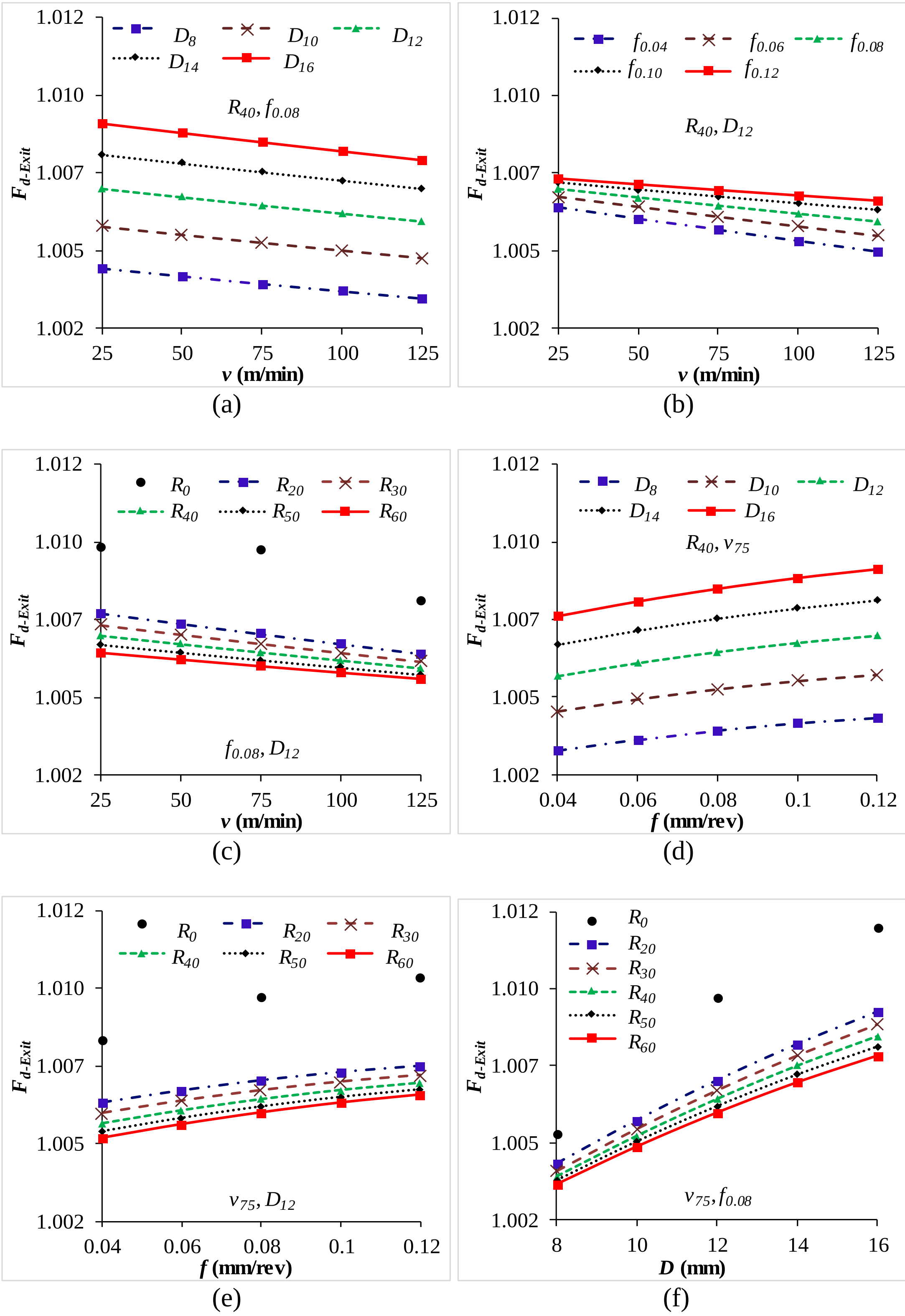

Figure 3.32 Variation of $F_{d\text{-}Exit}$ with respect to v at different (a) D, (b) f and (c) R. $F_{d\text{-}Exit}$ with respect to f at different (d) D and (e) R. (f) $F_{d\text{-}Exit}$ with respect to D at different R for E270 syntactic foam.

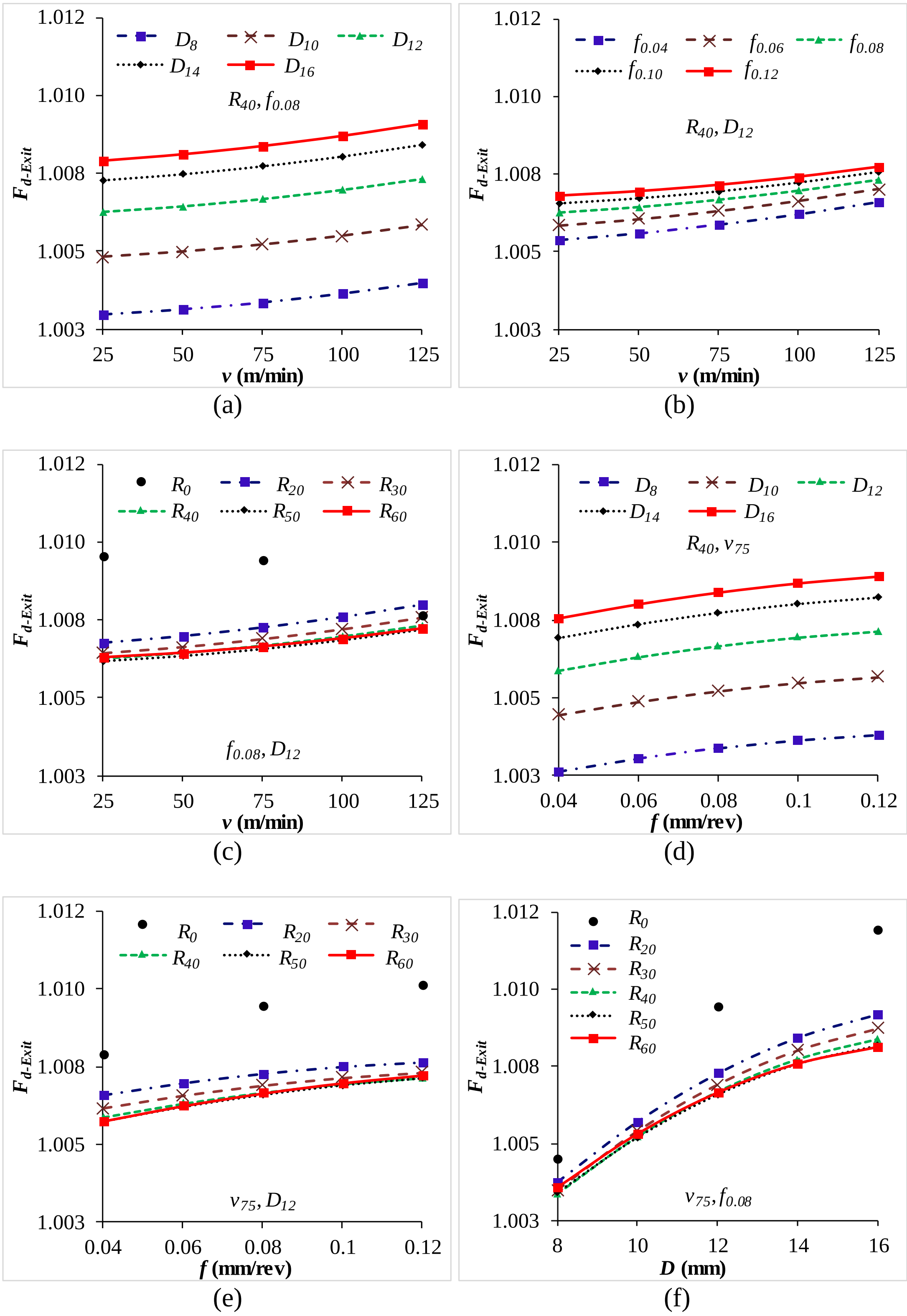

Figure 3.33 Variation of $F_{d\text{-}Exit}$ with respect to v at different (a) D, (b) f and (c) R. $F_{d\text{-}Exit}$ with respect to f at different (d) D and (e) R. (f) $F_{d\text{-}Exit}$ with respect to D at different R for E350 syntactic foam.

F_{d-Exit} is found to increase with increasing feed and drill diameter as shown in Figure 3.31d, Figure 3.32d and Figure 3.33d for all the syntactic foams. F_{d-Exit} increases in the range of 19-41, 21-39 and 16-34% for E200, E270 and E350 SFs respectively with increasing feed from $f_{0.04}$ - $f_{0.12}$. As feed increases, thrust force increases due to increased friction between tool and foam leading to higher values of F_{d-Exit} (Basavarajappa et al. 2011, Gaitonde et al. 2011). Figure 3.31e, Figure 3.32e and Figure 3.33e show variation of feed and filler content as a function of F_{d-Exit} for E200, E270 and E350 SFs respectively. F_{d-Exit} increases with increasing feed and decreasing filler content. Compared to that of neat epoxy, F_{d-Exit} reduces by 51-54, 38-41 and 24-27 % for E200, E270 and E350 SFs respectively with increasing feed from $f_{0.04}$ - $f_{0.12}$. The variation of F_{d-Exit} with drill diameter and filler content is presented in Figure 3.31f, Figure 3.32f and Figure 3.33f for all the syntactic foams. With increasing drill diameter from D_8 - D_{16}, F_{d-Exit} increases in the range of 130-147, 129-132 and 105-120 for E200, E270 and E350 SFs respectively. Thrust force increases with increasing drill diameter due to the increased contact area of the drilled hole leading to higher F_{d-Exit} values (El-Sonbaty et al. 2004, Palanikumar 2011). Figure 3.34 shows a scanning electron micrograph of a part of a drilled hole. Comparing Figure 3.34a and Figure 3.34b, it is clear that the amount of damage occurred using smaller drill diameter is lesser than larger diameter drill.

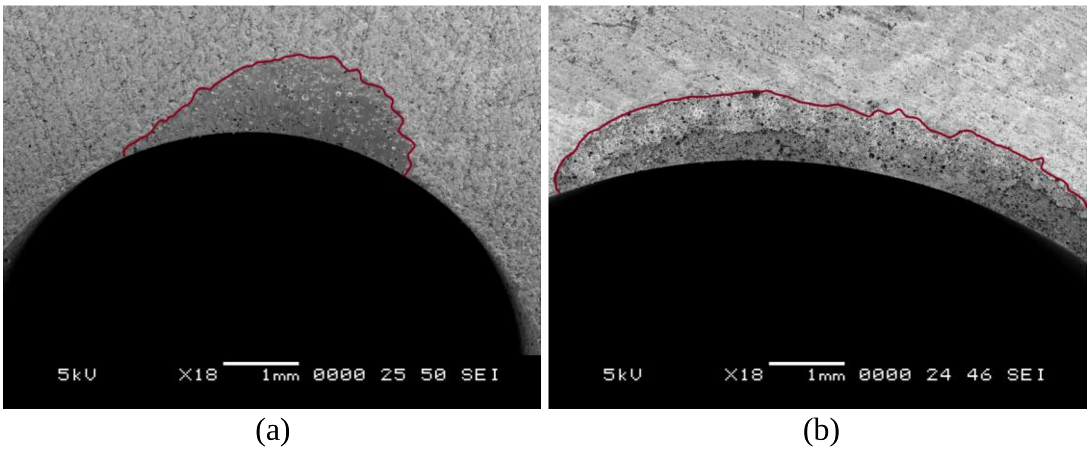

(a) (b)

Figure 3.34 Microscopic observations of E350 syntactic foam exit side drilled using (a) *D*8 and (b) *D*16 for damage assessment. Damage area is marked with a red line.

3.2.7 Grey relation analysis

3.2.7.1 E200 syntactic foam

It is observed from Table 3.14 that the conditions for minimizing all the responses for E200 syntactic foam are not same. Higher cutting speed is desired for reducing F_t, K_f, F_{d-Exit} whereas lower cutting speed is required to minimize R_a, CYL, C_{e-Exit}. Lower feed minimizes F_t, CYL, F_{d-Exit} while higher feed minimizes R_a, K_f, C_{e-Exit}. Similarly, all the responses except surface roughness can be minimized by using smaller diameter drills. The trade-off between various process parameters for minimizing the responses requires multi-response optimization. Hence, in this work, GRA is used for finding a specific combination of process parameters to minimize all the responses in drilling of syntactic foams.

Table 3.14 Input parameter settings for minimizing the responses in drilling of E200.

Response	Minimizing condition
Thrust force (F_t)	$v_{125} f_{0.04} R_{60} D_8$
Surface roughness (R_a)	$v_{25} f_{0.12} R_{60} D_{16}$
Sp. cutting coefficient (K_f)	$v_{125} f_{0.12} R_{60} D_8$
Cylindricity (CYL)	$v_{25} f_{0.04} R_{60} D_8$
Exit side circularity error (C_{e-Exit})	$v_{25} f_{0.12} R_{60} D_8$
Exit side damage factor (F_{d-Exit})	$v_{125} f_{0.04} R_{60} D_8$

The first step in GRA is to normalize the experimental data (Table 3.2, Table 3.4, Table 3.6, Table 3.8, Table 3.10 and Table 3.12) using smaller-the-better characteristic since the objective is to minimize the responses. Equation 2.11 is used for data normalization and results are presented in Table 3.15.

The second step in GRA is computing the grey relation coefficients using the normalized data (Table 3.15). Equation 2.12 is used for calculating the grey relation coefficients of the responses and results are presented in Table 3.16.

Table 3.15 Normalized data (Smaller is better) of E200 syntactic foam.

R	v	f	D	F_t	R_a	K_f	CYL	$C_{e\text{-}Exit}$	$F_{d\text{-}Exit}$
20	25	0.04	8	0.833	0.154	0.143	0.886	0.896	0.676
			12	0.667	0.461	0.143	0.886	0.597	0.489
			16	0.417	0.558	0.000	0.786	0.403	0.122
		0.08	8	0.750	0.180	0.571	0.886	0.925	0.605
			12	0.417	0.546	0.429	0.843	0.851	0.431
			16	0.167	0.743	0.429	0.686	0.642	0.011
		0.12	8	0.667	0.322	0.714	0.829	0.940	0.599
			12	0.333	0.635	0.651	0.771	0.896	0.361
			16	0.000	0.924	0.619	0.271	0.672	0.000
	75	0.04	8	0.917	0.154	0.429	0.886	0.836	0.691
			12	0.750	0.262	0.333	0.843	0.485	0.518
			16	0.500	0.549	0.143	0.743	0.261	0.182
		0.08	8	0.750	0.170	0.571	0.871	0.896	0.659
			12	0.500	0.483	0.524	0.786	0.776	0.489
			16	0.250	0.624	0.500	0.571	0.642	0.152
		0.12	8	0.750	0.305	0.810	0.814	0.933	0.623
			12	0.417	0.550	0.714	0.743	0.873	0.401
			16	0.167	0.805	0.714	0.071	0.642	0.062
	125	0.04	8	0.917	0.000	0.429	0.871	0.799	0.788
			12	0.750	0.166	0.333	0.814	0.463	0.556
			16	0.583	0.435	0.286	0.586	0.000	0.331
		0.08	8	0.833	0.127	0.714	0.843	0.881	0.698
			12	0.583	0.183	0.619	0.700	0.754	0.491
			16	0.333	0.488	0.571	0.000	0.537	0.134
		0.12	8	0.750	0.149	0.810	0.786	0.896	0.647
			12	0.500	0.361	0.778	0.071	0.806	0.489
			16	0.167	0.717	0.714	0.000	0.619	0.092
40	25	0.04	8	0.917	0.180	0.429	1.000	0.918	0.712
			12	0.750	0.522	0.333	0.900	0.813	0.501
			16	0.500	0.700	0.143	0.814	0.754	0.167
		0.08	8	0.750	0.455	0.571	0.886	0.925	0.687
			12	0.500	0.548	0.524	0.871	0.888	0.489
			16	0.250	0.802	0.500	0.771	0.791	0.092
		0.12	8	0.667	0.483	0.714	0.843	0.978	0.646
			12	0.417	0.641	0.714	0.814	0.903	0.401
			16	0.083	0.929	0.667	0.643	0.851	0.076
	75	0.04	8	0.917	0.166	0.429	0.971	0.873	0.730
			12	0.750	0.438	0.333	0.871	0.791	0.531
			16	0.583	0.550	0.286	0.743	0.694	0.331
		0.08	8	0.833	0.344	0.714	0.886	0.918	0.716
			12	0.583	0.522	0.619	0.800	0.828	0.496
			16	0.333	0.709	0.571	0.700	0.776	0.107

R	v	f	D	F_t	R_a	K_f	CYL	$C_{e\text{-}Exit}$	$F_{d\text{-}Exit}$
		0.12	8	0.750	0.406	0.810	0.829	0.948	0.700
			12	0.500	0.539	0.778	0.757	0.888	0.431
			16	0.250	0.901	0.762	0.557	0.813	0.098
	125	0.04	8	0.917	0.124	0.429	0.886	0.821	0.825
			12	0.750	0.242	0.333	0.843	0.754	0.683
			16	0.583	0.493	0.286	0.729	0.612	0.331
		0.08	8	0.833	0.236	0.714	0.871	0.896	0.736
			12	0.667	0.299	0.714	0.771	0.799	0.501
			16	0.417	0.559	0.643	0.486	0.739	0.197
		0.12	8	0.833	0.312	0.905	0.829	0.933	0.721
			12	0.583	0.518	0.841	0.700	0.873	0.491
			16	0.250	0.712	0.762	0.271	0.799	0.152
60	25	0.04	8	1.000	0.199	0.714	1.000	0.940	0.750
			12	0.833	0.571	0.524	0.971	0.896	0.580
			16	0.667	0.767	0.429	0.886	0.791	0.301
		0.08	8	0.917	0.461	0.857	0.971	0.978	0.721
			12	0.750	0.743	0.810	0.886	0.896	0.511
			16	0.500	0.806	0.714	0.814	0.806	0.202
		0.12	8	0.833	0.483	0.905	0.871	1.000	0.571
			12	0.583	0.745	0.841	0.857	0.963	0.431
			16	0.333	1.000	0.810	0.700	0.888	0.107
	75	0.04	8	1.000	0.199	0.714	1.000	0.910	0.908
			12	0.917	0.484	0.714	0.929	0.851	0.611
			16	0.750	0.753	0.571	0.786	0.701	0.361
		0.08	8	0.917	0.406	0.857	0.957	0.925	0.727
			12	0.750	0.549	0.810	0.829	0.866	0.511
			16	0.583	0.709	0.786	0.743	0.791	0.301
		0.12	8	0.917	0.473	1.000	0.871	0.985	0.696
			12	0.667	0.582	0.905	0.814	0.925	0.511
			16	0.417	0.903	0.857	0.629	0.821	0.152
	125	0.04	8	1.000	0.162	0.714	0.971	0.896	1.000
			12	0.917	0.426	0.714	0.871	0.791	0.736
			16	0.833	0.518	0.714	0.729	0.672	0.521
		0.08	8	1.000	0.236	1.000	0.957	0.925	0.810
			12	0.833	0.462	0.905	0.829	0.821	0.623
			16	0.667	0.641	0.857	0.714	0.769	0.436
		0.12	8	0.917	0.312	1.000	0.857	0.978	0.721
			12	0.750	0.613	0.968	0.743	0.888	0.668
			16	0.583	0.744	0.952	0.529	0.806	0.224

Table 3.16 Grey relation coefficients of E200 syntactic foam.

R	v	f	D	F_t	R_a	K_f	CYL	$C_{e\text{-}Exit}$	$F_{d\text{-}Exit}$
20	25	0.04	8	0.750	0.372	0.368	0.814	0.827	0.607
			12	0.600	0.481	0.368	0.814	0.554	0.494
			16	0.462	0.531	0.333	0.700	0.456	0.363
		0.08	8	0.667	0.379	0.538	0.814	0.870	0.559
			12	0.462	0.524	0.467	0.761	0.770	0.468
			16	0.375	0.661	0.467	0.614	0.583	0.336
		0.12	8	0.600	0.424	0.636	0.745	0.893	0.555
			12	0.429	0.578	0.589	0.686	0.827	0.439
			16	0.333	0.868	0.568	0.407	0.604	0.333
	75	0.04	8	0.857	0.372	0.467	0.814	0.753	0.618
			12	0.667	0.404	0.429	0.761	0.493	0.509
			16	0.500	0.526	0.368	0.660	0.404	0.379
		0.08	8	0.667	0.376	0.538	0.795	0.827	0.594
			12	0.500	0.492	0.512	0.700	0.691	0.494
			16	0.400	0.571	0.500	0.538	0.583	0.371
		0.12	8	0.667	0.418	0.724	0.729	0.882	0.570
			12	0.462	0.526	0.636	0.660	0.798	0.455
			16	0.375	0.719	0.636	0.350	0.583	0.348
	125	0.04	8	0.857	0.333	0.467	0.795	0.713	0.702
			12	0.667	0.375	0.429	0.729	0.482	0.530
			16	0.545	0.469	0.412	0.547	0.333	0.428
		0.08	8	0.750	0.364	0.636	0.761	0.807	0.624
			12	0.545	0.380	0.568	0.625	0.670	0.496
			16	0.429	0.494	0.538	0.333	0.519	0.366
		0.12	8	0.667	0.370	0.724	0.700	0.827	0.586
			12	0.500	0.439	0.692	0.350	0.720	0.494
			16	0.375	0.639	0.636	0.333	0.568	0.355
40	25	0.04	8	0.857	0.379	0.467	1.000	0.859	0.634
			12	0.667	0.511	0.429	0.833	0.728	0.500
			16	0.500	0.625	0.368	0.729	0.670	0.375
		0.08	8	0.667	0.478	0.538	0.814	0.870	0.615
			12	0.500	0.525	0.512	0.795	0.817	0.494
			16	0.400	0.717	0.500	0.686	0.705	0.355
		0.12	8	0.600	0.492	0.636	0.761	0.957	0.585
			12	0.462	0.582	0.636	0.729	0.838	0.455
			16	0.353	0.875	0.600	0.583	0.770	0.351
	75	0.04	8	0.857	0.375	0.467	0.946	0.798	0.649
			12	0.667	0.471	0.429	0.795	0.705	0.516
			16	0.545	0.526	0.412	0.660	0.620	0.428
		0.08	8	0.750	0.433	0.636	0.814	0.859	0.638
			12	0.545	0.511	0.568	0.714	0.744	0.498
			16	0.429	0.632	0.538	0.625	0.691	0.359

R	v	f	D	F_t	R_a	K_f	CYL	$C_{e\text{-}Exit}$	$F_{d\text{-}Exit}$
			8	0.667	0.457	0.724	0.745	0.905	0.625
		0.12	12	0.500	0.520	0.692	0.673	0.817	0.468
			16	0.400	0.834	0.677	0.530	0.728	0.357
			8	0.857	0.363	0.467	0.814	0.736	0.741
		0.04	12	0.667	0.398	0.429	0.761	0.670	0.612
			16	0.545	0.497	0.412	0.648	0.563	0.428
			8	0.750	0.395	0.636	0.795	0.827	0.654
	125	0.08	12	0.600	0.416	0.636	0.686	0.713	0.500
			16	0.462	0.531	0.583	0.493	0.657	0.384
			8	0.750	0.421	0.840	0.745	0.882	0.641
		0.12	12	0.545	0.509	0.759	0.625	0.798	0.496
			16	0.400	0.635	0.677	0.407	0.713	0.371
			8	1.000	0.384	0.636	1.000	0.893	0.667
		0.04	12	0.750	0.538	0.512	0.946	0.827	0.543
			16	0.600	0.682	0.467	0.814	0.705	0.417
			8	0.857	0.481	0.778	0.946	0.957	0.641
	25	0.08	12	0.667	0.661	0.724	0.814	0.827	0.506
			16	0.500	0.721	0.636	0.729	0.720	0.385
			8	0.750	0.492	0.840	0.795	1.000	0.538
		0.12	12	0.545	0.662	0.759	0.778	0.931	0.468
			16	0.429	1.000	0.724	0.625	0.817	0.359
			8	1.000	0.384	0.636	1.000	0.848	0.844
		0.04	12	0.857	0.492	0.636	0.875	0.770	0.562
			16	0.667	0.669	0.538	0.700	0.626	0.439
			8	0.857	0.457	0.778	0.921	0.870	0.646
60	75	0.08	12	0.667	0.526	0.724	0.745	0.788	0.506
			16	0.545	0.632	0.700	0.660	0.705	0.417
			8	0.857	0.487	1.000	0.795	0.971	0.622
		0.12	12	0.600	0.544	0.840	0.729	0.870	0.506
			16	0.462	0.837	0.778	0.574	0.736	0.371
			8	1.000	0.374	0.636	0.946	0.827	1.000
		0.04	12	0.857	0.465	0.636	0.795	0.705	0.654
			16	0.750	0.509	0.636	0.648	0.604	0.511
			8	1.000	0.395	1.000	0.921	0.870	0.725
	125	0.08	12	0.750	0.482	0.840	0.745	0.736	0.570
			16	0.600	0.582	0.778	0.636	0.684	0.470
			8	0.857	0.421	1.000	0.778	0.957	0.641
		0.12	12	0.667	0.563	0.940	0.660	0.817	0.601
			16	0.545	0.661	0.913	0.515	0.720	0.392

Finally, grey relation grade is computed by averaging grey relation coefficients using Equation 2.16. Table 3.17 presents the grey relation grades of the measured responses along with the ranks. Highest value (0.819) of grey relation grade is noted to be for $v_{125} f_{0.08} R_{60} D_8$ and is the optimized condition for response minimization. By performing drilling at this parameter setting, responses can be effectively minimized to achieve best hole quality.

Table 3.17 Grey relation grade and rank of E200 syntactic foam.

v	f	D	R_{20}		R_{40}		R_{60}	
			γ_i	Rank	γ_i	Rank	γ_i	Rank
25	0.04	8	0.623	40	0.699	13	0.764	7
		12	0.552	62	0.611	46	0.686	19
		16	0.474	78	0.545	65	0.614	44
	0.08	8	0.638	35	0.664	26	0.777	5
		12	0.575	59	0.607	49	0.700	12
		16	0.506	74	0.561	61	0.615	43
	0.12	8	0.642	34	0.672	24	0.736	9
		12	0.591	54	0.617	42	0.690	15
		16	0.519	71	0.589	57	0.659	29
75	0.04	8	0.647	31	0.682	21	0.785	4
		12	0.544	66	0.597	51	0.699	14
		16	0.473	79	0.532	70	0.607	50
	0.08	8	0.633	36	0.688	16	0.755	8
		12	0.565	60	0.597	52	0.659	28
		16	0.494	76	0.546	64	0.610	47
	0.12	8	0.665	25	0.687	18	0.789	3
		12	0.590	55	0.612	45	0.682	22
		16	0.502	75	0.588	58	0.626	37
125	0.04	8	0.645	33	0.663	27	0.797	2
		12	0.535	67	0.589	56	0.686	20
		16	0.456	80	0.515	73	0.610	48
	0.08	8	0.657	30	0.676	23	0.819	1
		12	0.547	63	0.592	53	0.687	17
		16	0.447	81	0.518	72	0.625	38
	0.12	8	0.646	32	0.713	10	0.776	6
		12	0.533	69	0.622	41	0.708	11
		16	0.484	77	0.534	68	0.624	39

Furthermore, it is necessary to analyze the effects of process parameters on the machining performance at the optimized condition ($v_{125} f_{0.08} R_{60} D_{8}$). This is performed using the average analysis and results are presented in Table 3.18. Response table (Table 3.18) is used to draw the grey relation grade graph and is presented in Figure 3.35. It is observed from Figure 3.35 and Table 3.18 that the drill diameter is having a significant effect on the drilling performance at the optimized condition followed by cutting speed. ANOVA is performed on the grey relation grades to compute the percentage contribution of process parameters at the optimized condition and the results are presented in Table 3.19. From Table 3.19 it is clear that the drill diameter (53.64%) has a significant effect on the machining performance followed by the cutting speed (41.38%).

Table 3.18 Response table for grey relation grade of E200 syntactic foam.

Level	Mean grey relation grade			
	v	*f*	*R*	*D*
1	0.5624	0.6274	0.6153	0.7001
2	0.6120	0.6225	0.6195	0.6174
3	0.6932	0.6177	0.6328	0.5501
Delta	0.1308	0.0097	0.0175	0.1500
Rank	2	4	3	1

Table 3.19 ANOVA for grey relation grade of E200 syntactic foam.

Source	DF	Adj SS	Adj MS	F-Value	P-Value	% Contribution
v	2	0.2352	0.1176	702.67	0.00	41.38
f	2	0.0013	0.0006	3.78	0.03	0.22
R	2	0.0045	0.0023	13.48	0.00	0.79
D	2	0.3049	0.1525	910.93	0.00	53.64
*v*f*	4	0.0036	0.0009	5.35	0.00	0.63
*v*R*	4	0.0013	0.0003	1.99	0.11	0.23
*v*D*	4	0.0016	0.0004	2.44	0.06	0.29
*f*R*	4	0.0006	0.0002	0.93	0.46	0.11
*f*D*	4	0.0054	0.0013	7.99	0.00	0.94
*R*D*	4	0.0020	0.0005	2.99	0.03	0.35
Error	48	0.0080	0.0002			
Total	80	0.5685				

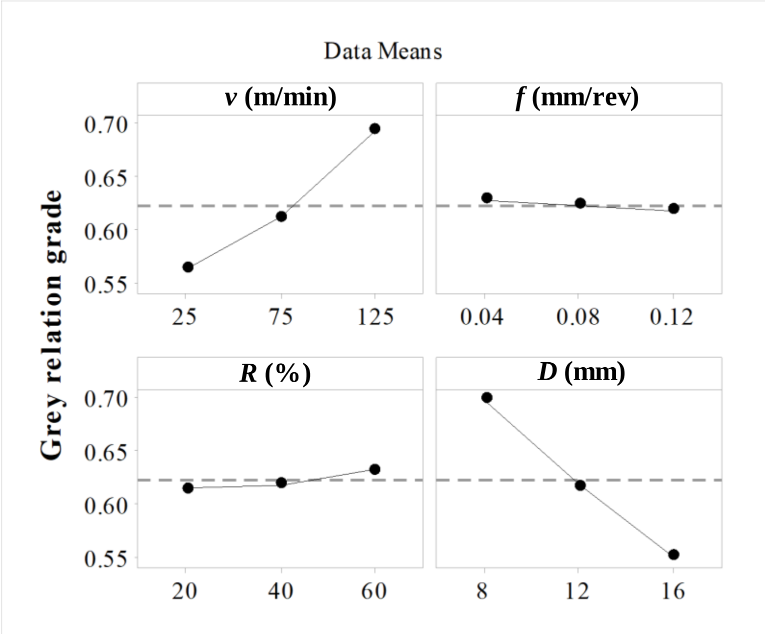

Figure 3.35 Grey relation grade graph for E200 syntactic foam.

3.2.7.2 E270 syntactic foam

Table 3.20 presents the conditions for minimizing the responses. It is observed from Table 3.20 that the conditions for minimizing all the responses are not same. The trade-off between various process parameters for minimizing the responses leads to multi-response optimization using GRA. Table 3.21 presents the normalized experimental data of the responses for comparison computed using Equation 2.11. Equation 2.12 is used for calculating the grey relation coefficients of the responses using the normalized data (Table 3.21) and results are presented in Table 3.22.

Table 3.20 Input parameter settings for minimizing the responses in drilling of E270.

Response	Minimizing condition
Thrust force (F_t)	$v_{125} f_{0.04} R_{60} D_8$
Surface roughness (R_a)	$v_{25} f_{0.12} R_{60} D_{16}$
Sp. cutting coefficient (K_f)	$v_{125} f_{0.12} R_{60} D_8$
Cylindricity (CYL)	$v_{25} f_{0.04} R_{60} D_8$
Exit side circularity error (C_{e-Exit})	$v_{25} f_{0.12} R_{60} D_8$
Exit side damage factor (F_{d-Exit})	$v_{125} f_{0.04} R_{60} D_8$

Table 3.21 Normalized data (Smaller is better) of E270 syntactic foam.

R	*v*	*f*	*D*	F_t	R_a	K_f	*CYL*	$C_{e\text{-}Exit}$	$F_{d\text{-}Exit}$
20	25	0.04	8	0.867	0.314	0.273	0.820	0.772	0.718
20	25	0.04	12	0.667	0.656	0.091	0.787	0.614	0.296
20	25	0.04	16	0.467	0.848	0.000	0.590	0.281	0.080
20	25	0.08	8	0.733	0.357	0.545	0.787	0.842	0.711
20	25	0.08	12	0.533	0.675	0.545	0.656	0.614	0.263
20	25	0.08	16	0.133	0.916	0.341	0.492	0.386	0.016
20	25	0.12	8	0.733	0.477	0.818	0.721	0.947	0.639
20	25	0.12	12	0.467	0.797	0.758	0.656	0.789	0.197
20	25	0.12	16	0.000	0.935	0.591	0.197	0.719	0.000
20	75	0.04	8	0.867	0.143	0.273	0.803	0.684	0.795
20	75	0.04	12	0.733	0.388	0.273	0.770	0.544	0.479
20	75	0.04	16	0.467	0.517	0.000	0.525	0.175	0.158
20	75	0.08	8	0.800	0.143	0.682	0.770	0.825	0.742
20	75	0.08	12	0.533	0.471	0.545	0.607	0.561	0.379
20	75	0.08	16	0.200	0.604	0.409	0.377	0.316	0.125
20	75	0.12	8	0.733	0.330	0.818	0.705	0.895	0.722
20	75	0.12	12	0.467	0.515	0.758	0.508	0.702	0.213
20	75	0.12	16	0.133	0.777	0.682	0.066	0.386	0.034
20	125	0.04	8	0.867	0.092	0.273	0.803	0.526	0.894
20	125	0.04	12	0.733	0.217	0.273	0.705	0.351	0.623
20	125	0.04	16	0.533	0.423	0.136	0.393	0.088	0.313
20	125	0.08	8	0.800	0.134	0.682	0.705	0.667	0.811
20	125	0.08	12	0.533	0.369	0.545	0.492	0.579	0.446
20	125	0.08	16	0.267	0.590	0.477	0.279	0.140	0.183
20	125	0.12	8	0.733	0.330	0.818	0.557	0.667	0.725
20	125	0.12	12	0.400	0.423	0.697	0.459	0.579	0.379
20	125	0.12	16	0.133	0.713	0.682	0.000	0.316	0.080
40	25	0.04	8	0.867	0.358	0.273	1.000	0.754	0.811
40	25	0.04	12	0.733	0.620	0.273	0.852	0.526	0.396
40	25	0.04	16	0.600	0.854	0.273	0.672	0.404	0.213
40	25	0.08	8	0.800	0.471	0.682	0.934	0.895	0.784
40	25	0.08	12	0.600	0.664	0.636	0.738	0.702	0.346
40	25	0.08	16	0.333	0.927	0.545	0.607	0.561	0.107
40	25	0.12	8	0.733	0.599	0.818	0.770	0.965	0.690
40	25	0.12	12	0.533	0.797	0.818	0.705	0.930	0.323
40	25	0.12	16	0.200	0.979	0.727	0.459	0.596	0.054
40	75	0.04	8	0.867	0.244	0.273	0.885	0.754	0.846
40	75	0.04	12	0.733	0.455	0.273	0.770	0.491	0.612
40	75	0.04	16	0.600	0.734	0.273	0.541	0.228	0.324
40	75	0.08	8	0.800	0.343	0.682	0.770	0.860	0.820
40	75	0.08	12	0.600	0.529	0.636	0.656	0.614	0.479
40	75	0.08	16	0.333	0.818	0.545	0.492	0.456	0.114

R	v	f	D	F_t	R_a	K_f	CYL	$C_{e\text{-}Exit}$	$F_{d\text{-}Exit}$
			8	0.733	0.396	0.818	0.721	0.930	0.781
		0.12	12	0.533	0.564	0.818	0.590	0.895	0.363
			16	0.267	0.857	0.773	0.377	0.491	0.116
			8	0.933	0.129	0.545	0.836	0.579	0.928
		0.04	12	0.733	0.315	0.273	0.738	0.474	0.803
			16	0.600	0.482	0.273	0.525	0.000	0.379
			8	0.800	0.284	0.682	0.738	0.807	0.822
	125	0.08	12	0.667	0.334	0.727	0.623	0.526	0.529
			16	0.400	0.596	0.614	0.443	0.386	0.213
			8	0.733	0.337	0.818	0.656	0.842	0.848
		0.12	12	0.600	0.506	0.879	0.508	0.614	0.363
			16	0.267	0.686	0.773	0.033	0.386	0.158
			8	0.933	0.469	0.545	1.000	0.842	0.845
		0.04	12	0.800	0.602	0.455	0.934	0.632	0.637
			16	0.733	0.997	0.545	0.721	0.614	0.302
			8	0.867	0.493	0.818	0.934	0.947	0.748
	25	0.08	12	0.667	0.948	0.727	0.787	0.895	0.468
			16	0.533	0.997	0.750	0.672	0.719	0.229
			8	0.867	0.732	1.000	0.836	1.000	0.663
		0.12	12	0.667	0.981	0.939	0.738	0.912	0.423
			16	0.400	1.000	0.864	0.492	0.807	0.125
			8	0.933	0.407	0.545	0.934	0.772	0.878
		0.04	12	0.867	0.544	0.636	0.852	0.579	0.670
			16	0.733	0.740	0.545	0.705	0.439	0.340
			8	0.867	0.452	0.818	0.902	0.877	0.818
60	75	0.08	12	0.733	0.631	0.818	0.738	0.789	0.515
			16	0.600	0.762	0.818	0.557	0.526	0.290
			8	0.867	0.601	1.000	0.803	0.912	0.759
		0.12	12	0.733	0.694	1.000	0.623	0.825	0.510
			16	0.467	0.878	0.909	0.492	0.737	0.175
			8	1.000	0.000	0.818	0.885	0.702	1.000
		0.04	12	0.867	0.477	0.636	0.754	0.579	0.670
			16	0.733	0.574	0.545	0.623	0.105	0.471
			8	0.933	0.249	0.955	0.869	0.842	0.854
	125	0.08	12	0.733	0.563	0.818	0.672	0.667	0.546
			16	0.600	0.707	0.818	0.492	0.474	0.370
			8	0.867	0.263	1.000	0.738	0.877	0.782
		0.12	12	0.733	0.564	1.000	0.623	0.719	0.523
			16	0.467	0.871	0.909	0.426	0.544	0.213

Table 3.22 Grey relation coefficients of E270 syntactic foam.

R	v	f	D	F_t	R_a	K_f	CYL	$C_{e\text{-}Exit}$	$F_{d\text{-}Exit}$
20	25	0.04	8	0.789	0.422	0.407	0.735	0.687	0.639
			12	0.600	0.592	0.355	0.701	0.564	0.415
			16	0.484	0.767	0.333	0.550	0.410	0.352
		0.08	8	0.652	0.438	0.524	0.701	0.760	0.634
			12	0.517	0.606	0.524	0.592	0.564	0.404
			16	0.366	0.856	0.431	0.496	0.449	0.337
		0.12	8	0.652	0.489	0.733	0.642	0.905	0.580
			12	0.484	0.711	0.673	0.592	0.704	0.384
			16	0.333	0.885	0.550	0.384	0.640	0.333
	75	0.04	8	0.789	0.369	0.407	0.718	0.613	0.709
			12	0.652	0.449	0.407	0.685	0.523	0.490
			16	0.484	0.509	0.333	0.513	0.377	0.373
		0.08	8	0.714	0.369	0.611	0.685	0.740	0.659
			12	0.517	0.486	0.524	0.560	0.533	0.446
			16	0.385	0.558	0.458	0.445	0.422	0.364
		0.12	8	0.652	0.427	0.733	0.629	0.826	0.642
			12	0.484	0.507	0.673	0.504	0.626	0.389
			16	0.366	0.691	0.611	0.349	0.449	0.341
	125	0.04	8	0.789	0.355	0.407	0.718	0.514	0.826
			12	0.652	0.390	0.407	0.629	0.435	0.570
			16	0.517	0.464	0.367	0.452	0.354	0.421
		0.08	8	0.714	0.366	0.611	0.629	0.600	0.726
			12	0.517	0.442	0.524	0.496	0.543	0.474
			16	0.405	0.549	0.489	0.409	0.368	0.380
		0.12	8	0.652	0.427	0.733	0.530	0.600	0.645
			12	0.455	0.464	0.623	0.480	0.543	0.446
			16	0.366	0.635	0.611	0.333	0.422	0.352
40	25	0.04	8	0.789	0.438	0.407	1.000	0.671	0.726
			12	0.652	0.569	0.407	0.772	0.514	0.453
			16	0.556	0.774	0.407	0.604	0.456	0.389
		0.08	8	0.714	0.486	0.611	0.884	0.826	0.699
			12	0.556	0.598	0.579	0.656	0.626	0.433
			16	0.429	0.873	0.524	0.560	0.533	0.359
		0.12	8	0.652	0.555	0.733	0.685	0.934	0.617
			12	0.517	0.711	0.733	0.629	0.877	0.425
			16	0.385	0.960	0.647	0.480	0.553	0.346
	75	0.04	8	0.789	0.398	0.407	0.813	0.671	0.765
			12	0.652	0.479	0.407	0.685	0.496	0.563
			16	0.556	0.653	0.407	0.521	0.393	0.425
		0.08	8	0.714	0.432	0.611	0.685	0.781	0.735
			12	0.556	0.515	0.579	0.592	0.564	0.490
			16	0.429	0.734	0.524	0.496	0.479	0.361

R	v	f	D	F_t	R_a	K_f	CYL	$C_{e\text{-}Exit}$	$F_{d\text{-}Exit}$
			8	0.652	0.453	0.733	0.642	0.877	0.696
		0.12	12	0.517	0.534	0.733	0.550	0.826	0.440
			16	0.405	0.777	0.688	0.445	0.496	0.361
			8	0.882	0.365	0.524	0.753	0.543	0.873
		0.04	12	0.652	0.422	0.407	0.656	0.487	0.717
			16	0.556	0.491	0.407	0.513	0.333	0.446
			8	0.714	0.411	0.611	0.656	0.722	0.738
	125	0.08	12	0.600	0.429	0.647	0.570	0.514	0.515
			16	0.455	0.553	0.564	0.473	0.449	0.389
			8	0.652	0.430	0.733	0.592	0.760	0.767
		0.12	12	0.556	0.503	0.805	0.504	0.564	0.440
			16	0.405	0.614	0.688	0.341	0.449	0.373
			8	0.882	0.485	0.524	1.000	0.760	0.763
		0.04	12	0.714	0.556	0.478	0.884	0.576	0.580
			16	0.652	0.995	0.524	0.642	0.564	0.417
			8	0.789	0.497	0.733	0.884	0.905	0.665
	25	0.08	12	0.600	0.907	0.647	0.701	0.826	0.485
			16	0.517	0.995	0.667	0.604	0.640	0.393
			8	0.789	0.651	1.000	0.753	1.000	0.598
		0.12	12	0.600	0.963	0.892	0.656	0.851	0.464
			16	0.455	1.000	0.786	0.496	0.722	0.364
			8	0.882	0.457	0.524	0.884	0.687	0.804
		0.04	12	0.789	0.523	0.579	0.772	0.543	0.603
			16	0.652	0.658	0.524	0.629	0.471	0.431
			8	0.789	0.477	0.733	0.836	0.803	0.733
60	75	0.08	12	0.652	0.575	0.733	0.656	0.704	0.508
			16	0.556	0.677	0.733	0.530	0.514	0.413
			8	0.789	0.556	1.000	0.718	0.851	0.675
		0.12	12	0.652	0.620	1.000	0.570	0.740	0.505
			16	0.484	0.804	0.846	0.496	0.655	0.377
			8	1.000	0.333	0.733	0.813	0.626	1.000
		0.04	12	0.789	0.489	0.579	0.670	0.543	0.602
			16	0.652	0.540	0.524	0.570	0.358	0.486
			8	0.882	0.400	0.917	0.792	0.760	0.774
	125	0.08	12	0.652	0.534	0.733	0.604	0.600	0.524
			16	0.556	0.631	0.733	0.496	0.487	0.443
			8	0.789	0.404	1.000	0.656	0.803	0.696
		0.12	12	0.652	0.534	1.000	0.570	0.640	0.512
			16	0.484	0.795	0.846	0.466	0.523	0.388

Equation 2.16 is used to calculate grey relation grade by averaging grey relation coefficients and results are presented in Table 3.23. Highest value (0.798) of grey relation grade is noted to be for $v_{25} f_{0.12} R_{60} D_8$ and is the optimized condition for response minimization. By performing drilling at this parameter setting, responses can be effectively minimized to achieve sound quality hole.

Table 3.23 Grey relation grade and rank of E270 syntactic foam.

v	f	D	R_{20}		R_{40}		R_{60}	
			γ_i	Rank	γ_i	Rank	γ_i	Rank
25	0.04	8	0.613	34	0.672	16	0.736	7
		12	0.538	57	0.561	49	0.631	31
		16	0.483	72	0.531	60	0.632	30
	0.08	8	0.618	33	0.703	11	0.746	5
		12	0.535	58	0.575	45	0.694	13
		16	0.489	71	0.546	55	0.636	28
	0.12	8	0.667	17	0.696	12	0.798	1
		12	0.591	43	0.649	23	0.738	6
		16	0.521	64	0.562	48	0.637	27
75	0.04	8	0.601	40	0.641	25	0.706	10
		12	0.535	59	0.547	54	0.635	29
		16	0.431	80	0.493	70	0.561	50
	0.08	8	0.630	32	0.660	18	0.729	8
		12	0.511	66	0.549	53	0.638	26
		16	0.439	78	0.504	67	0.571	46
	0.12	8	0.652	21	0.676	15	0.765	2
		12	0.531	61	0.600	41	0.681	14
		16	0.468	75	0.529	62	0.610	36
125	0.04	8	0.601	39	0.657	19	0.751	4
		12	0.514	65	0.557	52	0.612	35
		16	0.429	81	0.458	76	0.522	63
	0.08	8	0.608	38	0.642	24	0.754	3
		12	0.499	69	0.546	56	0.608	37
		16	0.433	79	0.480	73	0.558	51
	0.12	8	0.598	42	0.656	20	0.725	9
		12	0.502	68	0.562	47	0.651	22
		16	0.453	77	0.478	74	0.584	44

Furthermore, it is necessary to analyze the effects of process parameters on the machining performance at the optimized condition ($v_{25} f_{0.12} R_{60} D_8$). This is performed using the average analysis and results are presented in Table 3.24. Response table (Table 3.24) is used to draw the grey relation grade graph and is presented in Figure 3.36. It is observed from Figure 3.36 and Table 3.24 that the drill diameter is having a significant effect on the drilling performance at the optimized condition followed by cutting speed and feed. ANOVA is performed on the grey relation grades to compute the percentage contribution of process parameters at the optimized condition and the results are presented Table 3.25. From Table 3.25 it is clear that the drill diameter (53.36 %) has a significant effect on the machining performance followed by the cutting speed (34.84 %) and feed (5.58 %).

Table 3.24 Response table for grey relation grade of E270 syntactic foam.

Level	Mean grey relation grade			
	v	*f*	*R*	*D*
1	0.5367	0.6222	0.5795	0.6777
2	0.5825	0.5885	0.5889	0.5848
3	0.6633	0.5718	0.6140	0.5199
Delta	0.1266	0.0504	0.0345	0.1579
Rank	2	3	4	1

Table 3.25 ANOVA for grey relation grade of E270 syntactic foam.

Source	DF	Adj SS	Adj MS	F-Value	P-Value	% Contribution
v	2	0.2219	0.1110	457.34	0.00	34.84
f	2	0.0356	0.0178	73.28	0.00	5.58
R	2	0.0172	0.0086	35.47	0.00	2.70
D	2	0.3400	0.1700	700.56	0.00	53.36
*v*f*	4	0.0003	0.0001	0.28	0.89	0.04
*v*R*	4	0.0009	0.0002	0.93	0.46	0.14
*v*D*	4	0.0001	0.0000	0.10	0.98	0.01
*f*R*	4	0.0039	0.0010	4.04	0.01	0.62
*f*D*	4	0.0042	0.0011	4.37	0.00	0.67
*R*D*	4	0.0013	0.0003	1.39	0.25	0.21
Error	48	0.0116	0.0002			
Total	80	0.6371				

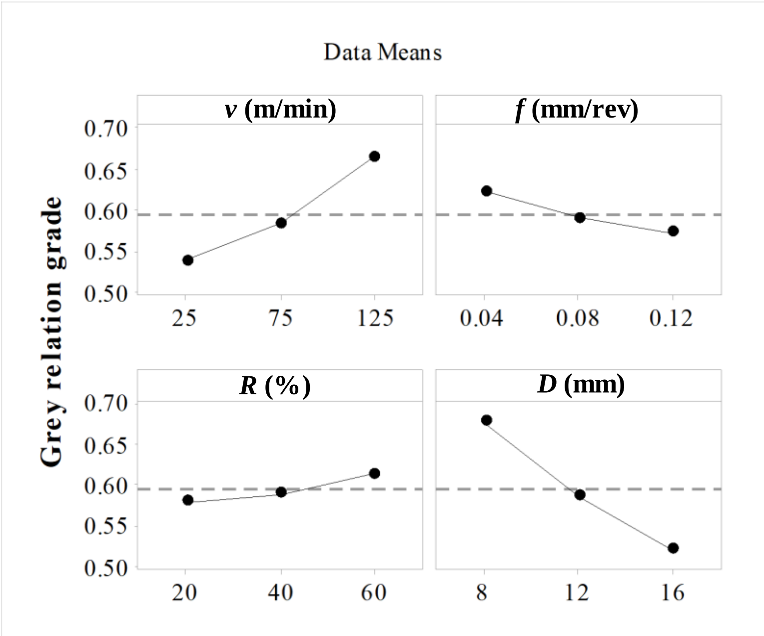

Figure 3.36 Grey relation grade graph for E270 syntactic foam.

3.2.7.3 E350 syntactic foam

The conditions for minimizing the responses of E350 syntactic foam is presented in Table 3.26. It is observed from Table 3.26 that the conditions for minimizing all the responses are not same. The trade-off between cutting speed, feed and drill diameter for minimizing the responses leads to multi-response optimization using GRA.

Table 3.26 Input parameter settings for minimizing the responses in drilling of E350.

Response	Minimizing condition
Thrust force (F_t)	$v_{25} f_{0.04} R_{60} D_8$
Surface roughness (R_a)	$v_{25} f_{0.12} R_{60} D_{12}$
Sp. cutting coefficient (K_f)	$v_{25} f_{0.12} R_{60} D_8$
Cylindricity (CYL)	$v_{75} f_{0.04} R_{60} D_8$
Exit side circularity error (C_{e-Exit})	$v_{25} f_{0.12} R_{60} D_8$
Exit side damage factor (F_{d-Exit})	$v_{25} f_{0.04} R_{60} D_8$

Experimental data used in GRA must be pre-processed using smaller-the-better characteristic since the objective is to minimize the responses. Equation 2.11 is used for data normalization using experimental data (Table 3.2, Table 3.4, Table 3.6, Table 3.8, Table 3.10 and Table 3.12) and results are presented in Table 3.27. Equation 2.12 is used for calculating the grey relation coefficients of the responses and results are presented in Table 3.28.

Table 3.27 Normalized data (Smaller is better) of E350 syntactic foam.

R	v	f	D	F_t	R_a	K_f	CYL	$C_{e\text{-}Exit}$	$F_{d\text{-}Exit}$
20	25	0.04	8	0.882	0.679	0.484	0.854	0.905	0.946
			12	0.706	0.835	0.355	0.732	0.667	0.518
			16	0.353	0.807	0.000	0.439	0.429	0.220
		0.08	8	0.765	0.618	0.677	0.780	0.952	0.795
			12	0.588	0.880	0.677	0.585	0.762	0.411
			16	0.176	0.770	0.484	0.220	0.571	0.143
		0.12	8	0.706	0.360	0.806	0.707	0.952	0.786
			12	0.471	0.872	0.785	0.707	0.810	0.375
			16	0.118	0.866	0.710	0.073	0.643	0.054
	75	0.04	8	0.882	0.477	0.484	0.878	0.786	0.830
			12	0.647	0.821	0.226	0.805	0.524	0.411
			16	0.412	0.469	0.097	0.561	0.143	0.173
		0.08	8	0.765	0.381	0.677	0.780	0.833	0.821
			12	0.471	0.780	0.548	0.610	0.619	0.327
			16	0.235	0.641	0.532	0.488	0.286	0.149
		0.12	8	0.706	0.335	0.806	0.659	0.905	0.777
			12	0.471	0.925	0.785	0.659	0.762	0.196
			16	0.059	0.590	0.677	0.317	0.429	0.054
	125	0.04	8	0.824	0.434	0.290	0.878	0.690	0.750
			12	0.588	0.891	0.097	0.707	0.500	0.304
			16	0.412	0.222	0.097	0.317	0.000	0.089
		0.08	8	0.706	0.356	0.581	0.610	0.762	0.795
			12	0.588	0.873	0.677	0.610	0.524	0.185
			16	0.059	0.719	0.387	0.000	0.119	0.030
		0.12	8	0.529	0.313	0.613	0.732	0.643	0.580
			12	0.471	0.829	0.785	0.512	0.524	0.161
			16	0.000	0.387	0.645	0.024	0.071	0.000
40	25	0.04	8	0.882	0.457	0.484	0.927	0.905	1.000
			12	0.706	0.915	0.355	0.732	0.690	0.661
			16	0.588	0.636	0.387	0.488	0.500	0.446
		0.08	8	0.824	0.610	0.774	0.829	0.976	0.857
			12	0.706	0.893	0.806	0.756	0.881	0.351
			16	0.412	0.533	0.677	0.366	0.690	0.244
		0.12	8	0.765	0.598	0.871	0.780	1.000	0.911
			12	0.588	0.927	0.871	0.610	0.929	0.375
			16	0.353	0.805	0.839	0.122	0.762	0.179
	75	0.04	8	0.882	0.553	0.484	1.000	0.810	0.938
			12	0.765	0.780	0.484	0.878	0.619	0.399
			16	0.647	0.636	0.484	0.683	0.310	0.315
		0.08	8	0.824	0.669	0.774	0.780	0.833	0.786
			12	0.647	0.880	0.742	0.780	0.738	0.446
			16	0.412	0.598	0.677	0.488	0.405	0.089

R	v	f	D	F_t	R_a	K_f	CYL	$C_{e\text{-}Exit}$	$F_{d\text{-}Exit}$
			8	0.765	0.366	0.871	0.854	0.905	0.848
		0.12	12	0.588	0.833	0.871	0.659	0.762	0.268
			16	0.294	0.588	0.806	0.390	0.476	0.125
			8	0.941	0.327	0.677	0.829	0.714	0.839
		0.04	12	0.765	0.691	0.484	0.634	0.548	0.446
			16	0.588	0.312	0.387	0.390	0.119	0.125
			8	0.824	0.285	0.774	0.780	0.810	0.875
	125	0.08	12	0.647	0.866	0.742	0.732	0.595	0.339
			16	0.353	0.331	0.629	0.146	0.190	0.018
			8	0.765	0.323	0.871	0.659	0.833	0.768
		0.12	12	0.529	0.893	0.828	0.585	0.643	0.268
			16	0.176	0.492	0.742	0.073	0.143	0.042
			8	0.941	0.498	0.677	0.927	0.929	0.912
		0.04	12	0.824	0.980	0.613	0.878	0.857	0.589
			16	0.647	0.669	0.484	0.634	0.524	0.357
			8	0.882	0.638	0.871	0.829	0.976	0.825
	25	0.08	12	0.765	1.000	0.871	0.732	0.905	0.536
			16	0.529	0.910	0.774	0.488	0.762	0.251
			8	0.882	0.714	1.000	0.805	1.000	0.728
		0.12	12	0.706	0.945	0.957	0.610	0.952	0.415
			16	0.529	0.918	0.935	0.293	0.810	0.144
			8	0.941	0.452	0.677	1.000	0.833	0.946
		0.04	12	0.882	0.750	0.742	0.878	0.738	0.571
			16	0.706	0.530	0.581	0.683	0.452	0.339
			8	0.882	0.442	0.871	0.927	0.857	0.839
60	75	0.08	12	0.706	0.809	0.806	0.829	0.810	0.393
			16	0.471	0.766	0.726	0.512	0.452	0.220
			8	0.824	0.595	0.935	0.829	0.905	0.748
		0.12	12	0.706	0.835	0.957	0.805	0.833	0.393
			16	0.412	0.553	0.871	0.463	0.667	0.161
			8	1.000	0.295	0.871	0.854	0.738	0.834
		0.04	12	0.824	0.863	0.613	0.732	0.548	0.470
			16	0.647	0.719	0.484	0.585	0.190	0.244
			8	0.882	0.000	0.871	0.780	0.833	0.680
	125	0.08	12	0.706	0.780	0.806	0.707	0.667	0.339
			16	0.471	0.841	0.726	0.415	0.333	0.185
			8	0.824	0.269	0.935	0.780	0.833	0.571
		0.12	12	0.647	0.946	0.914	0.585	0.667	0.304
			16	0.412	0.881	0.871	0.268	0.381	0.054

Table 3.28 Grey relation coefficients of E350 syntactic foam.

R	v	f	D	F_t	R_a	K_f	CYL	$C_{e\text{-}Exit}$	$F_{d\text{-}Exit}$
20	25	0.04	8	0.810	0.609	0.492	0.774	0.840	0.903
			12	0.630	0.752	0.437	0.651	0.600	0.509
			16	0.436	0.722	0.333	0.471	0.467	0.391
		0.08	8	0.680	0.567	0.608	0.695	0.913	0.709
			12	0.548	0.807	0.608	0.547	0.677	0.459
			16	0.378	0.685	0.492	0.390	0.538	0.368
		0.12	8	0.630	0.439	0.721	0.631	0.913	0.700
			12	0.486	0.796	0.699	0.631	0.724	0.444
			16	0.362	0.788	0.633	0.350	0.583	0.346
	75	0.04	8	0.810	0.489	0.492	0.804	0.700	0.747
			12	0.586	0.736	0.392	0.719	0.512	0.459
			16	0.459	0.485	0.356	0.532	0.368	0.377
		0.08	8	0.680	0.447	0.608	0.695	0.750	0.737
			12	0.486	0.695	0.525	0.562	0.568	0.426
			16	0.395	0.582	0.517	0.494	0.412	0.370
		0.12	8	0.630	0.429	0.721	0.594	0.840	0.691
			12	0.486	0.869	0.699	0.594	0.677	0.384
			16	0.347	0.549	0.608	0.423	0.467	0.346
	125	0.04	8	0.739	0.469	0.413	0.804	0.618	0.667
			12	0.548	0.821	0.356	0.631	0.500	0.418
			16	0.459	0.391	0.356	0.423	0.333	0.354
		0.08	8	0.630	0.437	0.544	0.562	0.677	0.709
			12	0.548	0.798	0.608	0.562	0.512	0.380
			16	0.347	0.640	0.449	0.333	0.362	0.340
		0.12	8	0.515	0.421	0.564	0.651	0.583	0.544
			12	0.486	0.745	0.699	0.506	0.512	0.373
			16	0.333	0.449	0.585	0.339	0.350	0.333
40	25	0.04	8	0.810	0.479	0.492	0.872	0.840	1.000
			12	0.630	0.854	0.437	0.651	0.618	0.596
			16	0.548	0.579	0.449	0.494	0.500	0.475
		0.08	8	0.739	0.562	0.689	0.745	0.955	0.778
			12	0.630	0.824	0.721	0.672	0.808	0.435
			16	0.459	0.517	0.608	0.441	0.618	0.398
		0.12	8	0.680	0.554	0.795	0.695	1.000	0.848
			12	0.548	0.873	0.795	0.562	0.875	0.444
			16	0.436	0.720	0.756	0.363	0.677	0.378
	75	0.04	8	0.810	0.528	0.492	1.000	0.724	0.889
			12	0.680	0.695	0.492	0.804	0.568	0.454
			16	0.586	0.579	0.492	0.612	0.420	0.422
		0.08	8	0.739	0.601	0.689	0.695	0.750	0.700
			12	0.586	0.807	0.660	0.695	0.656	0.475
			16	0.459	0.554	0.608	0.494	0.457	0.354

R	v	f	D	F_t	R_a	K_f	CYL	$C_{e\text{-}Exit}$	$F_{d\text{-}Exit}$
		0.12	8	0.680	0.441	0.795	0.774	0.840	0.767
			12	0.548	0.750	0.795	0.594	0.677	0.406
			16	0.415	0.548	0.721	0.451	0.488	0.364
	125	0.04	8	0.895	0.426	0.608	0.745	0.636	0.757
			12	0.680	0.618	0.492	0.577	0.525	0.475
			16	0.548	0.421	0.449	0.451	0.362	0.364
		0.08	8	0.739	0.412	0.689	0.695	0.724	0.800
			12	0.586	0.788	0.660	0.651	0.553	0.431
			16	0.436	0.428	0.574	0.369	0.382	0.337
		0.12	8	0.680	0.425	0.795	0.594	0.750	0.683
			12	0.515	0.824	0.744	0.547	0.583	0.406
			16	0.378	0.496	0.660	0.350	0.368	0.343
60	25	0.04	8	0.895	0.499	0.608	0.872	0.875	0.851
			12	0.739	0.961	0.564	0.804	0.778	0.549
			16	0.586	0.601	0.492	0.577	0.512	0.437
		0.08	8	0.810	0.580	0.795	0.745	0.955	0.741
			12	0.680	1.000	0.795	0.651	0.840	0.519
			16	0.515	0.847	0.689	0.494	0.677	0.400
		0.12	8	0.810	0.636	1.000	0.719	1.000	0.648
			12	0.630	0.902	0.921	0.562	0.913	0.461
			16	0.515	0.859	0.886	0.414	0.724	0.369
	75	0.04	8	0.895	0.477	0.608	1.000	0.750	0.903
			12	0.810	0.667	0.660	0.804	0.656	0.538
			16	0.630	0.515	0.544	0.612	0.477	0.431
		0.08	8	0.810	0.472	0.795	0.872	0.778	0.757
			12	0.630	0.723	0.721	0.745	0.724	0.452
			16	0.486	0.681	0.646	0.506	0.477	0.391
		0.12	8	0.739	0.552	0.886	0.745	0.840	0.665
			12	0.630	0.752	0.921	0.719	0.750	0.452
			16	0.459	0.528	0.795	0.482	0.600	0.373
	125	0.04	8	1.000	0.415	0.795	0.774	0.656	0.751
			12	0.739	0.785	0.564	0.651	0.525	0.486
			16	0.586	0.640	0.492	0.547	0.382	0.398
		0.08	8	0.810	0.333	0.795	0.695	0.750	0.610
			12	0.630	0.694	0.721	0.631	0.600	0.431
			16	0.486	0.758	0.646	0.461	0.429	0.380
		0.12	8	0.739	0.406	0.886	0.695	0.750	0.538
			12	0.586	0.903	0.853	0.547	0.600	0.418
			16	0.459	0.808	0.795	0.406	0.447	0.346

Lastly, grey relation grade is computed by averaging grey relation coefficients using Equation 2.16 and results are presented in Table 3.29 along with the ranks. Highest grey relation grade (0.802) is noted for $v_{25} f_{0.12} R_{60} D_{8}$ and is the optimized condition for response minimization. By performing drilling at this parameter setting, responses can be effectively minimized to achieve best hole quality.

Table 3.29 Grey relation grade and rank of E350 syntactic foam.

v	f	D	R_{20}		R_{40}		R_{60}	
			γ_i	Rank	γ_i	Rank	γ_i	Rank
25	0.04	8	0.738	11	0.749	6	0.767	4
		12	0.597	48	0.631	35	0.733	13
		16	0.470	72	0.508	66	0.534	61
	0.08	8	0.695	19	0.745	9	0.771	3
		12	0.608	45	0.682	22	0.748	7
		16	0.475	71	0.507	68	0.604	46
	0.12	8	0.672	26	0.762	5	0.802	1
		12	0.630	36	0.683	21	0.732	15
		16	0.510	65	0.555	53	0.628	38
75	0.04	8	0.674	25	0.741	10	0.772	2
		12	0.567	51	0.616	43	0.689	20
		16	0.430	77	0.519	64	0.535	60
	0.08	8	0.653	31	0.696	18	0.747	8
		12	0.544	57	0.647	34	0.666	28
		16	0.462	73	0.488	70	0.531	62
	0.12	8	0.651	33	0.716	16	0.738	12
		12	0.618	41	0.628	37	0.704	17
		16	0.457	74	0.498	69	0.540	59
125	0.04	8	0.618	40	0.678	23	0.732	14
		12	0.546	56	0.561	52	0.625	39
		16	0.386	81	0.433	75	0.508	67
	0.08	8	0.593	49	0.677	24	0.666	29
		12	0.568	50	0.612	44	0.618	42
		16	0.412	79	0.421	78	0.527	63
	0.12	8	0.546	55	0.655	30	0.669	27
		12	0.554	54	0.603	47	0.651	32
		16	0.398	80	0.433	76	0.544	58

Moreover, it is essential to analyze the effects of process parameters on the machining performance at the optimized condition ($v_{25} f_{0.12} R_{60} D_{8}$). This is performed using the average analysis and results are presented in Table 3.30. Response table (Table 3.30) is used to draw the grey relation grade graph and is presented in Figure 3.37. It is observed from Figure 3.37 and Table 3.30 that the drill diameter is having a significant effect on the drilling performance at the optimized condition followed by cutting speed and feed. The percentage contribution of process parameters at the optimized condition is computed by performing ANOVA on the grey relation grades and the results are presented in Table 3.31. From Table 3.31 it is clear that the drill diameter (68.77%) has a significant effect on the machining performance followed by the cutting speed (15.40%) and feed (11.21%). These observations offer guidelines for the industries to produce quality holes in GMB/Epoxy syntactic foams used for structural applications.

Table 3.30 Response table for grey relation grade of E350 syntactic foam.

Level	Mean grey relation grade			
	v	*f*	*R*	*D*
1	0.5582	0.6494	0.6056	0.7008
2	0.6088	0.6120	0.6058	0.6317
3	0.6584	0.5641	0.6139	0.4929
Delta	0.1002	0.0853	0.0083	0.2079
Rank	2	3	4	1

Table 3.31 ANOVA for grey relation grade of E350 syntactic foam.

Source	DF	Adj SS	Adj MS	F-Value	P-Value	% Contribution
v	2	0.1356	0.0678	159.27	0.00	15.40
f	2	0.0987	0.0494	115.93	0.00	11.21
R	2	0.0012	0.0006	1.41	0.26	0.14
D	2	0.6055	0.3027	711.04	0.00	68.77
*v*f*	4	0.0005	0.0001	0.26	0.90	0.05
*v*R*	4	0.0005	0.0001	0.30	0.88	0.06
*v*D*	4	0.0036	0.0009	2.12	0.09	0.41
*f*R*	4	0.0033	0.0008	1.95	0.12	0.38
*f*D*	4	0.0015	0.0004	0.89	0.48	0.17
*R*D*	4	0.0096	0.0024	5.62	0.00	1.09
Error	48	0.0204	0.0004			
Total	80	0.8804				

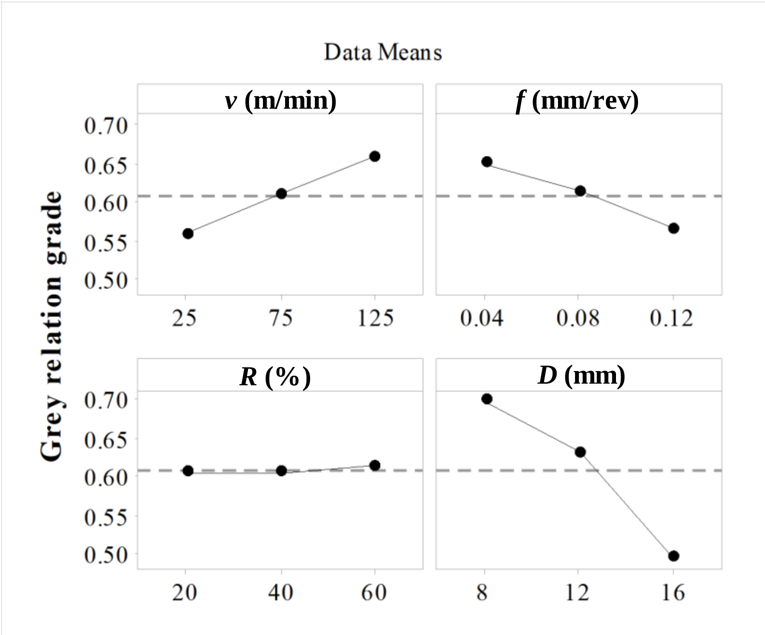

Figure 3.37 Grey relation grade graph for E350 syntactic foam.

Parameter settings for minimizing the responses based on prevailing GRA investigations on individual foams are $v_{125} f_{0.08} R_{60} D_8$, $v_{25} f_{0.12} R_{60} D_8$ and $v_{25} f_{0.12} R_{60} D_8$ for E200, E270 and E350 foams respectively. These parametric settings help industrial practitioners to achieve best quality holes in drilling of the GMB/Epoxy syntactic foams. Nevertheless, its worthwhile to investigate wall thickness effect on the quality of the drilled holes and is presented hereafter.

3.3 Influence of GMB wall thickness on drilling characteristics of SFs

From earlier investigations, it is observed that increasing GMBs content significantly improves the hole quality. Thereby, GMBs content is fixed at 60 vol.% for analyzing the influence of GMB wall thickness on the drilling characteristics of syntactic foams. Levels of the remaining process parameter are kept same as stated in the earlier investigations and are presented in Table 3.32 along with GMBs wall thickness. Three levels for each input process parameters are selected (Table 3.32) to consider the nonlinear effects among the parameters. Table 3.33 presents extracted values based on wall thickness from Table 3.2, Table 3.4, Table 3.6, Table 3.8, Table 3.10 and Table 3.12. Based on the values as presented in Table 3.33, mathematical models are proposed to study the interaction effects of wall thickness variations.

Table 3.32 Drilling process parameters.

Parameters	Levels		
	1	2	3
v	25	75	125
f	0.04	0.08	0.12
D	8	12	16
w	0.716	0.925	1.080

Table 3.33 Experimental layout plan and the measured average value of responses.

w	v	f	D	F_t	R_a	K_f	CYL	$C_{e\text{-}Exit}$	$F_{d\text{-}Exit}$
0.716	25	0.04	8	19.62	4.12	122.63	0.022	0.024	1.003
			12	39.24	2.81	163.50	0.024	0.030	1.004
			16	58.86	2.11	183.94	0.030	0.044	1.007
		0.08	8	29.43	3.20	91.97	0.024	0.019	1.003
			12	49.05	2.20	102.19	0.030	0.030	1.005
			16	78.48	1.97	122.63	0.035	0.042	1.007
		0.12	8	39.24	3.12	81.75	0.031	0.016	1.004
			12	68.67	2.19	95.38	0.032	0.021	1.005
			16	98.10	1.29	102.19	0.043	0.031	1.008
	75	0.04	8	19.62	4.12	122.63	0.022	0.028	1.001
			12	29.43	3.11	122.63	0.027	0.036	1.004
			16	49.05	2.16	153.28	0.037	0.056	1.006
		0.08	8	29.43	3.39	91.97	0.025	0.026	1.003
			12	49.05	2.88	102.19	0.034	0.034	1.005
			16	68.67	2.32	107.30	0.040	0.044	1.007
		0.12	8	29.43	3.15	61.31	0.031	0.018	1.003
			12	58.86	2.77	81.75	0.035	0.026	1.005
			16	88.29	1.63	91.97	0.048	0.040	1.008
	125	0.04	8	19.62	4.25	122.63	0.024	0.030	1.001
			12	29.43	3.32	122.63	0.031	0.044	1.003
			16	39.24	2.99	122.63	0.041	0.060	1.005
		0.08	8	19.62	3.99	61.31	0.025	0.026	1.002
			12	39.24	3.19	81.75	0.034	0.040	1.004
			16	58.86	2.56	91.97	0.042	0.047	1.005
		0.12	8	29.43	3.73	61.31	0.032	0.019	1.003
			12	49.05	2.66	68.13	0.040	0.031	1.003
			16	68.67	2.20	71.53	0.055	0.042	1.007
0.925	25	0.04	8	29.43	3.03	183.94	0.010	0.013	1.003
			12	49.05	2.54	204.38	0.014	0.025	1.005
			16	58.86	1.08	183.94	0.027	0.026	1.007
		0.08	8	39.24	2.94	122.63	0.014	0.007	1.004
			12	68.67	1.26	143.06	0.023	0.010	1.006
			16	88.29	1.08	137.95	0.030	0.020	1.008
		0.12	8	39.24	2.06	81.75	0.020	0.004	1.004
			12	68.67	1.14	95.38	0.026	0.009	1.006
			16	107.91	1.07	112.41	0.041	0.015	1.008
	75	0.04	8	29.43	3.26	183.94	0.014	0.017	1.003
			12	39.24	2.75	163.50	0.019	0.028	1.004
			16	58.86	2.03	183.94	0.028	0.036	1.007
		0.08	8	39.24	3.09	122.63	0.016	0.011	1.003
			12	58.86	2.43	122.63	0.026	0.016	1.005
			16	78.48	1.95	122.63	0.037	0.031	1.007

w	v	f	D	F_t	R_a	K_f	CYL	$C_{e\text{-}Exit}$	$F_{d\text{-}Exit}$
			8	39.24	2.54	81.75	0.022	0.009	1.004
		0.12	12	58.86	2.20	81.75	0.033	0.014	1.006
			16	98.10	1.52	102.19	0.041	0.019	1.008
			8	19.62	4.76	122.63	0.017	0.021	1.002
		0.04	12	39.24	3.00	163.50	0.025	0.028	1.004
			16	58.86	2.64	183.94	0.033	0.055	1.006
			8	29.43	3.84	91.97	0.018	0.013	1.003
	125	0.08	12	58.86	2.68	122.63	0.030	0.023	1.005
			16	78.48	2.15	122.63	0.041	0.034	1.007
			8	39.24	3.79	81.75	0.026	0.011	1.003
		0.12	12	58.86	2.68	81.75	0.033	0.020	1.005
			16	98.10	1.55	102.19	0.045	0.030	1.008
			8	29.43	2.78	183.94	0.010	0.006	1.003
		0.04	12	49.05	0.87	204.38	0.012	0.009	1.006
			16	78.48	2.10	245.25	0.022	0.023	1.007
			8	39.24	2.22	122.63	0.014	0.004	1.004
	25	0.08	12	58.86	0.79	122.63	0.018	0.007	1.006
			16	98.10	1.15	153.28	0.028	0.013	1.008
			8	39.24	1.92	81.75	0.015	0.003	1.005
		0.12	12	68.67	1.00	95.38	0.023	0.005	1.007
			16	98.10	1.11	102.19	0.036	0.011	1.009
			8	29.43	2.96	183.94	0.007	0.010	1.003
		0.04	12	39.24	1.78	163.50	0.012	0.014	1.006
			16	68.67	2.65	214.59	0.020	0.026	1.007
			8	39.24	3.00	122.63	0.010	0.009	1.004
1.080	75	0.08	12	68.67	1.55	143.06	0.014	0.011	1.007
			16	107.91	1.72	168.61	0.027	0.026	1.008
			8	49.05	2.39	102.19	0.014	0.007	1.004
		0.12	12	68.67	1.44	95.38	0.015	0.010	1.007
			16	117.72	2.56	122.63	0.029	0.017	1.009
			8	19.62	3.58	122.63	0.013	0.014	1.004
		0.04	12	49.05	1.33	204.38	0.018	0.022	1.006
			16	78.48	1.90	245.25	0.024	0.037	1.008
			8	39.24	4.75	122.63	0.016	0.010	1.005
	125	0.08	12	68.67	1.66	143.06	0.019	0.017	1.007
			16	107.91	1.42	168.61	0.031	0.031	1.008
			8	49.05	3.68	102.19	0.016	0.010	1.006
		0.12	12	78.48	1.00	109.00	0.024	0.017	1.008
			16	117.72	1.26	122.63	0.037	0.029	1.009

3.3.1 Development of mathematical models based on experimental data

Mathematical models for the considered responses ($F_t, R_a, K_f, CYL, C_{e-Exit}$ and F_{d-Exit}) are developed using the experimental data presented in Table 3.33. Since the process parameters (w, v, f and D) are considered at multi-levels, second-order mathematical models based on RSM are proposed for predicting the responses within the chosen range of process parameters. Regression equations for the different responses are developed using commercially available Minitab 14 software and are given as,

$$F_t = \begin{pmatrix} 77.73 - 94.32\times w - 0.53\times v + 226.59\times f - 6.45\times D + 14.39\times w^2 - 0.0001\times v^2 - \\ 2611.46\times f^2 + 0.18\times D^2 + 0.53\times w\times v + 70.64\times w\times f + 6.19\times w\times D + 0.27\times v\times \\ f - 0.003\times v\times D + 35.77\times f\times D \end{pmatrix} \tag{3.19}$$

$$R_a = \begin{pmatrix} 11.35 - 2.87\times w + 0.02\times v - 21.51\times f - 0.92\times D - 0.85\times w^2 - 3.73\times 10^{-5}\times v^2 - \\ 11.00\times f^2 + 0.03\times D^2 + 0.004\times w\times v + 9.64\times w\times f + 0.09\times w\times D + 0.02\times v\times f \\ -0.001\times v\times D + 0.17\times f\times D \end{pmatrix} \tag{3.20}$$

$$K_f = \begin{pmatrix} 119.09 + 142.91\times w - 1.33\times v - 830.49\times f - 2.10\times D - 34.7\times w^2 - 0.0002\times v^2 + \\ 6820.41\times f^2 + 0.09\times D^2 + 0.86\times w\times v - 1215.09\times w\times f + 5.88\times w\times D + 3.03\times v \\ \times f + 0.01\times v\times D - 30.16\times f\times D \end{pmatrix} \tag{3.21}$$

$$CYL = \begin{pmatrix} 0.02 + 0.03\times w + 1.28\times 10^{-5}\times v + 0.05\times f - 0.002\times D - 0.03\times w^2 + 5.78\times 10^{-7}\times v^2 \\ +0.278\times f^2 + 0.0001\times D^2 - 0.0001\times w\times v - 0.06\times w\times f + 0.0003\times w\times D - 0.0002 \\ \times v\times f + 4.17\times 10^{-6}\times v\times D + 0.01\times f\times D \end{pmatrix} \tag{3.22}$$

$$C_{e-Exit} = \begin{pmatrix} 0.12 - 0.19\times w - 0.0001\times v - 0.24\times f + 0.001\times D + 0.08\times w^2 - 7.41\times 10^{-8}\times \\ v^2 + 0.51\times f^2 + 0.0001\times D^2 + 0.0001\times w\times v + 0.20\times w\times f - 0.002\times w\times D - \\ 0.0002\times v\times f + 1.14\times 10^{-5}\times v\times D - 0.01\times f\times D \end{pmatrix} \tag{3.23}$$

$$F_{d-Exit} = \begin{pmatrix} 1.004 - 0.014\times w - 0.0001\times v + 0.032\times f + 0.0005\times D + 0.008\times w^2 - 2.09\times \\ 10^{-8}\times v^2 - 0.063\times f^2 + 5.70\times 10^{-7}\times D^2 + 0.0001\times w\times v - 0.007\times w\times f + 2.74 \\ \times 10^{-6}\times w\times D + 2.41\times 10^{-5}\times v\times f - 2.21\times 10^{-7}\times v\times D + 0.0001\times f\times D \end{pmatrix} \quad (3.24)$$

Equation 3.19-Equation 3.24 are used to predict the responses within the chosen range of input process parameters. ANOVA is used to validate proposed mathematical expressions adequacy (Table 3.34). According to ANOVA, the computed F-ratio should be more than the F-table for the models to be adequate. Higher CoD values indicate the adequacy of developed mathematical models for prediction. The average errors between the experimentally measured and predicted values are found to be 0.74, 4.5, 0.74, 0.95, 0.98 and 0.01% for F_t, R_a, K_f, *CYL*, $C_{e\text{-}Exit}$ and $F_{d\text{-}Exit}$ respectively indicates a good correlation is existing between the predicted and experimental values. Measurement of surface roughness in reinforced composites is less reliable, because the heterogeneous nature of composite material may lead to large deviations or improper results. Generally, surface roughness of machined surface is considered by averaging the value of several measurements. Deviations among the individual measurements may lead to high error percentage in surface roughness. However, the error between the measured and predicted values falls within 5% and hence the developed mathematical models can be effectively used as a tool in industrial practices to predict the machinability characteristics of varying wall thickness GMB reinforced epoxy foams during drilling.

3.3.2 Effects of individual parameters

Figure 3.38 shows the main effects plots for the responses. F_t increases with increasing *w*, *f*, *D* and slightly decreases with increasing *v* as seen from Figure 3.38a. Figure 3.38b shows that R_a increases with increasing *v* while decreases with increase in *w*, *f*, *D*. K_f increases as *w* and *D* increases while it declines with higher values of *v* and *f* (Figure 3.38c). *CYL* increases with increasing *f*, *v*, *D* and decreasing *w* as observed from Figure 3.38d. Figure 3.38e shows that $C_{e\text{-}Exit}$ increases with *D* and *v*, while decreasing trend is noted with *w* and *f*. Figure 3.38f shows increasing *w*, *f*, *D* increases the $F_{d\text{-}Exit}$ while it slightly decreases with increasing cutting speed.

Table 3.34 Summary of ANOVA results for the developed mathematical models.

Responses	Sum of squares		Degrees of freedom		Mean square		F-ratio	P-Value	CoD
	Regression	Residual	Regression	Residual	Regression	Residual			
F_t	5.02×10^{4}	1.77×10^{3}	14	66	3.59×10^{3}	26.83	133.78[a]	<0.001	0.9660
R_a	59.09	13.45			4.22	0.20	20.71[a]	<0.001	0.8145
K_f	1.33×10^{5}	1.16×10^{4}			9.53×10^{3}	175	54.43[a]	<0.001	0.9203
CYL	7.96×10^{-3}	3.61×10^{-4}			5.68×10^{-4}	5.00×10^{-6}	103.92[a]	<0.001	0.9566
C_{e-Exit}	1.33×10^{-2}	4.57×10^{-4}			9.48×10^{-4}	7.00×10^{-6}	137.10[a]	<0.001	0.9668
F_{d-Exit}	3.02×10^{-4}	9.00×10^{-6}			2.20×10^{-5}	1.41×10^{-7}	156.50[a]	<0.001	0.9708

[a]F-table = 2.36. Significance at 99 % confidence interval.

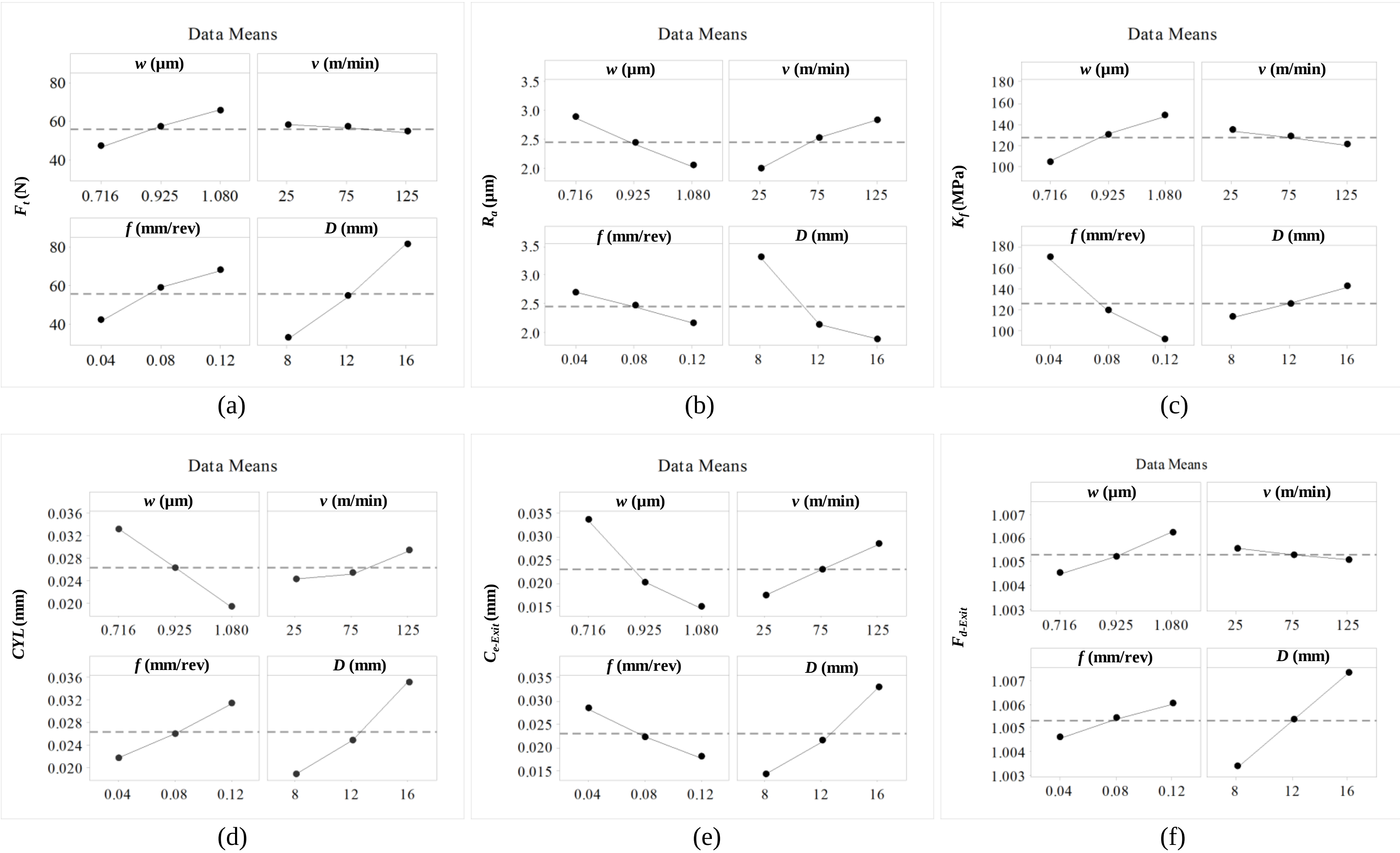

Figure 3.38 Main effects plot for (a) F_t (b) R_a (c) K_f (d) CYL (e) $C_{e\text{-}Exit}$ and (f) $F_{d\text{-}Exit}$.

3.3.3 Response surface plots for studying interaction effects

Interaction effects among the input process parameters are studied using response surface plots. The plots for varying wall thickness of GMBs are plotted using MATLAB software.

3.3.3.1 Thrust force

The variation of F_t with the input parameters such as w, v, f and D are graphed in Figure 3.39.

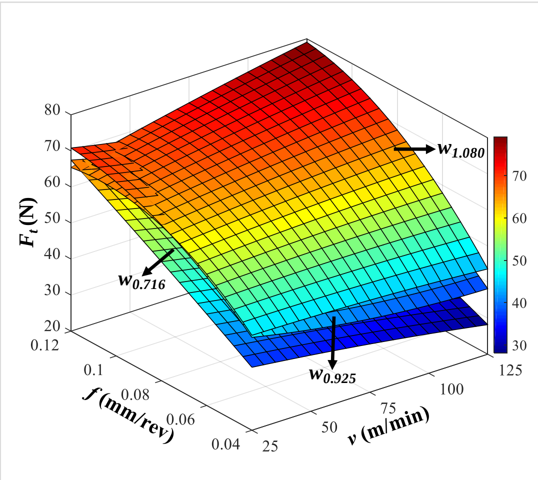

(a)

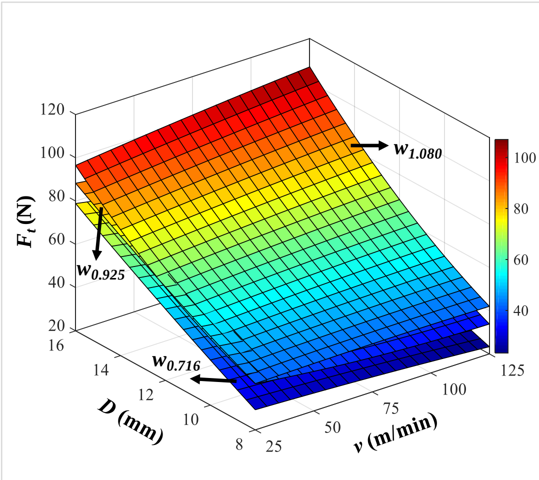

(b)

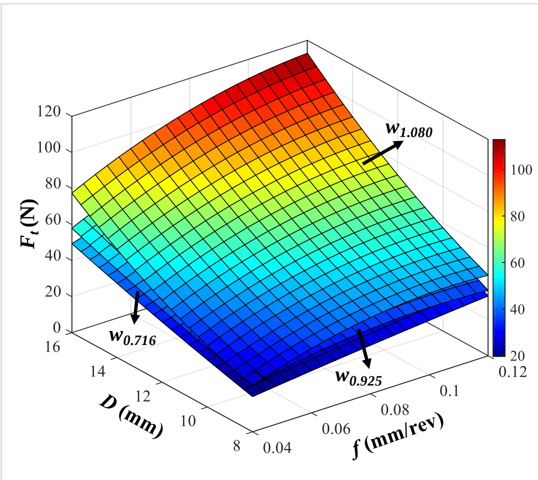

(c)

Figure 3.39 Response surface plots of (a) *v-f*, (b) *v-D* and (c) *f-D* on F_t for varying wall thickness.

F_t increases significantly with the increase in feed. Variation of F_t with increasing cutting speed is found to be very small (Figure 3.39a). Increasing feed from $f_{0.04}$ to $f_{0.12}$ increases F_t by 71, 66 and 81% for $w_{0.716}$, $w_{0.925}$ and $w_{1.080}$ respectively. It is known that increasing feed increases the contact area between twist drill and syntactic foam, which in turn increases metal removal rate resulting higher thrust forces. Also, increasing feed increases the cross-sectional area of undeformed chip which in turn increases the resistance for chip formation resulting in higher thrust force (Basavarajappa et al. 2011). F_t is found to be decreasing with increasing v for $w_{0.716}$ and $w_{0.925}$, while it slightly increases for $w_{1.080}$ (Figure 3.39b). Increasing v raises the tool and work material interface temperature, resulting in the softening of syntactic foam aided by poor thermal conductivity leading to decreased thrust force (Ameur et al. 2017). It is known that increasing GMB wall thickness increases the compressive strength and decreases the coefficient of thermal expansion of syntactic foams, which in turn improves the stiffness of the composite resulting in increased thrust force. F_t increases with D at all the levels of feeds as seen from Figure 3.39c. Increasing the drill diameter from D_8 to D_{16}, increases the thrust force by 74, 69 and 46% for, $w_{0.716}$, $w_{0.925}$ and $w_{1.080}$ respectively. As drill diameter increases, the contact area of the drilled hole increases leading to higher F_t (El-Sonbaty et al. 2004). It is also noted from Figure 3.39 that increasing GMBs wall thickness increases the thrust force. Increasing wall thickness from $w_{0.716}$ to $w_{1.080}$ increases the F_t by 39.84%. This is due to increasing wall thickness of GMBs increases the compressive strength of SFs due to increased collapse strength of GMBs (from 6.9 to 44.8 MPa), which in turn increases cutting resistance of the material for drill advancement resulting in higher thrust forces (Basavarajappa et al. 2011, Gupta et al. 2006, Wouterson et al. 2005).

3.3.3.2 Surface roughness

Figure 3.40 presents the response surface plots of surface roughness for varying GMB wall thickness. Surface roughness increases with increasing cutting speed and decreasing feed (Figure 3.40a). Increasing feed from $f_{0.04}$ to $f_{0.12}$ decreases R_a by 27, 35 and 51% for $w_{0.716}$, $w_{0.925}$ and $w_{1.080}$ respectively. It is known that increasing feed decreases the machining temperature due to the reduced contact time between drill and specimen leading to lower roughness values (Campos Rubio et al. 2008). Increasing cutting speed increases surface roughness while decreasing trend is observed with increasing drill diameter except for the SF reinforced with $w_{1.080}$ as observed from Figure 3.40b. R_a increases by 15, 56 and 72% for $w_{0.716}$, $w_{0.925}$ and $w_{1.080}$ respectively with increasing cutting speed from v_{25} to v_{125}. Increasing cutting speed increases the temperature at the tool-work material interface aided by the poor thermal conductivity of syntactic foams resulting in the rough surface (Gaitonde et al. 2011).

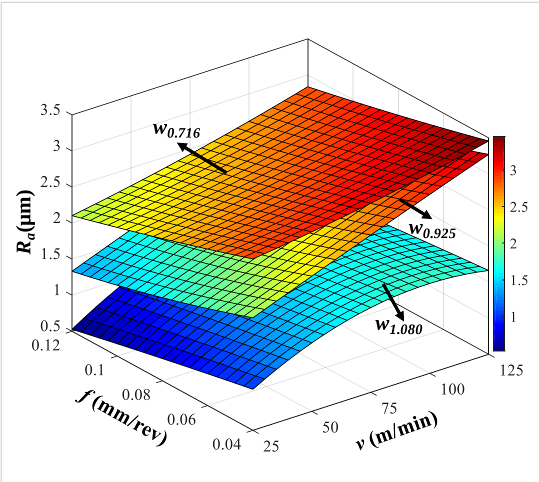

(a)

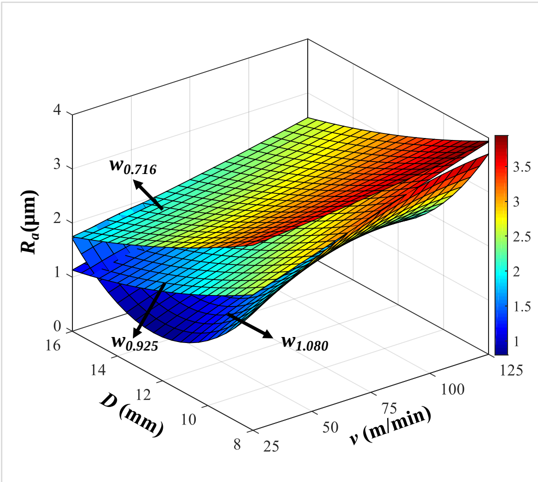

(b)

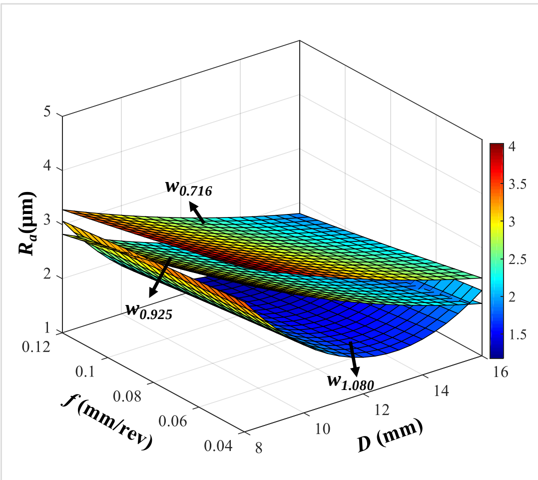

(c)

Figure 3.40 Response surface plots of (a) *v-f*, (b) *v-D* and (c) *f-D* on R_a for varying wall thickness.

Figure 3.40c shows the variation of R_a at different feed and drill diameter. Increasing diameter from D_8 to D_{16} decreases R_a in the range of 35-47% for varying wall thickness. Increasing drill diameter at a given cutting speed reduces the rotational speed of the cutting tool. This reduces the rubbing of cutting tool against drilled hole wall resulting reduced interface temperature, which in turn decreases R_a values (Khashaba et al. 2010). However, the surface roughness is found to be increasing beyond D_{12} for syntactic foam with thick-walled GMB due to higher thrust forces. This may be due to the effect of thrust force being more severe than the effect of decreased interface temperature. Syntactic foam with thick-walled GMBs ($w_{1.080}$) exhibits lower surface roughness values as compared to thin-walled GMBs ($w_{0.716}$ and $w_{0.925}$) as evident from Figure 3.40. Increasing wall thickness from $w_{0.716}$ to $w_{1.080}$ decreases surface roughness by 30% due to the increased thermal stability of syntactic foams with increasing GMBs wall thickness (Zeltmann et al. 2017). Figure 3.41 presents the micrographs showing the texture of drilled hole surface. Surface roughness of E200-60 foam is found to be higher than E350-60 foam due to the presence of broken GMBs as shown in Figure 3.41a. Thick-walled GMBs being stiffer (due to higher collapse strength), produces an effective burnishing effect than that of thin-walled ones. This leads to the smearing of epoxy matrix on the broken GMBs resulting lower roughness values (Figure 3.41b).

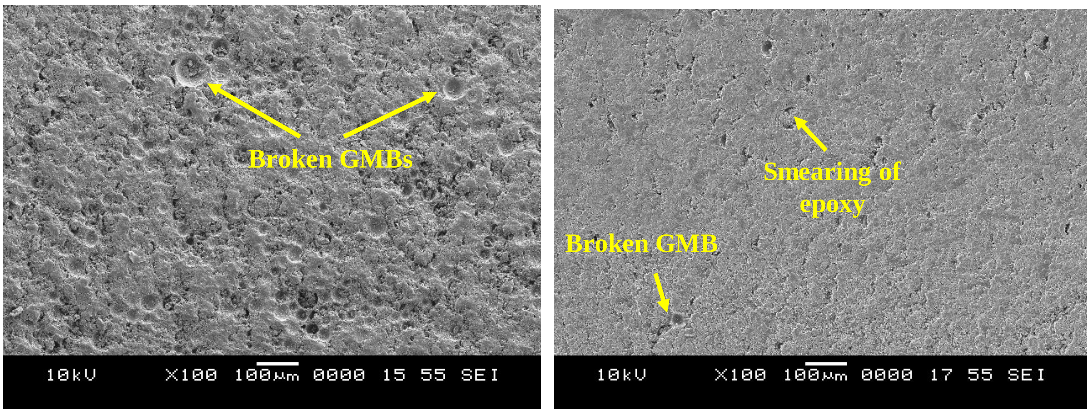

(a) (b)

Figure 3.41 Scanning electron micrographs of (a) E200-60 and (b) E350-60 syntactic foams showing drilled hole surface.

3.3.3.3 Specific cutting coefficient

K_f is found to be decreasing with increasing cutting speed and decreasing feed (Figure 3.42a). Increasing feed from $f_{0.04}$ to $f_{0.12}$ decreases K_f by 40, 50 and 56% for $w_{0.716}$, $w_{0.925}$ and $w_{1.080}$ respectively. At lower feeds, the shear model could not fit the chip formation process effectively as the syntactic foams is subjected to lower strain rates resulting in higher specific cutting coefficient (Basavarajappa et al. 2011).

Figure 3.42b shows the variation of K_f with v at different D. K_f decreases by 19 and 25% with the increasing cutting speed for SF with $w_{0.716}$ and $w_{0.925}$, while it increases by 8% for $w_{1.080}$. K_f depends on the thrust force generated during drilling (Davim et al. 2003). As explained earlier, increasing cutting speed decreases thrust force in SFs with thin-walled GMBs resulting reduced K_f values, whereas it increases with thick-walled GMB due to increased thrust force with increasing speed.

K_f is found to be decreasing with the rise in f and increases with increasing D (Figure 3.42c). Increasing drill diameter from D_8 to D_{16} increases K_f in the range of 11-43% for varying wall thickness. Increasing thrust force with increasing drill diameter leads to higher K_f (Davim et al. 2003). Figure 3.42 also shows that increasing GMBs wall thickness increases the K_f. Increasing GMBs wall thickness from $w_{0.716}$ to $w_{1.080}$ increases K_f by 41% because of increased thrust force (Gaitonde et al. 2010, Gupta et al. 2006).

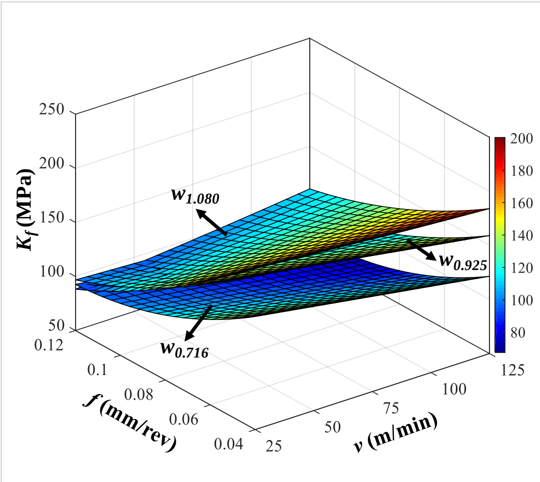

(a)

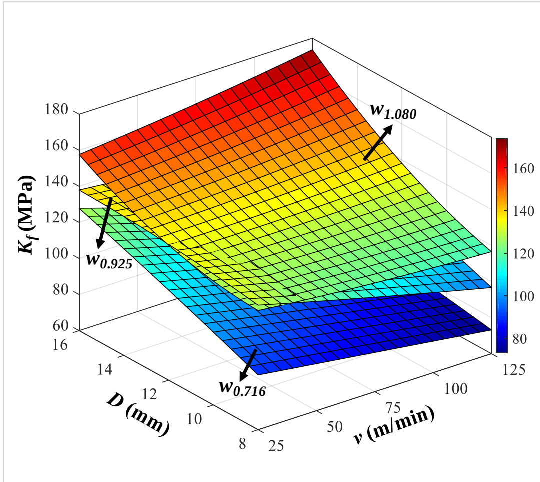

(b)

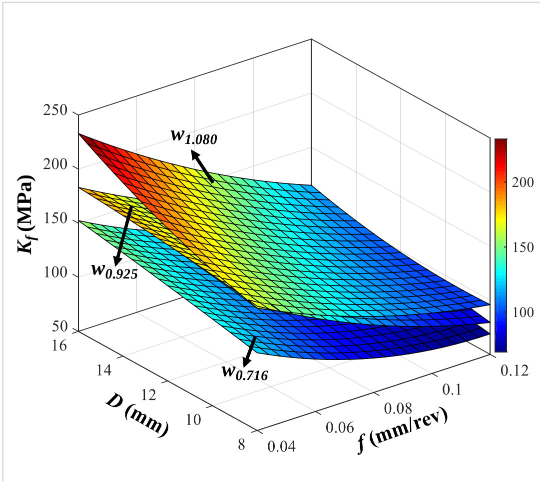

(c)

Figure 3.42 Response surface plots of (a) *v*-*f*, (b) *v*-*D* and (c) *f*-*D* on K_f for varying wall thickness.

3.3.3.4 Cylindricity

CYL increases with increasing v at all the levels of feeds as seen in Figure 3.43a. Increasing feed from $f_{0.04}$ to $f_{0.12}$ increases *CYL* by 40, 77 and 72% for $w_{0.716}$, $w_{0.925}$ and $w_{1.080}$ respectively. Better tool stability at lower feeds results in reduced *CYL* (Gowda et al. 2014, Sultan et al. 2015). *CYL* increases with increasing v and D (Figure 3.43b). Increasing speed form v_{25} to v_{125} increases *CYL* by 29, 24 and 8% for $w_{0.716}$, $w_{0.925}$ and $w_{1.080}$ respectively. At higher v the vibration of the cutting tool increases, which leads to the scatting of machine main shaft resulting in higher *CYL* (Kurt et al. 2008). Figure 3.43c shows the variation of *CYL* with f and D. *CYL* increases by 57, 127 and 159% for $w_{0.716}$, $w_{0.925}$ and $w_{1.080}$ respectively for increasing the D from D_8 to D_{16}. Increasing D increases the F_t generated during the process, which in turn increases the CYL (Gowda et al. 2014). Increasing w decreases CYL of the drill hole significantly, i.e. 41% (Figure 3.43). It is known that the thermal and dimensional stability of SFs increase with increasing GMBs wall thickness, which subsequently reduces CYL of drilled holes (Park et al. 2005, Zeltmann et al. 2017).

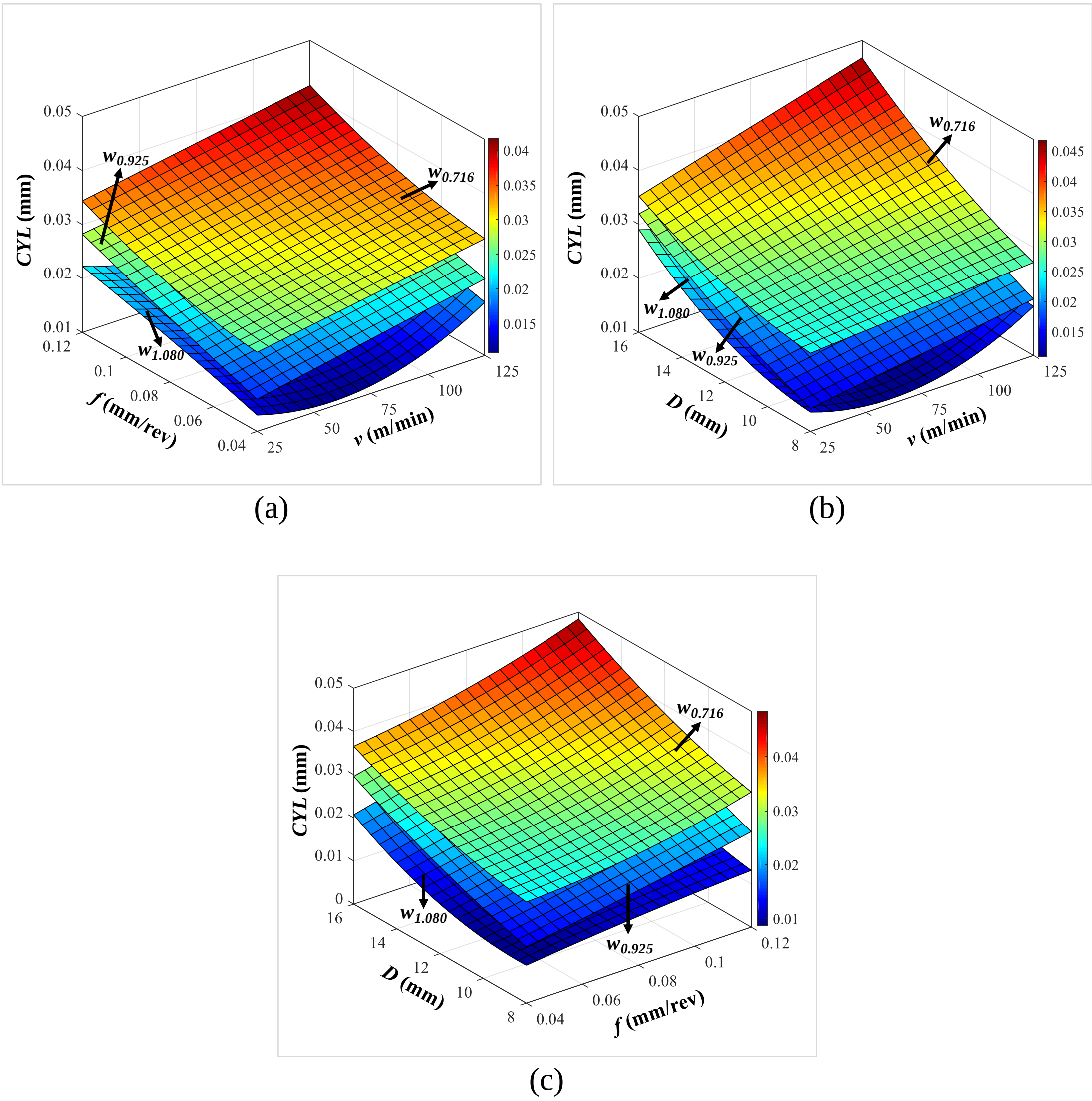

Figure 3.43 Response surface plots of (a) *v-f*, (b) *v-D* and (c) *f-D* on *CYL* for varying wall thickness.

3.3.3.5 Exit side circularity error

Figure 3.44 presents the influence of GMBs wall thickness, cutting speed, feed and drill diameter on the circularity error. It is found that increasing the feed decreases the circularity error of the drilled holes (Figure 3.44a). Increasing feed from $f_{0.04}$ to $f_{0.12}$ decreases C_{e-Exit} in the range of 31-61% for varying wall thickness. Increasing feed decreases the work-tool contact time due to increased tool traverse speed. This reduces the rubbing action of tool against the drilled hole wall which in turn decreases circularity error. Increasing feed also increases the friction between drill and foam. However, frictional heat generated may not be sufficient enough to decrease SF stiffness which results in a quality hole (Campos Rubio et al. 2008).

Circularity error increases by 32, 78 and 163% for $w_{0.716}$, $w_{0.925}$ and $w_{1.080}$ respectively with increased cutting speed (Figure 3.44b). Increasing cutting speed increases rubbing of the tool against drilled wall resulting in higher surface distortion leading to higher C_{e-Exit} values (Campos Rubio et al. 2008). C_{e-Exit} is found to be increasing with increasing feed and drill diameter (Figure 3.44c). Increasing drill diameter increases the thrust force owing to higher contact area resulting in higher circularity error (El-Sonbaty et al. 2004, Giasin and Ayvar-Soberanis 2017).

Increasing GMBs wall thickness decreases the circularity error by 56%. Reinforcing the epoxy matrix with thick-walled GMBs significantly improves the mechanical and thermal properties of syntactic foams resulting in the increased stiffness of syntactic foams which in turn helps to reduce the circularity error of drilled holes (Gaitonde et al. 2012, Zeltmann et al. 2017).

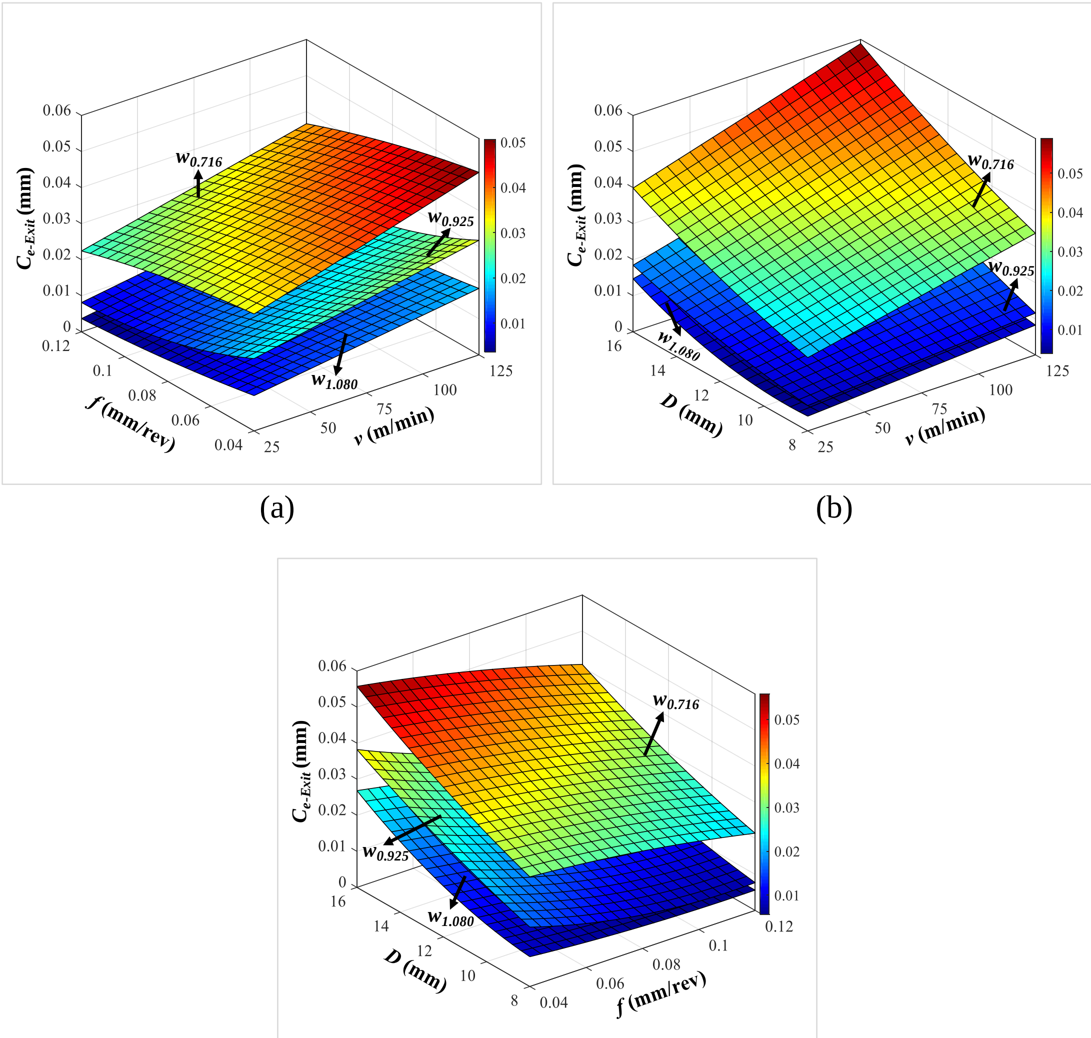

Figure 3.44 Response surface plots of (a) *v*-*f*, (b) *v*-*D* and (c) *f*-*D* on $C_{e\text{-}Exit}$ for varying wall thickness.

3.3.3.6 Exit side damage factor

Figure 3.45a shows the variation of F_{d-Exit} with cutting speed and feed. It is observed that increasing feed from $f_{0.04}$ to $f_{0.12}$ increases the damage factor by 34, 27 and 24% for $w_{0.716}$, $w_{0.925}$ and $w_{1.080}$ respectively. Increasing f increases F_t due to the increased cutting resistance of syntactic foam leading to higher values of F_{d-Exit} (Palanikumar 2011). Increasing v increases damage factor for the SF with $w_{1.080}$ GMB while decreasing trend is observed for other SFs (Figure 3.45b). F_{d-Exit} solely depends on the F_t developed during the drilling process (Palanikumar 2011). Increasing speed from

v_{25} to v_{125} decreases F_{d-Exit} by 41 and 22% for $w_{0.716}$ and $w_{0.925}$ respectively while it is seen to be increasing by 25% for $w_{1.080}$. SF reinforced with thick-walled GMBs exhibits higher cutting resistance for the advancement of tool into the work material leading to higher thrust forces which result in higher F_{d-Exit} values.

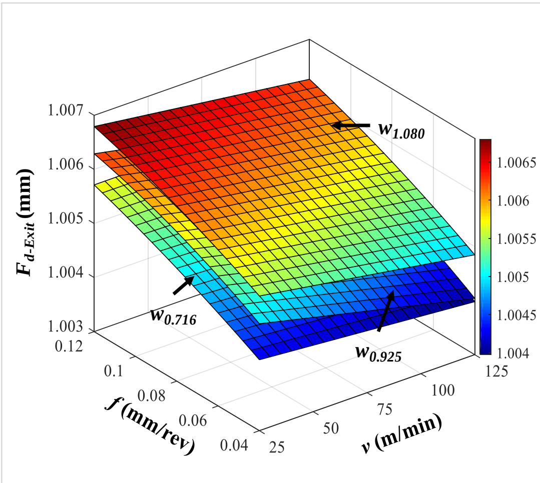

(a)

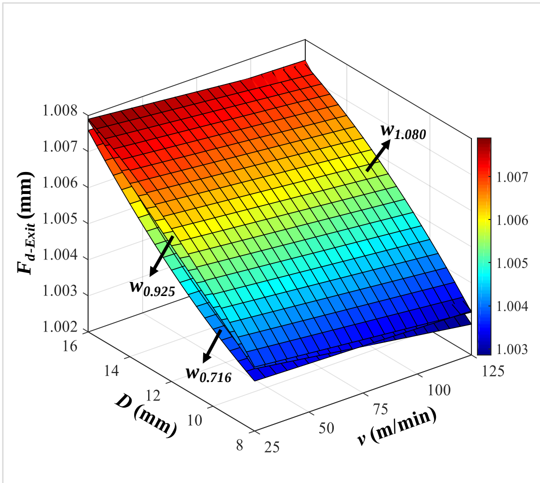

(b)

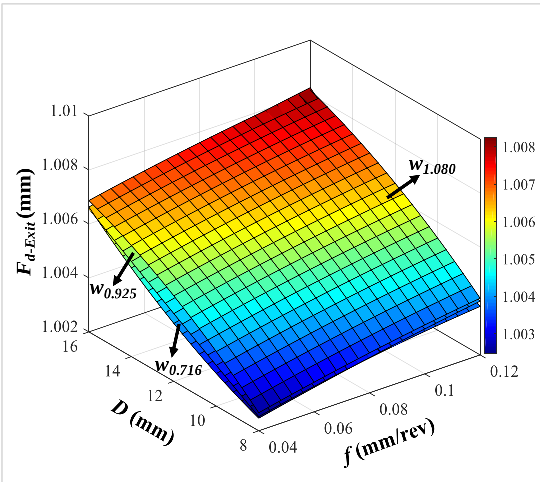

(c)

Figure 3.45 Response surface plots of (a) *v-f*, (b) *v-D* and (c) *f-D* on $F_{d\text{-}Exit}$ for varying wall thickness.

However, delamination factor decreases with increasing cutting speed for $w_{0.716}$ and $w_{0.925}$ due to thermal softening of SF as a result of increased friction between cutting edges and work material. Increasing drill diameter increases the F_{d-Exit} by 204, 156 and 128% for $w_{0.716}$, $w_{0.925}$ and $w_{1.080}$ respectively (Figure 3.45c). With increasing D, F_t

increases due to the increased contact area of hole leading to higher F_{d-Exit} values (El-Sonbaty et al. 2004, Palanikumar 2011). Increasing GMB wall thickness from $w_{0.716}$ to $w_{1.080}$ increases the $F_{d\text{-}Exit}$ by 40% owing to increased thrust forces. Figure 3.46 shows the microscopic image of exit side of the drilled hole. Syntactic foam reinforced with thin-walled GMBs suffers less damage (Figure 3.46a and Figure 3.46b) as compared to that with thick-walled GMBs (Figure 3.46c and Figure 3.46d). Increasing GMB wall thickness increases thrust forces which in turn increases the damage on the exit side of the drilled hole. GRA is inevitable as RSM based optimum conditions are not same for all the responses even in the case of wall thickness variations.

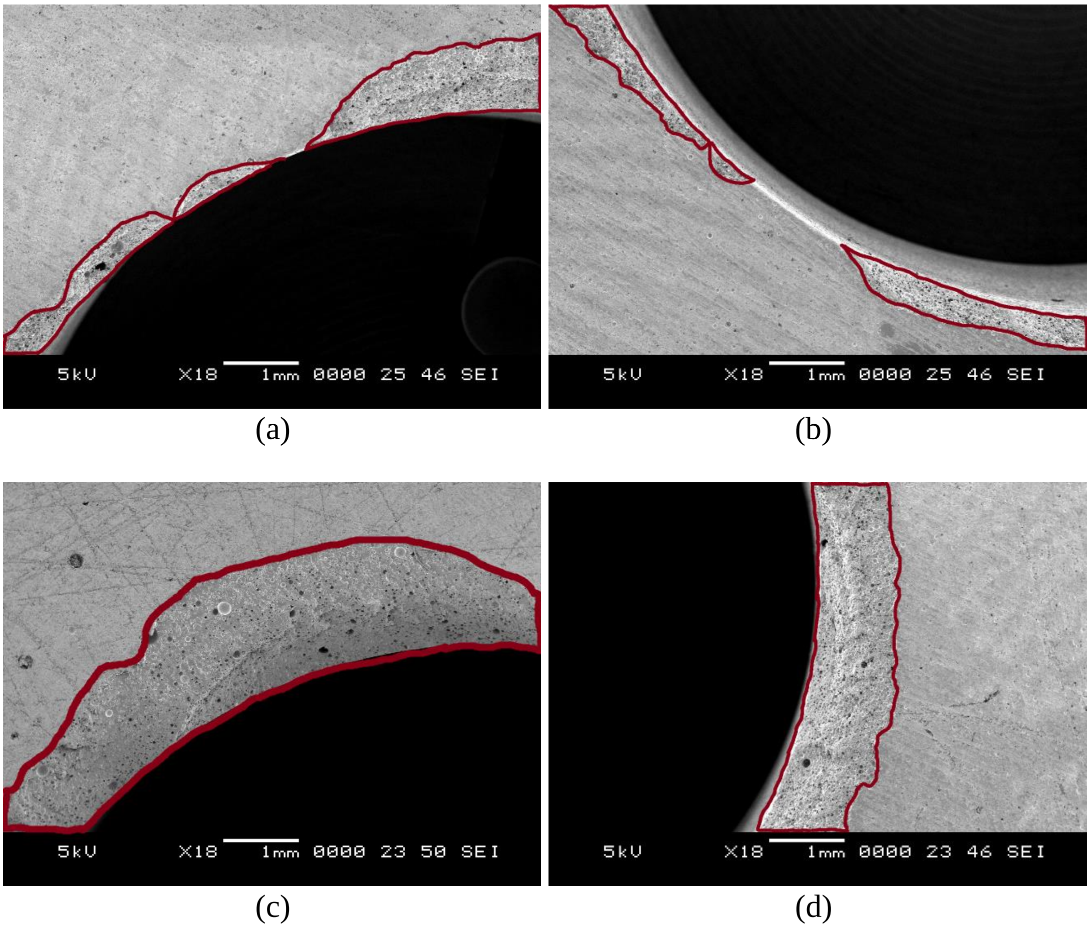

Figure 3.46 Microscopic observation of representative (a-b) E200 and (c-d) E350 syntactic foam exit side for damage assessment.

3.3.4 Grey relation analysis

It is observed from Table 3.35 and main effect plots (Figure 3.38) that the conditions for minimizing all the responses are not same.

Table 3.35 Input parameter settings for minimizing the responses.

Response	Minimizing condition
Thrust force (F_t)	$w_{0.716}v_{125}f_{0.04}D_8$
Surface roughness (R_a)	$w_{1.080}v_{25}f_{0.12}D_{16}$
Sp. cutting coefficient (K_f)	$w_{0.716}v_{125}f_{0.12}D_8$
Cylindricity (CYL)	$w_{1.080}v_{25}f_{0.04}D_8$
Exit side circularity error (C_{e-Exit})	$w_{1.080}v_{25}f_{0.12}D_8$
Exit side damage factor (F_{d-Exit})	$w_{0.716}v_{125}f_{0.04}D_8$

Lower GMBs wall thickness is desired for reducing F_t, K_f, F_{d-Exit} whereas thick-walled GMBs are required to minimize R_a, CYL, C_{e-Exit}. Higher cutting speed decreases F_t, K_f, F_{d-Exit} while lower cutting speed minimizes R_a, CYL, C_{e-Exit}. Lower feed minimizes F_t, CYL, F_{d-Exit} while higher level of feed is required to minimize R_a, K_f, C_{e-Exit}. Similarly, all the responses except surface roughness can be minimized by using smaller diameter drills. The trade-off between various process parameters for minimizing the responses necessitates multi-response optimization. Hence, in the present investigation GRA is used for finding a specific combination of process parameters to minimize the responses in drilling investigations of GMB reinforced epoxy matrix.

First step in GRA is to normalize the experimental data using smaller-the-better characteristic since the objective is to minimize the responses. Equation 2.11 is used for data normalization and results are presented in Table 3.36. Second step in GRA is computing the grey relation coefficients using the normalized data (Table 3.36). Equation 2.12 is used for calculating the grey relation coefficients of the responses and results are presented in Table 3.37.

Table 3.36 Normalized data (Smaller is better).

w	v	f	D	F_t	R_a	K_f	CYL	$C_{e\text{-}Exit}$	$F_{d\text{-}Exit}$
0.716	25	0.04	8	1.000	0.160	0.667	0.688	0.632	0.757
			12	0.800	0.492	0.444	0.646	0.526	0.591
			16	0.600	0.666	0.333	0.521	0.281	0.320
		0.08	8	0.900	0.393	0.833	0.646	0.719	0.728
			12	0.700	0.645	0.778	0.521	0.526	0.524
			16	0.400	0.701	0.667	0.417	0.316	0.223
		0.12	8	0.800	0.413	0.889	0.500	0.772	0.583
			12	0.500	0.646	0.815	0.479	0.684	0.447
			16	0.200	0.874	0.778	0.250	0.509	0.131
	75	0.04	8	1.000	0.160	0.667	0.688	0.561	0.910
			12	0.900	0.414	0.667	0.583	0.421	0.621
			16	0.700	0.654	0.500	0.375	0.070	0.379
		0.08	8	0.900	0.345	0.833	0.625	0.596	0.734
			12	0.700	0.472	0.778	0.438	0.456	0.524
			16	0.500	0.614	0.750	0.313	0.281	0.320
		0.12	8	0.900	0.404	1.000	0.500	0.737	0.704
			12	0.600	0.501	0.889	0.417	0.596	0.524
			16	0.300	0.787	0.833	0.146	0.351	0.175
	125	0.04	8	1.000	0.127	0.667	0.646	0.526	1.000
			12	0.900	0.362	0.667	0.500	0.281	0.743
			16	0.800	0.444	0.667	0.292	0.000	0.534
		0.08	8	1.000	0.193	1.000	0.625	0.596	0.816
			12	0.800	0.395	0.889	0.438	0.351	0.633
			16	0.600	0.554	0.833	0.271	0.228	0.451
		0.12	8	0.900	0.260	1.000	0.479	0.719	0.728
			12	0.700	0.529	0.963	0.313	0.509	0.677
			16	0.500	0.646	0.944	0.000	0.316	0.245
0.925	25	0.04	8	0.900	0.435	0.333	0.938	0.825	0.728
			12	0.700	0.559	0.222	0.854	0.614	0.546
			16	0.600	0.926	0.333	0.583	0.596	0.253
		0.08	8	0.800	0.458	0.667	0.854	0.930	0.644
			12	0.500	0.881	0.556	0.667	0.877	0.398
			16	0.300	0.926	0.583	0.521	0.702	0.188
		0.12	8	0.800	0.680	0.889	0.729	0.982	0.569
			12	0.500	0.911	0.815	0.604	0.895	0.359
			16	0.100	0.929	0.722	0.292	0.789	0.097
	75	0.04	8	0.900	0.378	0.333	0.854	0.754	0.757
			12	0.800	0.505	0.444	0.750	0.561	0.576
			16	0.600	0.687	0.333	0.563	0.421	0.285
		0.08	8	0.800	0.420	0.667	0.813	0.860	0.705
			12	0.600	0.586	0.667	0.604	0.772	0.439
			16	0.400	0.708	0.667	0.375	0.509	0.242

w	v	f	D	F_t	R_a	K_f	CYL	$C_{e\text{-}Exit}$	$F_{d\text{-}Exit}$
			8	0.800	0.559	0.889	0.688	0.895	0.654
		0.12	12	0.600	0.644	0.889	0.458	0.807	0.435
			16	0.200	0.816	0.778	0.292	0.719	0.141
			8	1.000	0.000	0.667	0.792	0.684	0.864
		0.04	12	0.800	0.443	0.444	0.625	0.561	0.575
			16	0.600	0.534	0.333	0.458	0.088	0.401
			8	0.900	0.231	0.833	0.771	0.825	0.736
	125	0.08	12	0.600	0.523	0.667	0.521	0.649	0.466
			16	0.400	0.657	0.667	0.292	0.456	0.312
			8	0.800	0.245	0.889	0.604	0.860	0.673
		0.12	12	0.600	0.524	0.889	0.458	0.702	0.446
			16	0.200	0.809	0.778	0.208	0.526	0.174
			8	0.900	0.499	0.333	0.938	0.947	0.700
		0.04	12	0.700	0.980	0.222	0.896	0.895	0.437
			16	0.400	0.669	0.000	0.688	0.649	0.248
			8	0.800	0.639	0.667	0.854	0.982	0.629
	25	0.08	12	0.600	1.000	0.667	0.771	0.930	0.393
			16	0.200	0.910	0.500	0.563	0.825	0.161
			8	0.800	0.715	0.889	0.833	1.000	0.550
		0.12	12	0.500	0.946	0.815	0.667	0.965	0.295
			16	0.200	0.918	0.778	0.396	0.860	0.073
			8	0.900	0.453	0.333	1.000	0.877	0.728
		0.04	12	0.800	0.751	0.444	0.896	0.807	0.422
			16	0.500	0.531	0.167	0.729	0.596	0.233
			8	0.800	0.443	0.667	0.938	0.895	0.641
1.080	75	0.08	12	0.500	0.809	0.556	0.854	0.860	0.277
			16	0.100	0.767	0.417	0.583	0.596	0.136
			8	0.700	0.596	0.778	0.854	0.930	0.567
		0.12	12	0.500	0.836	0.815	0.833	0.877	0.277
			16	0.000	0.554	0.667	0.542	0.754	0.087
			8	1.000	0.297	0.667	0.875	0.807	0.636
		0.04	12	0.700	0.864	0.222	0.771	0.667	0.340
			16	0.400	0.720	0.000	0.646	0.404	0.155
			8	0.800	0.002	0.667	0.813	0.877	0.511
	125	0.08	12	0.500	0.780	0.556	0.750	0.754	0.233
			16	0.100	0.841	0.417	0.500	0.509	0.107
			8	0.700	0.271	0.778	0.813	0.877	0.422
		0.12	12	0.400	0.947	0.741	0.646	0.754	0.204
			16	0.000	0.881	0.667	0.375	0.544	0.000

Table 3.37 Grey relation coefficients.

w	v	f	D	F_t	R_a	K_f	CYL	$C_{e\text{-}Exit}$	$F_{d\text{-}Exit}$
0.716	25	0.04	8	1.000	0.373	0.600	0.615	0.576	0.673
			12	0.714	0.496	0.474	0.585	0.514	0.550
			16	0.556	0.600	0.429	0.511	0.410	0.424
		0.08	8	0.833	0.452	0.750	0.585	0.640	0.648
			12	0.625	0.585	0.692	0.511	0.514	0.512
			16	0.455	0.626	0.600	0.462	0.422	0.392
		0.12	8	0.714	0.460	0.818	0.500	0.687	0.545
			12	0.500	0.586	0.730	0.490	0.613	0.475
			16	0.385	0.799	0.692	0.400	0.504	0.365
	75	0.04	8	1.000	0.373	0.600	0.615	0.533	0.848
			12	0.833	0.461	0.600	0.545	0.463	0.569
			16	0.625	0.591	0.500	0.444	0.350	0.446
		0.08	8	0.833	0.433	0.750	0.571	0.553	0.653
			12	0.625	0.486	0.692	0.471	0.479	0.512
			16	0.500	0.565	0.667	0.421	0.410	0.424
		0.12	8	0.833	0.456	1.000	0.500	0.655	0.628
			12	0.556	0.500	0.818	0.462	0.553	0.512
			16	0.417	0.701	0.750	0.369	0.435	0.377
	125	0.04	8	1.000	0.364	0.600	0.585	0.514	1.000
			12	0.833	0.439	0.600	0.500	0.410	0.660
			16	0.714	0.474	0.600	0.414	0.333	0.518
		0.08	8	1.000	0.382	1.000	0.571	0.553	0.730
			12	0.714	0.452	0.818	0.471	0.435	0.577
			16	0.556	0.529	0.750	0.407	0.393	0.477
		0.12	8	0.833	0.403	1.000	0.490	0.640	0.648
			12	0.625	0.515	0.931	0.421	0.504	0.607
			16	0.500	0.585	0.900	0.333	0.422	0.398
0.925	25	0.04	8	0.833	0.470	0.429	0.889	0.740	0.648
			12	0.625	0.531	0.391	0.774	0.564	0.524
			16	0.556	0.872	0.429	0.545	0.553	0.401
		0.08	8	0.714	0.480	0.600	0.774	0.877	0.584
			12	0.500	0.808	0.529	0.600	0.803	0.454
			16	0.417	0.872	0.545	0.511	0.626	0.381
		0.12	8	0.714	0.610	0.818	0.649	0.966	0.537
			12	0.500	0.849	0.730	0.558	0.826	0.438
			16	0.357	0.876	0.643	0.414	0.704	0.356
	75	0.04	8	0.833	0.446	0.429	0.774	0.671	0.673
			12	0.714	0.503	0.474	0.667	0.533	0.541
			16	0.556	0.615	0.429	0.533	0.463	0.412
		0.08	8	0.714	0.463	0.600	0.727	0.781	0.629
			12	0.556	0.547	0.600	0.558	0.687	0.471
			16	0.455	0.631	0.600	0.444	0.504	0.398

w	v	f	D	F_t	R_a	K_f	CYL	$C_{e\text{-}Exit}$	$F_{d\text{-}Exit}$
			8	0.714	0.531	0.818	0.615	0.826	0.591
		0.12	12	0.556	0.584	0.818	0.480	0.722	0.469
			16	0.385	0.731	0.692	0.414	0.640	0.368
			8	1.000	0.333	0.600	0.706	0.613	0.787
		0.04	12	0.714	0.473	0.474	0.571	0.533	0.541
			16	0.556	0.517	0.429	0.480	0.354	0.455
			8	0.833	0.394	0.750	0.686	0.740	0.655
	125	0.08	12	0.556	0.512	0.600	0.511	0.588	0.484
			16	0.455	0.593	0.600	0.414	0.479	0.421
			8	0.714	0.398	0.818	0.558	0.781	0.605
		0.12	12	0.556	0.512	0.818	0.480	0.626	0.474
			16	0.385	0.724	0.692	0.387	0.514	0.377
			8	0.833	0.499	0.429	0.889	0.905	0.625
		0.04	12	0.625	0.961	0.391	0.828	0.826	0.470
			16	0.455	0.602	0.333	0.615	0.588	0.399
			8	0.714	0.581	0.600	0.774	0.966	0.574
	25	0.08	12	0.556	1.000	0.600	0.686	0.877	0.452
			16	0.385	0.847	0.500	0.533	0.740	0.373
			8	0.714	0.637	0.818	0.750	1.000	0.526
		0.12	12	0.500	0.902	0.730	0.600	0.934	0.415
			16	0.385	0.859	0.692	0.453	0.781	0.350
			8	0.833	0.478	0.429	1.000	0.803	0.648
		0.04	12	0.714	0.667	0.474	0.828	0.722	0.464
			16	0.500	0.516	0.375	0.649	0.553	0.395
			8	0.714	0.473	0.600	0.889	0.826	0.582
1.080	75	0.08	12	0.500	0.724	0.529	0.774	0.781	0.409
			16	0.357	0.682	0.462	0.545	0.553	0.367
			8	0.625	0.553	0.692	0.774	0.877	0.536
		0.12	12	0.500	0.753	0.730	0.750	0.803	0.409
			16	0.333	0.528	0.600	0.522	0.671	0.354
			8	1.000	0.416	0.600	0.800	0.722	0.579
		0.04	12	0.625	0.786	0.391	0.686	0.600	0.431
			16	0.455	0.641	0.333	0.585	0.456	0.372
			8	0.714	0.334	0.600	0.727	0.803	0.506
	125	0.08	12	0.500	0.695	0.529	0.667	0.671	0.395
			16	0.357	0.759	0.462	0.500	0.504	0.359
			8	0.625	0.407	0.692	0.727	0.803	0.464
		0.12	12	0.455	0.904	0.659	0.585	0.671	0.386
			16	0.333	0.808	0.600	0.444	0.523	0.333

Finally, grey relation grade is computed by averaging grey relation coefficients using Equation 2.16. Table 3.38 presents the grey relation grades of the measured responses along with the ranks. Highest value (0.741) for grey relation grade is noted to be for

$w_{1.080}v_{25}f_{0.12}D_8$ and is the optimized condition for response minimization. By performing drilling at this parameter setting, responses can be effectively minimized to achieve best hole quality.

Table 3.38 Grey relation grade and rank.

v	f	D	$w_{0.716}$		$w_{0.925}$		$w_{1.080}$	
			γ_i	Rank	γ_i	Rank	γ_i	Rank
25	0.04	8	0.640	28	0.668	20	0.697	6
		12	0.556	56	0.568	49	0.684	9
		16	0.488	79	0.559	53	0.499	71
	0.08	8	0.651	24	0.672	18	0.702	4
		12	0.573	46	0.616	34	0.695	7
		16	0.493	76	0.559	54	0.563	52
	0.12	8	0.621	31	0.716	2	0.741	1
		12	0.565	51	0.650	25	0.680	12
		16	0.524	61	0.558	55	0.587	39
75	0.04	8	0.661	21	0.638	29	0.698	5
		12	0.579	41	0.572	47	0.645	27
		16	0.493	77	0.501	70	0.498	72
	0.08	8	0.632	30	0.652	23	0.681	11
		12	0.544	58	0.570	48	0.619	33
		16	0.498	73	0.505	68	0.494	74
	0.12	8	0.679	13	0.683	10	0.676	16
		12	0.567	50	0.605	37	0.657	22
		16	0.508	66	0.538	60	0.501	69
125	0.04	8	0.677	14	0.673	17	0.686	8
		12	0.574	45	0.551	57	0.586	40
		16	0.509	65	0.465	81	0.474	80
	0.08	8	0.706	3	0.676	15	0.614	35
		12	0.578	42	0.542	59	0.576	44
		16	0.518	63	0.494	75	0.490	78
	0.12	8	0.669	19	0.646	26	0.620	32
		12	0.601	38	0.578	43	0.610	36
		16	0.523	62	0.513	64	0.507	67

Furthermore, it is necessary to analyze the effects of process parameters on the machining performance at the optimized condition ($w_{1.080}v_{25}f_{0.12}D_8$). This is performed using the average analysis and results are presented in Table 3.39. Response table

(Table 3.39) is used to draw the grey relation grade graph and is presented in Figure 3.47. It is observed from Figure 3.47 and Table 3.39 that the drill diameter is having a significant effect on the drilling performance at the optimized condition followed by the interaction between cutting speed and GMB wall thickness.

Table 3.39 Response table for grey relation grade.

Level	Mean grey relation grade			
	w	*v*	*f*	*D*
1	0.57879	0.611966	0.58657	0.66941
2	0.59137	0.588715	0.589384	0.59777
3	0.61035	0.579827	0.604553	0.51332
Delta	0.03156	0.032139	0.017983	0.15609
Rank	3	2	4	1

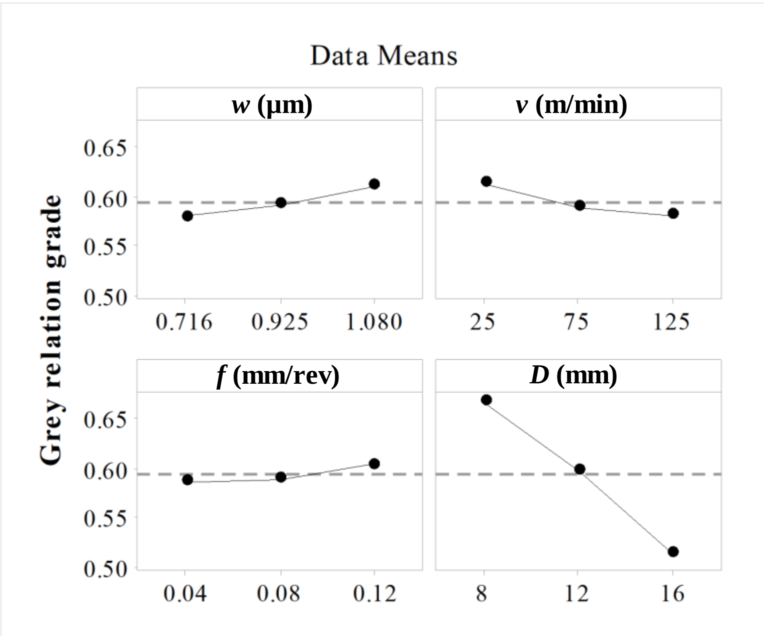

Figure 3.47 Grey relation grade graph.

ANOVA is performed on the grey relation grades to compute the percentage contribution of process parameters at the optimized condition and the results are presented in Table 3.40. From Table 3.40 it is clear that the drill diameter has a significant effect on the machining performance followed by the interaction between GMB wall thickness and cutting speed. Thick walled microballoons (SID-350Z having weight saving potential of ~48%) performed better as compared to thin walled ones (SID-200Z). These observations offer guidelines for the industries to produce quality holes in GMB/Epoxy syntactic foams used for structural applications.

Table 3.40 ANOVA for grey relation grade.

Source	DF	Adj SS	Adj MS	F-Value	P-Value	% Contribution
w	2	0.014	0.007	19.86	0.00	3.19
v	2	0.015	0.007	21.66	0.00	3.48
f	2	0.005	0.003	7.36	0.00	1.18
D	2	0.330	0.165	480.16	0.00	77.15
$w*v$	4	0.026	0.006	18.70	0.00	6.01
$w*f$	4	0.002	0.000	1.15	0.35	0.37
$w*D$	4	0.013	0.003	9.51	0.00	3.05
$v*f$	4	0.003	0.001	1.85	0.14	0.59
$v*D$	4	0.002	0.001	1.73	0.16	0.55
$f*D$	4	0.002	0.001	1.72	0.16	0.55
Error	48	0.016	0.000			
Total	80	0.427				

3.4 Chip morphology and tool wear

Low magnification micrographs of chips formed from neat epoxy and E350-60 are presented in Figure 3.48a and Figure 3.48b, respectively. Foam chips have fractured along multiple places, unlike the neat epoxy chips. Foam chips are desired as they are easily removed from the machined surfaces, avoiding entangling around the cutting tool.

Figure 3.48c shows representative images of neat epoxy chips produced during drilling at different cutting speeds and feeds for D_{16}. Ribbons type chips are formed at lower feed and increasing cutting speed did not show any significant effect on the chip morphology. Washer type helical chips are formed until $f_{0.08}$ but higher feed results in discontinuous ribbon type chips at lower cutting speed.

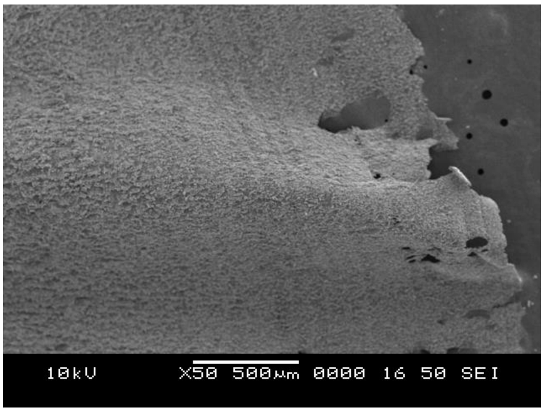

(a)

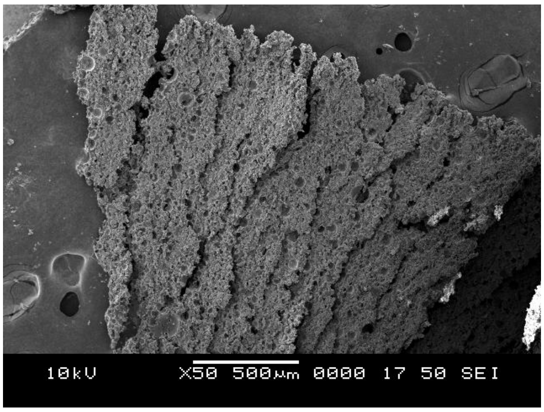

(b)

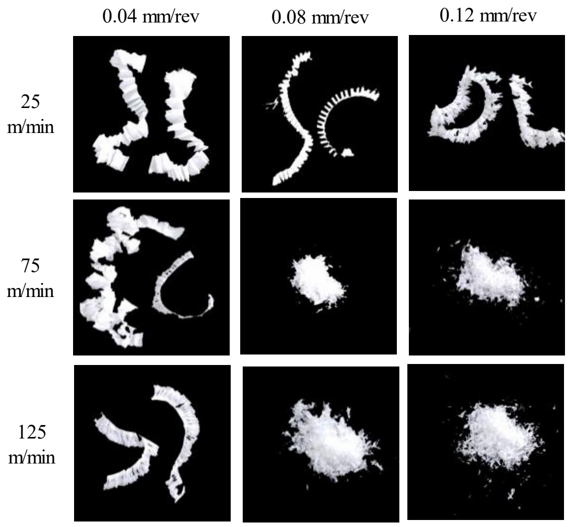

(c)

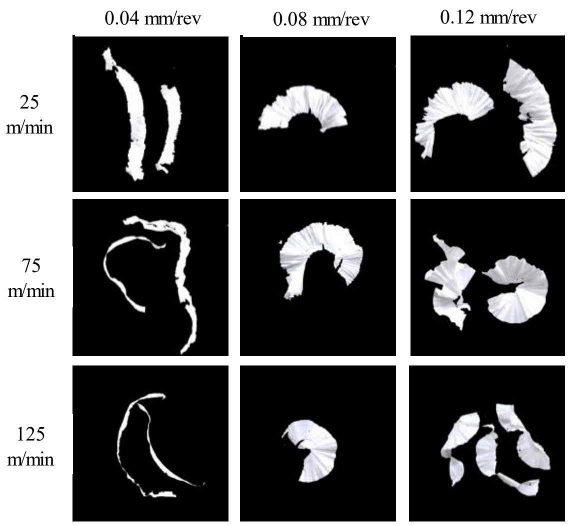

(d)

Figure 3.48 Micrographs of (a) neat epoxy and (b) E350-60 at the same magnification. Types of chips formed at different cutting speeds and feeds in drilling of (c) neat epoxy and (d) E350-60 foam for D_{16}.

At intermediate levels of feed and cutting speed, powdery chips are formed. This ductile to brittle transition in the chip forming mechanism in neat epoxy specimens is interesting. Chips formed in the drilling of syntactic foam at different cutting speed and feeds is presented in Figure 3.48d. Ribbon type chips are formed in all the type of syntactic foams, unlike powdery ones under some conditions in neat epoxy. The variation in drill diameter, GMB volume fraction and wall thickness do not exhibit any significant effect on the shape and size of the chips produced. The cutting tools are inspected using a confocal microscope (LEXT, OLS4000, OLYMPUS, Japan) post drilling operation. Figure 3.49 presents confocal microscopic images of the cutting tools used in the present investigation post drilling operation. The tools did not show any signs of tool wear even though GMB is brittle and abrasive in nature. This may be ascribed to the superior wear resistance of drill due to TiAlN coating. Also, the variation of thrust force with increasing cutting speed is found to be negligible indicating insignificant tool wear.

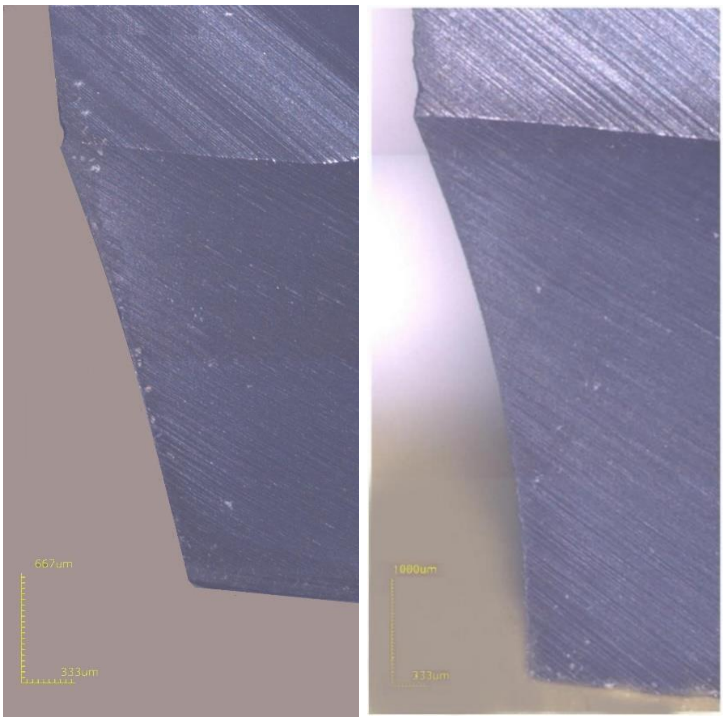

(a) (b)

Figure 3.49 Confocal microscope image of (a) D_8 and (b) D_{16} drill bit post drilling operation.

Conclusive remarks of this study are presented hereafter.

4 CONCLUSIONS

In the present work, a detailed investigation is carried out to evaluate the machinability characteristics in drilling of glass microballoon/epoxy syntactic foams. Syntactic foam samples are fabricated by dispersing hollow glass microballoons in epoxy matrix using manual stir casting method. Nine types of syntactic foams samples with 20, 40 and 60 vol.% of GMBs in epoxy matrix are fabricated using three different density grades of GMBs. The drilling experiments are conducted as per full factorial design with coated solid tungsten carbide twist drills using a vertical CNC machine. Three levels are selected for each of the process parameters with three replicates for each test condition. Cutting speed, feed, GMB content, GMB wall thickness and drill diameter are taken as input parameters, while thrust force, surface roughness, specific cutting coefficient, cylindricity, exit side circularity error and exit side damage factor are taken as the responses for evaluating the quality of drilled hole.

The second-order mathematical models of the responses are developed using the experimental data based on response surface methodology. ANOVA is used to check the adequacy of the developed models. Higher R-squared values indicate the adequacy of developed mathematical models for prediction. The errors between the experimentally measured and predicted values are found to be small indicating a good correlation is existing between the predicted and experimental values. Individual effect plots are plotted using the developed mathematical models by varying one parameter at a time, while the other parameters are kept at the intermediate level in their chosen range. These plots are used as a quick reference to understand the general trend between the chosen individual input parameters and to identify the most dominant parameter influencing the responses. Interaction effects of the input process parameters on responses are studied by varying two parameters at the same time in the mathematical models while keeping the other two parameters in the intermediate levels of their chosen range.

Finally, a multi-response optimization is performed using GRA to identify a specific combination of process parameters that produce a good quality hole in drilling of GMB/Epoxy foams by minimizing the responses (F_t, R_a, K_f, CYL, $C_{e\text{-}Exit}$, and $F_{d\text{-}Exit}$).

The main conclusions are summarized as follows:

Density

- Experimental density of all the syntactic foams is lower than the neat epoxy resin. Compared to neat epoxy, density reduction of syntactic foams is in the range of 18-53% indicating significant weight saving potential.
- Density of syntactic foams decreases with increasing GMB content and decreasing GMB wall thickness.
- Experimental density is found to be lower than theoretical density for all the syntactic foams indicating the presence of hollow microballoons and air entrapment in the matrix resin during processing.
- Matrix porosity in syntactic foams increases with volume fraction and wall thickness of GMB.

Thrust force

- Thrust force decreases with the increase in cutting speed for E200 and E270 foams, whereas it slightly increases for E350 foam.
- Thrust force of all the syntactic foams increases with increasing feed and drill diameter while decreases with increasing GMB content.
- A combination of lower feed, drill diameter, and higher filler content, cutting speed leads to minimum thrust force in E200 and E270 foams, while it is beneficial to select the lower cutting speed for E350 foam.
- Drill diameter has a significant effect on the thrust force followed by feed and GMB content, while the influence of cutting speed is found to be negligible.
- Thrust force generated in drilling of syntactic foams decreases in the range of 40-55% as compared to neat epoxy.

Surface roughness

- Surface roughness of all the foams increases with increasing cutting speed while decreases with the increasing feed and GMB content.

- Surface roughness is found to be decreasing with increasing drill diameter for E200 and E270 syntactic foams, whereas it decreases with increasing drill diameter up to D_{12} and later observed to be increasing for E350 syntactic foam.
- In comparison to surface roughness of neat epoxy, roughness in foams is observed to be increased by 14-20 times. Nevertheless, in foams, surface roughness decreases by 30% with the increasing glass microballoons content.
- Surface roughness of the drilled hole is highly influenced by drill diameter followed by cutting speed and feed.
- Surface roughness can be minimized by using higher levels of feed, filler content and drill diameter with lower values of cutting speed during drilling of E200 and E270 foams, whereas intermediate drill diameter (D_{12}) is preferred for drilling E350 syntactic foam.

Specific cutting coefficient

- Increasing feed and GMB content decreases specific cutting coefficient for all the syntactic foams, while it increases with increasing drill diameter.
- Specific cutting coefficient decreases with increasing cutting speed for E200 and E270 foams while it marginally increases for E350 syntactic foam.
- Minimum specific cutting coefficient in drilling E200 and E270 foams is achieved at a combination of lower feed, drill diameter and higher filler content, cutting speed, whereas lower cutting speed is found to be advantageous for drilling E350 foam.
- Feed and GMB content are observed to be the dominant parameters influencing specific cutting coefficient in drilling of E200 and E350 syntactic foams. Specific cutting coefficient of E350 foam is highly influenced by drill diameter followed by cutting speed.
- Specific cutting coefficient of syntactic foams decreases in the range of 40-55% as compared to those of neat epoxy.

Cylindricity

- Cylindricity of all the syntactic foams increases with increasing feed and drill diameter but decreases with increasing GMB content. Increasing cutting speed increases cylindricity of E200 and E270 syntactic foams while it decreases up to v_{75} and later found to be increasing beyond for E350 foam.
- Among input process parameters, drill diameter is the most dominant factor influencing the cylindricity of drilled holes followed by feed and GMB content. Effect of cutting speed on cylindricity is observed to be insignificant.
- Cylindricity of syntactic foams decreases in the range of 46-69% as compared to those of neat epoxy.

Exit side circularity error

- Circularity error of all the syntactic foams increases with increasing cutting speed and drill diameter, while it decreases with increasing feed and GMB content.
- Higher GMB content and feed along with lower cutting speed and drill diameter is essential for minimizing the circularity error.
- Drill diameter is the significant factor followed by GMB content in minimizing the circularity error of the holes in drilling E200 foam. However, drill diameter followed by cutting speed and feed is found to be the dominant factors for reducing the circularity error of E270 and E350 foams.
- As compared to neat epoxy, circularity error reduces in the range of 18-67% for the syntactic foams.

Exit side damage factor

- Damage factor is dependent on the thrust force developed during drilling process. Damage factor of all the syntactic foams increases with increasing feed and drill diameter but decreases with increasing GMB content.
- Lower feed and drill diameter along with higher cutting speed and GMB content is found to be the optimal condition for minimizing the damage factor of E200 and E270 syntactic foams.

- Drill diameter followed by feed and GMB content is seen to be the significant factors influencing the damage factor of the drilled hole.
- As compared to neat epoxy, damage factor of syntactic foams decreases in the range of 26-42%.

Grey relation analysis

- Grey relational analysis is performed to identify the optimal drilling conditions to produce quality holes in drilling of GMB/Epoxy syntactic foams.
- Highest grey relation grade (0.819) in drilling of E200 syntactic foam is obtained at a combination of $v_{125}f_{0.08}R_{60}D_{8}$ and performing machining at this optimized condition produces a good quality hole.
- Similarly, $v_{25}f_{0.12}R_{60}D_{8}$ is found to be the optimized condition for both E270 and E350 syntactic foams for producing quality holes.
- At the optimized condition, drill diameter (53-69%) has a significant effect on the quality of drilled hole followed by cutting speed (15-41%).

Effect of GMB wall thickness

- Increasing wall thickness of GMBs increases the compressive strength of SFs, which in turn increases cutting resistance of the material for drill advancement resulting in higher thrust forces. Increasing GMBs wall thickness increases the thrust force by 40%.
- Surface roughness is found to be decreased by 30% with increasing GMB wall thickness due to the improved thermal stability of syntactic foams. Further, thick-walled GMBs being stiffer produces an effective burnishing effect than that of thin-walled ones resulting lower surface roughness values.
- Cylindricity and circularity error is found to be decreased by 41 and 56% respectively with increasing GMB wall thickness because of the improved mechanical and thermal properties of syntactic foams.
- Increasing GMBs wall thickness increases specific cutting coefficient and exit side damage factor. Increasing GMBs wall thickness from $w_{0.716}$ to $w_{1.080}$

increases specific cutting coefficient and damage factor by 40% owing to the increased thrust forces.

- Grey relation optimization results reveal that performing machining at a combination of higher particle wall thickness and feed with lower cutting speed and drill diameter ($w_{1.080}v_{25}f_{0.12}D_8$) effectively minimizes the responses and helps in obtaining the best quality hole.
- At the optimized condition, drill diameter (77%) has a profound effect on the machining performance followed by the interaction between cutting speed and GMB wall thickness (6%).

Presented comprehensive investigation offer guidelines to achieve best quality holes in drilling operations for industries utilizing lightweight foam components.

SCOPE OF FUTURE WORK

The effects of other input process parameters like drill point angle, helix angle, chisel edge width, type of coolant and type of drill on quality of hole need to be addressed. Mathematical models based on artificial neural network can be developed to improve the accuracy of predicting the responses. Numerical models can be developed for predicting the critical thrust force responsible for drilling induced damage. Comparative analysis on the quality of the holes produced using convention drilling process and non- conventional machining process such as water jet machining, abrasive jet machining, laser drilling and ultrasonic drilling can be worth investigating. Further, the influence of heat generated on quality of hole in drilling GMB/Epoxy syntactic foams can be worth investigating.

REFERENCES

Abrao, A. M., Faria, P. E., Rubio, J. C. Campos, Reis, P. and Davim, J. Paulo. (2007). "Drilling of fiber reinforced plastics: A review." *Journal of Materials Processing Technology*, 186(1), 1-7.

Akhil, K. T., Shunmugesh, K., Aravind, S. and Pramodkumar, M. (2017). "Optimization of Drilling Characteristics using Grey Relational Analysis (GRA) in Glass Fiber Reinforced Polymer (GFRP)." *Materials Today: Proceedings,* 4(2), 1812-1819.

Ameur, M. F., Habak, M., Kenane, M., Aouici, H. and Cheikh, M. (2017). "Machinability analysis of dry drilling of carbon/epoxy composites: cases of exit delamination and cylindricity error." *The International Journal of Advanced Manufacturing Technology,* 88(9), 2557-2571.

ASTM C271-16, *Standard Test Method for Density of Sandwich Core Materials*, ASTM International, PA, USA.

Basavarajappa, S., Venkatesh, Abay, Gaitonde, V. N. and Karnik, S. R. (2011). "Experimental Investigations on Some Aspects of Machinability in Drilling of Glass Epoxy Polymer Composites." *Journal of Thermoplastic Composite Materials,* 25(3), 363-387.

Box, George EP and Draper, Norman R. (1987), *Empirical model-building and response surfaces*. John Wiley & Sons, New York.

Budov, V. V. (1994). "Hollow glass microspheres. use, properties, and technology (Review)." *Glass and Ceramics,* 51(7), 230-235.

Campos Rubio, J., Abrao, A. M., Faria, P. E., Correia, A. Esteves and Davim, J. Paulo. (2008). "Effects of high speed in the drilling of glass fibre reinforced plastic: Evaluation of the delamination factor." *International Journal of Machine Tools and Manufacture,* 48(6), 715-720.

Campos Rubio, Juan C., Abrao, Alexandre M., Eustaquio Faria, Paulo, Correia, Antonio Esteves and Davim, Joao Paulo. (2008). "Delamination in High Speed Drilling of Carbon Fiber Reinforced Plastic (CFRP)." *Journal of Composite Materials,* 42(15), 1523-1532.

Campos Rubio, Juan Carlos, Silva, Leandro Jose da, Leite, Wanderson de Oliveira, Panzera, Tulio Hallak, Filho, Sergio Luiz Moni Ribeiro and Davim, Joao Paulo. (2013). "Investigations on the drilling process of unreinforced and reinforced polyamides using Taguchi method." *Composites Part B: Engineering,* 55, 338-344.

Chung, Deborah DL. (2010), *Composite materials: science and applications*. Springer Science & Business Media, New York.

Cochran, Joe K. (1998). "Ceramic hollow spheres and their applications." *Current*

Opinion in Solid State and Materials Science, 3(5), 474-479.

Colloca, Michele, Gupta, Nikhil and Porfiri, Maurizio. (2013). "Tensile properties of carbon nanofiber reinforced multiscale syntactic foams." *Composites Part B: Engineering,* 44(1), 584-591.

Davim, J.Paulo, Reis, Pedro, Lapa, Vitor and Conceicao Antonio, C. (2003). "Machinability study on polyetheretherketone (PEEK) unreinforced and reinforced (GF30) for applications in structural components." *Composite Structures,* 62(1), 67-73.

Dodiuk, Hanna and Goodman, Sidney H. (2014). "Introduction." *Handbook of Thermoset Plastics*, William Andrew Publishing, Boston, 1-12

Donaldson, SL and Miracle, D. (2001), *ASM Handbook Composites*. ASM International, Ohio.

El-Sonbaty, I., Khashaba, U. A. and Machaly, T. (2004). "Factors affecting the machinability of GFR/epoxy composites." *Composite Structures,* 63(3), 329-338.

Eneyew, Eshetu D. and Ramulu, Mamidala. (2014). "Experimental study of surface quality and damage when drilling unidirectional CFRP composites." *Journal of Materials Research and Technology,* 3(4), 354-362.

Faria, P. E., Campos, R. F., Abrao, A. M., Godoy, G. C. D. and Davim, J. P. (2008). "Thrust Force and Wear Assessment When Drilling Glass Fiber-Reinforced Polymeric Composite." *Journal of Composite Materials,* 42(14), 1401-1414.

Feito, N., Diaz-Alvarez, J., Lopez-Puente, J. and Miguelez, M. H. (2018). "Experimental and numerical analysis of step drill bit performance when drilling woven CFRPs." *Composite Structures,* 184, 1147-1155.

Gaitonde, V. N., Karnik, S. R., Mata, Francisco and Davim, J. Paulo. (2009). "Study on Some Aspects of Machinability in Unreinforced and Reinforced Polyamides." *Journal of Composite Materials*, 43(7), 725-739.

Gaitonde, V. N., Karnik, S. R., Rubio, J. Campos, Abrao, A. M., Correia, A. Esteves and Davim, J. Paulo. (2011). "Surface roughness analysis in high-speed drilling of unreinforced and reinforced polyamides." *Journal of Composite Materials,* 46(21), 2659-2673.

Gaitonde, V. N., Karnik, S. R., Rubio, J. Campos, Correia, A. Esteves, Abrao, A. M. and Davim, J. Paulo. (2008). "Analysis of parametric influence on delamination in high-speed drilling of carbon fiber reinforced plastic composites." *Journal of Materials Processing Technology,* 203(1), 431-438.

Gaitonde, V. N., Karnik, S. R., Rubio, J. Campos, Correia, A. Esteves, Abrao, A. M. and Davim, J. Paulo. (2011). "A study aimed at minimizing delamination during drilling of CFRP composites." *Journal of Composite Materials,* 45(22), 2359-2368.

Gaitonde, V. N., Karnik, S. R., Rubio, Juan Carlos Campos, de Oliveira Leite, Wanderson and Davim, J. P. (2012). "Experimental studies on hole quality and machinability characteristics in drilling of unreinforced and reinforced polyamides." *Journal of Composite Materials,* 48(1), 21-36.

Gaitonde, V.N., Karnik, S.R., Mata, Francisco and Davim, J. Paulo. (2010). "Modeling and Analysis of Machinability Characteristics in PA6 and PA66 GF30 Polyamides through Artificial Neural Network." *Journal of Thermoplastic Composite Materials,* 23(3), 313-336.

Gaugel, Simon, Sripathy, Prithvi, Haeger, Andreas, Meinhard, Dieter, Bernthaler, Timo, Lissek, Fabian, Kaufeld, Michael, Knoblauch, Volker and Schneider, Gerhard. (2016). "A comparative study on tool wear and laminate damage in drilling of carbon-fiber reinforced polymers (CFRP)." *Composite Structures,* 155, 173-183.

Giasin, K., Ayvar-Soberanis, S. and Hodzic, A. (2015). "An experimental study on drilling of unidirectional GLARE fibre metal laminates." *Composite Structures,* 133, 794-808.

Giasin, Khaled and Ayvar-Soberanis, Sabino. (2017). "An Investigation of burrs, chip formation, hole size, circularity and delamination during drilling operation of GLARE using ANOVA." *Composite Structures,* 159, 745-760.

Gowda, B. M. Umesh, Ravindra, H. V., Jain, S. Prathik, Raj, Mohinder N., Prakesh, G. V. Naveen and Ugrasen, G. (2014). "Comparative Study of Surface Roughness and Cylindricity of Aluminium Silicon Nitride Material Using MRA GMDH & Pattern Recognition Technique in Drilling." *Procedia Materials Science,* 6, 1770-1779.

Gowda, B. M. Umesh, Ravindra, H. V., Prakash, G. V. Naveen, Nishanth, P. and Ugrasen, G. (2015). "Optimization of Process Parameters in Drilling of Epoxy Si3N4 Composite Material." *Materials Today: Proceedings,* 2(4), 2852-2861.

Groover, Mikell P. (2007), *Fundamentals of modern manufacturing: materials processes, and systems*. John Wiley & Sons, New Jersey.

Gupta, Nikhil, Karthikeyan, C. S., Sankaran, S. and Kishore. (1999). "Correlation of Processing Methodology to the Physical and Mechanical Properties of Syntactic Foams With and Without Fibers." *Materials Characterization,* 43(4), 271-277.

Gupta, Nikhil, Pinisetty, Dinesh and Shunmugasamy, Vasanth Chakravarthy. (2013), *Reinforced polymer matrix syntactic foams: effect of nano and micro-scale reinforcement*. Springer Science & Business Media, New York.

Gupta, Nikhil, Priya, Shashank, Islam, Rashed and Ricci, William. (2006). "Characterization of Mechanical and Electrical Properties of Epoxy-Glass Microballoon Syntactic Composites." *Ferroelectrics,* 345(1), 1-12.

Gupta, Nikhil and Ricci, William. (2006). "Comparison of compressive properties of layered syntactic foams having gradient in microballoon volume fraction and wall thickness." *Materials Science and Engineering: A,* 427(1), 331-342.

Gupta, Nikhil and Woldesenbet, Eyassu. (2004). "Microballoon Wall Thickness Effects on Properties of Syntactic Foams." *Journal of Cellular Plastics,* 40(6), 461-480.

Gupta, Nikhil, Zeltmann, Steven E., Shunmugasamy, Vasanth Chakravarthy and Pinisetty, Dinesh. (2014). "Applications of Polymer Matrix Syntactic Foams." *JOM,* 66(2), 245-254.

Hocheng, H. and Tsao, C. C. (2006). "Effects of special drill bits on drilling-induced delamination of composite materials." *International Journal of Machine Tools and Manufacture,* 46(12), 1403-1416.

Hu, Guohe and Yu, Demei. (2011). "Tensile, thermal and dynamic mechanical properties of hollow polymer particle-filled epoxy syntactic foam." *Materials Science and Engineering: A,* 528(15), 5177-5183.

Jayavardhan, M. L., Bharath Kumar, B. R., Doddamani, Mrityunjay, Singh, Ashish K., Zeltmann, Steven E. and Gupta, Nikhil. (2017). "Development of glass microballoon/HDPE syntactic foams by compression molding." *Composites Part B: Engineering,* 130, 119-131.

Karnik, S. R., Gaitonde, V. N., Rubio, J. Campos, Correia, A. Esteves, Abrao, A. M. and Davim, J. Paulo. (2008). "Delamination analysis in high speed drilling of carbon fiber reinforced plastics (CFRP) using artificial neural network model." *Materials & Design,* 29(9), 1768-1776.

Kaw, Autar K. (2005), *Mechanics of composite materials*. CRC press, New York.

Khashaba, U. A. (2004). "Delamination in drilling GFR-thermoset composites." *Composite Structures,* 63(3), 313-327.

Khashaba, U. A., El-Sonbaty, I. A., Selmy, A. I. and Megahed, A. A. (2010). "Machinability analysis in drilling woven GFR/epoxy composites: Part I – Effect of machining parameters." *Composites Part A: Applied Science and Manufacturing,* 41(3), 391-400.

Khashaba, U. A., El-Sonbaty, I. A., Selmy, A. I. and Megahed, A. A. (2012). "Drilling analysis of woven glass fiber-reinforced/epoxy composites." *Journal of Composite Materials*, 47(2), 191-205.

Kilickap, E. (2010). "Optimization of cutting parameters on delamination based on Taguchi method during drilling of GFRP composite." *Expert Systems with Applications,* 37(8), 6116-6122.

Kim, D. and Ramulu, M. (2004). "Drilling process optimization for graphite/bismaleimide–titanium alloy stacks." *Composite Structures*, 63(1), 101-114.

Kim, Ho Sung and Khamis, Mohammad Azhar. (2001). "Fracture and impact behaviours of hollow micro-sphere/epoxy resin composites." *Composites Part A: Applied Science and Manufacturing*, 32(9), 1311-1317.

Kim, Ho Sung and Plubrai, Pakorn. (2004). "Manufacturing and failure mechanisms of syntactic foam under compression." *Composites Part A: Applied Science and Manufacturing,* 35(9), 1009-1015.

Kishore, Shankar, Ravi and Sankaran, S. (2005). "Gradient syntactic foams: Tensile strength, modulus and fractographic features." *Materials Science and Engineering: A,* 412(1), 153-158.

Koopman, M., Gouadec, G., Carlisle, K., Chawla, K. K. and Gladysz, G. (2004). "Compression testing of hollow microspheres (microballoons) to obtain mechanical properties." *Scripta Materialia,* 50(5), 593-596.

Krishnaraj, Vijayan, Prabukarthi, A., Ramanathan, Arun, Elanghovan, N., Senthil Kumar, M., Zitoune, Redouane and Davim, J. P. (2012). "Optimization of machining parameters at high speed drilling of carbon fiber reinforced plastic (CFRP) laminates." *Composites Part B: Engineering,* 43(4), 1791-1799.

Kumar, Yogendra and Singh, Hari. (2014). "Multi-response Optimization in Dry Turning Process Using Taguchi's Approach and Utility Concept." *Procedia Materials Science,* 5, 2142-2151.

Kurt, M., Kaynak, Y. and Bagci, E. (2008). "Evaluation of drilled hole quality in Al 2024 alloy." *The International Journal of Advanced Manufacturing Technology,* 37(11), 1051-1060.

Lin, S. C. and Chen, I. K. (1996). "Drilling carbon fiber-reinforced composite material at high speed." *Wear,* 194(1), 156-162.

Manakari, Vyasaraj, Parande, Gururaj, Doddamani, Mrityunjay, Gaitonde, V. N., Siddhalingeshwar, I. G., Kishore, Shunmugasamy, Vasanth Chakravarthy and Gupta, Nikhil. (2015). "Dry sliding wear of epoxy/cenosphere syntactic foams." *Tribology International,* 92, 425-438.

Merino-Perez, Julian Luis, Royer, Raphael, Merson, Eleanor, Lockwood, Aiden, Ayvar-Soberanis, Sabino and Marshall, Matthew B. (2016). "Influence of workpiece constituents and cutting speed on the cutting forces developed in the conventional drilling of CFRP composites." *Composite Structures,* 140, 621-629.

Mohan, N. S., Kulkarni, S. M. and Ramachandra, A. (2007). "Delamination analysis in drilling process of glass fiber reinforced plastic (GFRP) composite materials." *Journal of Materials Processing Technology,* 186(1), 265-271.

Mohan, N. S., Ramachandra, A. and Kulkarni, S. M. (2005). "Influence of process parameters on cutting force and torque during drilling of glass–fiber polyester reinforced composites." *Composite Structures,* 71(3), 407-413.

Montgomery, Douglas C. (2017), *Design and analysis of experiments*. John wiley & sons, New York.

Nagpal, Geeta, Uddin, Moin and Kaur, Arvinder. (2014). "Grey Relational Effort Analysis Technique Using Regression Methods for Software Estimation." *International Arab Journal of Information Technology,* 11(5), 437-446.

Nikhil, Gupta and Ruslan, Nagorny. (2006). "Tensile properties of glass microballoon-epoxy resin syntactic foams." *Journal of Applied Polymer Science,* 102(2), 1254-1261.

Palanikumar, K. (2011). "Experimental investigation and optimisation in drilling of GFRP composites." *Measurement*, 44(10), 2138-2148.

Palanikumar, K., Campos Rubio, J., Abrao, A. M., Esteves Correia, A. and Davim, J. Paulo. (2008). "Influence of Drill Point Angle in High Speed Drilling of Glass Fiber Reinforced Plastics." *Journal of Composite Materials,* 42(24), 2585-2597.

Palanikumar, K., Karunamoorthy, L. and Karthikeyan, R. (2006). "Assessment of factors influencing surface roughness on the machining of glass fiber-reinforced polymer composites." *Materials & Design,* 27(10), 862-871.

Palanikumar, K., Latha, B., Senthilkumar, V. S. and Davim, J. Paulo. (2012). "Analysis on Drilling of Glass Fiber–Reinforced Polymer (GFRP) Composites Using Grey Relational Analysis." *Materials and Manufacturing Processes,* 27(3), 297-305.

Park, Soo-Jin, Jin, Fan-Long and Lee, Changjin. (2005). "Preparation and physical properties of hollow glass microspheres-reinforced epoxy matrix resins." *Materials Science and Engineering: A,* 402(1), 335-340.

Pihtili, Hasim and Canpolat, Nusret. (2009). "Investigation of Different Reinforced Composite Materials for Surface Roughness and Capacity of Being Drilled." *Journal of Composite Materials,* 43(19), 2071-2080.

Pinisetty, Dinesh, Shunmugasamy, Vasanth C. and Gupta, Nikhil. (2015). "Hollow Glass Microspheres in Thermosets - Epoxy Syntactic Foams." *Hollow Glass Microspheres for Plastics, Elastomers, and Adhesives Compounds,* William Andrew Publishing, Oxford, 147-174.

Porfiri, Maurizio and Gupta, Nikhil. (2009). "Effect of volume fraction and wall thickness on the elastic properties of hollow particle filled composites." *Composites Part B: Engineering,* 40(2), 166-173.

Rajamurugan, T. V., Shanmugam, K. and Palanikumar, K. (2013). "Analysis of delamination in drilling glass fiber reinforced polyester composites." *Materials & Design,* 45, 80-87.

Raju, Bhadrabasol Revappa, Suresha, Bheemappa, Swamy, Ragera Parameshwarappa and Kanthraju, Bannangadi Swamy Gowda. (2013). "Assessment of Cutting Parameters Influencing on Thrust Force and Torque during Drilling Particulate Filled

Glass Fabric Reinforced Epoxy Composites." *Journal of Minerals and Materials Characterization and Engineering,* 1, 101-109.

Ramesh, B., Elayaperumal, A., Satishkumar, S., Kumar, Anish, Jayakumar, T. and Dinakaran, D. (2016). "Influence of cooling on the performance of the drilling process of glass fibre reinforced epoxy composites." *Archives of Civil and Mechanical Engineering*, 16(1), 135-146.

Ravichandran, G, Raju, K, Varadarajan, YS and Suresha, B. (2016). "Performance of HSS and carbide drills on micro filler filled glass fabric reinforced epoxy composites." *Polymers Research Journal*, 10(4), 175-185.

Reddy, A Ramanjaneya, Reddy, K Siva Bhushan, Hussain, P, Reddy, B Sidda and Babu, S Sudhakar. (2013). "An experimental study using design of experiment method to compare the performance of solid carbide and Hss drills in drilling of GFRP composite material." *International Journal of Mechanical Engineering and Robotics Research*, 2(4), 216-221.

Shahapurkar, Kiran, Garcia, Carlos D., Doddamani, Mrityunjay, Mohan Kumar, G. C. and Prabhakar, Pavana. (2018). "Compressive behavior of cenosphere/epoxy syntactic foams in arctic conditions." *Composites Part B: Engineering,* 135, 253-262.

Sheikh-Ahmad, Jamal Y. (2009), *Machining of polymer composites*. Springer, New York.

Sheth, Saurin and George, P. M. (2016). "Experimental investigation, prediction and optimization of cylindricity and perpendicularity during drilling of WCB material using grey relational analysis." *Precision Engineering*, 45, 33-43.

Shutov, F. A. (1986). "Syntactic polymer foams." *Advances in Polymer Science*, Springer, Berlin, Heidelberg, 63-123.

Singh, Amrinder Pal, Sharma, Manu and Singh, Inderdeep. (2013). "A review of modeling and control during drilling of fiber reinforced plastic composites." *Composites Part B: Engineering*, 47, 118-125.

Singh, Inderdeep, Rakesh, Pawan Kumar and Malik, Jagannath. (2012). "Predicting forces and damage in drilling of polymer composites: soft computing techniques." *Mechatronics and Manufacturing Engineering*, Woodhead Publishing, United Kingdom, 227-258.

Sreenivasulu, Reddy and Rao, CS. (2012). "Application of gray relational analysis for surface roughness and roundness error in drilling of Al 6061 alloy." *International journal of lean thinking,* 3(2), 67-78.

Sultan, A. Z., Sharif, Safian and Kurniawan, Denni. (2015). "Effect of Machining Parameters on Tool Wear and Hole Quality of AISI 316L Stainless Steel in Conventional Drilling." *Procedia Manufacturing*, 2, 202-207.

Swetha, C. and Kumar, Ravi. (2011). "Quasi-static uni-axial compression behaviour of hollow glass microspheres/epoxy based syntactic foams." *Materials & Design,* 32(8), 4152-4163.

Teti, R. (2002). "Machining of Composite Materials." *CIRP Annals,* 51(2), 611-634.

Tsao, C. C. and Hocheng, H. (2004). "Taguchi analysis of delamination associated with various drill bits in drilling of composite material." *International Journal of Machine Tools and Manufacture,* 44(10), 1085-1090.

Tsao, C. C. and Hocheng, H. (2008). "Evaluation of thrust force and surface roughness in drilling composite material using Taguchi analysis and neural network." *Journal of Materials Processing Technology,* 203(1), 342-348.

Vankanti, Vinod Kumar and Ganta, Venkateswarlu. (2014). "Optimization of process parameters in drilling of GFRP composite using Taguchi method." *Journal of Materials Research and Technology,* 3(1), 35-41.

Velayudham, A. and Krishnamurthy, R. (2007). "Effect of point geometry and their influence on thrust and delamination in drilling of polymeric composites." *Journal of Materials Processing Technology,* 185(1), 204-209.

Wang, Lijun, Zhang, Jing, Yang, Xu, Zhang, Chun, Gong, Wei and Yu, Jie. (2014). "Flexural properties of epoxy syntactic foams reinforced by fiberglass mesh and/or short glass fiber." *Materials & Design,* 55, 929-936.

Wang, Xin, Kwon, Parick Y., Sturtevant, Caleb, Kim, Dave and Lantrip, Jeff. (2013). "Tool wear of coated drills in drilling CFRP." *Journal of Manufacturing Processes,* 15(1), 127-135.

Wouterson, Erwin M., Boey, Freddy Y. C., Hu, Xiao and Wong, Shing-Chung. (2005). "Specific properties and fracture toughness of syntactic foam: Effect of foam microstructures." *Composites Science and Technology,* 65(11), 1840-1850.

Xu, Jinyang, An, Qinglong, Cai, Xiaojiang and Chen, Ming. (2013). "Drilling machinability evaluation on new developed high-strength T800S/250F CFRP laminates." *International Journal of Precision Engineering and Manufacturing,* 14(10), 1687-1696.

Yi-Jen, Huang, Chia-Hao, Wang, Yu-Lin, Huang, Gangjian, Guo and R., Nutt Steven. (2010). "Enhancing specific strength and stiffness of phenolic microsphere syntactic foams through carbon fiber reinforcement." *Polymer Composites,* 31(2), 256-262.

Yung, K. C., Zhu, B. L., Yue, T. M. and Xie, C. S. (2009). "Preparation and properties of hollow glass microsphere-filled epoxy-matrix composites." *Composites Science and Technology,* 69(2), 260-264.

Zeltmann, Steven Eric, Chen, Brian and Gupta, Nikhil. (2017). "Thermal expansion and dynamic mechanical analysis of epoxy matrix–borosilicate glass hollow particle syntactic foams." *Journal of Cellular Plastics*, 54(3), 463-481.

Zhang, Xin, Wang, Pengfei, Zhou, Yihao, Li, Xiaotuo, Yang, En-Hua, Yu, T. X. and Yang, Jinglei. (2016). "The effect of strain rate and filler volume fraction on the mechanical properties of hollow glass microsphere modified polymer." *Composites Part B: Engineering*, 101, 53-63.

Zhu, Bailin, Ma, Jing, Wang, Jian, Wu, Jun and Peng, Dongsheng. (2012). "Thermal, dielectric and compressive properties of hollow glass microsphere filled epoxy-matrix composites." *Journal of Reinforced Plastics and Composites*, 31(19), 1311-1326.

LIST OF PUBLICATIONS

INTERNATIONAL JOURNALS

1. Ashrith H. S., Mrityunjay Doddamani, Vinayak Gaitonde and Nikhil Gupta (2018). "Hole Quality Assessment in Drilling of Glass Microballoon/Epoxy Syntactic Foams." *JOM,* 70(7), 1289-1294. (**Springer, 2.145**).

2. Ashrith H. S., Mrityunjay Doddamani, Vinayak Gaitonde and Nikhil Gupta (2018). "Influence of materials and machining parameters on drilling performance of syntactic foams." *Materials Performance and Characterization*. 7(1), 495-514. (**ASTM**).

3. Ashrith H. S., Mrityunjay Doddamani and Vinayak Gaitonde (2018). "Effect of wall thickness and cutting parameters on drilling of glass microballoon/epoxy syntactic foam composites." *Composite Structures*. 211, 318-336. (**Elsevier, 4.101**).

INTERNATIONAL CONFERENCES

1. Ashrith H. S., Mrityunjay Doddamani, Vinayak Gaitonde and Nikhil Gupta (2017). "Surface roughness evaluation in drilling of syntactic foams." *International Conference on Advances in Polymer Science and Technology*, November 23-25, 2017, Indian Institute of Technology, New Delhi, India.

2. Ashrith H. S., Mrityunjay Doddamani, Vinayak Gaitonde and Nikhil Gupta (2017). "Machinability study of syntactic foams". *International Conference on Precision, Meso, Micro and Nano Engineering*, December 06-09, 2017, Indian Institute of Technology, Madras, Chennai, India.

3. Ashrith H. S., Mrityunjay Doddamani and Vinayak (2018). "Evaluation of circularity error in drilling of syntactic foam composites." *International Conference on Design, Materials & Manufacture*. January 29-31, 2018, NITK, Surathkal, India. DOI: 10.1063/1.5029641

4. Ashrith H. S., Mrityunjay Doddamani and Vinayak Gaitonde (2018). "Experimental investigation on the machinability characteristics in drilling of epoxy syntactic foam." *International Engineering Symposium*. March 6-13, 2018, Kumamoto University, Japan.

BIO-DATA

1. **Name** : Ashrith H. S.
2. **Father's Name** : H. S. Shivegowda
3. **Date of Birth** : 02nd June 1987
4. **Nationality** : Indian
5. **Marital Status** : Married
6. **Address** : Department of Mechanical Engineering
   National Institute of Technology Karnataka
   Surathkal, PO Srinivasnagar 575 025
   Karnataka, India.
7. **Mobile Number** : +91 9844883545
8. **E-mail id.** : *ashuhiriyal@gmail.com*
9. **Educational Qualification** :

Qualification	University/Board	Year of Passing
Ph. D. (Mechanical Engineering)	National Institute of Technology Karnataka	Pursuing
M. Tech. (Mechanical Engineering)	Visvesvaraya Technological University, Belgaum	2011
B. E. (Mechanical Engineering)	Visvesvaraya Technological University, Belgaum	2009